

Lancaster University



Analysis of the Role of CIZ1 in Regulation of DNA Replication

by

James Tollitt

PhD Thesis in Biomedical and Life Sciences

Lancaster University

Faculty of Health and Medicine

Biomedical Life Sciences

September 2020

Declaration

I declare that the content of this thesis is my own work and has not been submitted by myself in substantially the same form for the award of a higher degree elsewhere. Any sections of the thesis which have been published have been clearly identified.

A handwritten signature in black ink, appearing to read 'James Tollitt', with a horizontal line underneath it.

James Tollitt

Acknowledgements

Firstly, I would like to thank Dr Nikki Copeland for the support throughout my many years of studies at Lancaster University. You once told me that success was a mixture of hard work and luck. However, any success I have experienced during my PhD is a direct consequence of the opportunities that you have been generous to afford to me. I would also like to thank my secondary supervisor Dr Sarah Allinson for the support, and assistance both in the lab and during lab meetings.

Secondly, throughout my PhD studies I have been lucky enough to share the lab with a number of brilliant individuals: Dr Urvi Thacker, Dr Tekle Pauzaite, Freya Ferguson, and Natasha Falkingham. My PhD would have been considerably more challenging without the help, conversations, and most importantly trading cell culture at weekends. Tekle in particular, I would like to thank for hundreds of trips to get coffee and cake we shared, as well as letting me meet your two energetic dogs. Beyond labmates I would like to thank Dr Monica Staniek, Alex Hardgrave, Jack Martin, Kim Fabian and many more for the trips to the pub, cycling outings, and shared lunches.

Thirdly, I would like to thank my family. Your support has always been given without question whether this is financial, emotional, or providing a house with a garden during a pandemic lockdown.

Finally, and critically, I would like to thank Rebecca Freeman. My PhD began at the same time as our relationship. The two have formed the focus of my life during this time. They could not be more different. A PhD is challenging, stressful, and at times disheartening. You, however, are the antithesis of this always there with love, support, and kindness without question. Thank-you always.

List of Figures

Figure 1.1 – <i>E. coli</i> Replication	9
Figure 1.2 – The Metazoan Cell Cycle	10
Figure 1.3 – DNA Replication Licensing	17
Figure 1.4 – DNA Replication Initiation	21
Figure 1.5 - CIZ1 Promotes Replication initiation through interactions with Cyclins	27
Figure 1.6 – The Quantitative Model of the Cell Cycle	29
Figure 1.7 – Oncogene Activation Induces Replication Stress	36
Figure 1.8 – Synthetic Lethality	41
Figure 1.9 – The DDR to DSBs	44
Figure 1.10 – The Replication Stress Response	46
Figure 3.1 – DNA Combing Schematic	79
Figure 3.2 – DNA Replication Event Schematic	81
Figure 3.3 – Measuring Replication Fork Rate	82
Figure 3.4 – Measuring IOD Using DNA Combing	83
Figure 3.5 – Measure Replication Fork Stalling Through IdU: CldU Length Ratio	85
Figure 3.6 – Measure Replication Fork Stalling Through Measuring Replication Fork Asymmetry.	86
Figure 3.7 – Measuring Replication Fork Restart Rate	87
Figure 3.8 – Analysis and quality control of Yoyo1 Stained Lambda Phage DNA	90
Figure 3.9 – Analysis of antibody labelled Lambda Phage ssDNA	92
Figure 3.10 – pH optimisation of DNA combing of NIH 3T3 DNA	95
Figure 3.11 – Single labelling of combed DNA from NIH 3T3 cells	97
Figure 3.12 – Dual labelling of DNA combed from NIH 3T3 cells	99
Figure 3.13 – Quality control of nuclei isolated from NIH 3T3 cells	101
Figure 3.14 – Degradation of DNA During Cell Isolation	103
Figure 3.15 – Degradation of DNA During Nuclei Isolation	104
Figure 3.16 – Centrifuging Nuclei Effects DNA Integrity	106
Figure 3.17 – Freeze Thaw Effects DNA Integrity	108
Figure 3.18 – Enriching Long DNA Fibres by Electrophoresis	110
Figure 3.19 – Labelling of <i>in vitro</i> reactions with multiple nucleotides	112
Figure 3.20 – Labelling of Replication on Combed DNA From <i>in vitro</i> Replication Experiments	114
Figure 3.21 – Patterns of DNA replication	116

Figure 4.1 – CRIPSR CAS9 mediated genome editing	123
Figure 4.2 – crRNA Sequences targeting CIZ1	125
Figure 4.3 – Generation of CIZ1 null NIH 3T3 cells	126
Figure 4.4 – Analysis of Cell Cycle Profiles of WT and CIZ1 KO Cell lines	128
Figure 4.5 – Cell Cycle re-entry Profiles of WT and CIZ1 null cells	130
Figure 4.6 – Loss of CIZ1 changed the timing of cell cycle re-entry	132
Figure 4.7 – Loss of CIZ1 Changed the way cells entered quiescence	135
Figure 4.8 – Loss of CIZ1 altered serum dependence	138
Figure 4.9 – Loss of CIZ1 altered the restriction point	141
Figure 4.10 – Loss of CIZ1 moderates the DDR to HU	143
Figure 4.11 – Generation of stably transfected CIZ1 ^{AB} Cell line	146
Figure 4.12 – Analysis of asynchronous CIZ1 ^{AB} cell lines	147
Figure 4.13 – CIZ1 ^{AB} cell cycle re-entry post-quiescence mirrors WT cells	149
Figure 4.14 – 24-hour monitoring of a release of CIZ1 ^{AB} cells into S-phase	150
Figure 4.15 – Analysis of the restriction of the CIZ1 ^{AB} cells	151
Figure 4.16 – Response to HU treatment in CIZ1 ^{AB} cells.	153
Figure 4.17 – A model for how loss of CIZ1 induces cellular changes	162
Figure 5.1 – Overview of approaches used for mammalian cell cycle synchronisation	167
Figure 5.2 – Purification of Cyclin A-CDK2	170
Figure 5.3 - High concentrations of CIZ1-N471 block DNA replication initiation	172
Figure 5.4 – Comparison of WT, CIZ1 KO and CIZ1 ^{AB} Nuclei S Phase Entry <i>in vitro</i>	175
Figure 5.5 – CIZ1 Titration promotes cyclin A loading onto CIZ1 KO nuclei <i>in vitro</i>	177
Figure 5.6 – Titration of Cyclin A into G1 extracts promotes replication initiation at a narrow range of concentrations	179
Figure 5.7 – Recombinant CIZ1 rescues CIZ1 KO nuclei, and restores optimal CDK thresholds <i>in vitro</i>	181
Figure 5.8. CIZ1-N471 Expands concentrations of Cyclin A/CDK2 that can promote DNA replication initiation	183
Figure 5.9 – CIZ1-N471 increases the range of cyclin A-CDK that promotes initiation of DNA replication	185
Figure 5.10 – Increased cyclin A-CDK2 concentration changes optimal CIZ1 levels for CIZ1 KO Nuclei	187
Figure 5.11- Measuring Replication Kinetics in <i>in vitro</i> reactions	189

Figure 5.12. The effect of adding recombinant CIZ1 to a range of cyclin A/CDK2 concentrations in vitro	192
Figure 5.13 – Model for the effect of CIZ1 levels and thresholds for initiation of DNA replication	197
Figure-5.14- Model for the effect of increased CIZ1	199
Figure 6.1 - Sources of DNA Replication Stress	207
Figure 6.2. Replication dynamics of cell treated with CDC7 inhibitors PHA-767491 or XL-413	210
Figure 6.3-Replication dynamics of WT and CIZ1 KO NIH 3T3 Cells	212
Figure 6.4. CIZ1 ^{AB} reverses the DRS phenotype in CIZ1KO cells	214
Figure 6.5. CIZ1 KO increases activation of cryptic replication origins	216
Figure 6.6. CIZ1 ^{AB} reverses the activation of cryptic replication origins in CIZ1 KO cells	218
Figure 6.7. CIZ1 KO cells have impaired ability to restart forks after replication challenge with HU n	220
Figure 6.8 Measuring Replication Dynamics 24 hours after HU Mediated Replication Stress	224
Figure 6.9 A Model for the Tumour Suppressor Function of CIZ1	229
Figure 7.1 – Surveying CIZ1 alterations in cancers in the cancer genome atlas	241
Figure 7.2-A Model for how CIZ1 Loss Reduces Genome Stability.	246

List of Tables

Table 1.1 – Comparison of genome sizes, DNA replication fork rates and genome architecture across the domains of life	7
Table 1.2 – The major CDKs, cyclin binding partners, and their role in cell cycle control.	12
Table 2.1 – Recipe of auto induction broth	53
Table 2.2 – Western blot antibodies, suppliers, targets, and species.	61
Table 2.3 – Recipe for <i>in vitro</i> replication assay buffers	66
Table 2.4 – Primers Used for Generating CIZ1 Cells Using CRISPR Cas9	67
Table 2.5 – Antibodies used for DNA combing experiments	74
Table 7.1 – CIZ1 alterations observed in cancers	239

List of Abbreviations

ANOVA – Analysis of Variance

APC – Anaphase Promoting Complex

ARS – Autonomously Replicating Sequence

ATM – Ataxia Telangiectasia Mutant

ATP – Adenosine Triphosphate

ATR – Ataxia Telangiectasia and Rad3-Related Protein

BCA – Bicinchoninic Acid

BRCA1 – Breast cancer type 1 susceptibility protein

BRCA2 – Breast cancer type 2 susceptibility protein

BrDU – Bromodeoxyuridine

CAK – CDK Activating Kinase

CAPS – N-Cyclohexyl-3-Aminopropanesulfonic Acid

CDK – Cyclin Dependent Kinase

CD4 – Cluster of Differentiation 4

CDC – Cell Division Cycle

CDT1 – Chromatin Licensing and DNA Replication Factor 1

CFS – Common Fragile Sites

CHK1 – Checkpoint Kinase 1

CHK2 – Checkpoint Kinase 2

CldU – Chlorodeoxyuridine

CMG – Cdc45-MCM-GINS

CIZ1 – CIP1 Interacting Zinc Finger Protein 1

CIZ1 KO – CIZ1 null NIH 3T3 cells generated by CRISPR/Cas9

CIZ1^{AB} – Stably Transfected GFP-CIZ1 Expressing CIZ1 KO1 NIH 3T3 Cells

CPD – Cyclobutene Pyrimidine Dimers

CPK – Creatine Phosphokinase

CRISPR – Clustered Regularly Interspaced Short Palindromic Repeats

CTP – Cytidine Triphosphate

DDR – DNA Damage Response

DDK – Dbf4-dependent kinase

DMEM – Dulbecco's Modified Eagle's Medium

DNA – Deoxyribonucleic Acid
DRS – DNA Replication Stress
DSB – Double Strand Break
dsDNA – Double Strand DNA
DTT – Dithiothreitol
EDTA - Ethylenediaminetetraacetic Acid
EdU – 5-Ethynyl-2'-Deoxyuridine
GDP – Guanosine diphosphate
GINS – Go-Ichi-Ni-San
GTP – Guanosine triphosphate
HBS – HEPES Buffered Saline
HEPES – (4-(2-hydroxyethyl)-1-piperazineethanesulfonic acid)
HR – Homologous Recombination
IdU – Iododeoxyuridine
IOD – Inter Origin Distance
IPTG – Isopropyl β -D-1-thiogalactopyranoside
ITs – inhibitory S-phase Kinase Threshold
LB – Lysogeny Broth
MAT1 - CDK-activating kinase assembly factor
MCM – Minichromosome Maintenance
MES – 2-(N-morpholino)ethanesulfonic Acid
MPM – Malignant Pleural Mesothelioma
MRN – MRE 11-RAD50-NBS1
MTH2 – MutT homolog2
NCZ – Neocarzinostatin
NHEJ – Non-Homologous End Joining
ORC – Origin Recognition Complex
PAM – Protospacer Adjacent Motif
PARP – Poly-ADP Ribose Polymerase
PBS – Phosphate Buffered Saline
PCNA – Proliferating Chain Nuclear Antigen
PCR – Polymerase Chain Reaction
PIPES - 1,4-Piperazinediethanesulfonic Acid

PMSF – Phenylmethylsulphonyl Fluoride
PRC – Polycomb Repressive Complexes
PreRC – Pre-Replication Complex
PreIC – Pre-Initiation Complex
RB – Retinoblastoma
RNA – Ribonucleic Acid
RPA – Replication Protein A
SCF - Skp, Cullin, F-box Containing Complex
SDS-PAGE – Sodium Dodecyl Sulphate–Polyacrylamide Gel Electrophoresis
siRNA – Small Interfering RNA
SSB – Single Strand Break
ssDNA – Single Strand DNA
SUMO – Small ubiquitin-like modification
TBE – Tris Borate EDTA
TLS – Translesion Synthesis
TBS – Tris Buffered Saline
Ts – S-phase Kinase Threshold
UV – Ultraviolet
Xi – inactive X chromosome
Xist - X-inactive specific transcript
XP – Xeroderma Pigmentosum
YAP – Yes-associated protein
UPS – Ubiquitin Proteasome System
UTP – Uridine Triphosphate

Abstract

Metazoan DNA replication is a finely controlled event. The driving force promoting cell division is increasing kinase levels as cells progress from G1 to Mitosis. Phosphorylation of cell cycle driving targets is driven through motifs surrounding phosphorylation sites in proteins. Dysregulation of these events results in an alteration of the DNA replication programme inducing DNA replication stress. This can result in an erosion of genome stability, driving cancer progression. Mutation in multiple oncogenes has the effect of altering CDK networks, and replication timing.

CIZ1 is a DNA replication factor. It plays a role in co-ordinating the spatiotemporal localisation of Cyclin A and Cyclin E surrounding the G1/S transition. CIZ1's activity is controlled by CDK mediated phosphorylations, when hypo-phosphorylated, CIZ1 promotes nuclear matrix localisation of Cyclin A. Evidence suggests that CIZ1 has both oncogenic and tumour suppressor functions. However, the mechanisms that link CIZ1 to cancer remain unclear. CIZ1 may act as a kinase sensor modifying how cells respond to CDK networks.

Here, to determine the role of CIZ1 in cell cycle progression, and DNA replication two independent CIZ1 KO cell lines were produced. There were no detectable differences in cell cycle profiles using EdU and flow cytometry. However, analysis of cell cycle re-entry kinetics after release from quiescence showed that CIZ1 KO cells bypass restriction point earlier than parental cell lines. In addition, CIZ1 KO cells express cyclin A earlier than parental cell lines, consistent with the earlier timing of restriction point.

Significantly, cell free DNA replication analysis of CIZ1 KO cell lines and parental cell lines revealed CIZ1 KO cells showed a defect in cyclin A chromatin loading that could be reversed by titration of CIZ1. This suggests that CIZ1 aids localisation of cyclin A to chromatin.

Furthermore, CIZ1 KO cell lines require 2-fold higher cyclin A-CDK2 levels to initiate DNA replication in vitro, and this effect is reversed by addition of CIZ1 which reduces this level to

the optimal level for the parental cells. In addition, analysis of the interplay between CIZ1 and cyclin A-CDK2 showed that the threshold CDK activity to promote DNA replication is modulated by the levels of CIZ1.

Analysis of the DNA replication kinetics of CIZ1 KO cell lines by DNA combing identified a DNA replication stress phenotype, characterised by a change in DNA replication dynamics, including a reduced fork rate and increased origin firing. The DRS phenotype was reversed by CIZ1 addback (CIZ1^{AB}). In addition, CIZ1 KO cells showed defects in recovery from DRS inducing agent hydroxyurea and this defect was reversed in CIZ1^{AB} cell lines. Together this data indicates that CIZ1 is involved in regulating cellular responses to CDK activity, that CIZ1 KO induces altered replication timing and replication stress. These observations provide mechanistic insight into the role that CIZ1 plays in tumorigenesis.

Table of Contents	
Declaration	i
Acknowledgements.....	ii
List of Figures.....	iii
List of Abbreviations.....	vii
Abstract	x
Chapter 1. General Introduction.....	1
1.1. Introduction	2
1.2. The DNA replication programme across the Domains of Life.....	3
1.3. The Cell Cycle	8
1.4. Deregulation of the cell cycle underpins tumorigenesis	14
1.5. Replication Licensing and Initiation.....	16
1.6. CIZ1	23
1.7. CIZ1 Interactions with Cyclin CDKs During the G1/S Transition.....	25
1.8. The quantitative model of cell cycle regulation by CDK and the Permissive Kinase Window	28
1.9. DNA Replication Stress	32
1.10. Targeting the Replication Stress Response in Cancer Therapeutics.....	36
1.11. DNA Damage Response	42
Chapter 2. Materials and Methods.....	50
2.1 E. coli.....	51
2.1.1. Bacterial Cell Culture	51
2.1.2. Preparing Competent Cells	51
2.1.3. Bacterial Transformation	52
2.1.4. Inducing Recombinant Protein Expression using IPTG	52
2.1.5. Inducing Recombinant Protein Using Auto induction Media.....	53
2.1.6. Purification of recombinant GST Tagged Proteins.....	54
2.1.7. Quantifying Protein Concentration	55
2.1.8. Purifying Plasmid DNA from <i>E. coli</i>	55
2.1.9 Quantifying DNA Concentration.....	55
2.1.10 Ethanol Precipitation	55
2.1.11. Agarose Gel Electrophoresis	56
2.1.12. Gel Extraction	56
2.1.13. Restriction Digests	56
2.1.14 PCR.....	57
2.2. Protein Extraction and SDS-PAGE.....	57

2.2.1. Casting SDS-PAGE gels	57
2.2.2. SDS-PAGE	57
2.2.3. Staining SDS-PAGE Gels.....	58
2.2.4. Isolation of Protein from 15 cm and 10 cm Cell Culture Plates.....	58
2.2.5. Isolation of Cytosolic and Chromatin Fractions Through CSK Fractionation.....	58
2.2.6. Isolating Whole cell extracts from 6 Well Plates	59
2.3. Western Blotting	59
2.3.1. Transferring Protein to Membranes	59
2.3.2. Probing Membranes	60
2.3.3. Normalising Loads Across Western Blot Samples	60
2.3.4. Antibodies	61
2.4. Mammalian Cell Culture	61
2.4.1. Growing Mammalian Cells	61
2.4.2. Passaging Mammalian Cells	62
2.4.3. Freezing Mammalian Cell Stocks	62
2.4.4. Double Thymidine Arrest of HeLa Cells and S phase Synchrony	62
2.4.5. Quiescence Synchronisation of NIH 3T3 Cells	63
2.4.6. EdU Labelling Fluorescence microscopy	63
2.4.7. Cell cycle analysis with EdU Labelling by Flow Cytometry	64
2.4.8. Mycoplasma Testing	64
2.5. <i>in vitro</i> DNA Replication Assays.....	65
2.5.1. Preparation of replication competent nuclei	65
2.5.2. Preparation of G ₁ Extracts from NIH 3T3 Cells	65
2.5.3. Preparation of S Phase Extracts from HeLa Cells.....	65
2.5.4. Preparation of 10x Premix Solution.....	66
2.5.5. Preparation of Creatine phosphokinase (CPK) Buffer.....	66
2.5.6. <i>In vitro</i> Cell Free DNA Replication Reactions.....	66
2.6 CRISPR/Cas9.....	67
2.6.1. Primer Design	67
2.6.2. Annealing Complimentary Oligonucleotides.....	68
2.6.3. Ligating Double Stranded Oligonucleotides into the GeneArt® CRISPR Nuclease Vector	68
2.6.4. Purifying Plasmid DNA	68
2.6.5. Sequencing GeneArt® CRISPR Nuclease Vector	68
2.6.6. Transfection of NIH3T3 Cells	69
2.6.7. Enrichment of Transfected CRISPR Cas9 Cells.....	69

2.7 DNA Combing	70
2.7.1. Pulse Labelling of Cells	70
2.7.2. Pulse Labelling of Nuclei in cell free DNA replication Assays.....	71
2.7.3. Producing Silanized Coverslips.	71
2.7.4. Purification of DNA	72
2.7.5. DNA Combing	73
2.7.6 Labelling and Imaging	73
2.7.5a. Imaging of Combed DNA	76
2.7.4b Analysis of Replication Tracks	76
2.8. Statistical Analysis	76
Chapter 3. Optimisation of DNA Combing for Cell Based and Cell Free analysis of DNA replication kinetics.....	78
3.1. Introduction	79
3.1.1 Introduction to DNA Combing.....	79
3.1.2. Using DNA Combing to Measure DNA Replication Dynamics	81
3.1.3 Chapter Aims	88
3.2. Optimising DNA Combing for Cell Based Experiments	89
3.2.1 Combing dsDNA from λ phage DNA	89
3.2.2. Optimisation of anti-ssDNA antibodies using Single Stranded λ Phage DNA.....	91
3.2.3. Combing YOYO1 Stained DNA from NIH 3T3	93
3.2.4. Optimisation of Dual Labelling with CldU and IdU in Cell Based Experiments.....	96
3.2.5. Dual labelling of nascent DNA using CldU and IdU.....	98
3.3. Establishing DNA combing of mammalian Cell free DNA replication assays.	100
3.3.1. Validating Replication Competence of G1 Nuclei.....	100
3.3.2. Method Development for Improving DNA Combing of <i>in vitro</i> DNA replication assays.....	102
3.3.3. <i>in vitro</i> labelling methods.....	111
3.3.4. Labelling of Nucleotides of DNA from <i>in vitro</i> Replication Experiments	113
3.4. Chapter Discussion	115
Chapter 4. Cell Cycle Analysis of CIZ1 Null Murine Fibroblasts	120
4.1. Introduction	121
4.1.1 Introduction to CRIPSR Cas9	121
4.1.2. Chapter Aims	123
4.2. Generating CIZ1 Null Cells using CRISPR-Cas9	124
4.3. Characterisation of CIZ1 Null Cells	127
4.3.1. Loss of CIZ1 Does Not Affect the Asynchronous Cell Cycle Profile of NIH 3T3 Cells	127

4.3.2. CIZ1 KO Cells display Altered Cell Cycle Profiles During Cell Cycle Re-entry Post Quiescence.....	129
4.3.3. Analysis of cell cycle exit into quiescence in WT and CIZ1 KO murine fibroblasts	134
4.3.4. Analysis of the timing for Restriction point in WT and CIZ1 null fibroblasts.....	137
4.3.5. Loss of CIZ1 Causes a Moderate Shift in the Restriction Point in Post Quiescence Cells	141
4.3.6. Loss of CIZ1 Results in a Prolonged DDR to Hydroxyurea	142
4.4. Generating and Characterising CIZ1 ^{AB} Cells	145
4.4.1. Ectopic Expression of CIZ1 in CIZ1 KO1 NIH 3T3 Cells.....	145
4.4.2. Asynchronous Cell Cycle Profiles of GFP-CIZ1 Addback Cells.....	147
4.4.3. CIZ1 ^{AB} cells display WT cell cycle re-entry kinetics.	148
4.4.4. Altered 'Restriction Point' of CIZ1 KO cells is rescued by Ectopic Expression of GFP CIZ1.....	152
4.4.5. CIZ1 ^{AB} cells reverse defects in cellular response to Hydroxyurea	153
4.5. Chapter Discussion	156
Chapter 5. CIZ1 defines the CDK activity thresholds for the initiation of DNA replication <i>in vitro</i>	163
5.1. Introduction to <i>in vitro</i> Replication Experiments.....	164
5.1.1. Cell Fusion Experiments.....	164
5.1.2. Identification of Replication Origins and Fork Dynamics <i>in vitro</i>	164
5.1.3. Metazoan Cell Free DNA Replication Assays.....	165
5.1.4. Chapter Aims	169
5.2 Expression of Recombinant CIZ1 and Cyclin A-CDK2 for use in Cell Free DNA Replication Assays.....	169
5.3 Using <i>in vitro</i> Reactions to Investigate Interplay Between CIZ1-N471 and Cyclin A/CDK2	171
5.3.1 Cell Free Analysis of the Initiation Phase of DNA Replication.....	171
5.3.2 <i>In vitro</i> analysis of CIZ1 null fibroblasts during the initiation phase of DNA replication.....	174
5.3.3. CIZ1 is required for efficient Cyclin A chromatin association <i>in vitro</i>	176
5.2.4 Cyclin A/CDK2 promotes initiation of DNA replication in a narrow concentration range.....	178
5.3.5. Recombinant CIZ1 can promote WT like DNA replication initiation kinetics in CIZ1 null nuclei.....	180
5.3.6. CIZ1 Expands the range of concentrations of Cyclin A/CDK2 that promote DNA replication initiation.	182
5.3.7. Recombinant CIZ1 can enhances activity of Cyclin A/CDK2 <i>in vitro</i>	184
5.4. DNA combing of Cell free DNA replication assays <i>in vitro</i>	188

5.4.1. Replication fork velocities are reduced in CIZ1 KO nuclei in cell free DNA replication assays	188
5.4.2. Cyclin A and CDK2 Co-operate to Promote Optimal DNA Replication <i>in vitro</i>	190
5.5. Chapter Discussion	194
5.5.1. CIZ1 Shifting Kinase Thresholds May Induce DRS.....	194
5.5.2. CIZ1 Disruption of Kinase Thresholds may be Linked to its Role in Cancers	198
5.5.3. Analysis of Cell Free DNA Replication Kinetics	200
Chapter 6 Analysis of DNA Replication Kinetics in CIZ1 KO by DNA Combing	204
6.1. Introduction	205
6.1.2 Aims	208
6.2. Results.....	208
6.2.1. Using DNA Combing to Measure Changes in DNA Replication Dynamics.	208
6.2.2. CIZ1 KO Induces a DNA Replication Stress Phenotype	212
6.2.3. CIZ1 ^{AB} reverses the DNA replication stress phenotype observed in CIZ1 KO Cells.	213
6.2.4. CIZ1 KO Results in Increased Origin Activation, consistent with DRS.	215
6.2.5. Evaluation of the role of CIZ1 in cellular responses to increased DRS.	219
6.2.6 CIZ1 KO cell lines show defective origin activation 24 Hours after HU Treatment.	223
6.3. Chapter Discussion	226
6.3.1. CIZ1 Null cells undergo DRS and have increased sensitivity to DRS inducing agents	226
6.3.2 A potential model for the role of DRS in tumourigenesis in CIZ1 KO mice	227
Chapter 7. General Discussion	230
7.1. Summary of Results.....	231
7.2. Loss of CIZ1 Alters the kinetics of cell cycle re-entry from Quiescence	232
7.3. Loss of CIZ1 Alters Replication Dynamics which Could Result in Genome Instability .	234
7.4. Loss of CIZ1 Promotes an altered DDR	236
7.5. The Quantitative Model: CIZ1 as a Kinase Sensor at G1/S Phase Transition	238
7.6. CIZ1's Links to Tumorigenesis	239
7.7. Phenotypes Observed upon Loss of CIZ1 Consistently have Links to Epigenetics	242
7.8. Future Work	243
7.9. Concluding remarks.....	245

Chapter 1.

General Introduction

1.1. Introduction

Cancers result from a deregulation of the pathways that control the cell cycle. Arguably, the major pathways involved in this are the Cyclin/Cyclin dependent kinase (CDK) networks. As cells progress through the cell division cycle each stage is governed by phosphorylation from CDKs (Stern & Nurse, 1996; Uhlmann et al., 2011). Dysregulation of CDK networks results in aberrant DNA replication, mitotic defects, DNA damage, and increased mutation rate. These pathways, or regulators of these pathways, are frequently mutated early in cancers providing the growth advantage that allows tumorigenesis (Mol et al., 2013). This is followed by a prolonged erosion of cell cycle control, promoting genome instability as further mutations are acquired that underpin the development of cancer.

A major barrier to cancer occurs at the G1/S phase transition, the point where cells commit to the cell cycle, and begin replicating their DNA. This is governed through phosphorylation of key replication licensing proteins by CDKs, further into the cell cycle further phosphorylation of these same proteins by CDKs promote their inhibition preventing re-replication of the genome, ensuring that the cell cycle is unidirectional (Pauzaite et al., 2017). This process is also accompanied by a switch between the primary Cyclin activating CDK2, from Cyclin E to Cyclin A. Cyclin A has roles in regulating both DNA replication, and mitosis (Hégarat et al., 2020). This switch is thought to be governed by a localisation change promoted by nuclear matrix anchoring protein Cip1 interacting zinc finger protein 1 (CIZ1) (Copeland et al., 2015).

There is increasing evidence that CIZ1 can perform oncogenic like functions. CIZ1 is frequently overexpressed or alternatively spliced in numerous common cancers, including lung, bladder, and prostate cancers (Higgins et al., 2012; Liu et al., 2015; Chen et al., 2019). Loss of CIZ1 has also been shown *in vitro* to possess a tumour suppressor function, increasing tumorigenesis, and promoting lymphoproliferative disorders in mice (Nishibe et al., 2013;

Ridings-Figueroa et al., 2017). This dual, yet contrasting, phenotype is one shared by other proteins, notably, p21 a CDK inhibitor, and interacting partner of CIZ1 (Mitsui et al., 1999; Abbas & Dutta, 2009; Ohkoshi et al., 2016; Georgakillas et al., 2017). The exact function of CIZ1 is unclear, although it is clear that CIZ1 functions around the G1/S phase checkpoint and can promote the activation of a number of pathways that contribute to cell cycle progression: CDK signalling, and YAP signalling. (Coverley et al., 2005; Copeland et al., 2010, Copeland et al., 2015; Lei et al., 2016). Additionally, CIZ1 may play a role in DNA damage responses (DDR), as CIZ1 ablation results in increased sensitivity to DNA damage and over-expression of CIZ1 is associated with tumorigenesis (Coverley et al., 2005; Higgins et al., 2012; Nishibe et al., 2013; Lei et al., 2015; Wang et al., 2018). The focus of this project is to understand the role that CIZ1 plays in DNA replication initiation process, and how it contributes to DNA replication stress.

This chapter will introduce the main concepts crucial to this report: Cyclin/CDK signalling, CIZ1 biology, DNA Replication Stress, tumorigenesis, the DNA damage response, and the quantitative model of cell cycle progression. These will provide the basis for understanding the results that will follow. Results in this thesis demonstrate that loss of CIZ1 induces changes to cell cycle re-entry timing, altered responses to CDK signalling *in vitro*, an aberrant DNA damage response to replication stress, and a change in DNA replication dynamics consistent with DNA replication stress. Together these phenotypes link CIZ1 with cell cycle regulation, critically during the G1/S transition. These results have implication for mechanisms that underpin the link between CIZ1 and tumorigenesis.

1.2. The DNA replication programme across the Domains of Life

Licensing of replication origins by replication factors has to occur at thousands of putative origins across the metazoan genome. The DNA replication programme describes the organisation of DNA replication initiation, elongation, and termination that is required for

accurate, timely, replication of a genome (Ganier et al., 2019). The replication programme varies widely across the domains of life, with evolution needing to solve different problems as genome size increased, chromosomes became separated, and the need to respond to replication challenges became more important for the survival of a species, or individual. This section will summarise the adaptations that occurred throughout the evolution of the three domains of life (Table 1.1).

Each kingdom has specific mechanisms to ensure the timely and accurate copying of DNA. Different organisms have different problems that need to be solved when replicating DNA. Proteobacteria, such as *E. coli*, have small genomes encoded on a circular chromosome of 4.6 Mbp. This is orders of magnitude smaller than those of higher eukaryotes. The *E. coli* replication origin (OriC) lies proximal to genes encoding DNA replication proteins, such as DnaA and DnaN, the bacterial orthologues of the origin recognition complex (ORC) and proliferating cell nuclear antigen (PCNA) respectively (Section 1.5) (Mackiewicz et al., 2004). Small circular chromosomes enable timely and efficient duplication that facilitates a doubling time of approximately 20 minutes (Gibson et al., 2018).

It is worth noting that other species of bacteria, although a minority, utilize multiple replication origins during DNA synthesis (Gao et al., 2015). Bacterial origins are sequence dependent, DnaA binds at conserved 9-mer repeats (TT^A/T^TTNCACA) (Speck & Messer, 2001). DNA melting occurs at adjacent AT rich sequences. The minimum sequence for OriC recognition has been determined to be 163 bp, although this does display deficiencies in initiating multiple simultaneous rounds of replication per cell division (Stepankiw et al., 2009). After initiation, DNA replication occurs rapidly (relative to eukaryotes) with replication forks traveling bidirectionally at velocity of 60 kb/min (Mechali, 2010). This rapid speed is required to ensure duplication of the 4.6 Mbp within the 20-minute cell division cycle (Gibson et al., 2018).

In evolutionary history, Archaea branched from eukaryotes more recently than bacteria. At first appearances, archaeal genomes resemble closely those of Bacteria: DNA is arranged on a single, circular gene rich chromosome. Counter-intuitively, Archaea DNA replication proteins appear more similar to eukaryotes. Many replication proteins sequence shares more homology with eukaryotes than Bacteria, including ORC, the DNA polymerases and PCNA (Edgell & Doolittle, 1997; Robinson & Bell, 2005; Wu et al., 2014). Computational analysis of numerous archaeal genomes identified OriC like regions in some, but not all of test archaea species (Lopez et al., 2002). As in bacteria, these origins were located closely within the genome to the genes of replication proteins including CDC6 (Luo & Gao, 2019). However, multiple species, such as *Sulfolobus acidocaldarius*, and *Sulfolobus solfataricus*, have been identified which contain multiple putative origins. Furthermore, deletion of origins in certain strains does not prevent replication initiation, indicating that in some species a conserved origin sequence is not required. Following initiation from a single, multiple or, a non-canonical origin of replication in archaea proceeds at an intermediate rate between Bacteria, and Eukaryota, at approximately 20 kbp/min. This is slower than Bacteria yet remains an order of magnitude more rapid than eukaryotes (Kelman & Kelman, 2018).

Eukaryotes use conserved mechanisms for origin specification, loading and activation of the DNA replication machinery. Eukaryotes differ from their prokaryotic counterparts through the use of multiple linear chromosomes. Typically, the chromosomes are much larger and less gene dense in eukaryotes than archaea or prokaryotes, and eukaryote genome length varies widely (Coelho et al., 2013). Fungal species range from 9 Mbp in the methylotrophic yeast *Hansenula polymorpha* to 180 Mbp in the ectomycorrhizal fungus: *Cenococcum geophilum*. Typically, genome size is roughly 40 Mbp (Mohanta & Bae, 2015) that compares to gigabase genomes of higher Eukaryotes. The increased genome size, and the presence of multiple linear chromosomes requires multiple replication origins to facilitate efficient and timely duplication of the genome. The DNA replication process begins with the specification

of putative DNA replication origins. In Fungi this process is facilitated by specific DNA sequences called autonomously replicating sequences (ARS), that are conserved AT rich regions (Dhar et al., 2012).

The yeast *Saccharomyces cerevisiae*, like *E. coli* replicates its DNA in half an hour, it has a 12 Mbp genome (3-fold higher than *E. coli*), this genome is organised into 16 discrete chromosomes (Engel et al., 2014). *S. cerevisiae* genomes contain an estimated 520 ARSs. The ARS of *S. cerevisiae* include sites adjacent to genes encoding replication proteins including members of the minichromosome maintenance (MCM) 2-7 complex (Wang & Gao, 2019). Deep sequencing of *S. cerevisiae* revealed that DNA replication origins are activated at different times during S phase, some early, some mid and some late suggesting a temporally controlled DNA replication program (Muller et al., 2014). In addition, there are preferred replication origins and cryptic replication origins that are activated under times of replication stress to complete duplication of the genome before cell division (Santocanale et al., 1999; Brambati et al., 2018). This flexibility in origin usage is characteristic of eukaryotic replication programmes. The *S. cerevisiae* replication forks proceed at a median rate between 1.5 - 2.5 kbp/min (Rivin & Fangman, 1980; Yousefi & Rowicki, 2019). This rate is far below that observed in prokaryotes, when compounded with multiple chromosomes, and a larger genome this explains the need for multiple simultaneously replication origins to ensure DNA replication is completed within half an hour.

Unsurprisingly, the DNA replication programme in Animalia is increasingly complicated. Animalia replication origins are not sequence specific, and initially, it was thought that DNA replication origins occurred at random, yet transcriptionally inactive sequences within the genome. ORC bind DNA in a manner more dependent on the structure of the supercoiled DNA than the sequence itself, driven more by epigenetics than genetic sequence (Hyrien et al., 2015).

The *Homo sapien* genome is approximately 3 Gbp, orders of magnitude longer than either fungi or prokaryota encoded in 23 pairs of chromosomes that are less gene rich than bacteria or fungi (Piovesan et al., 2019). Due to the lack of sequence specificity the number of replication origins in the human genome is unknown, it is thought to be between 7000, and 10000 (Prioleau & MacAlpine, 2016). Analogous to the replication programme in yeast, DNA replication origin usage changes during S phase. This results in distinct temporally regulated activation of early, mid and late S phase replication origins. Similarly, there are dormant origins that are fired in response to replication challenge. The replication fork speed is between 1 – 3 kbp/min (Mechali, 2010). Challenges to the replication programmed can result in uncompleted replication, re-replication, or increased mutation frequency. All these properties can lead to tumorigenesis or cell death highlighting the importance of a correctly regulated DNA replication programme.

Type of Cell	Genome Size	DNA Organisation	Number of Origins	Replication Fork Velocity (kbp/min)
Bacteria	4.6 Mbp	1 Circular Chromosome	1	60
Archaea	Variable	1+ Circular Chromosome	1 +	20
Yeast	12 Mbp	16 Linear Chromosomes	520	1.5-2.5
Human	3 Gbp	23 Linear Chromosome Pairs	7000-10000	1-3

Table 1.1- Comparison of genome sizes, DNA replication fork rates and genome architecture across the domains of life.

1.3. The Cell Cycle

The cell cycle is the co-ordinated series of events that occur during cellular division. During this process, the genome of the cell must be duplicated, precisely and accurately (Section 1.2), and the cell must divide into two, with each daughter cell receiving one copy of the duplicated genome. The means by which cells achieve these two goals has diverged and varies significantly across the domains of life in terms of timing, regulation, and mechanism. This process is achieved by binary fission in bacteria. Eukaryotes utilise the mitotic spindle to orientate and segregate the genome equally into daughter cells that completes the more complex mitotic cell cycle of higher eukaryotes.

The simplest form of the cell cycle is found in bacteria such as *Escherichia coli* (*E. coli*) which can rapidly duplicate their cells, with a doubling time of 20 minutes in optimal conditions (Fossum et al., 2007). Briefly, *E. coli* replicate their ~4,600,000 base pair circular genome bi-directionally from a single origin of replication known as *OriC* (Blattner et al., 1997). *E. coli* cells elongate and partition into two identical daughter cells (Figure 1.1a). Interestingly, insertion of an additional *OriC* into the *E. coli* chromosome produces cells that replicate as normal and displayed no abnormal growth characteristics showing the capability of even basic life forms to select origins (Wang et al., 2011).

In optimal conditions, *E. coli* can initiate two rounds of DNA replication from already replicated *OriC* to increase the rate of cellular division (Figure 1.1b). After duplication of the genome, each daughter cell receives a copy of the *E. coli* genome during rolling circle replication allowing *E. coli* to double their cell number in 20 minutes, compared to 40 minutes if the chromosome was replicated from a single origin (Wawrzyniak et al., 2017).

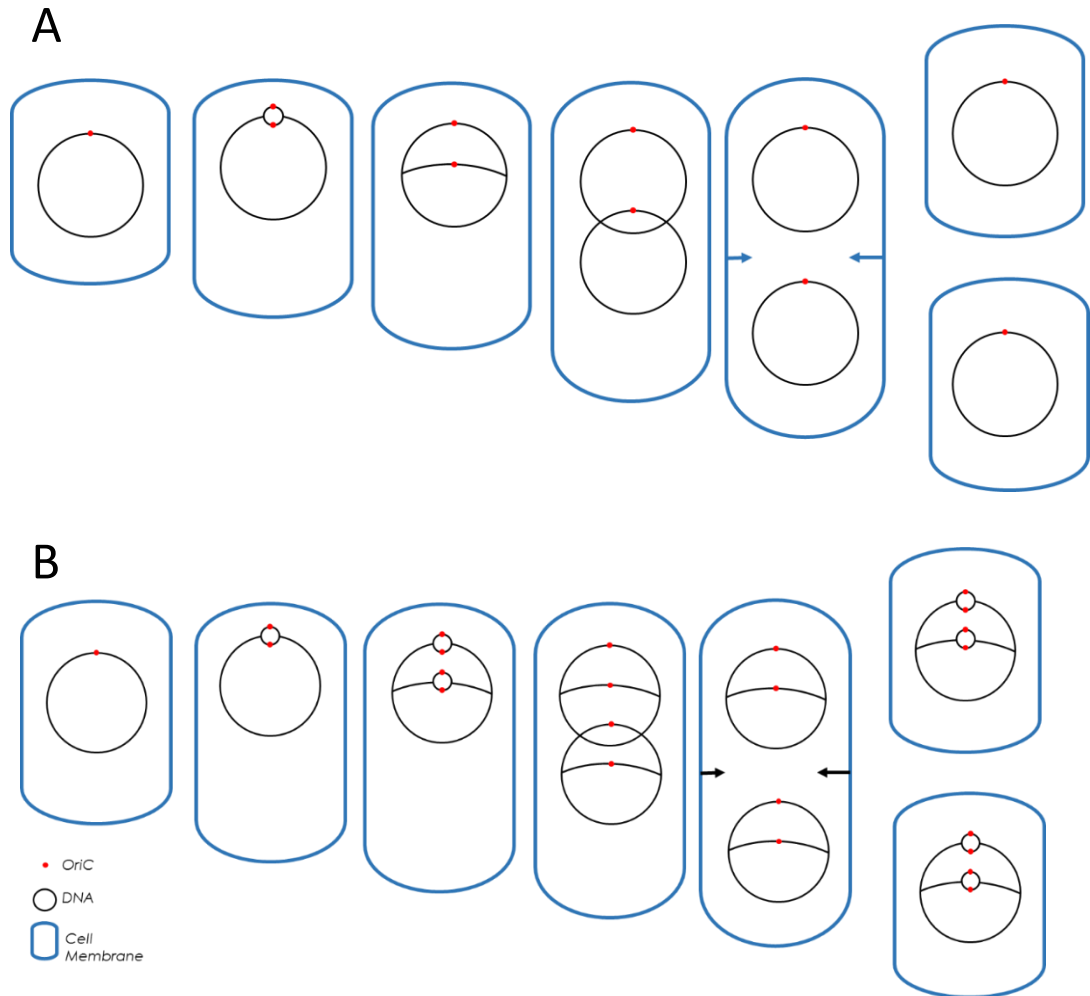


Figure 1.1-E. coli Replication A) Schematic for the replication of *E. coli*, one of the simplest cell cycles found across the domains of life. Replication proceeds from a single origin of replication *OriC*. The entire chromosome is then replicated from this point. After replication sister chromosomes are separated by decatenation. B) A schematic showing how *E. coli* can initiate two rounds of DNA replication during a cell division to maximise growth time. A feature not found in eukaryotic cells. This is known as rolling circle replication and shows bacteria can utilize multiple replication origins under specific conditions. See this paper for latest details (Japaridze et al., 2020).

With mammalian cells the control, timing and maintenance of cellular duplication is more complex. There are a logistical challenges mammalian cells must overcome for successful genome duplication. The large human genome (~3.5 Gbps), would take over 18 days for complete duplication if DNA replication initiated from a single origin analogous to *E. coli* (Kapusta et al., 2017), this is also impossible as human DNA is separated into 23 chromosome pairs. Yet, in human fibroblast cells, DNA replication can be completed in

between 6 – 8 hours (Griffiths, 1984). Precise and accurate duplication is achieved through separation of the two major events of cellular duplication: DNA replication, which occurs in S phase, and Cellular division, which occurs in M phase. These events are separated by two gap phases (G1 and G2) where cells prepare for these events, and if needed arrest the cell cycle (Figure 1.2).

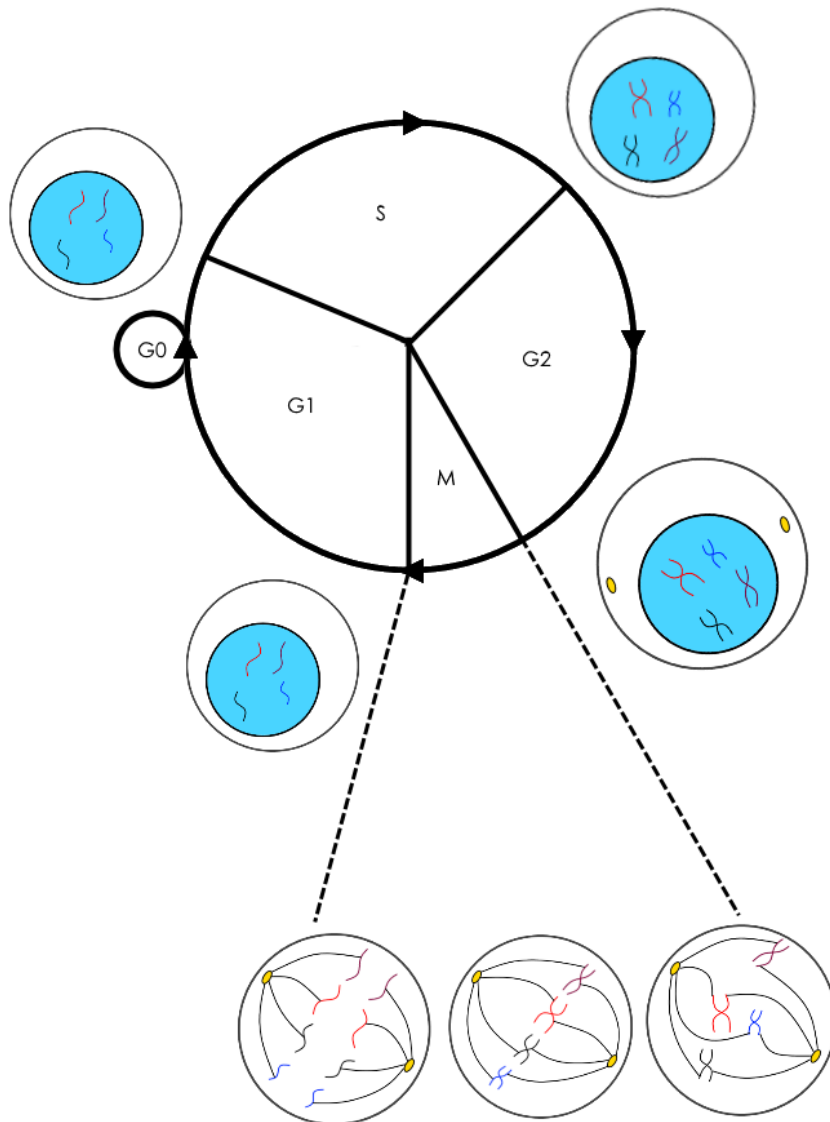


Figure 1.2-The metazoan cell cycle A schematic for the eukaryotic mitotic cell cycle. Displaying the 4 key cell cycle stages and the unidirectional progression. DNA replication occurs in S phase, and mitosis and cytokinesis occur in M phase. These 2 events are separated by the 2 gap phases G1 and G2.

In G1, phase cells commit to entering the cell cycle and completing duplication after stimulation by extracellular signals. Key events include replication origin licensing, the multistep process of loading of replication factors that results in recruitment and activation of the DNA helicase and polymerase proteins (Fragkos et al., 2015), and Rb phosphorylation a process which activates a positive feedback loop resulting in the commitment to S phase (Nishitani & Lygerou, 2002; Narasimha et al., 2014).

In mammalian S phase, the timing of replication origin firing is essential for cellular function. In early S phase, the euchromatin is preferentially replicated, with replication origin activation showing a positive correlation with actively transcribed genes in early S-phase (Sequeira-Mendes et al., 2009). Euchromatin is less tightly packed than heterochromatin making it more accessible to the replication machinery. Conversely, in late S phase DNA replication occurs at heterochromatic sites within the nucleus and areas close to the nuclear lamina (Rhind & Gilbert, 2013). The ends of chromosomes, the telomeres are replicated throughout S phase with different replication times being associated with different localizations after replication (Arnoult et al., 2010).

In G2, cells ensure that DNA replication is completed accurately, enabling an increase in CDK activity leading to initiation of the assembly of the mitotic spindle and provide a checkpoint to prevent damaged cells entering mitosis (Kousholt et al., 2012). In M phase cells divide and segregate their genome equally between 2 daughter cells. Errors in mitosis can result in chromosomal translocations and uneven partitioning of chromosome leading to aneuploidy, a common feature in cancer, mitotic defects also contribute to tumour resistance to immunotherapy (Lengauer, 1998; Levine & Holland, 2018).

Unidirectional progression through the eukaryotic cell cycle is driven by the activity of cyclin dependent kinases (CDKs). CDKs are kinase proteins with remarkable target promiscuity. They are expressed at high levels throughout the cell cycle (Arooz et al., 2000) and their

activation is tightly controlled. CDK activity requires dimerization with partner proteins, known as cyclins, and an activating phosphorylation catalysed by the CDK activating kinase (CAK), a ternary complex composed of cyclin H, MAT1, and CDK7 (Lolli & Johnson, 2005). There are approximately 20 cyclin and CDK proteins identified that have a diverse range of functions including regulation of RNA splicing to spermatogenesis (Peyressatre et al., 2015). The best characterised Cyclins and CDKs have roles in cell cycle progression (Table 1.2).

CDK	Cyclin	Cell Cycle Role
CDK1	Cyclin A Cyclin B	G2 Mitosis
CDK2	Cyclin A Cyclin E	Late G1 + S Phase Late G1
CDK4 CDK6	Cyclin D	Early G1

Table 1.2- The major CDKs, cyclin binding partners, and their role in cell cycle control. Adapted from Peyressatre et al. (2015).

Briefly, as a cell re-enters the cell cycle after exit from mitosis commitment to the cell cycle requires activity of growth factors. These mitogens promote the transcription of cyclin D the activity of which commits cells to the cell cycle through phosphorylation of the retinoblastoma protein (pRB) (Albrecht & Hansen, 1999; Moser et al., 2018). The phosphorylation of pRB promotes the transcription of cyclin E, cyclin A, and many other proteins through activation of the E2F transcription pathway (Müller & Helin, 2000; Thwaites et al., 2019). Cyclin D degradation is required prior to S phase as its activity blocks the activity of processivity factor PCNA and CDK2 (Fukami-Kobayashi & Mitsui, 1999; Qie & Diehl, 2020). Cyclin E/CDK2 promotes S phase entry, a notable event being phosphorylation events that trigger the unwinding of DNA through loading of the CMG complex allowing recruitment of the replicative polymerases (Li et al., 2011; Pauzaite et al., 2017). Cyclin A/CDK2 is active through S phase, promoting continuation. It is noteworthy that nuclei isolated from post-

quiescent mouse fibroblast cells can be initiated to replicate by cyclin A/CDK2 yet cyclin E/CDK2 requires further replication factors suggesting a role for cyclin A/CDK2 in DNA replication initiation (Coverley et al., 2002).

This appears to contrast with analyses of cyclin function in cell-based systems, knockout of both isoforms of Cyclin E: Cyclin E1 & Cyclin E2 are embryonically lethal. However individual knockouts are not cell cycle deficient due to redundancies between targets (Caldon & Musgrove, 2010). Cyclin E1/E2 null cells can be generated by growing embryos with WT placentas, Cyclin E null cells generated in this manner displayed reduce ability to re-enter the cell cycle following quiescence, through disturbed MCM helicase loading onto DNA, this behaviour appears independently of CDK2 activity (Geng et al., 2007). Cyclin A2 ablation allows normal cell cycle progression in mouse fibroblast cells due to compensation by increased Cyclin E activity, concurrent loss of Cyclin A2 and CDK2 however does suppress tumorigenesis and cell proliferation (Kalaszczynska et al., 2009; Gopinathan et al., 2014).

In G2 phase, Cyclin A is paired with CDK1 before being exchanged for cyclin B, which quickly promotes its own nuclear import triggering mitosis, there is a level of redundancy between CDK1, and CDK2, ablation of CDK2 results in a compensatory increase in CDK1 levels to allow cell cycle progression (Gavet & Pines, 2010; Gopinathan et al., 2015). The last act of the cyclin B-CDK1 complex is the activation of the anaphase promoting complex (APC/C^{Cdh1}).

APC/C^{Cdh1} mediates the metaphase to anaphase transition by proteasome mediated destruction of cohesin, resolution of the centromeres and separation of the sister chromatids. Finally, APC/C^{Cdh1} results in the destruction of cyclin B by ubiquitylation, reducing CDK activity to a low level enabling PP2A to reset the CDK phosphoproteome to a basal level as cells enter G1 phase of the cell cycle after mitotic exit (Sivakumar & Gorbsky, 2015). Deregulation of these regulatory mechanisms results in tumorigenesis.

1.4. Deregulation of the cell cycle underpins tumorigenesis

Deregulation of the cell cycle leads to the uncontrolled proliferation of cells known as cancer. Cancer is a significant healthcare problem in the developed world. Public health efforts in the developing world over the last century have seen an increase in antiseptic techniques, advances in surgery, the development of antibiotics, and increased food and water hygiene has increased the life expectancy. In the UK, life expectancy for a person born between 1910 – 1912 was 55 years for females and 52 years for males. 100 years later, this has risen to 83 years for females and 79 years for males (Office of National Statistics, 2015). With increased life expectancy, and increased surveillance, there is increased time to develop mutations that underpin, transformation and acquisition of additional characteristics associated with over-proliferation and cell survival leading to cancer. Due to increased longevity, current estimates suggest that in the UK over half of people born after 1960 will be diagnosed with cancer during their lifespan (Ahmad et al., 2015). Fortunately, research into cancer causes and treatments have caused a decrease in mortality from cancer, dropping over a fifth between 1971 and 2012 (Oke et al., 2015).

Cancer is a genetic disease, primarily caused through mutation of genes arising through environmental stress. A number of genes are involved in cancer development that are characterised by their activity. For example, mutations in genes that increases their activity are known as oncogenes. This increase in activity tends to increase cellular growth and can be mediated by duplication of the gene, mutation of the promoter, point mutations causing increased activity (Vogelstein et al., 2013). This contrasts with tumour suppressor proteins that prevent untimely cellular division. Mutations in tumour suppressors, or changes to their transcription regulation, lead to a loss of function and loss of their activity promote tumorigenesis (Payne & Kemp, 2005; Botezatu et al., 2019). Tumour suppressors are often involved in halting the cell cycle following DNA damage or cellular stress and include the classic example of a tumour suppressor gene is p53 a master regulator of the cell cycle (Yan

et al., 2011; Marcel et al., 2015). Examples of both these types of genes, and their functions will be discussed in the following sections.

Knowledge of common hereditary mutations that increase cancer incidence allows the opportunity for screening, and early intervention. The most well categorised mutations of this class are tumour suppressors BRCA1 and BRCA2. Without intervention women carrying hereditary loss of function BRCA1 mutations have a 70 % risk of contracting breast cancer (Semmler et al., 2019). Both BRCA1 and BRCA2 play roles in regulating homologous recombination to repair DNA in response to DSBs. Identification of genes that pre-dispose people to cancer allows for the development of targeted therapeutics. Poly ADP ribose polymerase (PARP) inhibition has been effective in treatment BRCA1 and BRCA2 mutated tumours (Frampton, 2015).

There are multiple types of mutations that result in oncogene activation. These include point mutations, or insertions/deletions within the coding sequence to the gene. These will typically result in a hyperactive or hyper stable version of the gene product. An example of this is RAS, a family of membrane coupled G-proteins that transduce signals from tyrosine kinases that promote cell division. Multiple mutations in RAS found in cancers block the hydrolysis of GTP-GDP 'locking' RAS proteins in a permanently activated state; this reduces cells dependences on growth signals, and promotes cell proliferation (Miller & Miller, 2012).

Another class of mutations that cause oncogene activation are mutations within the promotor region of the oncogene; typically, these will increase transcription of the oncogene, increasing protein levels. An example of this is the gene TERT in malignant pleural mesothelioma (MPM). MPM is the cancerous condition commonly associated with the inhalation of asbestos; MPM has very low survival rates. TERT is a component of telomerase, the enzyme that 'caps' DNA, cancer cells due to increased division rely on this to prevent

loss of telomeres and achieve replicative immortality. Mutations in the promoter that increase TERT mRNA levels have been identified in MLM cells (Tallet et al., 2014).

The third common class of mutation that causes oncogene activations is chromosomal rearrangements. This can include moving genes to areas in the genome with greater transcription levels, or fusion of multiple genes resulting in increased oncogenic activation. Examples of this include the BCR-ABL. This is a fusion of chromosome 9 and 22 fusing the genes BCR and ABL. BCR-ABL fusions are commonly found within common myeloid leukaemia cells. The BCR-ABL gene product results in increased cell signalling, promoting cell proliferation and suppressing apoptosis. (Quintas-Cardama & Cortes, 2009). Identification of mutations that promote cancer such as BCR-ABL allow development of targeted therapies (Rossari et al., 2018).

1.5. Replication Licensing and Initiation

The accurate and timely duplication of DNA in mammalian cells requires strict regulation. Perturbation of this system results in untimely inaccurate replication, resulting in activation of cell cycle checkpoints or an increase in DNA mutation rate. Increases in mutation rate can accelerate the progression of tumorigenesis. Multiple redundant regulatory and checkpoint pathways exist to safeguard the genome during DNA replication. Before S phase can begin, origins of replication must be selected and prepared for replication initiation. This process is termed replication licensing. Replication licensing results in the recruitment of proteins to putative origins known as pre-replication complexes (PreRCs).

Firstly, during the conclusion of mitosis, the origin recognition complex (ORC) forms a ring around DNA and marks putative origin sites. This complex is composed of subunits ORC1-6 and facilitates recruitment of two further proteins, CDC6 and Chromatin licensing and DNA replication factor 1 (CDT1). CDC6 is a AAA+ ATPase, ATP hydrolysis by CDC6 results in the recruitment and loading of two identical heterohexameric complexes. These complexes are each formed of six subunits, MCM2-7. These MCM2-7 complexes, upon replication initiation, function as the catalytic core of the DNA helicase. One ring is provided to one of the replisomes for each origin (Blichert et al., 2017) (Figure 1.3).

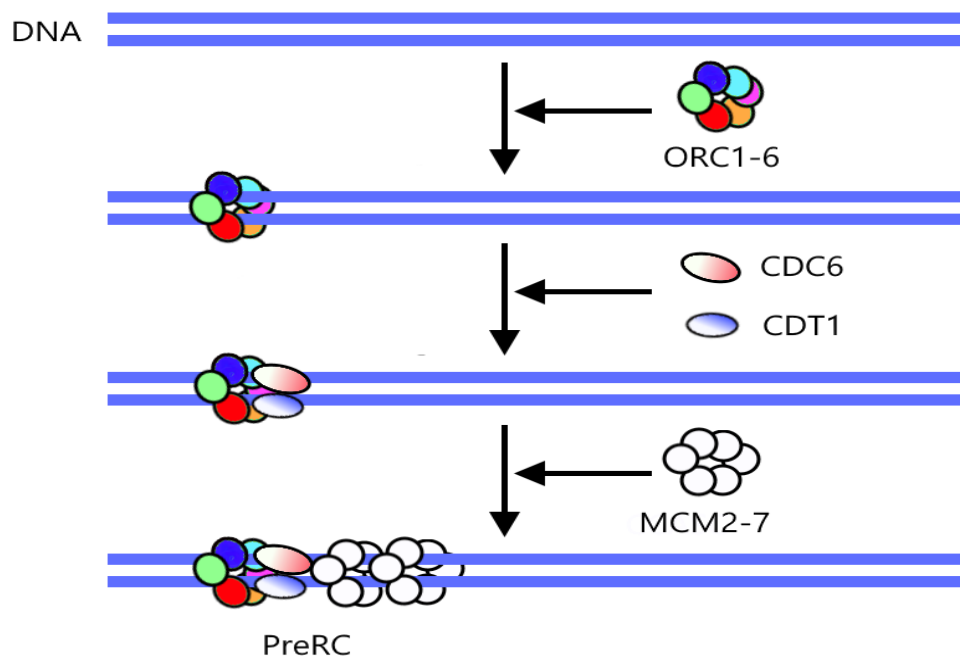


Figure 1.3 - DNA Replication Licensing During M and G1 phase replication origins are licensed. Origins are bound by the origin recognition complex (ORC1-6) in a DNA structure dependent manner. CDC6 and CDT1 are recruited to the ORC at putative origins. CDT1 and CDC6 promote recruitment of the MCM2-7 heterohexamer. Two MCM2-7 heterohexamers are recruited per origin. The ORC, CDC6, CDT1, MCM2-7 complex is known as a Pre-replication complex. More origins are licensed on the genome than are used during S phase.

Replication licensing is controlled through multiple levels of regulation. ORC1, ORC 6 and ORC2-5 are recruited to the nucleus through independent mechanisms mediated by chaperone proteins and CDK phosphorylation (Ghosh et al., 2011). The ORC is recruited to origins through conserved (in eukaryotes) basic residues in ORC1, binding requires ATP

binding of the AAA+ ATPase ORC1 (Kawakami et al., 2015). ORC binding requires subunits 1-5, whilst ORC 6 is required for efficient S phase entry. In yeast, depletion of ORC 6 in G1 resulted in loss of MCM2 chromatin association, reduced origin firing rates, and impaired S phase progression (Semple et al., 2006). Expression of ORC subunits is not cell cycle stage specific, as it is not the limiting step for replication initiation (Thome et al., 2000).

Deregulation of ORC activity and expression has not been found to be associated with cancer.

Conversely, CDC6 levels are tightly linked to cell cycle stage. CDC6 is degraded on the onset of S phase and accumulates at the beginning of the cell cycle. CDC6 expression is E2F regulated, requiring external growth signals to stimulate expression. CDC6 is essential for DNA replication, removal of CDC6 in tumour cells blocks initiation of DNA replication and impairs tumour growth. (Yan et al., 1998; Chen et al., 2016). Degradation of CDC6 is mediated by the activity of CDK2, phosphorylation of the N terminus of CDC6 by CDK2 and CDK1 promotes SCF mediated ubiquitination and degradation (Drury et al., 1997; Al Zain et al., 2015). The accumulation of CDC6 in G1 and degradation during S phase helps ensure that DNA replication is initiated only once per cell cycle. CDC6 expression is increased in breast cancers, and higher expression trends with lower survival rates (Mahaevappa et al., 2017).

CDT1 is regulated through numerous pathways. CDT1 expression is E2F mediated. CDT1 is inhibited by re-replication inhibiting protein geminin. Geminin blocks CDT1 binding both CDC6, and interacting with the MCM heterohexamer (Kushwaha et al., 2016). Geminin levels drop after mitosis, geminin is degraded by the APC/C ubiquitin ligase, geminin levels rise again during S phase as the APC/C is deactivated (Rizzardi & Cook, 2012). This allows CDT1 activity to be highest during replication licensing. Similarly, to CDC6, CDT1 levels are found higher in breast cancers, and higher expression trends with lower survival rates (Mahadevappa et al., 2017).

MCM2-7 act as the replicative helicase an essential role for replication. Loading of MCM2-7 at dormant origins is used for completing replication when cells are under replication stress (Ge et al., 2007). Loading of MCM2-7 onto chromatin is largely controlled by CDT1, itself controlled by the Ubiquitin Proteasome System (UPS) and geminin. Activation of MCM2-7 requires binding of MCM10, GINS, CDC45 (CMG), and phosphorylation by CDK2 and DDK. DNA is unwound upon CMG activation, double stranded DNA enters the hexameric ring at N-terminal zinc finger regions, the strand that is to become the leading strand is pulled down through the heterohexameric ring exiting through a C-terminal motor ring. An 'exit groove' formed by zinc finger regions in MCM3 and MCM5 provides a channel which the strand of DNA to become the lagging strand traverses (Yuan et al., 2020). After S Phase, MCM2-7 is inhibited by phosphorylation to prevent re-replication of DNA, phosphorylation of MCM4 by Cyclin A/CDK2 reduced the DNA binding of MCM2-7 (Moritani & Ishimi, 2013).

The phosphorylation of MCM2-7 complex is mediated by CDK2, CDK1, Cdc7 (the kinase component of DDK), ATM and ATR (Fei & Xu, 2018). Phosphorylation from CDK2 has two broad functions, to promote PreIC assembly, and to inhibit re-replication. CDK2 mediated phosphorylation of MCM3 at T772 promotes chromatin loading (Yeeles et al., 2015). Contrastingly, phosphorylation of MCM4 across numerous phosphorylation sites reduces chromatin association of the MCM2-7 complex (Tudzarova et al., 2016). The discrete roles of CDK signalling to enforce cell cycle unidirectionality. Phosphorylation of MCM subunits also play an important role in checkpoint activation and cell cycle arrest. ATR and ATM phosphorylates sites on MCM2 and MCM3 in response to stressed replication, inhibiting replication (Fei & Xu, 2018). CDK1 phosphorylation of MCM4 inhibits replication, preventing re-replication of DNA. CDC45 phosphorylation have a number of activities including promoting chromatin association and promoting binding of CDC45 to MCM2-7 (Li et al., 2011).

Licensed origins do not automatically initiate DNA replication. The activity of CDK and DDK are required for the recruitment of factors that are required to activate the replicative helicase complexes are required (Mailand & Diffley, 2005; Sheu & Stillman 2016; Rossbach & Sclafani, 2016). Site-specific phosphorylation on MCM subunits by CDK2 and DDK causes the recruitment of three proteins essential for replication initiation: MCM10, CDC45 and GINS. GINS is a multiunit protein complex formed of four subunits: Psf1, Psf2, Psf3 and Sld5. Together, MCM2-7, GINS and CDC45 form the CMG complex that forms the replicative helicase in mammalian cells, with MCM2-7 acting as the catalytic core (Li & O'Donnell, 2018). GINS also activates the polymerase activity of the RNA primase DNA polymerase α (DNA pol α), the polymerase responsible for synthesising short RNA primers that enable processive DNA synthesis by DNA pol δ and DNA pol ϵ in the replisome complex (De Falco et al., 2007; Zhou et al., 2018). The DNA polymerases are anchored on to DNA through the trimeric ring protein proliferating chain nuclear antigen (PCNA). This prevents dissociation of polymerases increasing processivity, as well as providing a binding site for cell cycle regulators, and regulating signals (Boehm et al., 2016). Replication continues bi-directionally from the replication origin through both leading and lagging strand synthesis (Figure 1.4).

Cyclin E/CDK2 and DDK phosphorylation along with the activity of the Sld3-Dpb11-Sld2 complex promotes the recruitment and activation of the CDC45, GINS, MCM2-7 (CMG) complex that serves as the eukaryotic replicative DNA helicase (Boos et al., 2011). Following unwinding of DNA, the replicative machinery is loaded onto the replication bubble to copy the DNA template bidirectionally. The replisome includes PCNA, a processivity factor analogous to the bacterial sliding clamp protein; DNA polymerase α that produces the RNA primers require to initiate DNA synthesis; DNA polymerase ϵ , which elongates the leading strand, and DNA polymerase δ , which elongates the lagging strand (Miyabi et al., 2011; Muzi-Falconi et al., 2003). Although it has been proposed that DNA polymerase δ often catalyses

The initial DNA on the leading strand but becomes replaced by DNA polymerase ϵ (Daigaku et al., 2015) (Figure 1.4).

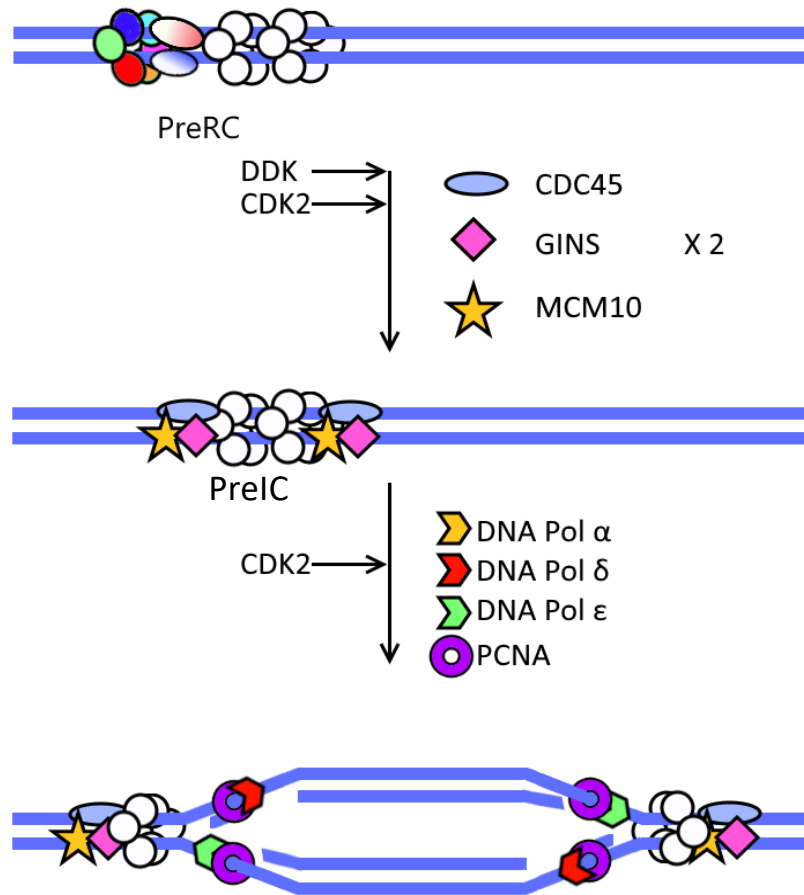


Figure 1.4 - DNA Replication Initiation Pre replication complexes are converted to Pre-initiation complexes in response to increasing CDK activity. The coordinated activity of CDK2 and DDK promotes recruitment of CDC45, GINS and MCM10 to MCM2-7 activating its helicase activity. Further Phosphorylation events facilitate the recruitment of PCNA the DNA polymerases delta, alpha and epsilon (replisome). Multiple interfaces between CMG, PCNA and polymerases facilitate bi-directional leading and lagging strand synthesis.

CDC45 has a number of interactions and regulatory mechanisms. Firstly, it is part of the CMG complex of the fully activated helicase. CDC45 interacts with MCM5, and 7, as well as the main replicative polymerases, topoisomerases, and primases (Broderick & Nasheuer, 2009). CDC45 in the CMG interfaces with MCM2, MCM5 and GINS (Simon et al., 2016). In response

to DNA damage, a CHK1 response promotes dissociation of CDC45, this is not simply due to inhibition of the CDK signals that promote CDC45 binding (Liu et al., 2006).

Activation of pre-RCs and pre-ICs requires numerous phosphorylation events. These are mediated through CDK and DDK. DDK activity is suppressed in events of replication stress, in yeast activation of S phase checkpoint results in activation of RAD53, interactions between RAD53 and DDK promote a dissociation from chromatin suppressing cell cycle progression (Larasati & Duncker et al., 2017).

PCNA has numerous functions, as well as anchoring the replisome to DNA it provides a platform for binding of a number of proteins, this requires multiple mechanisms of regulation. Roles involved include DNA replication, and DNA repair (Mailand et al., 2013).

PCNA expression is regulated by E2F4 (Ren et al., 2002). Phosphorylation of PCNA at tyrosine 211 stabilises chromatin bound DNA (Wang et al., 2006). Acetylation of PCNA prevents PCNA interacting with protein MutT homolog2 (MTH2), promoting degradation of PCNA (Yu et al., 2009). Mono-ubiquitination of PCNA is required to promote translesion synthesis across replication barriers. DNA polymerase η is recruited to mono-ubiquitinated PCNA at lysine 164 by RAD18 (Watanabe et al., 2004). Small ubiquitin-like modification (SUMOylation) of PCNA prevents DSB formation through maintenance of DNA repair pathways. In unperturbed replication, SUMOylation of lysine164 prevents TLS by suppression of ubiquitination of the same residue as well as recruiting SRS2P, a helicase that suppresses homologous recombination (HR) (Hoegge et al., 2002; Papouli et al., 2005).

The core polymerase enzymes are also subject to regulation. DNA pol δ is heterotetramer formed of p125, p68, p50 and p12. DNA pol delta remains anchored to the replisome through interactions with PCNA via a C-terminal PIP box of the p68 subunit of the polymerase (Lee et al., 2017). Replication stress results in the ubiquitination and degradation of the p12 subunit in an ATR dependent manner. Additional factors such as protein PDIP46

(DNA polymerase delta interacting protein 46) bind and activate DNA pol delta, through the P50 subunit. (Zhang et al., 2007). The eukaryotic DNA primase DNA pol alpha is regulated through phosphorylation. Phosphorylation by Cyclin E/CDK2 promotes primase activity in a manner not seen by Cyclin A/CDK2, differentiating the needs across G1, S and G2 phase (Voitenleitner et al., 1999).

The importance of the accurate DNA replication licensing, initiation and termination events ensure that DNA is replicated accurately and only once per cell cycle. Regulation of DNA replication licensing and activation is complex, multifaceted, and adaptable in response to damage and stress. Critically, almost every facet of DNA replication licensing and initiation is impacted by CDK mediated phosphorylation. Therefore, regulation of CDK activity is essential for the correct maintenance of replication initiation (Section 1.8).

1.6. CIZ1

Cip1 interacting zinc finger protein (CIZ1) is a protein found in higher mammalian organisms and there are regions of homology with the C-terminus in some vertebrates. In humans, CIZ1 is encoded by the CIZ1 gene located on chromosome 9. CIZ1 was first identified in 1999 (Mitsui et al., 1999) and there are no high-resolution structures of CIZ1, but it is predicted to be natively disordered in the N-terminal region, while the C-terminus is predicted to be more structured. The C terminus of CIZ1 contains a matrin type zinc finger domain (Ainscough et al., 2007). Matrin motifs are stabilised by a zinc ligand that function in RNA and DNA binding, and are commonly found in transcription factors (Klug, 2010; Font & Mackay, 2010). Functions of zinc finger containing proteins include regulation of chromatin folding, transcriptional regulation, and translation regulation.

A number of alternatively spliced CIZ1 isoforms have been identified (Coverley et al., 2005; Rahman et al., 2010; Higgins et al., 2012, Swarts et al., 2018). The best characterised CIZ1 isoform is the embryonic CIZ1 (ECIZ1) transcript identified in murine embryos that lacks the

N-terminal polyglutamine motif that aids expression (Coverley et al., 2005). Differential CIZ1 splicing is a common event in tumours and the functional significance of these variants are beginning to be determined. A cancer specific splice variant lacking exon 8 has been proposed as a biomarker for lung cancer (b-variant). This variant lacks the nuclear matrix attachment domain, and its expression was significantly increased in lung tumour samples compared to adjacent tissue (Higgins et al., 2012). Interestingly targeted depletion of CIZ1 b-variant in mouse xenografts caused reduced the growth of tumours suggesting that CIZ1 is required for tumour growth in this context and may serve as a viable target in certain cancers.

Contrastingly, CIZ1 also has been reported to act as a tumour suppressor, loss of CIZ1 in mice are sensitive to hydroxyurea mediated replication stress, and sensitive to retroviral insertional mutations, developing numerous leukaemias. CIZ1 null mice also develop lymphoproliferative disorders (Nishibe et al., 2013 Ridings-Figueroa et al., 2017) A summary of published mutations found in CIZ1 in cancers is summarised in Chapter 7.

Recently, CIZ1 activity has been associated with the inactive X chromosome (Xi) in female mouse cells. These findings showed that CIZ1 was recruited to Xi during early embryonic development. This interaction is through repeat E anchors in X-inactive specific transcript (Xist) RNA (Sunwo et al., 2017). This provides a further potential link to cancer as X chromosome inactivation is disrupted in a number of cancers (Ridings-Figueroa et al., 2017; Sunwoo et al., 2017). Loss of CIZ1, and long-term cell culture, results in compromised relocation of Xi that occurs as cells proliferate. This was accompanied by a change in the expression of genes regulated by polycomb repressive complexes (PRC1/2), PRC1/2 are transcriptional regulators that suppress transcription by modulating chromatin environments, similarly to CIZ1 PRC2 mutations have been observed to function contrastingly as both tumour suppressor, and oncogenes (Laugesen et al., 2016, Stewart et

al., 2019). Whether or not this change in behaviour is linked to CIZ1's role in cancer remains unclear, however deregulation of PRC1 and PRC2 can result on DNA replication stress in cultured cells, something CIZ1 null cells have been shown to be sensitive to (Nishibe et al., 2013; Piunti et al., 2017).

1.7. CIZ1 Interactions with Cyclin CDKs During the G1/S Transition

CIZ1 plays a role in the events of DNA replication initiation. CIZ1 binds to DNA the nuclear matrix fraction of chromatin, where it may anchor CDC6 to this site. The nuclear matrix is a collection of proteins, and ribonucleotides that aids in the organisation of chromosomes and within the nucleus. Organisation of the nuclear matrix differs across cell type and during tumorigenesis. The nuclear matrix is made up of lamin proteins which span the nuclear envelope linking the chromosomes to the cytoskeleton and composes the scaffold that remains after chromatin isolation, crosslinking and DNase digestion (Nickerson et al., 1997; Rynearson et al., 2011; Wasąg et al., 2016; Wilson et al., 2016). DNA attaches to the nuclear matrix through loops at matrix attachment regions (MARs) and scaffold attachment regions (SARs). The nuclear matrix plays a role in DNA replication, nascent DNA becomes associated to the nuclear matrix. Additionally, replication origins have been shown to be recruited to the nuclear matrix during late G1, and preRC/IC proteins are recruited to the nuclear matrix following mitosis (including ORC proteins, CDC6, CDT1, and MCM3), as well as Cyclin E and Cyclin A. Cyclin E NM recruitment is lost in cancers (Wilson et al., 2013).

CIZ1 can associate with cyclin A/CDK2 and cyclin E/CDK2 during the events of DNA replication potentially contributing to the spatiotemporal regulation of DNA replication firing (Pauzaite et al., 2017). CIZ1 can expand and increase the replication initiation activity of recombinant cyclin A/CDK2 *in vitro* (Coverley et al., 2005; Copeland et al., 2010).

Additionally, *in vitro* experiments have shown that phosphomimic versions of CIZ1 abolishes this effect (Copeland et al, 2015).

CIZ1 itself is regulated by the activity of cyclin-CDK mediated phosphorylation and contains several phosphorylation sites (Coverley et al., 2005; Copeland et al., 2015). CIZ1 is a substrate of cell cycle kinases, which have important functions surround the G1/S phase transition: Cyclin E/CDK2, cyclin A/CDK2 (Copeland et al., 2015). When CIZ1 is phosphorylated at sites T293 or T192 its replication activity is reduced *in vitro*. This activity is linked to CIZ1's ability to co-ordinate Cyclin A/CDK2 and Cyclin E/CDK2 during the G1/S transition, anchoring these kinases to the nuclear matrix, close in proximity to licensed origins (Coverley et al., 2005, Copeland et al., 2015).

CIZ1 interacts with G1/S cyclins through cyclin-binding motifs (K/RXL). As cells progress through the cell cycle from mitosis Cyclin E levels increase, here CIZ1 interacts with Cyclin E at the nuclear matrix. It appears that CIZ1 is recruited to regions of the nuclear matrix with high Cyclin E as depletion of CIZ1 by siRNAs does not impact cyclin E nuclear matrix localisation. Later, Cyclin A levels increase as cells reach late G1 and early S phase, this increase is accompanied by a switch in Cyclin binding to CIZ1, Cyclin E is displaced at the nuclear matrix on CIZ1 by Cyclin A. This localisation change of Cyclin A is CIZ1 dependent, depletion of CIZ1 by siRNA results in loss of the nuclear matrix localisation of Cyclin A (Copeland et al., 2010). This exchange ensures that Cyclin A/CDK2 becomes localised to sites that experience Cyclin E/CDK2 activity (Figure 1.5a).

Phosphorylation of CIZ1 by CDKs results in a loss of its DNA replication initiation activity, in cycling cells, these phosphorylations occur as cells enter S phase when replication initiation is no longer required. Phosphomimetic variants of CIZ1 no longer promote DNA replication *in vitro*. These phosphorylations are accompanied by a loss of the ability for CIZ1 to interact with Cyclin A. These phosphorylations do not restrict CIZ1's nuclear localisation, and CIZ1 can still interact with replication licensing factor CDC6 as this interaction is at a different binding

site. This implies that CIZ1 de-activation promotes replication after the onset of S phase (Copeland et al., 2015) (Figure 1.5b).

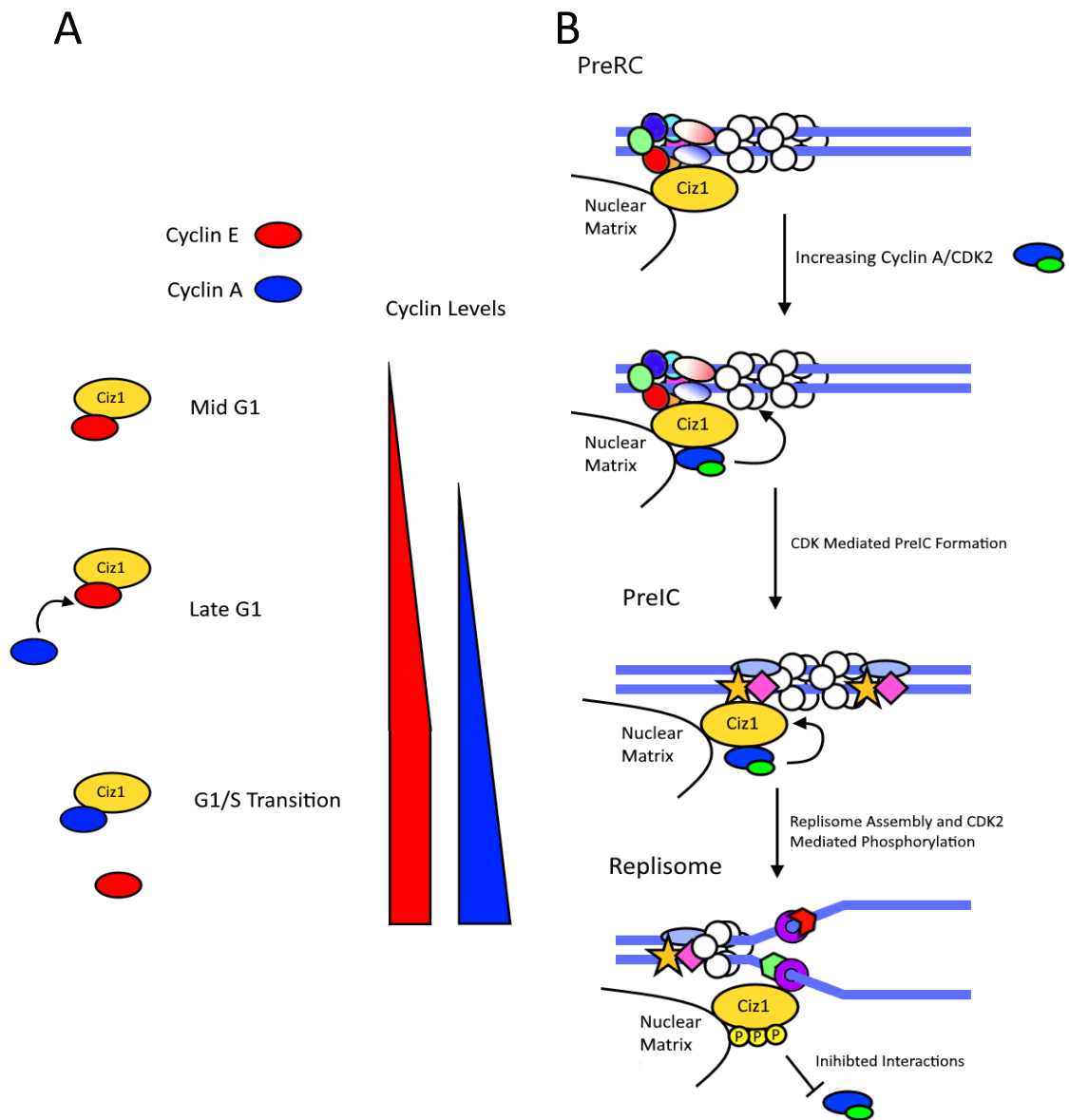


Figure 1.5-CIZ1 Promotes Replication initiation through interactions with Cyclins A) CIZ1 recruits Cyclin A/CDK2 to sites with Cyclin E activity. CIZ1 interacts with Cyclin E in mid G1 phase, as Cyclin A levels increase Cyclin A/CDK2 displaces Cyclin E, promoting a shift in the active Cyclin at CIZ1 enriched sites. Adapted from Copeland et al. (2010) B) Cyclin A is recruited to replication origins by CIZ1, Cyclin A/CDK2 promotes replication initiation, and then phosphorylates CIZ1 promoting release of Cyclin A/CDK2 from CIZ1 at the nuclear matrix. Adapted from Copeland et al (2015).

Together, these studies inform a model by which CIZ1 is localised to licensed origins through interactions with CDC6 and Cyclin E at the nuclear matrix. This promotes the activation of these origins through Cyclin E (and later Cyclin A) mediated CDK2 phosphorylation. As cells progress towards S phase Cyclin A accumulates and is brought to these 'selected' origins by CIZ1. Cyclin A mediated phosphorylation then promotes replication origin firing, and then later CIZ1 phosphorylation promotes the dissociation of Cyclin A/CDK 2 and CIZ1. Preventing replication initiation at fired origins. Therefore, it appears that CIZ1 acts as a 'kinase sensor' translating levels of Cyclin A, and Cyclin E to their activity (Pauzaite et al., 2017). Disruption of this could result in aberrant Cyclin/CDK signalling. Localisation changes of G1/S cyclins are sufficient to induce DNA replication stress and result in mitotic defects (Bagheri-Yarmand et al., 2010). Correct regulation of CDK activity and the timing of the phosphorylation of CDK substrates is important for cell cycle regulation.

1.8. The quantitative model of cell cycle regulation by CDK and the Permissive Kinase Window

The cell cycle is regulated by the activity of cyclin dependent kinases, which oscillates from low in G1 phase to high during mitosis. The organisation of the cell cycle can be recapitulated by a single cyclin-CDK fusion protein in fission yeast (Coudreuse & Nurse, 2010; Gutierrez-Escribano & Nurse, 2015). The thresholds that determine the cell cycle phase transitions appears to be governed by the intrinsic CDK activity rather than by a specific activity of any cyclin-CDK complex. The quantitative model, originally proposed by Stern & Nurse (1996), provides a molecular basis for the G1/S and G2/M transitions of the cell cycle. The hypothesis that this project intends to test relies on the "kinase model of DNA replication". This states that DNA replication initiation is only possible within a tightly controlled window of kinase activity. There is a low kinase activity threshold (T_S) below which replication cannot occur, and a higher inhibitory kinase threshold (iT_S) above which replication is blocked.

Additionally, there is a third increase kinase threshold at which mitosis can begin (T_M)

(Pauzaite et al., 2016) (Figure 1.6).

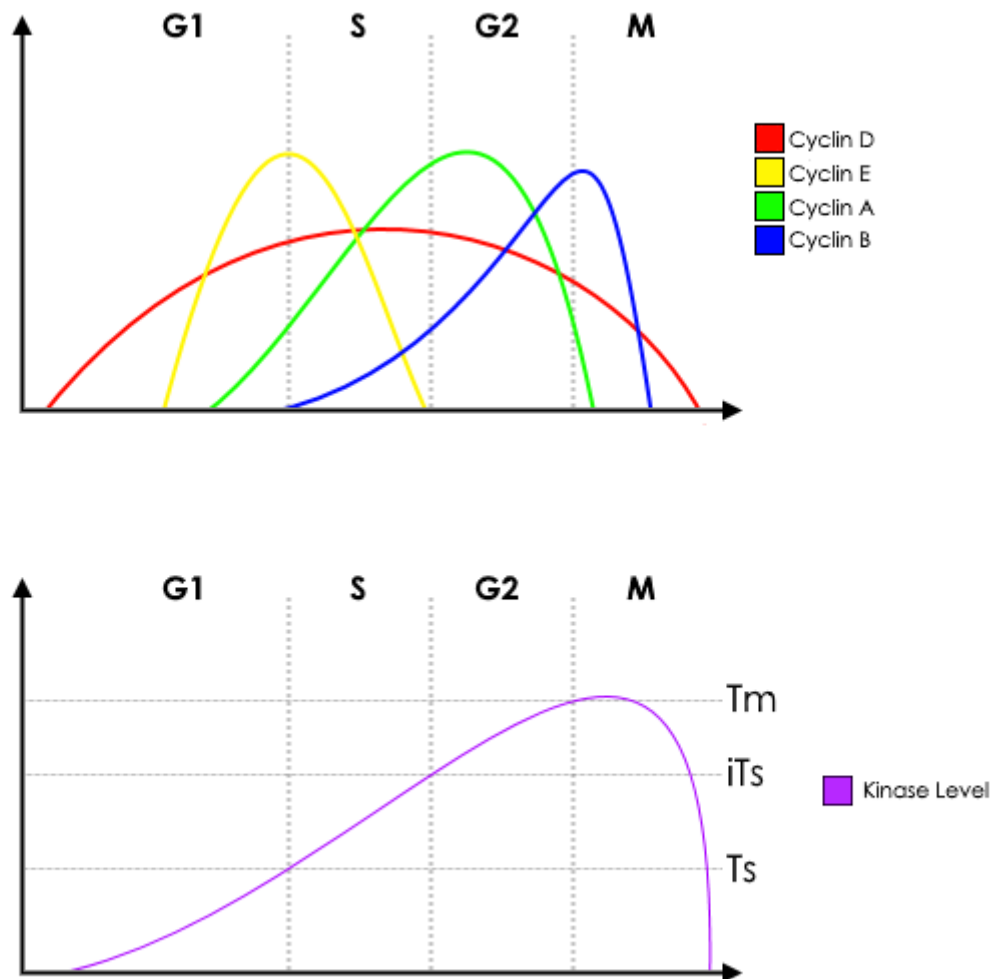


Figure 1.6 – The Quantitative Model of the Cell Cycle A schematic showing kinase level changes across the cell cycle, and the thresholds present throughout the cell cycle. Kinase level increase is primarily driven through the temporally controlled expression of cyclins which activate cyclin dependent kinase binding partners.

The lower kinase activity (T_S) is set primarily through the activity of two kinases: CDK2 complexed with cyclin A or cyclin E, and Dbf4-dependent kinase (DDK). The activity of these two kinases is required to convert preRCs into preICs (Fragkos et al., 2015). CDKs also phosphorylate other replication factors such as Sld2 and Sld3 part of the budding yeast

PreIC, which promotes the recruitment of further factors such as GINS and pol ϵ (Araki, 2010). Without this activity, licensed origins could not recruit the replicative polymerases Pol δ and Pol ϵ and replication cannot occur.

The inhibitory higher kinase activity iT_3 that prevents DNA replication initiation is driven through a number of mechanisms. In general, higher kinase levels lead to phosphorylation of key replication proteins that targets them for removal from the nucleus or destruction by ubiquitination. These include ORC1 and CDT1 (Guarino et al., 2011; Mendez et al., 2002).

Within the quantitative model lies the ability to control whether cells lie in dormant quiescence (G0) or enter the cell cycle into S phase, here there is a kinase threshold, the restriction point. Whether cells enter the cell cycle straight away, or enter quiescence is governed by p21 levels at mitosis and G1. Cells that divide with high p21, typically have hypophosphorylated RB, low CDK activity and will enter G0 or need external signals to promote cell cycle entry (Moser et al., 2018). Cells which divide with low intracellular p21 levels enter G1 with higher CDK activity, leading to hyperphosphorylation of RB, and rapidly begin a further round of cell division. (Moser et al., 2018). CDK activity, is key for RB phosphorylation, control over cell cycle entry above and below the restriction point threshold governs cell division rates. Once the G1/S transition is passed, p21 is degraded by the ubiquitin proteasome system through the activity of CRL4^{Cdt2} and SCF^{Skp2} E3 ligases. p21 levels at G2/M are linked to DNA damage within the S phase of the previous cell cycle. DNA damage promotes a DDR, which results in the accumulation of p53 through G1, triggering an accumulation of p21. These cells will not enter S phase even in high serum conditions due to CDK inhibition keeping the kinase level below the threshold (Barr et al., 2017). The cell cycle is driven by these two thresholds, the RP, and the G1/S phase transition, both in turn governed by kinase levels. The RP is promoted by an increase in kinase activity opposed by p21 inhibition of CDKs. Between the restriction point and the G1/S transition cells can return

to their G_0 state, however this becomes impossible after the G1/S transition. Degradation of p21 by the UPS promotes high CDK levels driving proliferation through the cell cycle. p21 levels will accumulate through S and G2 allowing DNA repair however cells commit to division. This drives the unidirectionality of the cell cycle, driven by a one-way kinase level increase protecting against re-replication (Heldt et al., 2018).

The presence of these precise kinase thresholds coupled with the increasing kinase activity throughout the stages of the cell cycle, followed by resetting upon activation of the APC/C ensures DNA replication and mitosis occur only at the correct time as well as ensuring origins do not fire more than once per cell cycle (Spencer et al., 2013). Consequently, the activity of CDKs ensure the unidirectional progression of the cell cycle.

Recently, the molecular mechanisms that underpin the quantitative model of CDK activity have begun to be determined. Swaffer et al. (2016), demonstrated that CDK substrates can be roughly grouped into their sensitivity to CDK activity. This can be roughly split into early (phosphorylated, G1/S), intermediate, and late (phosphorylated G2/M). In this report, re-ordering of the cell cycle, DNA synthesis before on set of M phase was achieved through dephosphorylation and subsequent re-phosphorylation of the early targets. Additionally, cells arrested in G1/S phase exposed to high CDK activity simultaneously phosphorylated early and late CDK targets, and concurrently entered S phase and M phase. Intermediate kinase targets appeared to be regulated by cyclin specificity, the absence of G1/S cyclins resulted in a decrease in the rate of intermediate targets increasing gradually over the cell cycle. Swaffer et al. (2016) proposed a model where early and late targets are driven through global increases in kinase activity and intermediate targets are regulated by cyclin/CDK specificity.

More recently, Ord et al., (2019) demonstrated that cyclin specific phosphorylation is triggered by three major sequence specific factors. Firstly, threonine residues are less

efficiently phosphorylated than serine residues, bifurcating targets to late and early phosphorylation. Secondly, the distances between CDK phosphorylation sites, and changes in combinations of CDK phosphorylation sites could dictate the activity and time required to phosphorylate them. This effect could be reduced by addition of cyclin specific docking sites this could be how mid targets are more specifically regulated by the specific Cyclin-CDKs. Thirdly, through specific cyclin docks, S phase CDK recognised an RxL motif and M phase CDKs recognised an LxF motif, the order of phosphorylation can be reversed by altering which motif is present. Together these two reports enrich the quantitative model of the cell cycle. Early and late targets are defined by being more readily phosphorylated, mediated through phosphorylation patterns and serine threonine switching. This allows cell cycle progression using only 1 CDK (Gutierrez-Escribano & Nurse, 2015). However, phosphorylation thresholds are fine tuned in mid targets by the presence of cyclin specific binding docks, allowing the fine control of 1000s of different targets involved in cell cycle progression.

A key thing to note is that bringing cyclins into close contact with targets through docking ports was key to defining thresholds, a role that CIZ1 plays during the G1/S transition (Copeland et al., 2010). CIZ1 also interacts with p21, the protein involved with setting the kinase level after mitosis (Moser et al., 2018). *In vitro* CIZ1 appears to regulate CDK activity at the G1/S transition (Coverley et al., 2005), if CIZ1 is altering the S phase threshold this may result in deregulated CDK signalling. Deregulation of CDK signalling will result in a phenomenon known as DNA replication stress (Jones et al., 2012; Shimura et al., 2013; Llobet et al., 2019) which could help uncover the role CIZ1 plays in tumour development.

1.9. DNA Replication Stress

DNA Replication stress (DRS) is defined as the stalling and slowing of DNA replication forks, this can be caused by oncogenic mutation, external stresses, or collisions with transcription events. Replication stress triggers the DDR and activates the S phase checkpoint. This allows

cells to repair DNA or in circumstances where repair is not possible to undergo programmed cell death. If cells can bypass this 'tumorigenesis barrier' during sustained replication stress, mutation rates increase resulting in cancer developments (Bartkova et al., 2006). Sustained replication stress leads to genome instability, which underlies many of the hallmarks of cancer. DRS is characterised by slow replication forks and activation of cryptic origin sites (Gaillard et al., 2015).

DRS can be mediated by a number of factors including oncogene activation (RAS, myc, BCL-2), overexpression of cyclin D/E or regulators of the DNA replication process (CDC6), or reduction of factors that stabilise ssDNA such as RPA (Sideridou et al., 2011; Kotsantis et al., 2016; Macheret & Halazonetis, 2018; Primo & Teixeira, 2020). There are a number of mechanisms by which oncogene activation induces replication stress. These include collisions with transcription machinery, collision with abnormal DNA structures (e.g. G quadruplexes), abnormal origin licensing, impaired origin firing, or depletion of nucleotide pools, or replication when nucleotide pools are low (Primo & Teixeira, 2019). All of these result in a slowdown or increased stalling of replication forks resulting in genome instability.

Prolonged replication stress causes damage to DNA; this is most noticeable at common fragile sites (CFS), which are sites that are likely to break during replication stress. These sites often share characteristics: CFS are commonly located in late replicating regions of the DNA (Beau et al., 1998). CFS commonly are AT rich containing interrupted AT repeat regions (Zlotorynski et al., 2003), addition of these AT rich patterns to genes in yeast increases DNA fragility (Zhang et al., 2007; Glover et al., 2017). Recently, databases of the ~125 identified CFS have been established, identifying over 4000 protein coding regions within them.

Notably the most common conditions linked to genes within CFS were neoplasia. Functions of proteins within CFS included DNA repair, and mitotic spindle checkpoint proteins (Kumar et al., 2019). The tumour suppressor gene: fragile histidine triad protein (FHIT) that functions

in regulation of nucleotide metabolism lies within a CFS commonly damaged in response to carcinogens and mutated in a number of cancers (Limas & Cook, 2019).

Cells have developed mechanisms to protect from the effects of replication stress. DRS could result in under replicated DNA, that could result in cell death through apoptosis, the removal of the cell from the cell cycle via senescence, or if allowed to replicate through a mitotic catastrophe. The activation of dormant 'cryptic' origins within the genome enables complete duplication of the genome under DRS conditions. Activation of cryptic origins is observed when MCM2-7 proteins are lowered. In 'normal' growth conditions, MCM2-7 deficient cells replicate at a rate comparable to control. However, when replication is challenged by nucleotide synthesis inhibitor hydroxyurea replicate rates were drastically lowered (Ge et al., 2007).

There are two major results of DRS: under replicated DNA due to under licensed origins, slow DNA replication forks, or reduced origin firing. In the absence of complete duplication of the genome under-replicated DNA proceeding through mitosis can cause loss of genomic integrity. The second result of DRS is stalled replication forks, failure to replicate through stalled forks will result in mitotic catastrophe. Cells have mechanisms to replicate through stalled forks, but these mechanisms are error prone and can also result in DNA damage. This implicates replication stress as a source for genome instability, explaining why DRS has been proposed as a hallmark of cancer (Macheret & Halazonetis, 2015).

Replication through DNA lesions using trans-lesion synthesis (TLS), which utilizes alternative DNA polymerase enzymes to replicate past lesions. These include the Y family of DNA polymerases, principally Pol η (Sale, 2013). This polymerase commonly replicates through bulky cyclobutane pyrimidine dimers (CPDs) caused by UV damage, utilizing an enlarged more open active site than replicative polymerases pol δ and pol ϵ (Biertümpfel et al., 2010). Loss of Pol η in xeroderma pigmentosum v (XP-V) results in an increased photosensitivity

(Black, 2016). TLS lack the proofreading ability present in the principal replicative polymerases: pol δ and pol ϵ . *S. cerevisiae* Pol η has a single base substitution rate of 950 per 100,000 base pairs, compared with ≤ 1.3 and ≤ 0.2 for pol δ and pol ϵ respectively. Furthermore, *S. cerevisiae* pol η has a single insertion or deletion rate of 93 per 100,000 bp, compared to 1.3 and 0.5 in pol δ and pol ϵ respectively (McCulloch & Kunkel, 2008). Increased TLS has been linked to multiple cancer types; furthermore, it has been implicated as a mechanism for tumours to develop resistance to chemotherapy (Zafar & Eoff, 2017).

Another mechanism by which cells resolve replication stress due to stalled forks is through homologous repair (HR). HR relies on a homologous sequence of DNA from sister chromatid to repair. If HR is not possible the more error prone non-homologous end joining (NHEJ) pathway is used. HR is often disrupted in cancer, notable mutations in HR tumour suppressor proteins BRCA1/BRCA2 confer severe cancer risk, woman who carry BRCA1 mutations have a 70 % chance of developing breast cancer in their lifetimes (Semmler et al., 2019). Failure to resolve replication stress can result in genome instability in a multiple ways. This can include point mutations due to TLS, large-scale chromosomal re-arrangements, changes in chromosome number due to mitotic error, addition, or deletion of DNA (Bishop & Schiestl, 2002; Sishc & Davis, 2017).

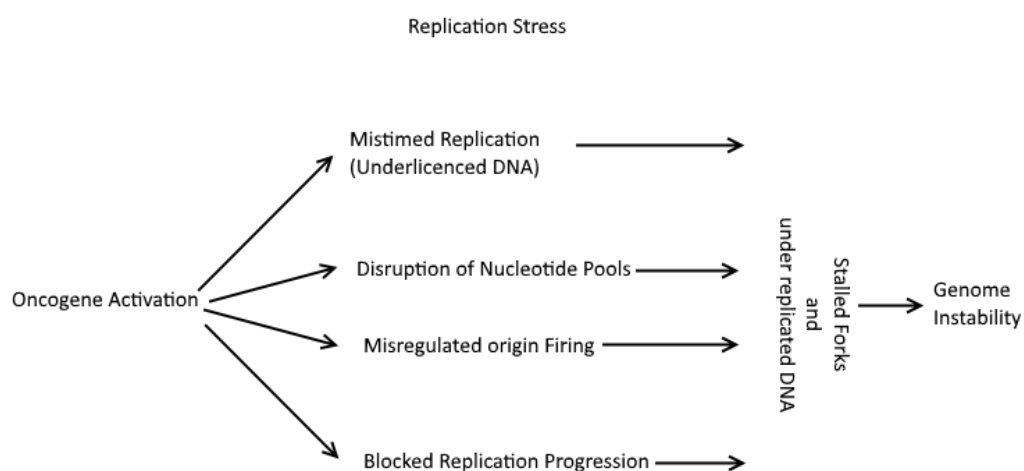


Figure 1.7- Oncogene Activation Induces Replication Stress. *Oncogene activation can result in multiple phenotypes. Many of these phenotypes summarised in this figure result in the slowing or stalling of replication forks i.e. replication stress. These lead to increased DNA damage at CFS and under replication of DNA. If left unchecked for a prolonged time oncogene induced replication stress results in genome instability,*

The second defence against replication stress is the ATR Chk1 checkpoint response. This is discussed in detail in Section 1.11. Interestingly, DRS is a feature of many tumour cells and this can be targeted by DRS inducing factors to selectively kill cancer cells. In mice, CHK1 inhibition can kill tumours with high levels of replication stress derived from overexpression of MYC transcription factors. This was ineffective in tumours that did not display increased DRS. These cancer cells rely on the checkpoint response to complete DNA replication without catastrophe (Murga et al., 2011). This chronic DRS is a potential avenue to explore for personalised anticancer treatments.

1.10. Targeting the Replication Stress Response in Cancer Therapeutics

Previous sections described both replication stress, the causes of replication stress, and the cellular response to replication stress. Clearly, minimising replication stress and developing robust mechanisms to protect against its effect is vital for the long-term survival and health

of multicellular organisms. Recently, due to weaknesses in tumour cells response to replication stress. Replication stress has become a target for cancer therapeutics.

Many approved cancer therapeutics function by inducing replication stress in the rapidly replicating tumour cells. These classes of drugs can function by inhibition of DNA and RNA synthesis (5-Fluorouracil), or by inhibition of nucleotide biosynthesis (Hydroxyurea, mercaptopurine, or methotrexate). These drugs have no preference between proliferating 'healthy' cells and rapidly proliferating tumour cells. Tumour cells are more sensitive to these drugs as they are proliferating more rapidly, therefore DRS is induced in these tumour cells promoting apoptosis, additionally, tumour cells often rely on the DRS to prevent catastrophic replication defects (O'Neil et al., 2017). Consequently, drugs of this class are associated with a number of side effects that would cause discomfort or danger to the patient. Side effects include nausea, fatigue, immunosuppression, and diarrhoea (Formen & O'Connor, 2018). Clearly, such drugs are not ideal unless no better option is available.

Conventional chemotherapeutics include drugs that compete with dCTP for DNA incorporation, preventing DNA elongation and inducing DRS by stalling replication forks (Cytarabine and gemcitabine) (Uhbi et al., 2019). Cytarabine promoted remission of acute myeloid leukaemia by 60-80 % in young adults (Wu et al., 2017).

Another family of conventional drugs that induce DNA damage are DNA alkylating and cross-linking agents. These drugs block replication through physical linking of DNA bases (both neighbouring and disparate). Cisplatin is an example of this class of drug (Uhbi et al., 2019). Cisplatin has been used to treat multiple cancer types including lung, testicular, and ovarian cancers. Cisplatin promotes apoptosis, inducing both inter-strand and intra-strand cross links, this occurs at any point in the cell cycle (Aldossary, 2019). Side effects of cisplatin are severe commonly including anaemia, bone marrow failure, and sepsis. In rare occurrences, cisplatin treatment causes cardiac arrest, and acute leukaemia (NICE, 2020²).

Finally, another class of conventional of chemotherapeutic drugs that induce DNA replication stress are the topoisomerase inhibitors. These prevent the resolution of DNA supercoiling induced by DNA replication, blocking continued replication, and inducing DSB (Ubhi et al., 2019). An example of this type of chemotherapeutic is doxorubicin (Nitiss, 2009).

Doxorubicin is used to treat numerous cancers including leukaemia, lymphoma, and breast cancer. The various replication stress inducing cancer therapeutics have responses that vary across cancer type, and individual. They all commonly share severe side effects. Clearly, more targeted, lower side effect chemotherapeutics need to be developed as cancer treatment becomes more personalised.

More recently, targeted drugs have been developed that exploit weaknesses in tumour cells DDR to induce catastrophic damage to the cell. The first of these developed was Olaparib, a PARP inhibitor. BRCA1 and 2 are tumour suppressor genes that function within the DNA repair programme BRCA1 was first discovered in 1994, around the same time BRCA2 was identified (Swensen et al., 1994; Wooster et al., 1995), both genes were discovered due to heredity breast cancer cases. Women with BRCA1/2 mutations without intervention have a 40 – 60 % chance of developing breast cancers. Screening families of those effected by BRCA mutations has proved preventative (Chen & Parmigianim, 2007; Bryant et al. 2005).

Small cell lung cancer, representing 15 % of lung cancers, displays replication stress caused by the activation of oncogenes and the loss of TS functions (Bian & Lin, 2019). Therefore, a potential mechanism for the treatment of SCLC via targeting replication stress. One potential candidate is WEE1, which is a CDK1 inhibitor that regulates the G2/M checkpoint and prevents the untimely onset of mitosis. SCLC cells and other cancer cells are under constitutive replication stress. Cells under constitutive DRS often fail to complete DNA replication before mitosis. WEE1 is a kinase that targets CDK2 and CDK1 through inhibitory phosphorylation, preventing the signals that would promote mitosis. WEE1 also inhibits the

firing of fully licenced replication origins through inhibition of CDK2 (Moiseeva et al., 2019). The mechanism by which WEE1 inhibition functions as a cancer treatment is that WEE1 inhibition would allow cells to enter mitosis when DNA replication is not finished, this would result in a mitotic catastrophe causing the death of daughter cells. In p53 mutant cancer cells, WEE1 depletion reduced cell proliferation, as well as sensitising cells to ionising radiation (Yin et al., 2017). Furthermore, chemical inhibition of WEE1 in SCLC by AZD1775 revealed that numerous SCLC cell lines were sensitive to WEE 1 inhibition (Sen et al., 2017). AZD1775 is currently undergoing clinical trial. Modern strategies have been developed to increase the potency of AZD1775, repurposing it as a proteolysis targeting chimera (PROTAC), to selectively target WEE1 for degradation by the ubiquitin proteasome system reducing dose required, and promoting G2/M accumulation (Li et al., 2020).

A third potential target is ATR inhibition. It is a component of the SSB DNA damage checkpoint activated by long stretches of RPA the single strand binding protein. ATRi has been shown *in vitro* to be effective at sensitising cancer cell lines to radiotherapy, by preventing the DNA damage response (DDR), in cells damaged by radiation, and allowing the cell cycle to progress through to mitosis. This resulted in mitotic catastrophe that induced cell death (Dillon et al., 2017). Currently there are multiple ATRi in clinical trial, both as a single treatment, and in combinational therapy with other treatments such as Olaparib and radiotherapy (Cancer Research UK, 2020; National Institute of Health ,2020¹, National Institute of Health ,2020², National Institute of Health ,2020³, El-Maouche et al., 2020).

Another potential target in the DDR pathway is CHK1. CHK1 lies directly downstream of ATR in the DDR. Again, inhibition of this in cells under constitutive DRS (tumour cells) would result in erosion of the S phase checkpoint, resulting in mitosis in the presence of under-replicated DNA, which would result in mitotic catastrophe that would cause cell death (Ubhi

& Brown, 2019). A number of CHK1 inhibitors have been trialled, although a number were discontinued due to poor tolerability and toxicity (Muageri-Sacca et al., 2013).

The common theme behind a number of these DRS targeting cancer therapeutics is the concept of synthetic lethality. Synthetic lethality is the phenomenon whereby a drug blocks or impedes one arm of a redundant pathway. 'Healthy' cells, cells can use another arm of the pathway to ensure DNA repair (O'Neil et al., 2017) (Figure 1.8), but the exact mechanism by which PARPi is synthetically lethal is unclear. One theory is that PARP proteins are responsible for SSB repair such as BER, BRCA1/2 negative cells are defective in HR, a major mechanism for the repair of DSBs. When PARP is inhibited, SSB become DSBs, which in healthy cells can be repaired, but in BRCA1/2 cells cannot resulting in catastrophic DNA damage (Morales et al., 2014). PARPi is damaging to healthy cells, but the damage is exacerbated in HR deficient cells (Murai et al., 2012; Hopkins et al., 2019). Additionally, PARP inhibition traps enzymes PARP1 and PARP2 at damaged DNA foci, which are more challenging to repair than SSBs alone.

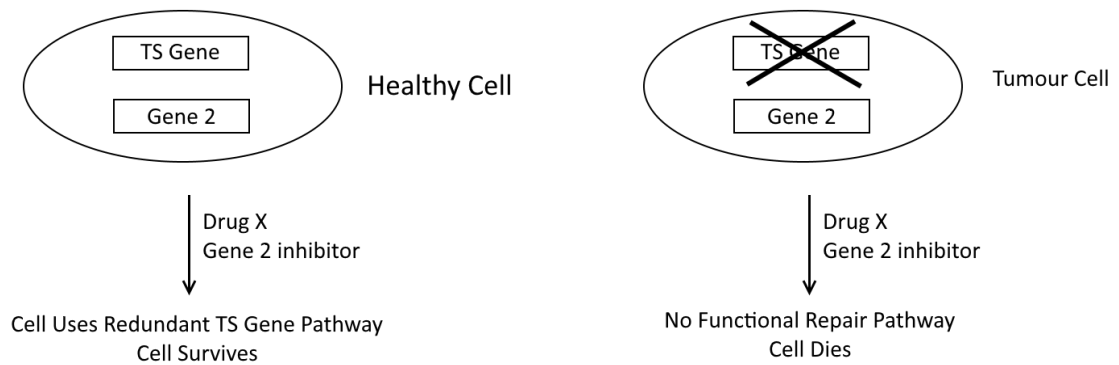


Figure 1.8 - Synthetic Lethality Synthetic lethality is the concept that a cancers mutation background results in a drug that is not lethal to 'healthy' cells becomes lethal to tumour cells. One mechanism by which this occurs is summarised here. DNA repair can be achieved by 2 pathways, one involves TS gene, the other involves gene 2. In healthy cells, inhibition of gene 2 is not lethal, DNA is repaired through the TS gene pathway. The cancer cells are TS gene negative, inhibition of gene 2 here leaves no pathway by which DNA can be repaired. Drug X causes the death of the tumour cells but allows survival of healthy cells, hence synthetic lethality.

The development of PARP inhibition was a breakthrough in cancer therapeutics. However, common to many targeted therapies there is the issue of resistance. Since clinical use of Olaparib became widely available several resistance mechanisms have been identified in tumours, the mechanisms by which cells develop resistant to PARPi is unclear. Some examples are by restoration of HR pathways, increase egress of drug, stabilization of stalled forks and reduced PARP trapping (Francica & Rottenberg, 2018; Noordermeer & Attikum 2019).

1.11. DNA Damage Response

Mammalian cells face numerous replication challenges. These can be from external sources, such as UV light, inhaled carcinogens, or, they can be from internal sources, oncogene activation, or reactive oxygen species (ROS). The key result of all these challenges is an increase in the rate of DNA damage. This damage can exist in multiple ways. UV light results in bulk adducts such as CPDs. Oncogene activation can result in an increase in single strand breaks, stalled replication forks can lead to an increase in DSBs. Unresolved this damage will result in increased mutations, cell death and mitotic catastrophe (Chatterjee & Walker, 2017). To compete with constant challenges to DNA replication across all the cells in an organism, mechanisms have evolved that repair DNA damage to allow replication to occur. A key mechanism is the DNA damage response (DDR) of the S phase checkpoint.

The DDR consists of a network of signals including proteins that sense DDR, these trigger a signal transduction pathway that results in the halting of the cell cycle. The major effectors of this response is the tumour suppressor 'guardian of the genome' p53. These prevent S phase progression buying the cell time to either repair DNA damage, remove the cell from the cell cycle completely (senescence), or in cases of irreparable damage safely remove the cell through apoptosis (Bartkova et al., 2006; Ciccia & Elledge, 2010). Together these pathways exist as the tumorigenesis barrier, preventing the accumulation of mutations in somatic cells. Bypass of this barrier can be key for cancer development

Double strand breaks (DSBs) are generated by a number of mechanisms, for example, exposure to X-rays. DSBs trigger the phosphorylation of the serine 139 residue of histone H2AX (gammaH2AX) by the protein ataxia telangiectasia mutant (ATM). H2AX phosphorylation is itself facilitated through a change in chromatin, through release of heterochromatin protein 1 ((HP1)-beta) from methylate histone H3 (H3K9me) in response to DSBs. The MRN (MRE 11, RAD50, NBS1) complex is recruited to DSBs independently of H2AX

phosphorylation, and can promote DNA repair in the absence of DNA (Yuan & Chen, 2010)

Together γ H2AX and the MRN complex provide the sites to recruit and activate further proteins in the DSB response (van den Bosch et al., 2003). The MRN complex recruits and activates the ATM kinase, which is largely responsible for the signal transduction in response to DSBs. ATM phosphorylates and activates a number of downstream proteins including checkpoint kinase 2 (CHK2). Chk2 in turn phosphorylates and activates p53, and CDC25. p53 phosphorylation results in the halting of the cell cycle, CDC25 phosphorylation results in the inactivation of the phosphatase, this prevents the activating phosphorylation of CDK2 resulting in cell cycle progression inhibition. This is compounded by p53 binding to the promoter of p21 and promoting expression and accumulation of p21, p21 directly inhibits CDKs restraining cell cycle progression (Jackson & Bartek, 2009; Liptenko et al., 2011) (Figure 1.9.).

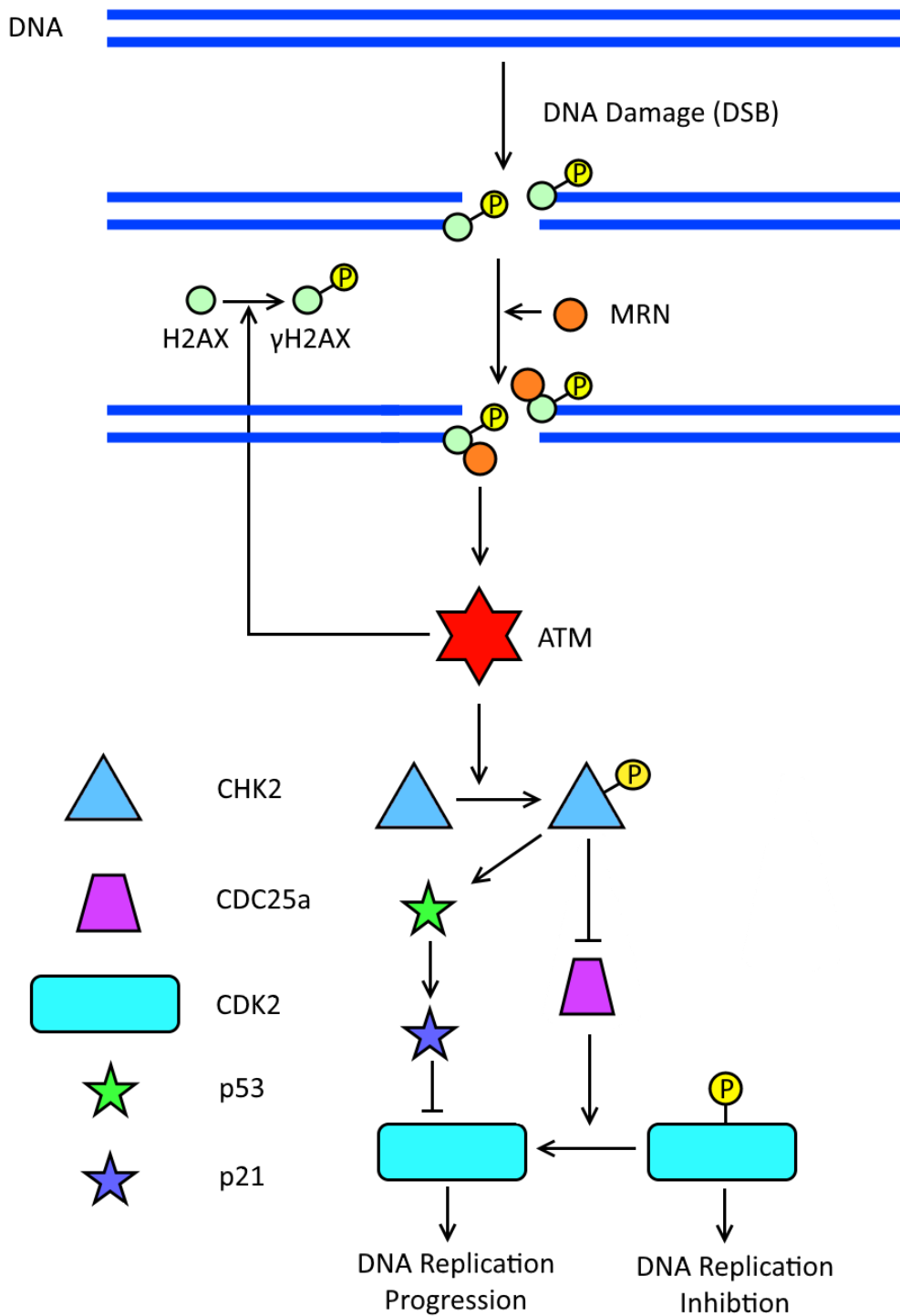


Figure 1.9 – The DDR to DSBs. Double strand breaks are DNA damage caused by multiple sources e.g. ionising radiation. DSBs are labelled by the MRN complex and gammaH2AX. These activate ATM promoting H2AX phosphorylation and activation of CHK2. CHK2 promotes inhibition of cell cycle progression through activation of p53 and inhibition of cdc25. Together these promote activation of p21 and inhibition of CDKs. p21 can induce senescence and p53 can promote apoptosis.

Single strand breaks (SSB) and replication stress both trigger the halting of the cell cycle through activation of ATM-related (ATR) kinase. ATR is a component of the replisome and mediates responses to DNA damage and replication stress, which causes a decoupling of replicative polymerase and replicative helicases, resulting in long strands of ssDNA coated in single strand binding protein RPA. RPA recruits TOPBP1 to the sites of DNA damage through direct binding, via the BRCT2 domain of TOPBP1, ATR binds ATRIP and ATRIP is recruited to stall forks by binding RPA, when together at stalled forks, mediated through RPA, TOPBP1 activates ATR activating its kinase activity allowing downstream effects to occur (Acevedo et al., 2016). ATR phosphorylates checkpoint kinase 1 (CHK1). CHK1 phosphorylates p53 and CDC25. This has the same effect as CHK2, restraint of the cell cycle and inhibition of CDKs (Figure 1.9). SSBs are repaired using multiple mechanisms. One mechanism is the error prone trans lesion synthesis (TLS), other involve PARP signalling (Abbots & Wilson, 2017) (Section 1.7). RPA increases genome integrity. Inhibition of RPA induces DNA replication stress, suppression of RPA results in activation of the Fanconi anaemia pathway, suppression of RPA in cells lacking the FA pathway displayed increase rates of DNA damage (Glanzer et al., 2014; Jang et al., 2016) The FA pathway coordinates the repair of inter-strand crosslinks (Ceccaldi et al., 2016)

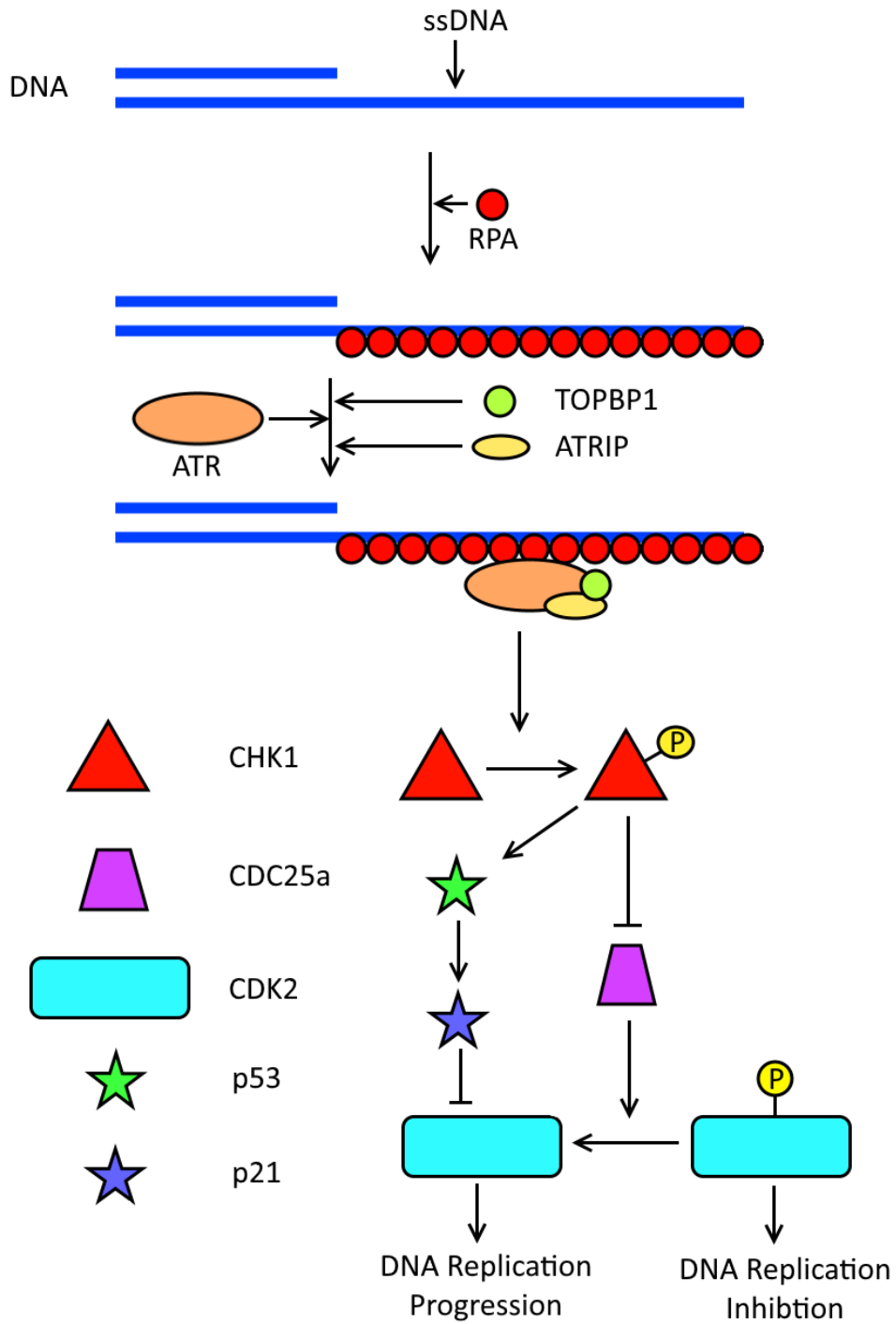


Figure 1.10 The replication stress response. Replication stress induces formation of long stretches of ssDNA that are recognised and coated with RPA. RPA coating recruits ATR, ATRIP, and TOPBP1 promoting activation of ATR. ATR phosphorylates and activates CHK1 which restrains the cell cycle through activation of p53, and p21.

Activation of cell cycle checkpoints through the DDR, halts cell cycle progression while cells respond to genotoxic stress. Initially, cells will attempt to repair DNA damage and if this is unsuccessful cells will either enter senescence or promote cell death. Responses to DNA damage vary across the stages of the cell cycle. Neocarzinostatin (NCZ) induces DSBs independently of cell cycle stage. Cells treated with NCZ in G1 rapidly halt the cell cycle at the G1/S checkpoint, cells treated during S phase continued through to G2 at low-moderate doses arresting at the following G2/M checkpoint, finally cells damaged at G2 or M rapidly arrested the cell cycle. The stage of the cell cycle damage occurs effects the repair pathways used to resolve it, after S phase DNA has a homologous chromatid which allows higher resolution repair (Chao et al., 2017). The major repair pathways from DSBs are HR, and NHEJ. NHEJ is more error prone than HR. If DNA cannot be repaired, then senescence is an option. p53 is activated upon DNA damage, and sustained p53 activation can result in apoptosis or senescence to remove the damaged cell from the cell cycle and prevent tumorigenesis (Qian et al., 2013). Constitutive p53 activation ensures that p21 expression is prolonged, leading to accumulation of p16^{ink4a} (Abbots & Wilson, 2017). p16^{ink4a} is an inhibitor of CDK4 and CDK6. Coupled with cyclin D these provide the major signal for the phosphorylation of pRB, which drives promotion of E2F transcription promoting cell cycle entry. Cells without this signal enter senescence, a permanently non-replicative state. Senescence in aging cells is linked to the strength of the promoter for p16^{ink4a} (Liu et al., 2019). The other option is apoptosis, this occurs when cells are under greater stress. Increasing doses of Doxorubicin in cells promotes a switch of cell fates from senescence to apoptosis (Altieri et al., 2012). This choice is partially due to acetylation status of p53. In high levels of stress, acetylation of K117 upregulates PUMA and NOX promoting apoptosis (Childs et al., 2014).

Cancers evade the DDR to be able to replicate their genome despite the presence of DNA damage and that leads to increased DNA mutation rates. Many of the proteins seen in the DDR are tumour suppressor genes. In fact, p53 is the most commonly mutated tumour

suppressor gene, mutated in up to 50 % of ovarian cancers (Olivier et al., 2010). Chk2 is a tumour suppressor gene (Hiroa et al., 2002). ATM is a tumour suppressor gene, qPCR analysis of nasopharyngeal carcinoma cells revealed reduced ATM expression (Bose et al., 2009). p21 displays different effects based on localization nuclear localised p21 acts as a tumour suppressor whereas cytoplasmic p21 has been reported to have oncogenic activity (Ohkoshi et al., 2015). CDC25 has been suggested as a therapeutic target for triple negative breast cancer (Liu et al., 2018). Collectively, these examples demonstrate the key role that the DDR plays in tumour development.

1.12 Aims:

In vitro experiments suggest that CIZ1 may be able to perturb the concentrations at which cyclin A/CDK2 can promote DNA replication initiation (Coverley et al., 2005; Copeland et al., 2010; Copeland et al., 2015). Permitting replication firing at both conditions lower and higher than when additional CIZ1 is not present. Coupling this with the observed overexpression and altered expression of CIZ1 in a number of cancers including breast and lung cancers may help to explain these effects (den Hollander et al., 2006; Higgins et al., 2012).

The overall aim of this project is to assess the role of CIZ1 in regulation of DNA replication. In particular, the role of CIZ1 in establishing the threshold of cyclin A-CDK2 that promotes initiation of DNA replication. To evaluate the effect of differential cyclin A-CDK2 cell free DNA replication approaches will be used. The rate of DNA replication will be determined using DNA combing using cell free and cell-based approaches.

A CIZ1 KO fibroblast cell line will be produced to further investigate the role that CIZ1 plays in the initiation of DNA replication and DNA replication fork dynamics. Hoping to identify a link between CIZ1 and DNA replication kinetics, to identify if this is a potential mechanism that underpins CIZ1's role in cancers. The principal experimental aims of this project are:

- Optimise the DNA combing technique for use in NIH 3T3 cells, and *in vitro* cell free replication assays (Chapter 3)
- Generate CIZ1 null cells using CRISPR CAS9 (Chapter 4)
- Identify alterations in cell cycle regulation upon loss of CIZ1 (Chapter 4)
- Investigate links between CIZ1 and Cyclin A/CDK2 activity at the G1/S transition (Chapter 5)
- Identify any alterations to the replication programme upon loss of CIZ1 (Chapter 6)
- Identify alterations to the DDR in CIZ1 null cells (Chapter 4/Chapter 6)

Chapter 2.

Materials and Methods

2.1 E. coli

2.1.1. Bacterial Cell Culture

To ensure aseptic technique all *E. coli* culture media was sterilised by autoclaving prior to use. All bacterial cell culture was performed in a laminar flow hood.

E. coli were grown in 10 ml primary culture of LB broth (MELFORD) (10 g/L tryptone, 10 g/L sodium chloride, 5 g/L yeast extract) supplemented with appropriate antibiotics and grown overnight at 37 °C, 150 rpm. Where required, primary cultures were inoculated into 75 ml cultures of LB broth supplemented with appropriate antibiotics. For bacteria transformed with pGEX-6P-3 plasmids or its derivatives LB liquid cultures and LB agar plates were supplemented with 100 µg/ml ampicillin (Melford). Top10 cells transformed with the GeneArt® CRISPR Nuclease Vector were grown on LB agar plates supplemented with 100 µg/ml ampicillin (Melford).

E. coli were grown on LB agar (Fisher Scientific, 40 g/l) plates at 37 °C. Bacteria were spread or streaked onto LB agar plates supplemented with appropriate antibiotics.

2.1.2. Preparing Competent Cells

BL21 (DE3) cells from an existing glycerol stock were grown overnight at 37 °C in a 5 ml LB broth culture. The following day, a 75 ml secondary culture was inoculated and grown for approximately two hours. The OD600 was measured every half hour until it reached 0.3 – 0.4. When the OD600 had reached 0.3 the bacterial culture was centrifuged for 10 minutes at 3000 rpm at 4 °C in an MSE Harrier 18/80R centrifuge.

The supernatant was discarded and the bacterial pellet was re-suspended in 30 ml of ice cold, filter sterilised CCMB80 buffer (10 mM potassium acetate, 80 mM CaCl₂, 20 mM MnCl₂, 10 mM MgCl₂, 10% v/v glycerol). The bacteria was incubated on ice for 20 minutes. After incubation, the bacteria were centrifuged for 10 minutes at 3000 rpm at 4 °C in an MSE

Harrier 18/80R centrifuge. The supernatant was discarded and the bacterial pellet was re-suspended in 4 ml of ice cold, filter sterilised CCMB80 buffer. Competent cells were stored in 50 µl aliquots at -80 °C.

Competent cells were tested by transformation with pGEX-6P-3 relative to a negative control plate. After transformation cells were grown on plates containing 100 µg/ml ampicillin (Melford) cells were deemed competent if sufficient growth on transformed cells, and no growth on control cells. Cells were also tested for ability to express recombinant protein using an IPTG induction.

2.1.3. Bacterial Transformation

100 ng of plasmid DNA was added to 50 µl of competent cells (prepared as in Section 2.1.3.) on ice for half an hour. Following incubation, the transformation mixture was heat shocked at 42 °C in a heat block for 2 minutes. Samples were then placed on ice for 5 minutes. Samples were mixed with 300 µl of super optimal broth with catabolite repression (SOC) media (Invitrogen) and incubated whilst shaking at 37 °C for 1 hour. Following incubation, the transformation mixture was spread onto LB agar plates supplemented with appropriate antibiotics (100 µg/ml ampicillin or 50 µg/ml kanamycin) as appropriate.

2.1.4. Inducing Recombinant Protein Expression using IPTG

BL21 (DE3) cells were transformed with pGEX-6P-3 plasmids with appropriate inserts as. After overnight incubation colonies were selected and inoculated into 5 ml of LB broth supplemented with appropriate antibiotics and incubated at 37 °C overnight. The bacterial culture was transferred to 75 ml of LB broth supplemented with appropriate antibiotics and incubated at 37 °C. After 1 hour, 1 ml of bacterial culture was taken and its OD600 measured using a spectrophotometer using LB broth as a blank. This was repeated every 30 minutes until the OD600 reached between 0.4 – 0.6.

When the OD600 was between 0.4 and 0.6, 1 ml of the bacterial culture was removed centrifuged and re-suspended in SDS-PAGE loading buffer. IPTG was added to the bacterial culture at a concentration of 0.4 μ M. Every hour for 3 hours 1 ml of bacteria was removed, centrifuged, and prepared for SDS-PAGE.

2.1.5. Inducing Recombinant Protein Using Auto induction Media

To ensure that protein was expressed in a correctly folded soluble form, expression of recombinant protein is slowed by incubation of bacteria at 20 °C for 20 hours in auto induction media (Table 2.1) which slows the rate of protein expression. *E. coli* transformed with a pGEX-6P-3 plasmid with appropriate inserts were grown overnight in 5 ml LB broth. 5 ml of the primary culture were inoculated into 75 ml of LB broth and grown overnight. The 75 ml culture was added to 750 ml of autoinduction media and cultured overnight. Bacteria were harvested after 16-20 hours.

Component	Concentration
Ammonium Sulphate	25 mM
Potassium Phosphate	50 mM
Sodium Phosphate	50 mM
Glycerol	5 g/l
Glucose	2.78 mM
α Lactose	5.84 mM
MgSO ₄	1 mM
FeCl ₃	50 μ M
CaCl ₂	20 μ M
MnCl ₂	10 μ M
ZnSO ₄	10 μ M
CoCl ₂	2 μ M
CuCl ₂	2 μ M
NiCl ₂	2 μ M
Na ₂ MoO ₄	2 μ M
Na ₂ SeO ₃	2 μ M
H ₃ BO ₃	2 μ M
Tryptone	10 g/l
Yeast Extract	5 g/l
Ampicillin	100 μ g/ml

Table 2.1 – Recipe of auto induction broth

2.1.6. Purification of recombinant GST Tagged Proteins

Bacteria were sub—cultured in 5 ml cultures prior to being grown overnight in auto-induction media. All steps were performed at 4 °C, or on ice. Bacteria were harvested by centrifugation using a JLA 8.1000 rotor (Beckman Coulter) at 4500 RPM for 15 minutes in an Avanti J-26 XP centrifuge. If bacteria were to be stored for later purification bacteria pellets were resuspended in 25 ml of supernatant, placed into a 50 ml falcon tube, centrifuged at 4500 RPM for 15 minutes, supernatant discarded and pellets were flash frozen in liquid nitrogen then stored at -80 °C.

Pellets were re-suspended in 25 ml of HEPES buffered saline (HBS) (50 mM HEPES pH 7.8, 135 mM NaCl, 3 mM EDTA, 1 mM DTT) supplemented with 2 cComplete™ EDTA-free Protease Inhibitor Cocktail tablets (ROCHE), and 1 mM phenylmethylsulfonyl fluoride (PMSF) (Sigma Aldrich). Concurrently, 750 µl of glutathione sepharose beads were re-suspended in 50 ml of HBS and incubated on a roller for 1 hour.

To lyse the *E. coli*, cells were sonicated four times for 15 seconds with a 1 minute rest between each sonication to prevent heating. Lysed bacteria was centrifuged at 40,000 x *g* for 30 minutes using a JA-25.50 Rotor (Beckman Coulter) in an Avanti J-26 XP centrifuge and cell lysate removed. Glutathione sepharose beads were rehydrated by incubation in buffer for 30 minutes in HBS. After swelling, beads were harvested by centrifugation at 1000 RPM for 1 minute, and discarding supernatant. The cell lysate was mixed with glutathione sepharose beads and incubated for 1 hour on a vertical rotator.

Beads were washed 5 times in 10 ml HBS supplemented with 1 mM DTT, and cComplete™ EDTA-free Protease Inhibitor centrifuging bead solution at 1,000 RPM for 1 minute between each wash and discarding supernatant. Beads were washed 3 times in 10 ml 3C cleavage buffer (50 mM Tris HCl pH 7.0, 150 mM NaCl, 2 mM DTT). Beads were transferred to 1.5 ml Eppendorf tubes and filled up to capacity with 3C buffer. After the final wash a 50 µl sample

was removed for analysis by SDS-PAGE. 10 μ l of PreScission 3C Protease (GE Healthcare Life Science) was added and samples were incubated overnight on a vertical rotor.

Following proteolysis, beads were removed from solution by two 6 second pulse centrifugations through Pierce spin columns (Thermo Fisher Scientific). 50 μ l Samples of beads, and supernatant were removed for analysis using SDS-PAGE. Protein was stored in 20 μ l aliquots in liquid nitrogen.

2.1.7. Quantifying Protein Concentration

Protein concentration was calculated using the protocol outlined in the Pierce BCA protein assay kit (Thermo Scientific).

2.1.8. Purifying Plasmid DNA from *E. coli*

E. coli were prepared from glycerol stocks or fresh transformations. 10 ml of bacteria was grown overnight at 37 °C in LB broth. Bacteria were harvested by centrifugation at 4500 RPM for 10 minutes. Plasmid DNA was isolated following the protocol outline in the GeneJET plasmid miniprep kit (Thermo Fisher Scientific). When higher concentrations of DNA were required plasmids were eluted in 25 μ l elution buffer.

2.1.9 Quantifying DNA Concentration

DNA concentration was measured using a NanoDrop 2000c spectrophotometer (Thermo Fisher Scientific) following manufacturer's instructions.

2.1.10 Ethanol Precipitation

To increase DNA concentrations after miniprep or gel extraction ethanol precipitations were used. The volume of the sample was determined and 0.1 volumes of 3 M sodium acetate (pH 5.2), and 3 volumes of 100% ethanol were added. Samples were incubated at -20 °C

overnight, centrifuged at 14,000 x *g* for 30 minutes. Pelleted DNA was rinsed with 100 µl of 70 % ethanol. Samples were centrifuged at 14,000 x *g* for 15 minutes. The supernatant was removed, pellets were air dried for 15 minutes on ice to allow remaining ethanol to evaporate. DNA was dissolved in tris acetate ESTA (TAE) (40 mM Tris-acetate, 1 mM EDTA, pH 8.3) to produced desired concentration.

2.1.11. Agarose Gel Electrophoresis

DNA samples were prepared in 6 x DNA loading buffer (NEB), mixing one part loading buffer with 5 parts of DNA sample. Agarose gels were prepared by dissolving agarose in Tris borate EDTA solution (TBE) (89 mM Tris borate, 2 mM EDTA, pH 8.3). Agarose was dissolved by heating in a microwave, replacing any water lost through boiling. 0.01 % (v/v) gel red, or SYBR safe was added when the agarose solution had cooled sufficiently. Agarose was poured into a gel tank and left to set, with appropriate comb. Samples were loaded into wells along with a DNA ladder (as indicated in figure). Gels were run in TBE buffer at 120 V for 90 minutes, or until the dye reached the end of the gel. Gels were imaged using the Bio-Rad Chemidoc MP imaging system

2.1.12. Gel Extraction

DNA from agarose gels was isolated using the protocol outlined in the GeneJET gel extraction kit (Thermo Fisher Scientific).

2.1.13. Restriction Digests

All restriction enzymes were purchased from New England Biolabs. 1 µg of DNA was digested overnight at 37 °C following the manufacturer instructions.

2.1.14 PCR

PCR reactions were prepared using the PfuUltra II Fusion HS DNA Polymerase (Agilent) following manufacturer's instructions. PCR conditions were different between primers and templates using manufacturer's optimised program templates.

2.2. Protein Extraction and SDS-PAGE

2.2.1. Casting SDS-PAGE gels

Gels were casted using the Bio-Rad Mini-PROTEAN® tetra handset system. Resolving gels were prepared using a specified concentration of polyacrylamide (typically 10 % (v/v)), 0.38 M Tris pH 8.8, 0.1 % w/v sodium dodecyl sulphate (SDS), 0.06 % w/v ammonium persulphate (sigma). 10 µl of Tetramethylethylenediamine (TEMED) was added prior to pouring. Gels were poured between spacer plates; a thin layer of isopropanol was added on top to remove bubbles. After the resolving gel had set, isopropanol was removed using filter paper. A stacking gel was prepared with concentration 5 % v/v polyacrylamide, 83 mM Tris pH 6.8, 0.07 % w/v SDS, 0.03 % w/v APS. Directly prior to pouring, 5 µl of TEMED was added. A 10 or 15 well comb was added and the gel was allowed to set. Gels were used immediately or stored at 4 °C wrapped in wet blue roll and saran wrap.

2.2.2. SDS-PAGE

Samples were run on either a 4–15% Mini-PROTEAN® TGX™ Precast Protein Gels (Bio-Rad) or 10 % self-cast gels resolving gels with 5 % stacking gels (Section 2.2.1.). Gels were run in a Mini-PROTEAN Tetra Cell tank (Bio-Rad). Mini-PROTEAN® TGX™ Precast Protein Gels at 200 V for approximately 35 minutes, or until dye front reached the base of the gel. Hand casted gels were run at 100 V for approximately 1 hour, or until sample dye reached the base of the gel.

2.2.3. Staining SDS-PAGE Gels

Protein on gels were stained with the ThermoFisher Scientific GelCode blue safe protein stain, or InstantBlue® Coomassie Protein Stain (Abcam).

2.2.4. Isolation of Protein from 15 cm and 10 cm Cell Culture Plates

Media was removed from plates. Cells were rinsed in 10 ml (5 ml for 10 cm plates) PBS supplemented with 1 mM DTT and aspirated. Cells were incubated in 10 ml (5 ml for 10 cm plates) PBS, 1 mM DTT at 4 °C for 5 minutes. PBS 1 mM DTT was removed, and plates were placed at 45 ° and incubated at 4 °C for 5 minutes. Remaining pooled buffer was aspirated, cells were scraped using a cell scraper to the bottom of the plate until all cells had been visibly removed from the surface. Cells slurry was collected, and the total volume was made up to 200 µl (100 µl for 5 cm plates) with buffer. 80 µl (40 µl for 5 cm plates) of 4 x loading buffer was added and PMSF to 1 µM. Samples were boiled at 95 °C for 10 minutes and stored at -20 °C.

2.2.5. Isolation of Cytosolic and Chromatin Fractions Through CSK Fractionation

To isolate cytosolic and chromatin fractions, cells were incubated in cytoskeletal buffer (CSK, 10 mM PIPES pH 6.8, 100 mM NaCl, 300 mM sucrose, 1 mM EDTA, 1 mM MgCl₂, 1 mM DTT, ROCHE complete Protease inhibitors) and harvested by scrape harvesting (Section 2.2.4.)

Cell slurry was split equally into two tubes. One was the total protein sample, and 40 µl (20 for 10 cm plates) of 4x SDS-PAGE loading buffer and 1 mM PMSF was added, prior to heating to 95 °C for 10 minutes. The other tube was used to separate the chromatin and cytosolic fractions. Cytosolic and chromatin fractions were isolated by addition of 5 µL 10 % (v/v) Triton X-100 for 5 minutes on ice, centrifuged at 14,000 x *g* for 5 minutes. 40 µl 4X SDS-PAGE loading buffer and 1 mM PMSF were added to the supernatant (cytosolic and nucleosolic proteins). The pellet (Chromatin) was resuspended directly in 100 µl 4X SDS-PAGE loading

buffer and 1 mM PMSF. Samples were heated to 95 °C for 10 minutes. Samples were stored at -20 °C.

2.2.6. Isolating Whole cell extracts from 6 Well Plates

Media was aspirated from wells; wells were washed with 1 ml PBS and 100 µl of 1 x SDS-PAGE loading buffer supplemented with 1 mM PMSF and protease inhibitors were added to wells. Cells were incubated at room temperature for 10 minutes on a rocker, rotating the plate by 90 ° halfway through. Plates were placed at 45 ° for 2 minutes. Whole cell extracts (WCE) were collected by pipetting against the surface of the well 3 times to ensure separation. Samples were incubated at 95 °C for 10 minutes. Samples were stored at -20 °C.

2.3. Western Blotting

2.3.1. Transferring Protein to Membranes

2.3.1a. Transferring Protein to Nitrocellulose Membrane

For western blot analysis proteins were run on SDS-PAGE then transferred to an Amersham™ Protran™ 0.45 µm nitrocellulose blotting membrane (GE Healthcare Life Sciences) using a semi dry transfer system. 8 pieces of filter paper and 1 piece of nitrocellulose membrane was cut for each gel (9 cm x 7 cm per gel). Filter paper, membrane, and protein gels were each soaked in transfer buffer: 0.75 mM Trizma® base (Sigma Aldrich), 10 µM CAPS (Sigma Aldrich), 10 % (v/v) ethanol, 0.01 % (w/v) SDS. 4 layers of filter paper were stacked on the base of the transfer system, then the nitrocellulose membrane, SDS-PAGE gel, and the final 4 filter paper layers. Protein transfers were run at 1 mA/cm² for 90 minutes.

2.3.1b. Transferring Protein to a Polyvinylidene Difluoride (PVDF) Membrane

For western blot analysis proteins were run on SDS-PAGE then transferred to an Amersham Hybond P 0.2 PVDF western blotting membrane (GE Healthcare Life Sciences) using a semi

dry transfer system. Filter paper and membrane were prepared as in 2.3.1a. Membrane was hydrated in 98 % ethanol and soaked in transfer buffer (0.75 mM Trizma[®] base (Sigma Aldrich), 10 μ M CAPS (Sigma Aldrich), 10 % (v/v) ethanol, 0.01 % (w/v) SDS) for 5 minutes. Components were stacked and transferred as in 2.3.1a.

2.3.2. Probing Membranes

Following transfer, membranes were blocked for 1 hour in 50 ml falcon tubes in 10 ml of blocking buffer (1 % (w/v) BSA, 0.05 M Tris (Sigma-Aldrich), 0.138 M NaCl (Sigma Aldrich), 0.0027 M KCl (Sigma Aldrich), 0.1% Tween-20), pH 8.0) on a roller. Following blocking, membranes were incubated with primary antibody at appropriate concentration (Table 2.2), in 5 ml of blocking buffer overnight at 4 °C. After the primary antibody incubation, membranes were washed 4 times for 5 minutes in 5 ml of blocking buffer. 5 ml of blocking buffer with an appropriate concentration of HRP conjugated secondary antibody was added for 1 hour. Membranes were washed 4 times for 5 minutes in 5 ml of washing buffer (0.05 M Tris (Sigma-Aldrich), 0.138 M NaCl (Sigma Aldrich), 0.0027 M KCl (Sigma Aldrich), 0.1% Tween-20 (supplier), pH 8.0).

Western blots were developed with the Bio-Rad Chemidoc MP imaging system. Blots were developed using Westar EtaC 2.0 or Westar supernova (Cyanogen) reagents. Developing times varied across different antibodies and samples.

2.3.3. Normalising Loads Across Western Blot Samples

Protein levels were equalised across western blots by comparing the levels of actin in cellular samples, and histone H3 in chromatin bound fractions, and *in vitro* experiments. Samples were loaded on SDS-PAGE gels at equal volumes, typically 10 μ l. SDS-PAGE gels were prepared and separated protein transferred to a nitrocellulose membrane. Blots were probed for actin or histone H3 and developed. Using the image lab software (BIO RAD) the

signal intensity was compared. To alter the volume to achieve equal loads values were standardising to the highest load and altering volumes loaded inversely proportionally. Gels for probing were reloaded with the altered volumes.

2.3.4. Antibodies

Antigen	Raised in	Usable Concentration (v/v)	Supplier
Rabbit IgG (HRP conjugated)	Goat	0.02 %	Abcam
Mouse IgG (HRP conjugated)	Goat	0.02 %	Sigma
MCM2	Mouse	0.2 %	BD biosciences
CIZ1	Rabbit	0.05 %	Covalabs – generated 2015.
Cyclin A	Mouse	0.2 %	Abcam Ab38
Cyclin E	Mouse	0.2 %	Santa Cruz biotechnology (HE12)
CDC6	Mouse	0.2 %	Santa Cruz Biotechnology (sc-9964)
PCNA	Mouse	0.2 %	Santa Cruz Biotechnology (sc56)
Actin	Mouse	0.05 %	Sigma
Histone H3	Rabbit	0.01 %	Abcam

Table 2.2.-Western blot antibodies, suppliers, targets, and species.

2.4. Mammalian Cell Culture

2.4.1. Growing Mammalian Cells

All passaging of cells was performed in a laminar flow hood using appropriate aseptic technique. Both S3 HeLa cells and NIH 3T3 cell were grown in GIBCO Dulbecco's modified eagle medium (DMEM) (1 g/l glucose, with pyruvate and glutaMAX), 10 % (v/v) labtech FBS, 1 % (v/v) GIBCO 100x penicillin streptomycin glutamine. A ThermoFisher Scientific Heracell 150i incubator was used. Cells were grown at 37 °C.

2.4.2. Passaging Mammalian Cells

Cells were passaged every 2 or 3 days unless being synchronised by quiescent release. Media was removed by serological pipetting and washing in 10 ml of D-PBS (GIBCO). Cells were then incubated in 10 ml of 0.05 % trypsin-EDTA (GIBCO) solution in D-PBS until cells no longer adhered to the base of plates (if being release from confluence a 0.1 % trypsin-EDTA solution was used for 4-5 minutes). The trypsin cell solution was split across the required number of plates containing 30 ml of DMEM.

2.4.3. Freezing Mammalian Cell Stocks

Cells were grown to approximately 50 % density in 15 cm dishes for general cell culture, or in 6 well plates for CRISPR-Cas9 treated cells prior to selection. For 15 cm plates, cells were washed in 10 ml of DPBS. Cells were trypsinised as described (Section 2.5.2). Cells were added to 10 ml D-MEM, inactivating the trypsin. The cell suspension was centrifuged at 500 x *g* for 5 minutes, the media was removed by pouring, the remaining cells were centrifuged at 500 x *g* for 1 minute, the remainder of media was removed by pipetting. The cell pellet was re-suspended in 15 ml of a 5 % (v/v) solution of dimethyl sulfoxide (DMSO) (SIGMA-Aldrich) in DMEM. Cells were separated into 1 ml aliquots in cryotubes. Cryotubes were added to a Mr. Frosty™ freezing container (Thermo Fisher Scientific) and frozen overnight at -80 °C and transferred to liquid nitrogen for long-term storage. The procedure for freezing cells from 6 well plates is identical, excluding PBS washes and trypsinisation were done in 2 ml, the cell trypsin solution was quenched in 2 ml of DMEM and only one 1 ml aliquot of each cell type was frozen.

2.4.4. Double Thymidine Arrest of HeLa Cells and S phase Synchrony

To produce S-phase cytosolic extracts for cell free replication assays the double thymidine synchrony method was used. For S phase synchrony of HeLa S3 cells were grown to 70 %

density in 15 cm cell culture dishes. Upon reaching the desired density, cells were incubated for 24 hours in 30 ml of DMEM and 2.5 mM thymidine (SIGMA ALDRICH). Following incubation, cells were washed in 10 ml DPBS, then 30 ml of fresh DMEM was added and cells incubated for 8 hours (Section 2.5.1). Following incubation, cells were washed in 10 ml of DPBS, buffer aspirated, 30 ml of DMEM + 2.5 mM thymidine was added and cells incubated for 16 hours. Following incubation, cells were washed in 10 ml DPBS, then 30 ml of fresh DMEM was added, this was treated as the 0 hour time point.

2.4.5. Quiescence Synchronisation of NIH 3T3 Cells

To produce a synchronous G1 population of NIH 3T3 cells, they were synchronised in G₀ by contact inhibition and serum depletion. Cells were cultured in 15 cm plates until they reached quiescence. Once confluent, media was replaced and cells incubated for a further 48 hours. Cells were then passaged either 1 in 4 on 15 cm plates, or 1 in 10 on 9 cm plates. This was treated as the 0 hour time point. Cells were harvested at 15 hours for reactions using G1 extracts or 17.5 hours for the production of late G1 nuclei for use in cell free assays.

2.4.6. EdU Labelling Fluorescence microscopy

EdU labelling was performed to measure the proportion of cells in S phase through fluorescence microscopy. Cells were grown in plates containing autoclaved coverslips. Cells were incubated with 10 μ M EdU (Thermo Fisher Scientific) 30 minutes (1 hour for flow samples) before harvesting coverslips were removed and placed in 24 well plates. Coverslips were removed and washed 3 x 3 minutes in 1 ml PBS. Coverslips were fixed with 0.2 ml 4 % PFA in PBS for 15 minutes at room temperature. PFA was removed and coverslips washed 3 x 3 minutes with 1 ml PBS.

EdU was fluorescently labelled using the Click-iT™ EdU Cell Proliferation Kit for Imaging (Thermo Fisher Scientific). Alexa Fluor 555 azide and Alexa Fluor 488 azide were used as

indicated. After labelling and washing coverslips were mounted onto glass slides with VECTASHIELD® Antifade Mounting Media with DAPI (Vector Laboratories).

EdU labelled and GFP fluorescent cells were imaged using a Zeiss Scope A1 fluorescent microscope. DAPI, Alexafluor 555, and GFP were imaged using the red, blue, and green filters respectively. Multi-channel images were generated using the Zeiss Zen software add channel process.

2.4.7. Cell cycle analysis with EdU Labelling by Flow Cytometry

1 hour before harvesting cells EdU was added to the media at a final concentration of 10 μ M. Cells were harvested by trypsinisation. Cell solution was quenched in 5 ml DMEM. Cells were centrifuged at 500 x *g* for 5 minutes. Pellets were washed 3 times in 1 % BSA PBS centrifuging for 5 minutes at 500 x *g* after each wash. Cells were permeabilised in 0.5 % triton X-100 for 20 minutes at 4 °C. Cells were centrifuged and washed 3 times in 1 % BSA PBS and centrifuged after each wash. Cells were labelled with 500 μ l of EdU labelling cocktail (from alexa fluor 488 azide Click-iT™ EdU Cell Proliferation Kit) for 30 minutes at 4 °C. Cells were washed 3 times in 0.1 % Triton X-100 in PBS and centrifuged after each wash. Propidium Iodide was added to a concentration of 50 μ g/ml. Cells were imaged using a Beckman Coulter CytoFLEX.

2.4.8. Mycoplasma Testing

Quarterly mycoplasma tests were performed as well as tests after generation of each new cell line. Tests were performed using the MycoAlert mycoplasma detection kit (Lonza). Upon a positive result cells were discarded and data obtained with infected cell lines were discarded.

2.5. *in vitro* DNA Replication Assays

2.5.1. Preparation of replication competent nuclei

Five 15 cm plates of NIH 3T3 cells were synchronised in G₀. Nuclei were harvested 17.5 hours after release from quiescence and cytosolic extracts 15 hours after release from quiescence. All steps were performed at 4 °C. Cells were washed in 10 ml of hypotonic buffer (20 mM HEPES (pH 7.8), 15 mM potassium acetate, 0.5 mM MgCl₂, 1 mM DTT), cells were incubated in 10 ml of hypotonic buffer for 5 minutes. Hypotonic buffer was removed and plates were left at an angle for a further 5 minutes. Any excess buffer was discarded and cells were scraped and harvested. Cells were dounce homogenised 7 times using the tight pestle and centrifuged for 5 minutes at 6000 RPM. The cytosolic extract was removed and the nuclei pellet was re-suspended in an equal volume (~200 µl) of hypotonic buffer. Nuclei were flash frozen and stored in 10 µl aliquots in liquid nitrogen.

2.5.2. Preparation of G₁ Extracts from NIH 3T3 Cells

G₁ extracts were prepared in the same manner as replication competent nuclei. Key differences were extracts were isolated at the 15.5 hour time point, cells were dounce homogenised 25 times, centrifugation was done at 14000 RPM for 15 minutes, and supernatant was stored discarding the pellet. Extracts were flash frozen and stored in 50 µl aliquots in liquid nitrogen.

2.5.3. Preparation of S Phase Extracts from HeLa Cells

S phase extracts were isolated in the same manner as G₁ extracts using double thymidine synchronisation (section 2.5.4). Extracts were isolated from 20 plates of S3 HeLa cells 1 hour after release from a double thymidine block. Extracts were flash frozen and stored in 50 µl aliquots in liquid nitrogen.

2.5.4. Preparation of 10x Premix Solution

10 x premix solutions were prepared to a final concentration of: 40 mM HEPES, pH 7.8, 7 mM MgCl₂, 1 mM DTT, 40 mM phosphocreatine (CALBIOCHEM/MERCK), 3 mM ATP, 0.1 mM GTP, 0.1 mM CTP, 0.1 mM UTP, 0.1 mM dATP, 0.1 mM dGTP, 0.1 mM dCTP. All nucleotides were added slowly to avoid unresolvable precipitation.

2.5.5. Preparation of Creatine phosphokinase (CPK) Buffer

CPK buffer was prepared with the following concentrations: 40 mM HEPES, pH 7.8, 7 mM MgCl₂, 1 mM DTT.

2.5.6. *In vitro* Cell Free DNA Replication Reactions

The volume of *in vitro* reactions changed depending on the experiment. Samples for counting using epifluorescence microscopy were typically from 10 µl reactions, Samples for analysis via western blotting or DNA combing were typically from 50 µl reactions. The ratio of each component added to each *in vitro* reaction are displayed in Table 2.3 Any protein or small molecule added to reactions were dissolved in CPK buffer.

Component	Ratio to extract
0.1 M MgCl ₂	1:50
10 µg/ml creatine phosphokinase (CPK)	1:50
Biotin-16-dUTP	1:50
Premix Solution	1:10

Table 2.3 – Recipe for *in vitro* replication assay buffers

Reactions were performed at 37 °C for 30 minutes. For analysis by Western blot, one third of the volume was removed and prepared for SDS-PAGE this was the total protein. 2 µL of 10 % (v/v) Triton X-100 was added to the remaining sample for 2 minutes, sample centrifuged at 12,000 x g for 5 minutes. The supernatant was removed and 20 µL 4 x SDS-PAGE buffer prior to heating to 95 for 10 minutes. The chromatin pellet was re-suspended in 30 µL 4 x SDS-PAGE buffer mixed with 90 µL of hypotonic buffer prior to heating to 95 °C for 10 minutes and samples stored at -20 °C until use.

2.6 CRISPR/Cas9

2.6.1. Primer Design

DNA oligonucleotide primers were designed by identifying protospacer adjacent motif (PAM) sequences early in the gene desired to be knocked out. PAM sequences are the target for the Cas9 nuclease they have the sequence NGG where N is any nucleotide. 20 nucleotides directly 5' of the chosen PAM sites were used as the template for the CRISPR primers. For insertion into the GeneArt® CRISPR nuclease vector (thermofisher) a 3' overhang was added with sequence GTTTT. For the complimentary oligonucleotide the 20 nucleotide target sequence was reverse transcribed. For insertion into the GeneArt® CRISPR nuclease vector (thermofisher) a 3' overhang was added with sequence CGGTG. DNA Oligonucleotides were synthesised by and purchased from Eurofins genomics. The 4 oligo nucleotides designed for generating CIZ1 knockout NIH3T3 cells are displayed in Table 2.4.

DNA Oligonucleotide Name	DNA Oligonucleotide Sequence
CIZ1 KO1 for	5' - TTGCTCCTACAGCAGTTGCAGTTTT- 3'
CIZ1 KO1 rev	5' -TCGAACTGCTGTAGGAGCAACGGTG - 3'
CIZ1 KO2 for	5' - CAAGGTATGGCAGTCCCCGGTTTT - 3'
CIZ1 KO2 rev	5' - CGGGGAACTGCCATACCTTGCGGTG - 3'

Table 2.4 – Primers Used for Generating CIZ1 Cells Using CRISPR Cas9

2.6.2. Annealing Complimentary Oligonucleotides

Oligonucleotides were dissolved in ultrapure DNase free water to yield a concentration of 200 μM . 5 μl of each primer were mixed with oligonucleotide annealing buffer and made up to 10 μl in DNase/RNase free water. Reaction mixtures were heated for 4 minutes at 95 $^{\circ}\text{C}$ then left at room temperature for 10 minutes. Once annealed the double stranded oligonucleotides were serially diluted from 50 μM to 5 nM in oligonucleotide annealing buffer. The 5 nM solution was either used or stored at -20 $^{\circ}\text{C}$.

2.6.3. Ligating Double Stranded Oligonucleotides into the GeneArt[®] CRISPR Nuclease Vector

20 μl ligation mixtures were prepared in DNase/RNase free water with concentrations 50 mM Tris HCl, pH 7.6, 10 mM MgCl_2 , 1 mM ATP, 1 mM DTT, 5% (w/v) polyethylene glycol-8000, 1.5 ng/ μl linearized CRISPR nuclease vector, 1 mM Tris HCl, pH 8, 100 μM EDTA, pH 8, 0.5 nM double stranded oligonucleotide. Ligation mixtures were gently mixed, then incubated at room temperature for 10 minutes. Ligation mixtures were transformed into TOP10 *E. coli* competent cells using the procedure outlined in Section 2.1.4.

2.6.4. Purifying Plasmid DNA

Single colonies were picked from LB agar plates following transformation and inoculated into 5 ml of LB broth supplemented with 100 $\mu\text{g}/\text{ml}$ ampicillin and grown overnight at 37 $^{\circ}\text{C}$. Plasmid DNA was purified from top 10 *E. coli* using the Thermo Fisher Scientific Gene JET plasmid Miniprep kit. Plasmid concentration was quantified using a Thermo Fisher Scientific nano drop 2000c spectrophotometer.

2.6.5. Sequencing GeneArt[®] CRISPR Nuclease Vector

Sequences inserted into the linearized GeneArt[®] CRISPR Nuclease Vector to be sent to be sequenced were diluted to 50 – 100 ng/ μl . Diluted plasmids were sequenced by eurofins

genomics using the U6 forward primer. The sequence of the U6 forward primer (5' - GGACTATCATATGCTTACCG - 3').

2.6.6. Transfection of NIH3T3 Cells

NIH 3T3 cell transfection was performed using the Amaxa® Cell Line Nucleofector® Kit R (Lonza). NIH 3T3 cells were grown to between 70 – 80 % confluence, cells trypsinised, and trypsin quenched with 5 ml of DMEM. Cells were harvested by centrifugation at 500 x *g* for 5 minutes, supernatant was removed, and then centrifuged for a further minute at 500 x *g*, and remaining supernatant removed. Cells were re-suspended in 100 µl of Kit R solution with 2µl DNA and transferred to electro cuvettes. Cells were transfected using the NIH 3T3 programme (U-030) using the Lonza nucleofector 2b electroporation system. Transfected cells were added to 30 ml of DMEM, plated on to 15 cm dishes and incubated.

2.6.7. Enrichment of Transfected CRISPR Cas9 Cells

24 hours following transfection with the GeneArt® CRISPR Nuclease Vector cells were to be selected and enriched. Successfully transfected cells were selected using CD4 expression. Cells were harvested by trypsinisation and centrifugation at 500 x *g* for 5 minutes. Cells were suspended in 2 ml of enrichment buffer (PBS, 0.1 % BSA, 2 mM EDTA) and centrifuged, this was repeated a further two times. After the final centrifugation cells were resuspended in 50 µl of enrichment buffer. Concurrently, 25 µl of Dynabeads® CD4 magnetic beads (Thermo Fisher Scientific) were placed on a magnetic separator for 1 minute, the supernatant was discarded and beads resuspended in 100 µl of enrichment buffer. The beads were placed on a magnetic separator, supernatant removed and resuspended in 25 µl of enrichment buffer. The cells and beads were added together and made up to 1 ml with enrichment buffer. The bead cell mixture was incubated at 4 °C on a rotator for 30 minutes.

Cells were placed on a magnetic separator for 1 minute, the supernatant was discarded and cells were re-suspended in 500 µl of enrichment buffer. This process was repeated 6 times. Cells were placed on a magnetic separator for 1 minute, beads re-suspended in 100 µl of DMEM and 10 µl DETACHaBEAD® CD4 for 45 minutes on a rotator. The supernatant was removed and stored; beads were washed in 500 µl of DMEM 3 times recovering the supernatant each time. Supernatants were made up to 4 ml and centrifuged at 500 X g for 5 minutes. Pellets were re-suspended in DMEM, cells were counted and diluted to approximately 5 cells/ml. Cells were plated into 96 well plates and incubated at 37 °C.

24 hours after enrichment, the number of cells in each well was determined by microscopy. Wells that contained single cells were selected to be grown further. They were grown up to 96 well plates via 24 well plates and 6 well plates. At this stage cells were frozen for storage in liquid nitrogen and cells were prepared for SDS-PAGE to determine which cells were CIZ1 knock outs.

2.7 DNA Combing

2.7.1. Pulse Labelling of Cells

This describes a basic pulse labelling; timings of pulses were typically 20 minutes for each nucleotide. However, incubation may vary and this will be indicated in the figure in the experimental design image.

2.7.1a. Dual labelling with IdU and CldU

Cells were cultured to 70-80 % confluence. Media replaced with 30 ml media supplemented with 25 µM iododeoxyuridine (IdU) and incubated for 20 minutes. Media was removed, cells were washed with 10 ml PBS. Cells were incubated in 30 ml of DMEM media + 250 µM chlorodeoxyuridine (CldU) for 20 minutes. Cells were then harvested by trypsinisation, and quenched in 5 ml DMEM. Cells were centrifuged at 500 x g for 5 minutes. Supernatant was

discarded, and cells were centrifuged at 500 x *g* for 1 minute to remove remaining media.

Cell pellets were encapsulated in agarose (Section 2.8.4).

2.7.1b. Single Labelling with EdU

Cells were prepared for DNA combing as in section 2.8.1a, except cells were incubated in 30 ml of DMEM supplemented with 10 μ M EdU for 1 hour at 37 °C to label DNA, all other steps were identical.

2.7.2. Pulse Labelling of Nuclei in cell free DNA replication Assays.

Nuclei were sequentially pulse labelled in S phase extracts (Section 2.6.3.), nuclei were pulse labelled with numerous modified nucleotides specified in experimental design. Between pulse labelling nuclei were centrifuged at 500 x *g* for 5 minutes then resuspended in fresh extracts with the second modified nucleotide.

2.7.3. Producing Silanized Coverslips.

22 mm by 22 mm by 0.5 mm square coverslips (Agar Scientific) were homogenously coated in a hydrophobic layer of trimethoxysilane for DNA combing experiments. All steps were performed in a fume hood. Coverslips were placed in Teflon racks in the bottom of autoclaved 250 ml heavy duty beakers. Coverslips were moved to clean beakers after every wash. Coverslips were rinsed in 120 ml of acetone (Fisher) for 1 minute. Coverslips were dried, transferred to a fresh beaker, and washed in 120 ml 50% (v/v) methanol for 20 minutes in an ultrasonic water bath. Coverslips were air dried, transferred to a fresh beaker then washed in 120 ml chloroform (Sigma Aldrich) for 20 minutes in an ultrasonic water bath. Coverslips were air dried and transferred to an ultrasonic water bath. Coverslips were washed for 20 minutes in 120 ml of piranha solution (70 % (v/v) sulfuric acid 99% (w/v), 30 % (v/v) hydrogen peroxide 35 % (w/v) in a 60 °C water bath. Coverslips were removed from

piranha solution and left until the majority of viscous acid had run off the coverslips.

Coverslips were washed in 120 ml of water in an ultrasonic water bath for 5 minutes.

Coverslips were washed in 120 ml of chloroform in an ultrasonic water bath for 5 minutes, followed by a water wash. Chloroform and water washes were repeated until viscous acid was visibly removed from the coverslip and air dried.

Coverslips were submerged in 120 ml of 0.1 % (v/v) (7-octen-1-yl) trimethoxysilane in heptane (Sigma Aldrich) overnight in a desiccator. Coverslips were washed in an ultrasonic waterbath for all subsequent steps. Coverslips were washed in heptane (Sigma Aldrich) for 5 minutes, coverslips removed, washed in 120 ml of water for 5 minutes, and washed in 120 ml of chloroform (Sigma Aldrich) for 5 minutes. Coverslips were air dried and silanized coverslips stored individually in 50 ml falcon tubes in the dark in a desiccator.

2.7.4. Purification of DNA

Following *in vitro* replication assays, reactions were centrifuged and suspended in 115 μ l of PBS and warmed to 42 °C. Concurrently, 1 % (w/v) low melting point agarose in PBS was prepared, melted at 65 °C and cooled to 42 °C for 15 minutes. 98 μ l of low melting point agarose was added to the warmed nuclei solution. The agarose nuclei solution was added to agarose plug moulds (BIO-RAD), 100 μ l per plug. Agarose was set at 4°C for 30 minutes. Plugs were digested overnight in 2 mg/ml proteinase K (Bio-Rad) at 42 °C.

Plugs were washed for 60 minutes in 10 ml of 0.2 μ m filtered TNE 50 buffer (10 mM Tris HCl, pH 7.5, 20 mM NaCl, 50 mM EDTA). This was repeated 3 further times, incorporating 1 mM PMSF on the penultimate wash. At this stage plugs could either be stored short term in the fridge or the DNA purified and combed. After the final wash in TNE 50, plugs were washed for half an hour in 2 ml of 0.2 μ m filtered MES EDTA buffer (50 mM MES (pH 5.7)). Plugs were warmed to 65 °C for 15 minutes in 0.2 μ m filtered MES EDTA buffer. Agarose plugs were

allowed to reach 42 °C, then 100 µl of 2 % (v/v) beta agarose 1 (New England Biolabs) added and incubated overnight, releasing the naked genomic DNA.

2.7.5. DNA Combing

DNA solution (from section 2.8.2) was slowly poured into a Teflon block with 25 x 25 x 4 mm milled well. DNA was combed using the KSV NIMA dip coater system (Biolin Scientific).

Silanised coverslips were clipped onto the combing apparatus and lowered into the DNA solution. Coverslips were incubated in the DNA solution for 10 minutes prior to removal from solution at 300 µm/second. Coverslips were glued to slides using cyanoacrylate glue on each corner. A second 22 x 22 mm coverslips was mounted on top of the coverslip with DNA bound to its surface using Prolong diamond anti-fade mountant (Thermo Scientific).

2.7.6 Labelling and Imaging

2.7.6a. Yoyo1 labelling

Samples from *in vitro* replication experiments were labelled using 0.1 µM YOYO - 1 iodide (ThermoFisher Scientific) prior to combing. DNA was imaged using a Zeiss LSM 880 confocal microscope.

2.7.6b. Antibody Labelling of IdU, CldU, and ssDNA

All wash steps were performed in coplin jars. After combing, coverslips were incubated at 60 °C for 1 hour. DNA was denatured in 0.5 M NaOH for 30 minutes at room temperature. Slides were washed 3 x 3 minutes in washing buffer (0.1 % v/v Tween 20, PBS, pH 7.4) slides transferred to a humidity chamber and blocked in 200 µl blocking buffer (3% BSA, 0.1 % v/v Tween 20, PBS 7.4) at 37 °C for 1 hour. Blocking buffer was removed and 50 µl of primary antibody solution 1 was added (Table 2.5). Primary antibody solutions were incubated overnight at 4 °C.

Slides were washed 3 x 3 minutes in washing buffer, transferred to a humidity chamber, 50

Solution	Antibody	Species Raised	Concentration	Supplier
Primary Antibody Solution 1	IdU	Mouse	1/20	BD Biosciences 347580
	CldU	Rat	1/125	Serotec OBT0030
Primary Antibody Solution 2	ssDNA	Mouse	1/50	Merck Millipore MAB3034
Secondary Antibody Solution 1	Anti-Rat IgG Alexa Fluor 488	Chicken	1/50	Thermo Fisher Scientific A-21470
	Anti-Chicken IgY Alexa Fluor 488	Goat	1/50	Thermo Fisher Scientific A-11039
	Anti-Mouse IgG Alexa Fluor 633	Goat	1/50	Thermo Fisher Scientific A-21050
Secondary Antibody Solution 2	Anti-Mouse IgG Alexa Fluor 568	Rabbit	1/50	Thermo Fisher Scientific A-11061
	Anti-Rabbit IgG Alexa Fluor 568	Goat	1/50	Thermo Fisher Scientific A-11036
Primary antibody solution 3	Digoxigenin	Mouse	1/50	Abcam (AB420)
Secondary antibody solution 3	Anti-Mouse IgG Alexa Fluor 633	Goat	1/50	Thermo Fisher Scientific A-21050

Table 2.5 – Antibodies used for DNA combing experiments

μl of secondary antibody solution 1 (Table 2.5) added and incubated at 37 °C for 30 minutes. Slides were washed 3 x 3 minutes in washing buffer, transferred to a humidity chamber and 50 μl of primary antibody solution 2 was incubated for 2 hours at room temperature. Slides were washed 3 x 3 minutes in washing buffer, 50 μl of secondary antibody solution 2 was added and incubated for 30 minutes at 37 °C. Slides were washed 3 x 3 minutes in washing buffer and slides mounted on a 22mm by 22mm square coverslip with ProLong™ Gold Antifade Mountant (Thermo Fisher Scientific)

2.7.6c. EdU Labelling (Denatured DNA)

All wash steps were performed in coplin jars. After combing, coverslips were incubated at 60 °C for 1 hour. DNA was denatured in 0.5 M NaOH for 30 minutes at room temperature. Slides were washed 3 x 3 minutes in washing buffer (0.1 % v/v Tween 20, PBS, pH 7.4). Slides were transferred to a humidity chamber and blocked in 200 µl blocking buffer (3% BSA, 0.1 % v/v Tween 20, PBS 7.4) at 37 °C for 1 hour, blocking buffer removed and 50 µl of EdU labelling cocktail was added and incubated at 37 °C for 30 minutes. Slides were washed 3 x 3 minutes in washing buffer, transferred to a humidity chamber and 50 µl of primary antibody solution incubated for 2 hours at room temperature. Slides were washed 3 x 3 minutes in washing buffer, 50 µl of secondary antibody solution 2 was added and incubated for 30 minutes at 37 °C. Slides were washed 3 x 3 minutes in washing buffer. Slides were mounted with 22mm by 22mm square coverslip with ProLong™ Gold Antifade Mountant (Thermo Fisher Scientific).

2.7.6d. EdU Labelling (dsDNA)

DNA was pre-labelled with YOYO-1, After combing DNA was treated exactly as in 2.8.4b. omitting the denaturing and antibody labelling steps. Additionally, Alexa fluor 555 azide was used rather than Alexa Fluor 488 azide. After the Click-It reaction and washing slides were mounted with 22mm by 22mm square coverslip with ProLong™ Gold Antifade Mountant (Thermo Fisher Scientific).

2.7.4e. Digoxigenin labelling

EdU labelling was performed as in 2.8.4c. After Edu Labelling and washing, cells were transferred to a humidity chamber where 50 µl of primary antibody solution 3 was added, incubated overnight at 4 °C. Slides were washed 3 x 3 minutes in washing buffer 50 µl of secondary antibody solution 3 was added and incubated at 37 °C for 30 minutes. Slides were washed 3 x 3 minutes in washing buffer, 50 µl of primary antibody solution 2 was added and

incubated for 2 hours at room temperature. Slides were washed 3 x 3 minutes in washing buffer, 50 µl of secondary antibody solution 2 was added and incubated for 30 minutes at 37 °C. Slides were washed 3 x 3 minutes in washing buffer. Slides were mounted with 22mm by 22mm square coverslip with ProLong™ Gold Antifade Mountant (Thermo Fisher Scientific).

2.7.5a. Imaging of Combed DNA

DNA combing images were captured using a Zeiss LSM 880 confocal microscope. ssDNA labelled with Alexafluor 568, IdU labelled with Alexafluor 633, and CldU labelled with alexafluor 488 were excited with the 568, 633, and 488 nm lasers respectively and captured using 568-640 nm, 638-747 nm, and 493-598 nm ranges. dsDNA labelled with YOYO1 and EdU labelled with Alexafluor 555 were excited with the 568 and 488 nm lasers respectively. For both experimental approaches each fluorophore was captured on a separate track to minimise bleed through effects .

2.7.4b Analysis of Replication Tracks

Lengths on DNA fibres were calculated with image J using the straight line measure tool. For each length the 2 furthest points colocalised to DNA were used to define the replication track.

2.8. Statistical Analysis

Where only two groups were involved the means were compared using the students T-test, p values were calculated with Microsoft excel. When multiple comparisons were required for a single factor (e.g. DNA Combing experiments) experimental means were compared using a one way analysis of variance (one-way ANOVA) followed by post-hoc pairwise comparisons by a Tukey's honestly significant difference (HSD) test using SPSS. When multiple comparisons were required across two factors (e.g.) a two way analysis of variance (two-

way ANOVA) was performed using SPSS followed by post-hoc pairwise comparisons using simple main effects analysis.

Chapter 3.

**Optimisation of DNA Combing for Cell Based
and Cell Free analysis of DNA replication
kinetics**

3.1. Introduction

3.1.1 Introduction to DNA Combing

DNA combing was first described by Bensimon et al. (1994). In this seminal paper, viral & bacterial genomes were stretched onto silanised cover slips using the force of a constant movement through an air water meniscus. This established the principle that uniformly stretched lengths of DNA could be visualised by fluorescence microscopy. This work was extended to refine the forces and optimal hydrophobic surfaces required to stretch DNA consistently and enabled measurement of the tensile strength of DNA (Bensimon et al., 1995). DNA combing was used by Michalet et al. (1997) to map deletions in disease genes using hybridised fluorescent DNA probes. Direct measurement of differences in distance allowed the observation and measurement of disease related genomic deletions. This approach was further modified using novel nucleotide analogues that are incorporated into nascent DNA during replication and imaged using immunofluorescent techniques (Jackson & Pombo, 1998) (Figure 3.1).

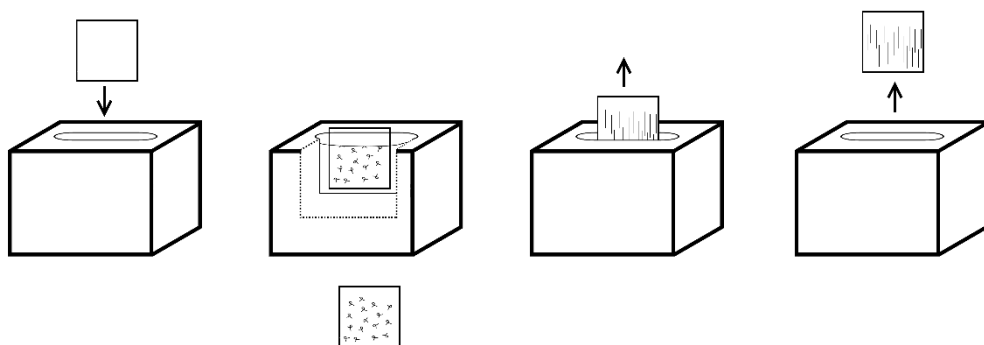


Figure 3.1-DNA Combing Schematic. A schematic diagram displaying the process of DNA combing. A silanized coverslip is placed into a DNA solution in a Teflon well. After a DNA binding step the coverslip is removed at a constant rate to allow uniform stretching of DNA.

Concurrently the fibre stretching assay was developed by Parra & Windle (1993). The major difference between DNA combing and fibre stretching is that fibre stretching uses cells lysed on slides tilted allowing the DNA solution to run down the slide, aligning the DNA. The first use of fibre stretching mapped fluorescent tags to DNA, a technique that was adapted with DNA combing by Michalet et al. (1997). This assay provides less consistent stretching, and DNA from single cells, but is less technically difficult, less time consuming, and requires less specific technical equipment than DNA combing.

DNA combing has primarily been used to measure and monitor DNA replication stress through high precision measurements of changes in DNA replication dynamics. Fluorescent labelling of modified nucleotides on combed DNA was first used by Jackson & Pombe (1998). In this paper, the dynamics of replication origin firing within replicons was measured using a single pulse labelled BrdU step. By extending the length of pulse labelling, differences in replication dynamics over time were observed. Merrick et al. (2004) further developed the dual labelled technique to measure DNA replication dynamics. This method remains in common use today and is used in Chapter 6 to investigate the effects of CIZ1 knock out on DNA replication kinetics. The use of sequential iododeoxyuridine (IdU) and chlorodeoxyuridine (CldU) treatments allowed high precision measurements of several replication parameters including replication fork velocity, origin firing, and DNA replication fork stalling. These parameters are often altered during DRS. For example, DNA damaging agents slow replication fork progression, blocking new origin firing, and increase replication fork stalling (Gaillard et al., 2015; Macheret et al., 2015; Técher et al., 2017). Together these early innovators provided the tools that are used ubiquitously today to monitor DNA replication dynamics.

3.1.2. Using DNA Combing to Measure DNA Replication Dynamics

To determine the rate of replication fork progression, it is necessary to differentiate between replication origin firing, elongation and termination events. The use of a single label does not allow this without the ability to control the simultaneous firing of all origins (possible in yeast) (Bianco et al., 2012; Hiraga et al., 2018). A sequential dual labelling approach with differentially labelled nucleotides is required to achieve discrimination as this produces unique patterns for each initiation, elongation and termination.

DNA combing typically used to determine replication fork velocity. This is achieved through two sequential equal length (typically 20 minutes) pulse-labelling steps with two different modified nucleotides (typically IdU, and CldU) (Figure 3.2).

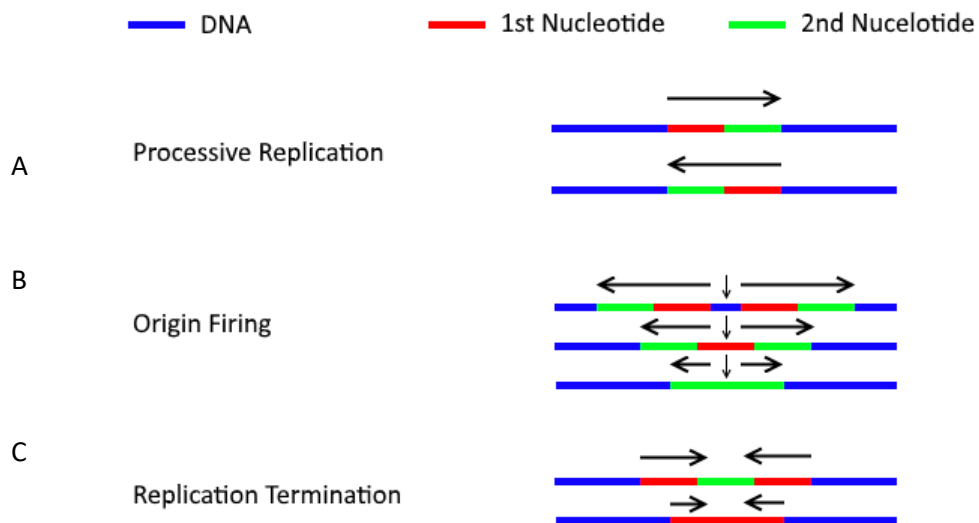


Figure 3.2.-DNA Replication Event Schematic. A schematic displaying how different replication events are visualised using a dual labelled DNA combing approach. A) An actively replicating fork is represented by neighbouring replication tracks from each nucleotide, the order of colours determines the direction. B) Origin firing is represented by symmetrical replication tracks. Timing of origin firing determines the appearance of origins. C) Similarly, termination events are represented by symmetrical patterns, however the second nucleotide appears at the centre (C).

To measure replication fork velocities, origin firing during the second pulse labelling step, and termination events are excluded from the dataset, as DNA replication either ended early (termination) or started late (origin firing). Both events prevent incorporation of the modified nucleotide to occur for the entire duration of the second pulse label and would inaccurately reduce fork speeds. For each remaining replication event the length of the second pulse labelling track is measured, this value is then converted to kbp/min using the known stretching factor (1 μm = 2 kbp) and incubation time. The median value of this provides an accurate measure for the replication fork velocity for a specific cell line in specific conditions. This is summarised in Figure 3.3.

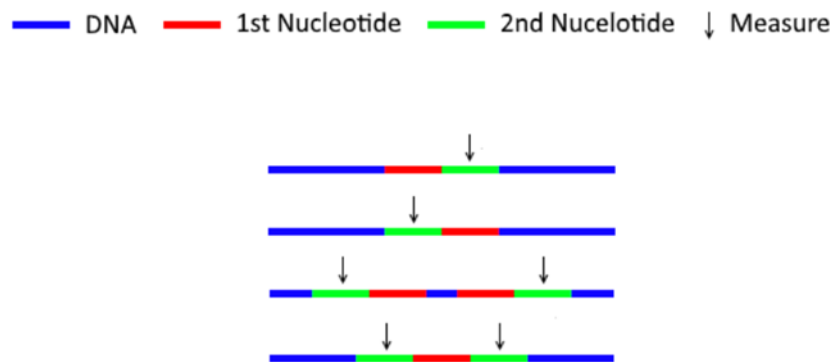


Figure 3.3-Measuring Replication Fork Rate. A schematic diagram displaying how to measure replication fork rate using DNA combing. Blue represents DNA, Red represents the first labelling nucleotide, Green represents the second labelling nucleotide.

Critically, the fork rate changes when cells are under DRS. DNA combing has been used to demonstrate DRS induction in pre-senescent and senescent cells is independent of replication timing changes. This research revealed that replication fork velocities slowed in pre-senescent and senescent cells, however replication timing remained unchanged. This

demonstrated the degradation of function of senescent cells over time (Rivera-Mulia et al., 2018).

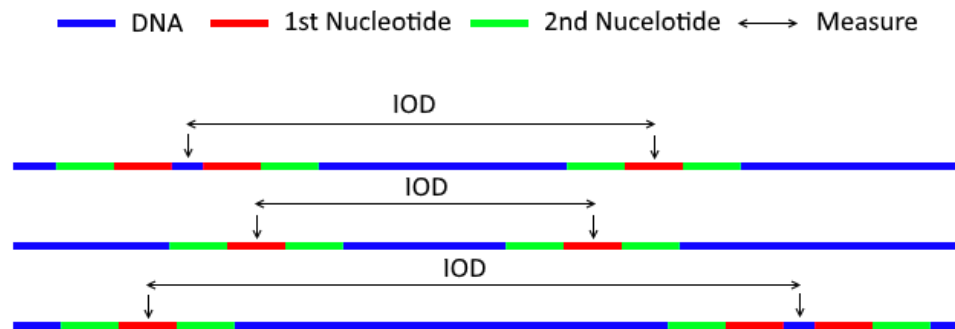


Figure 3.4 – Measuring IOD Using DNA Combing A graphical schematic displaying two representative images of DNA combing of neighbouring origins.

During DRS, cells activate ‘cryptic’ origins to facilitate timely completion of DNA replication (Courtot et al., 2018). Activation of cryptic origins can result in a reduction in the intra-origin distance (IoD) between replication origins and this value reduces the more cryptic origins activated. The activation of cryptic origins depletes replication factors, such as the ssDNA binding protein RPA, which can cause aberrant DNA replication and recombination events (Toledo et al., 2013). Incomplete replication would result in problems during mitosis, such as anaphase bridges.

IOD is measured using the same pulse labelling technique as used to measure replication fork velocity. Cycling cells are sequentially pulse labelled for equal time (typically 20 minutes) with two different modified nucleotides (typically IdU and CldU). For IOD measuring, termination events and processive replication fork patterns are excluded from analysis and adjacent origins on the same fibre of DNA are measured (Figure 3.4).

Median IOD changes as replication dynamics change. This technique has been used to demonstrate that as cells become terminally differentiated, their IOD becomes shorter. It

was proposed that this was due to chromatin becoming more tightly packed in more differentiated cells (Estefanía et al., 2012). This would cause a decrease in the speed of replication forks, so more active origins are required to replicate DNA in a timely manner.

A third parameter that can be measured through DNA combing is replication fork stalling. Cells under replication stress stall forks. Stalled forks activate cell cycle checkpoints and trigger the DDR. If stalled forks can be resolved, DNA replication can continue. If resolution is not possible, stalled forks are a major signal for the induction of apoptosis. Failure to manage stalled forks during S phase can result in incomplete replication of DNA, leading to mitotic defects, some of which promote growth defects and tumorigenesis (Pond et al., 2019).

For the first method of measuring replication fork stalling rates only the processing replication fork patterns are measured (Figure 3.2). If DNA replication is unperturbed, the replication forks rate is comparable between the first and the second pulse labelling and this would remain true if DNA replication is slowed during DRS. Therefore, unperturbed replication should produce dual labelled replication tracks with equal lengths. Whereas, if there is an increase in fork stalling rates, the fork rate for the first and second pulse labelling events will deviate. The ratio between the observed rates for the first and second pulse labels will shift away from 1 where there is extensive fork stalling (Tourrière et al., 2017).

Any increase in replication fork stalling, increases the probability of fork stalling during pulse labelling for both the first and the second modified nucleotide. Stalling events during the first pulse labelling cannot be distinguished from termination events during the first pulse labelling, both will be resolved as a single labelled replication track of the first nucleotide, as DNA replication will stall before the second pulse labelling. However, replication stalling events during the second nucleotide are detectable. Unstalled forks should maintain their IdU : CldU length ratio (i.e. 1). However, if replication forks are stalled during the second

CldU labelling the ratio will shift, as. CldU labelling will be reduced relative to IdU, resulting in a ratio shift away from 1 as fork stalling increases (Figure 3.5).

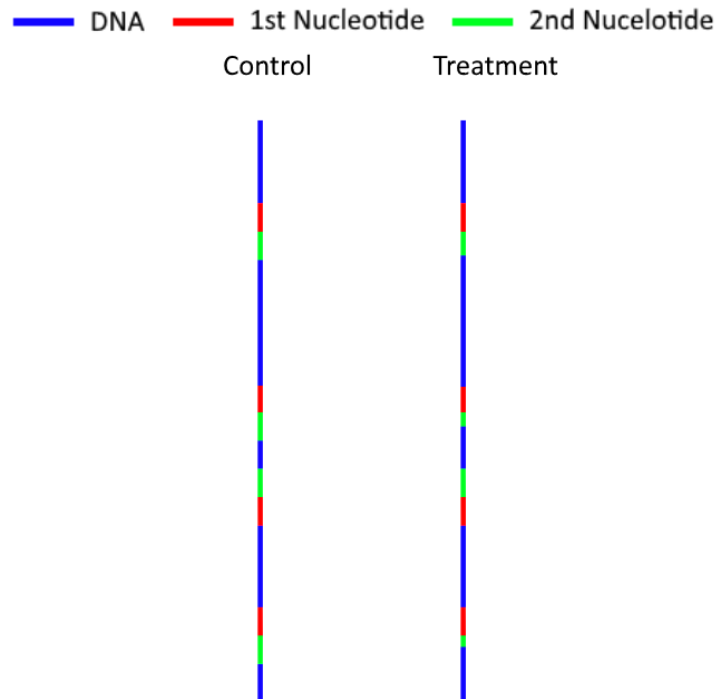


Figure 3.5 - Measure Replication Fork Stalling Through IdU:CldU Length Ratio – a graphical schematic displaying two representative images of DNA combing of processive replication tracks for samples where DNA fork stalling rates were not increased (control) and samples where replication fork stalling rate was increased (treatment).

The second method to measure replication fork stalling rates uses sequential pulse labelling reactions of equal length and determines the fork rate for both events. For this method, origins that are fired either before or during the first pulse labelling period are used (summarised in Figure 3.2). If fork stalling rates are low, both replication forks from each origin (sister replication forks) would progress at a similar rate, yielding sister replication tracks will be of comparable length. However, where replication fork stalling occurs, there is a deviation in the sister replication forks rate, leading to asymmetric fork rates (Quinet et al., 2017). This can be observed by plotting a scatter graph of the length of the second nucleotide pulse of the left track against the second nucleotide pulse of the right track of

sister replication tracks. Lower replication fork stalling rates lead to lower fork asymmetry. This results in a tight correlation between the left and the right track. Higher fork stalling rate reduces fork symmetry and produces a looser correlation between the lengths of the sister replication tracks. This can be measured either by the strength of the correlation between the track lengths, or an average of the ratio of the length of sister replication tracks (Figure 3.6).

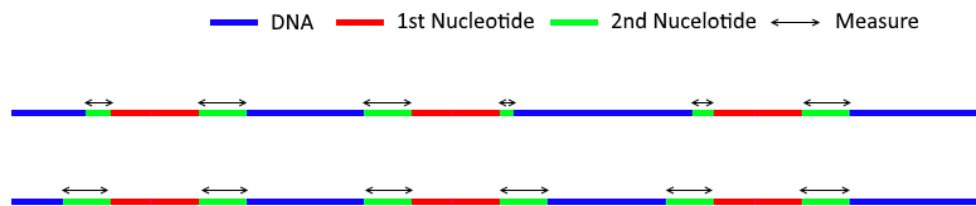


Figure 3.6 – Measuring Replication Fork Stalling Through Replication Fork Asymmetry. A graphical schematic displaying two representative images of DNA combing of processive replication tracks for samples where DNA fork stalling rates were not increased (control) and samples where replication fork stalling rate was increased (treatment).

This technique has been used to demonstrate that depletion of topoisomerase I increases the rate of fork stalling. Topoisomerase I acts at contact points between replication at transcription machinery. This experiment showed that siRNA depletion significantly increased replication fork asymmetry. Loss of topoisomerase I increased polymerase clashing as cells could no longer maintain replication (Tuduri et al., 2009).

Another parameter that can be measured at high resolution by DNA combing is replication fork restart rates. When cells are under replication stress processing replication forks can stall. This can be through collisions with transcription machinery or through the activation of the DDR. Changes in replication fork restart rates give information as to how well the cell is

able to respond to stress. Low concentrations of a drug may allow fork restart whereas high concentrations may prevent it. Changes in this can result in changes in how cells are able to respond to stress. To measure replication fork restart rates, cells are treated with one modified nucleotide (typically IdU) for 1 hour, followed by a 2 hour treatment with a drug or treatment that is expected to induce replication fork stalling (e.g. hydroxyurea), followed by a 20 minute treatment with a second modified nucleotide (typically CldU). This will reveal both stalled and restarted forks, as stalled forks will only be labelled with the first nucleotide, whereas restarted forks will be dual labelled (Figure 3.7).

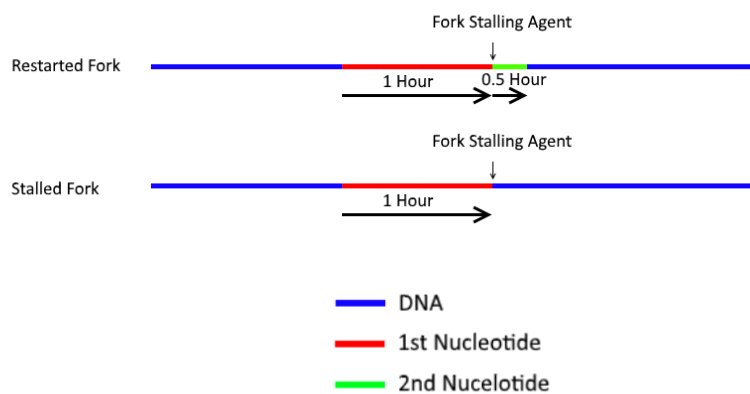


Figure 3.7- Measuring Replication Fork Restart Rate A) Schematic of approach to measure replication fork restart rate using DNA combing with representative images.

This technique has been used to demonstrate that depletion of the nuclease proteins XPF-ERCC1 and ARTEMIS results in a decrease in the rates that cells can restart forks stalled by hydroxyurea (Betous et al., 2018). It was proposed that these proteins could cleave DNA at stalled forks to promote a rapid restart of DNA replication at these sites. Similar to the mechanism of MUS81-EME1 after long period under DRS. This work identified a novel pathway for maintaining replicative integrity during DRS.

3.1.3 Chapter Aims

Consistent stretching of DNA is primarily dependent on three factors. Quality of isolated DNA, quality and consistency of coverslip coating of trimethoxysilane, and the pH of the final DNA solution. In this chapter, the basic parameters required for effective DNA combing will be determined and include:

- Validation of coverslip silanisation procedure
- Optimising of the pH for efficient DNA stretching and binding to a silanised coverslip.
- Verification of whether antibody labelling of ssDNA results in DNA stretched comparably to dsDNA
- Verification of single and dual nucleotide labelling methods
- Establish DNA combing parameters for combing of DNA from purified nuclei

3.2. Optimising DNA Combing for Cell Based Experiments

3.2.1 Combing dsDNA from λ phage DNA

The method used here utilised trimethoxysilane coated coverslips. Efficient coating requires a high level of cleanliness of coverslips and imperfections on the glass surface can disrupt the trimethoxysilane layer. A non-uniform silane coating results in non-linear stretched DNA preventing data analysis (Labit et al., 2008). In addition, the hydrophobicity of coverslips can be verified simply by observations of water droplets on coverslips that form near spherical beads on a hydrophobic surface. However, this gives no information as to whether the silanisation is uniform. To verify the silanisation technique and ensure that stretching forces are appropriate λ phage DNA was used. λ phage DNA has a known length of 48,000 bp. Stretching of DNA at 2 kbp/ μ m (Lebofsky & Bensimon, 2003) yields an average length of 14 μ m assuming that the combing process is working efficiently. To test the quality of the coverslip coating and to ensure that the force applied provides a consistent stretching factor, phage DNA was used as a molecular ruler. The Phage DNA was diluted, fluorescently labelled with yoyo1, and combed (Figure 3.8).

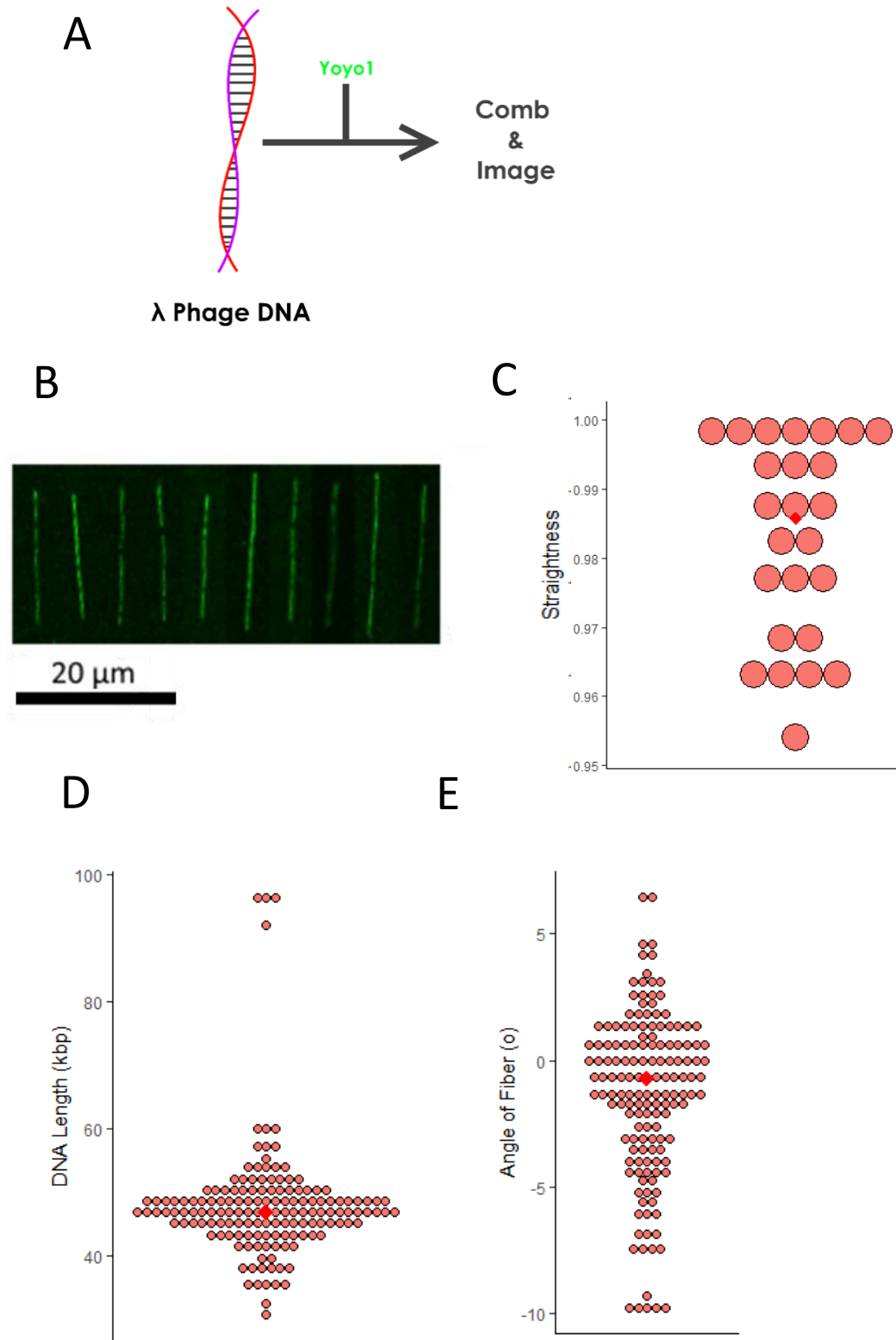


Figure 3.8. Analysis and quality control of Yoyo1 Stained Lambda Phage DNA A) A schematic of the experimental design. B) Representative images of yoyo1 stained combed lambda phage DNA. This figure is a mosaic of 10 randomly picked strands of DNA images. C) Straightness of combed DNA fibres. D) Observed lengths of combed DNA fibres ($N = 150$). E) Angle of combed fibres compared to a reference line ($N = 150$). Red diamonds on swarm plots indicate median values.

Visual inspection revealed that combing of λ DNA was successful, with straight, parallel DNA strands. This was confirmed by measuring the length of the DNA (L_{DNA}). The length between the start point and end point of each length of DNA was measured (L_{BF}). Straightness was measured using the following equation: $S = \frac{L_{BF}}{L_{DNA}}$. This compared the actual length of DNA, to the shortest possible length of DNA. The less straight a line is, the more curves it has, therefore the longer it is between 2 points. The closer to 1 the S value the more straight the lines and this experiment revealed an S value of 0.987. In addition, the DNA was parallel, consistently stretched and perpendicular to the air water meniscus that was used to stretch the DNA. The angles were consistent around a median angle of -1.5° . Critically, the range of measured angles of the fibres was very low ($-10^\circ - 7^\circ$) consistent with efficient DNA combing. λ phage DNA has a 48 kilobase genome making it a useful tool to determine that observed length is close to predicted length after DNA combing. The published DNA stretching factor of DNA combing is 2 kbp/ μm (Kaykov et al., 2016). The mean observed length was $23.4 \pm 4.7 \mu\text{m}$, corresponding to 47.4 kbp, demonstrating that consistent stretching is observed, and that this system is able to accurately quantitate the length of DNA fibres (Figure 3.8).

3.2.2. Optimisation of anti-ssDNA antibodies using Single Stranded λ Phage DNA

The next step was to optimise the labelling methods of ssDNA, and various modified nucleotides. This would allow experiments to measure replication dynamics to be able to be performed. The labelling of DNA with modified nucleotides requires fluorescent labelling after combing. For antibody-based labelling systems, DNA must be denatured to facilitate antibody accessibility and after denaturation the DNA is visualised with an anti-single stranded DNA antibody. However, EdU labelled DNA does not require denaturation and is double stranded when imaged. Critically, as analysis of both dsDNA and ssDNA would be performed, the labelling methods must produce consistent results. The epitopes for IdU, and CldU lie within the DNA double helix. DNA would need to be denatured, to expose the

epitopes, and allow antibody binding for labelling. This requires denaturation in 0.5 M NaOH and pH can affect the stretching of DNA. If the methods produced different results (in terms of DNA stretching) comparison between dsDNA and ssDNA approaches would be more complex. To verify that results from ssDNA and dsDNA labelling were comparable, the combing of λ DNA was performed but with NaOH denaturation, and antibody labelling of single stranded DNA (Figure 3.9).

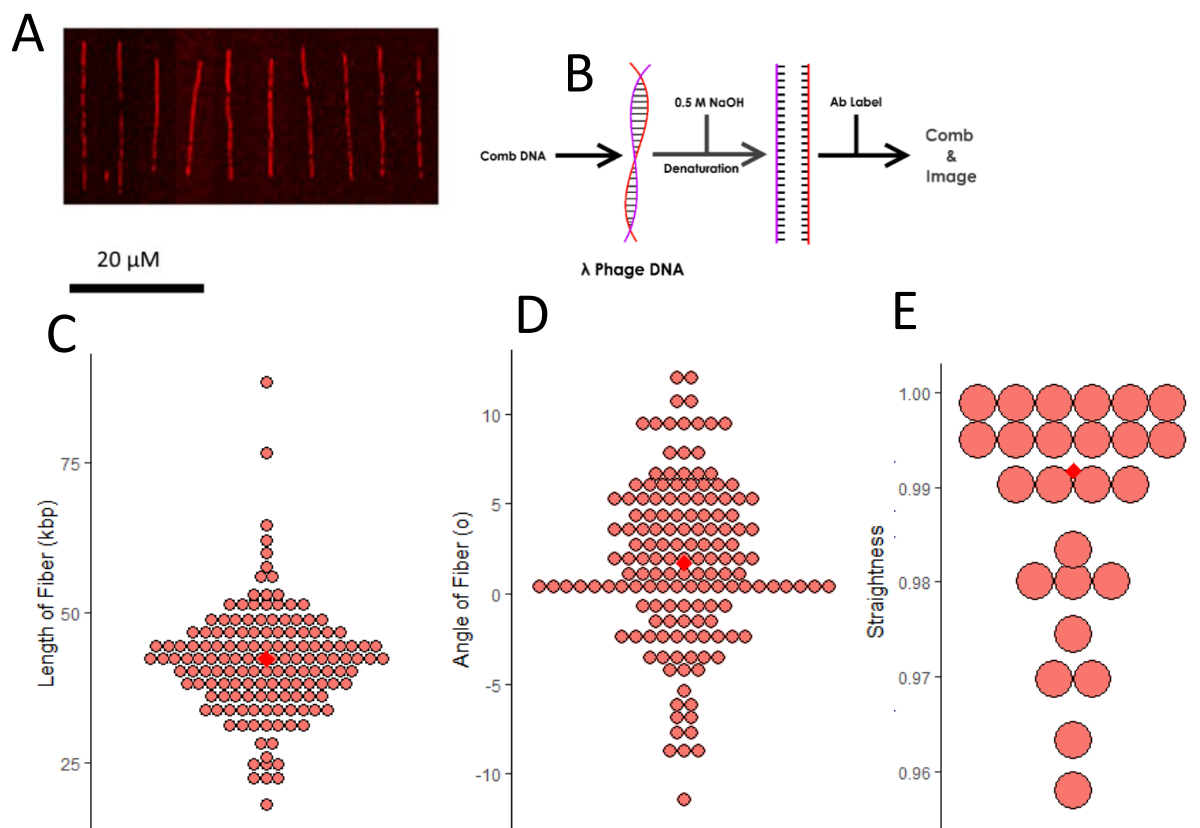


Figure 3.9. Analysis of antibody labelled Lambda Phage ssDNA A) Experimental overview. B) Representative images of yoyo1 stained combed lambda phage DNA. This figure is a mosaic of 10 randomly picked strands of DNA and were digitally aligned for presentation. C) Lengths of combed DNA fibres ($N = 150$). D) Angle of combed fibres ($N = 150$). E) Straightness of combed DNA fibres. Red point represents the median value in each plot.

Visual inspection of the DNA indicates that the DNA was successfully stretched (Figure 3.9a). The parameters determined for the denatured DNA were similar to those found for dsDNA (Figure 3.8). The DNA had an S value (straightness) of 0.926, comparable to yoyo 1 stained λ phage DNA, and there was no significant difference between the two values (T test, $p > 0.05$). The median length of DNA strands was $21.5 \mu\text{m}$ (43 kbp) ± 4.6 (Figure 3.9c). This data was normally distributed. This result is comparable to the expected length of λ phage DNA $24 \mu\text{m}$ (48 kbp). The yoyo1 stained double stranded λ phage had a median length of $24 \mu\text{m}$, a difference of less than $3.5 \mu\text{m}$, that was not significantly different (T test: $p > 0.05$). The data suggest that the two methods were compatible for combing efficiency, in terms of generating straight, and parallel DNA strands.

Both approaches yielded uniform, parallel DNA fibres that could be visualised, and length determined. These observations allow for the determination of DNA lengths using native and denatured DNA fibres. The major difference was with the quality of the imaging. Yoyo1 staining was continuous, whereas antibody labelling was more patchy and non-continuous. However, this problem is present in most published DNA combing research (Scwob et al., 2009). As the two methods were comparable, results between the two different methods could be compared with confidence.

3.2.3. Combing YOYO1 Stained DNA from NIH 3T3

All DNA combing experiments use DNA isolated from mouse fibroblast cell line NIH 3T3. This cell line was used because the cell free DNA replication assays utilise materials isolated from synchronised populations of cells (Section 2.5) that can be used to investigate the G1/S transition. In addition, most studies evaluating CIZ1 function have utilised murine cell fibroblasts of CIZ1 null mice. Consequently, using this cell line will ensure consistency between experimental approaches and as DNA is from the same source, the optimal binding and combing conditions should be the consistent in each approach.

The optimal pH for DNA combing typically lies between 5.1 and 5.8. To determine the optimal pH for murine fibroblasts, NIH 3T3 cells were grown to 80 % density and cells embedded in agarose. The purified DNA were resuspended in a MES buffer at a pH between pH 5.5 – 5.9 in 0.1 pH increments and labelled with Yoyo1. The DNA fibres were subsequently assessed for their degree of straightness and how parallel combed fibres are (Figure 3.10).

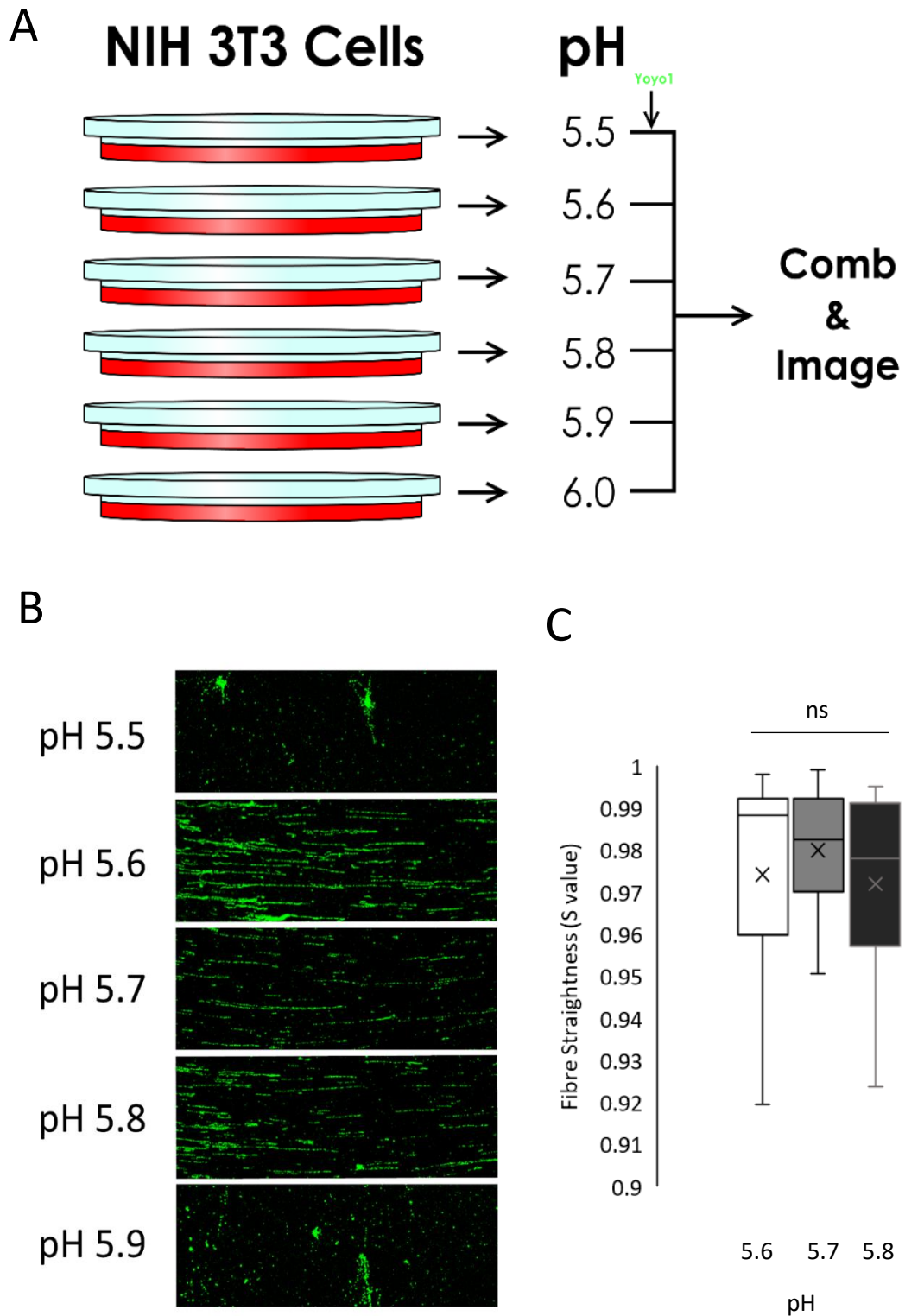


Figure 3.10-pH optimisation of DNA combing of NIH 3T3 DNA A) A schematic of the experimental design. B) Representative images of yoyo1 stained DNA at each of the pH values. C) Box and whisker plot of the straightness of the fibres from the 3 pH that successfully combed DNA.. The mean straightness of DNA did not vary significantly between pH 5.6-pH 5.8 (one-way ANOVA $P > 0.05$, $n = 3$ for each condition).

At pH 5.5 and pH 5.9, DNA did not efficiently adhere to or align on the silanised coverslip. At pH 5.6-5.8, the DNA was efficiently combed and produced straight DNA molecules (Median S values > 0.097). Additionally, there were no significant differences between any of these three data sets. Together this data suggests that the optimal pH range for efficient combing of DNA from NIH 3T3 cells is between 5.6 and 5.8. All experiments shown hereafter use pH 5.7 buffers.

3.2.4. Optimisation of Dual Labelling with CldU and IdU in Cell Based Experiments

To monitor DNA replication kinetics in NIH-3T3 cells, modified pyrimidine molecules IdU, CldU, and ethynyl-deoxyuridine (EdU) were used (Bianco et al., 2012). IdU and CldU require a denaturation step to reveal epitopes in double stranded DNA for immunofluorescence. IdU and CldU are fluorescently labelled using sandwiching of fluorescent antibody conjugates. In contrast, EdU does not require denaturation prior to labelling with azide-fluorophores using Click-It chemistry, which utilise the high energy C≡C bond to attach a fluorophore covalently to the nucleotide. As EdU does not require DNA denaturation to expose the binding epitope, EdU can be used to visualise both ssDNA, and dsDNA.

To establish parameters for visualisation of nascent DNA replication, NIH 3T3 cells were grown to 80 % confluence and cells pulse labelled with one of the three nucleosides (IdU, CldU, or EdU) for 30 minutes. The direct comparison of each nucleotide and allowed the replication fork rate to be determined for each nucleoside (Figure 3.11).

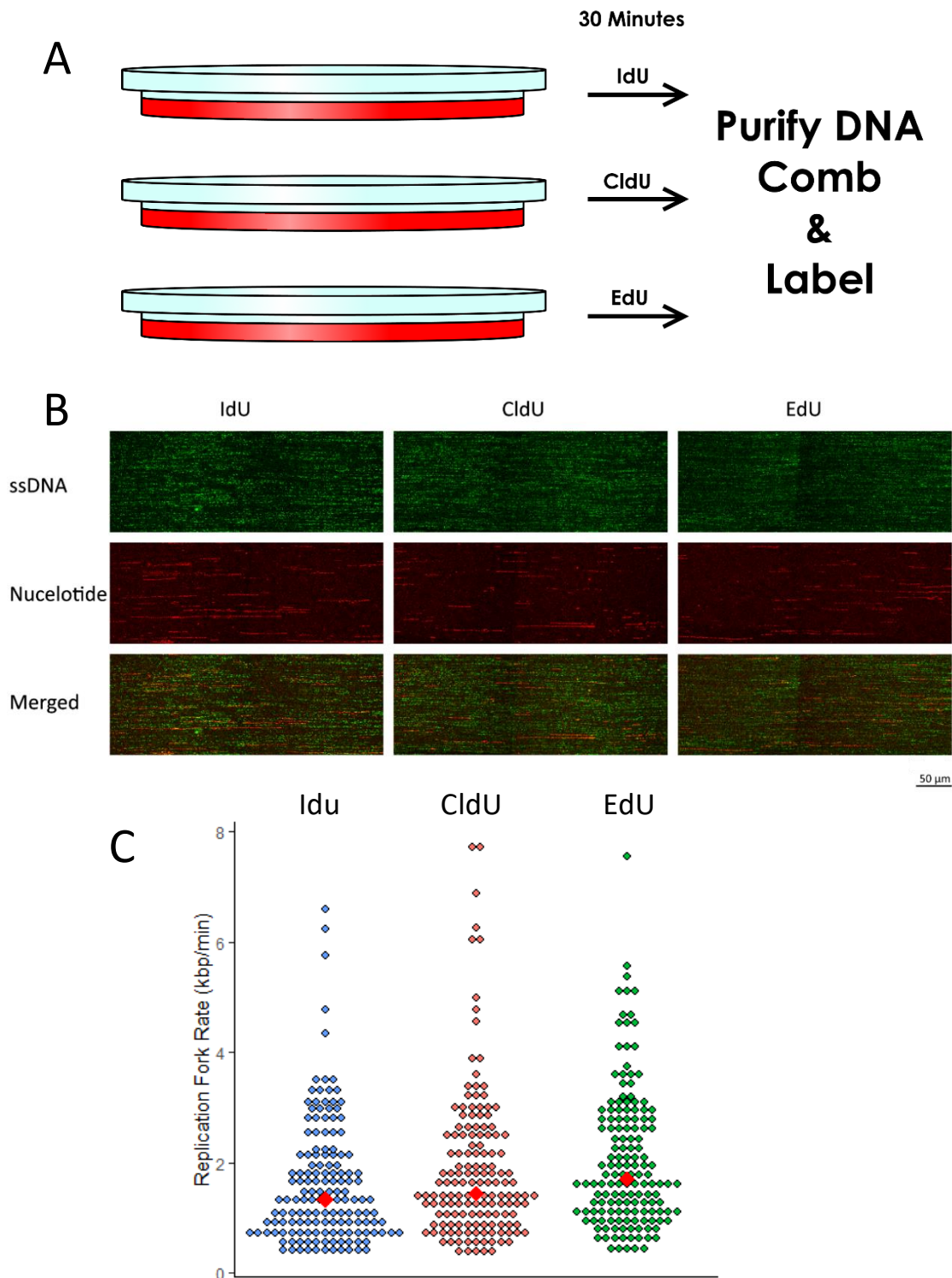


Figure 3.11 – Single labelling of combed DNA from NIH 3T3 cells A) Schematic for the design of the experiment B) Representative images of the combed labelled DNA. C) Replication fork rates from the single labelled fibres, for each nucleotide. Red diamonds on swarm plots indicate median values. The mean replication fork rate did not vary significantly between nucleotides used (one-way ANOVA $P > 0.05$, $n = 150$ for each condition).

To ensure that the nucleoside used was not affecting DNA replication fork progression rates, replication kinetics were determined for each pyrimidine analogue (Figure 3.11C).

Importantly, the replication track length for each of the pyrimidine analogues was similar (IdU: 1.3 kb/min, CldU 1.4 kb/min EdU 1.7 kb/min) and showed no significant differences.

Furthermore, the distribution of each of the different modified nucleotides, was comparable.

Together, this data indicates that each of the nucleotides, at the concentration used, do not significantly affect replication rates, suggesting that comparison across experiments using different labelling techniques is appropriate.

3.2.5. Dual labelling of nascent DNA using CldU and IdU.

Having demonstrated that CldU and IdU can efficiently label nascent DNA, sequential labelling can be used to dual label nascent DNA to analyse DNA replication kinetics. With a single labelling of DNA replication, the firing of an origin, termination of DNA replication and replication fork stalling are impossible to distinguish. However, dual labelling of DNA with two individual modified nucleotides reveals initiation, elongation, fork stalling and termination events.

In cell-based experiments, dual labelling of nascent DNA was performed using sequential labelling of IdU, followed by CldU (at a tenfold increase in concentration). This ensured that CldU was incorporated preferentially over IdU in the second labelling steps. Three plates of NIH 3T3 cells were labelled sequentially for 20 minutes with IdU and CldU. Cells were harvested, DNA was extracted, and DNA was combed (Figure 3.12)

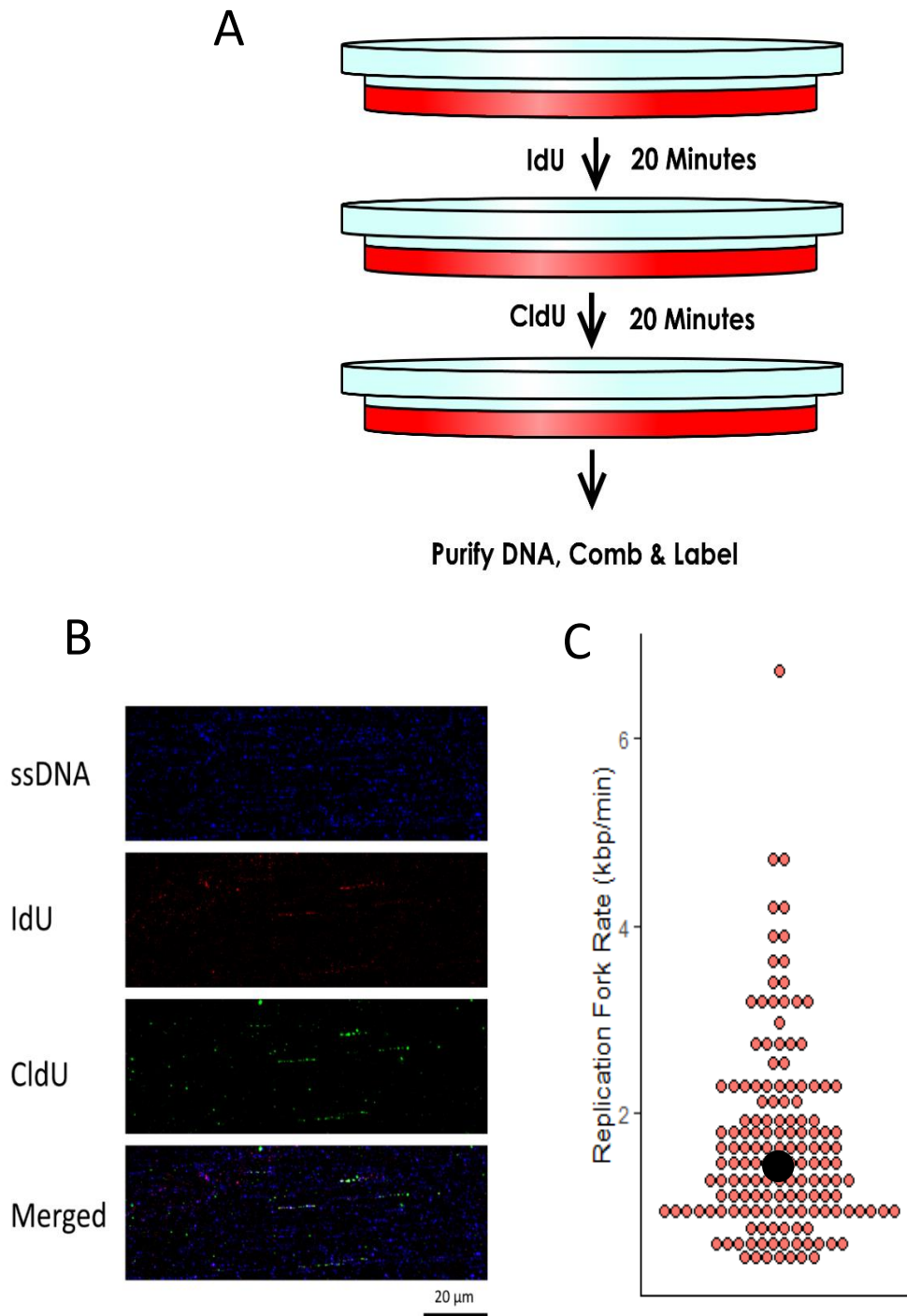


Figure 3.12-Dual labelling of DNA combed from NIH 3T3 cells. A) A schematic for the design of the experiment. B) Spectrally separated representative images of DNA from the experiment. C) Replication fork rates displayed as a beeswarm plot ($N = 150$). The median value is shown with a black dot

Visual inspection of images found defined tracks for CldU and IdU which colocalised to ssDNA, confirming that they represent DNA synthesis. After addition of CldU, there was a low level IdU signal due to small amounts of IdU remaining in cells after media change, that was colocalised with CldU. This approach provided sufficient signal to noise ratio to discriminate between ssDNA, IdU, and CldU independently to make high fidelity measurements on single molecules of DNA.

To determine replication fork velocity, 150 independent, dual labelled (IdU and CldU) replication tracks were measured and data plotted as a bee swarm plot (Figure 3.12C). This revealed the median replication fork velocity of $1.4 \text{ kbp}/\mu\text{m} \pm 0.4$. Together, these data indicate that the IdU and CldU dual labelling method is appropriate for measuring replication kinetics from NIH 3T3 cells. The optimisation of the method enabled experiments could be performed to measure how loss of CIZ1 effects DNA replication dynamics in NIH 3T3 cells (Chapter 6).

3.3. Establishing DNA combing of mammalian Cell free DNA replication assays.

3.3.1. Validating Replication Competence of G1 Nuclei

The cell cycle is regulated precisely by cyclin dependent kinases that establish the temporal regulation of the key transitions. Determination of the precise kinase activity that promotes the G1/S transition can be determined by careful titration of recombinant cyclin A-CDK2 into synchronous G1 cytosolic extracts and replication licensed late G1 nuclei (Chapter 5). This technique enables precise titration of proteins or small molecules and the impact on the initiation phase of DNA replication to be monitored (Copeland et al., 2010; Mariott et al., 2015).

Replication competent nuclei are defined as nuclei that have been synchronised in late G1 of the cell cycle and that enter S-phase in response to either an S-phase extract or addition of

recombinant cyclin A-CDK2 (Coverley et al., 2005; Copeland et al., 2010). Due to asynchrony that occurs during cell cycle re-entry from quiescence, there are nuclei that are already in S-phase, typically 10 % of the population. The nuclei that can be stimulated to initiate DNA replication by addition of an S-phase HeLa cytosolic extract are referred to as the replication competent population. To determine the quality of the nuclei two parallel reactions were set up for each batch of nuclei. The nuclei were reacted in an NIH 3T3 G₁ extract, and a HeLa S phase extract. The fraction of nuclei that were in S phase was calculated by fluorescent labelling of the biotin-16-dUTP nuclei with a streptavidin Alexa Fluor 555 conjugate (Figure 3.13).

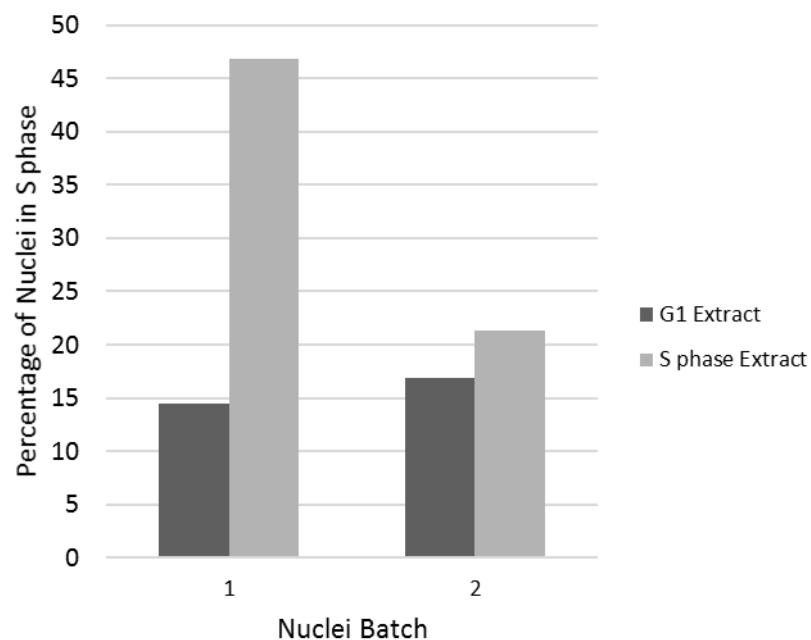


Figure 3.13- Quality control of nuclei isolated from NIH 3T3 cells. Nuclei were reacted in either G₁ (dark grey) or S phase (light grey) extracts. The proportion of nuclei in S phase was calculated by measuring incorporation of biotin 16 dUTP. (N = 2)

Comparison of synchronised nuclei (Figure 3.13) showed the number replicating nuclei in a G₁ extract is low (14.5 %). In contrast, addition of an S-phase extract that contains cyclin E-CDK2 and cyclin A-CDK2 promotes initiation of DNA replication, increasing the percentage of S-phase nuclei to 46.8 %, an over 3 fold increase. However, nuclei batch 2 were not replication competent and could not initiate DNA replication with a similar number in S-

phase as the G1 control (16.8% for G1 extract and 21.3 % in S-phase extract). These nuclei would not provide a significant signal to noise ratio so could not be used in future experiments. All isolated nuclei used here are validated this manner and nuclei that did not display a >2-fold increase in number of nuclei in S phase when comparing G1 reactions to S phase reactions were excluded from this analysis.

3.3.2. Method Development for Improving DNA Combing of *in vitro* DNA replication assays

Cell-free DNA replication assays enable titration of recombinant proteins to monitor chromatin binding or how factors affect DNA replication efficiency. In addition, cell free replication assays can also be used to identify mechanisms of action for novel inhibitors that are not able to cross the membranes of cells due to size or charge (Mariott et al., 2015). Hence, to gain greater resolution of the DNA replication process, this section aims to integrate the *in vitro* DNA replication system and DNA combing. However, this had proved unsuccessful due to fragmented strands of DNA produced during isolation or storage of nuclei. Isolated nuclei contained fragmented DNA and the short fibres are not long enough to accurately determine fork progression or to determine inter origin distance (IOD). Furthermore, replication fork velocity experiment results could be biased due to longer replication tracks being unable to be measured. The removal of fragmented DNA or modification to procedures to prevent formation of DNA fragments are required to investigate DNA replication kinetics and DNA replication stress *in vitro*.

There are a number of steps in the procedure used to produce replication competent nuclei that have the potential to induce small amounts of DNA damage. Any small amount of DNA damage can cause dramatic increases in DNA fragments that coat the coverslip and obscure long DNA strands in a DNA combing experiment. Adjacent nicks in DNA during combing will cause fragmentation of DNA as the DNA is stretched in the combing procedure. The major steps in the isolation procedure that could cause mechanical or chemical stress to the DNA

were assessed to determine the stage that induced short DNA fragments. These stages were: dissociation of the cells by trypsinisation versus hypotonic buffer and cell scraping. This is followed by dounce homogenisation to isolate nuclei from cells and centrifugation to harvest nuclei, flash freezing in liquid nitrogen, or preparation of cell free DNA replication assays.

As a first step, release of cells from the culture dish was performed using trypsinisation as this approach has been using in cell based DNA combing experiments without fragmentation of DNA. This could then be compared to the effects of mechanically scraping cells after hypotonic buffer incubation, followed by dounce homogenisation (Figure 3.14).

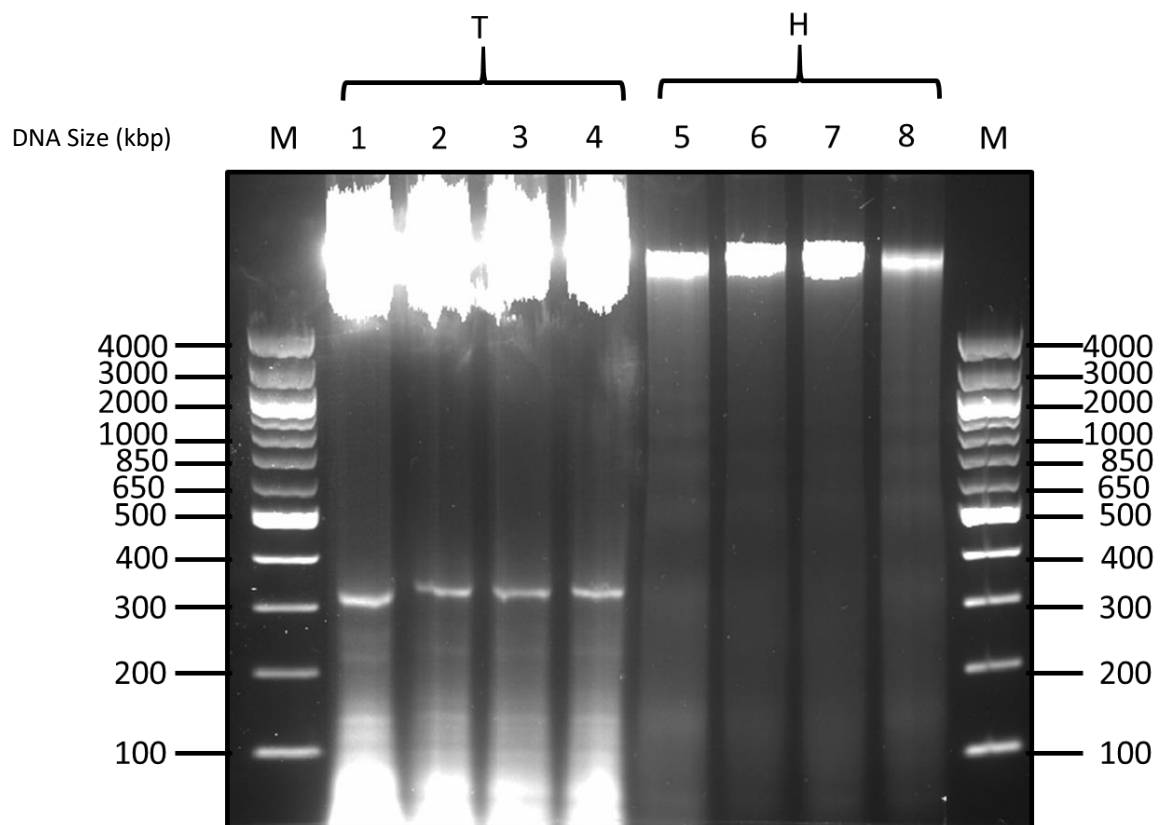


Figure 3.14 – Degradation of DNA During Cell Isolation Comparison of DNA damage induced by trypsinisation and scrape harvesting. M is molecular marker. Lane 1 – 4 are loaded with a proteinase k digest of cells harvested by trypsinisation. Lane 5-8 are loaded with a proteinase k digest of cells harvested by swelling in hypotonic buffer and scraping. T = trypsinised, H = Hypotonic buffer

Comparison of DNA fragmentation following harvesting by trypsinisation and mechanical scraping showed that both methods produced predominantly >4 kb DNA fragment and then

some evidence of smaller fragments at lower abundance. The trypsinised cells (Lane 1-4, Figure 3.18) had extensive low molecular weight DNA fragments <100bp and a band at approximately 300bp that were largely absent from the douced nuclei (Lanes 5-8). Although the amount of DNA was lower than that seen for trypsinised cells, it was mostly intact as it >4kpbs in length above the highest marker. These results demonstrate that scrape harvesting in hypotonic buffer step does not cause an increase in DNA damage relative to control DNA. Therefore, DNA damage occurs during the nuclei isolation, not the harvesting of the cells. Next, synchronised nuclei were prepared by existing approaches and analysed after each step in their isolation by agarose gel electrophoresis (Figure 3.15).

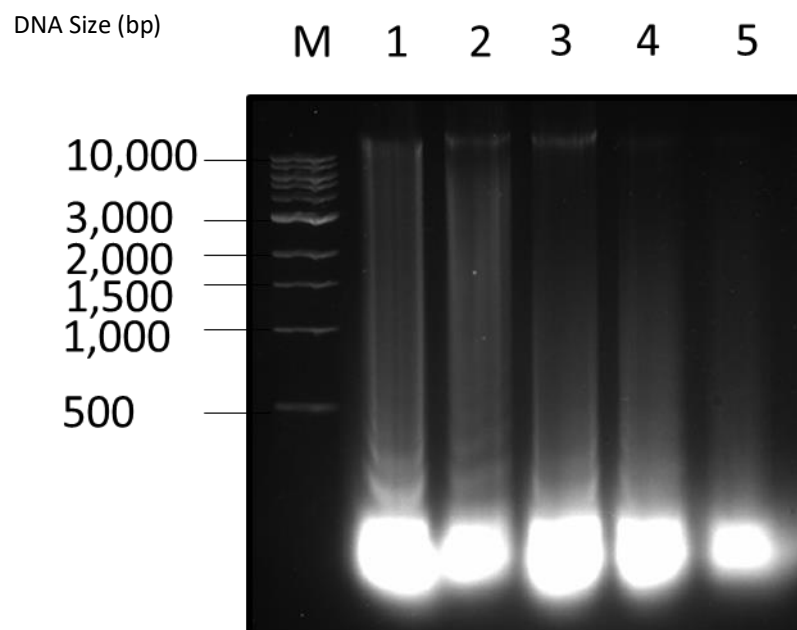


Figure 3.15 – Degradation of DNA During Nuclei Isolation How different stages of nuclei isolation caused different levels of DNA damage. M is molecular marker. Lane 1, DNA from scrape harvested cells. Lane 2, DNA after dounce homogenisation of cells. Lane 3, purified nuclear DNA after centrifugation. Lane 4, DNA extracted after snap freezing and freeze thawing. Lane 5, DNA after incubation in an S-phase cytosolic extract.

Analysis of DNA fragmentation at each step in the isolation of nuclei identified two steps as causing notable increases in the amount of smaller DNA fragments. These steps were (i) centrifugation and (ii) Snap freezing and thaw steps. This was characterised by a

disappearance of long DNA (10 kbp). When preparing DNA for DNA combing, vibration is well known to increase shearing of DNA and movement is kept to as little as possible. Anecdotal evidence suggests that specialist labs do not keep samples on the same bench as an active centrifuge or take them in lifts. Consequently, these results were anticipated as centrifugation can cause excessive force to be enacted on the nuclei during isolation. In addition, freezing can induce mechanical stress as ice crystals form in the freezing process that rupture the phosphodiester backbone. Since these are vital steps for both preparation and storage of nuclei for *in vitro* replication material the procedure may need to be modified.

To mitigate the damage to DNA caused by the physical stress of centrifugation, a number of modifications could be performed. For example, centrifuging nuclei onto sucrose cushions rather than the base of an Eppendorf tube may reduce impact and mechanical stress; this is a method that has been utilized to isolate nucleoli (Li & Lam, 2015). The increased density of the sucrose solution slows the separation of material during centrifugation, this may reduce the mechanical strain on DNA.

Another method to mitigate the damage to DNA from centrifugation would be to reduce the speed of centrifugation. Slower speeds could result in a lower force acting on the DNA as it hits the base of the Eppendorf tubes. This could protect the integrity of the DNA making it more suitable for combing. To test the effects of different centrifuge speeds cells were grown, synchronised and 17.5 hours after release cells were swelled in hypotonic buffer, scrape harvested, and dounce homogenised. The dounce homogenised sample was split into 3 equal sized volumes. Each sample was centrifuged at different rates ranging from 500 – 12,000 x G, additionally one sample was vortexed to shear DNA to be used as a positive control. After centrifugation samples were digested overnight in proteinase K then prepared for agarose gel electrophoresis on a 1.5 % agarose gel (Figure 3.16).

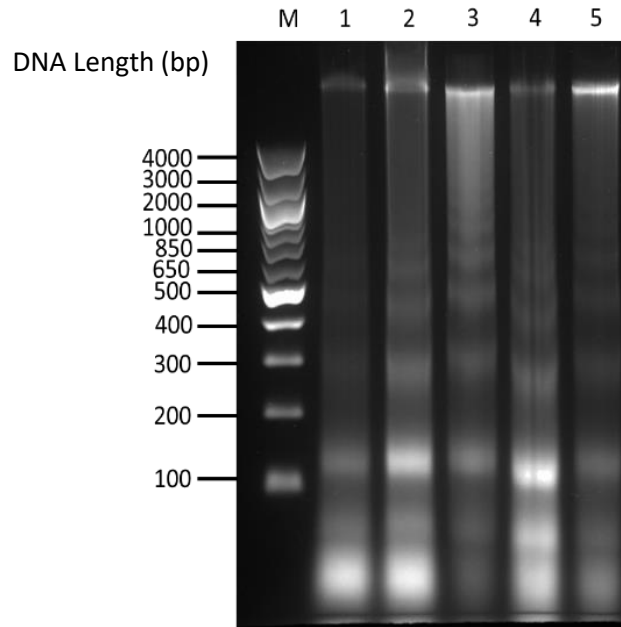


Figure 3.16 – Centrifuging Nuclei Effects DNA Integrity The effects of increasing centrifuge speed on DNA damage during isolation of nuclei for *in vitro* experiments. Lane 1 is loaded with a proteinase k digest of scrape harvested dounce homogenised cells. Lane 2 is a vortexed nuclei control to increase DNA shearing. Lanes 3-5 are harvested at 500, 6000, and 12000 x G respectively.

There was a little difference between the amount of small DNA fragments for samples centrifuged at speeds greater than 500 x G (Lane 4) and 12,000 x G (Lane 5) with these lanes showing band patterns similar to the vortexed DNA (Lane 2). Lane 3 was the 6000 x G samples which showed some signs of DNA damage but appeared to show an increased amount of longer DNA, and a pattern more similar to the negative control. The results suggest that centrifugation speeds of 6000 x g are sufficient to isolate nuclear materials and minimise DNA shearing.

Freeze thawing nuclei appears to cause significant damage to DNA (Figure 3.10). The simplest way to avoid this damage is to perform *in vitro* experiments directly after harvesting of nuclei. To assess the effect of snap-freezing nuclei prior to use, 2 plates were synchronised, and nuclei were harvested at the 17.5 hour time point. Nuclei from 1 plate

were frozen for use as a control and compared with fresh reagents after incubation with S-phase extracts. Nuclei were embedded in low melting point agarose and DNA was purified as described (Section 2.7.7a). DNA was labelled with Yoyo1 for both preparations (Figure 3.17).

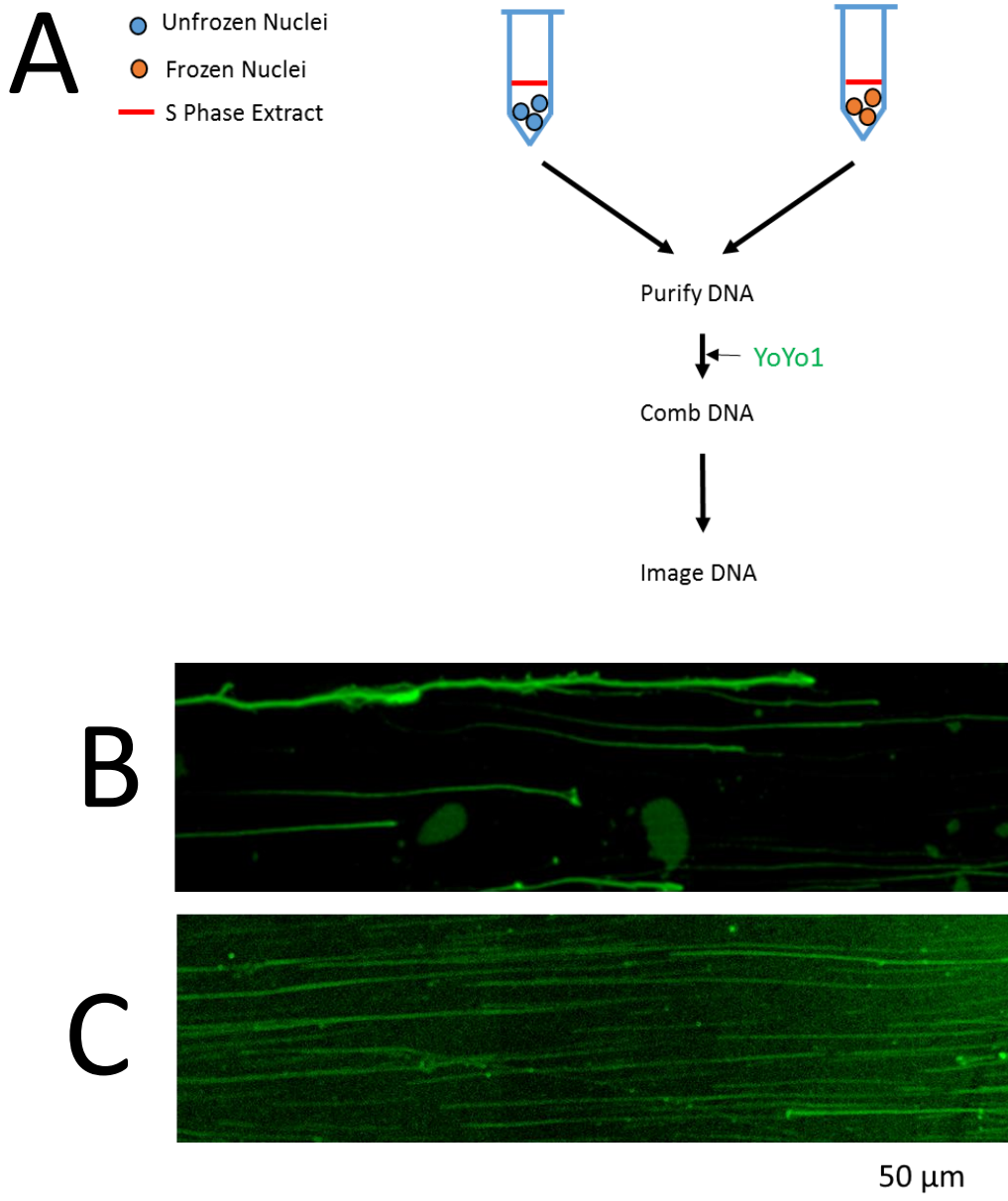


Figure 3.17-Freeze Thaw Effects DNA Integrity. Schematic for isolation of nuclei without freezing to test if they could be successfully combed. Samples were labelled with yoyo-1. Blue nuclei represent nuclei that have been thawed from liquid nitrogen storage. Orange nuclei represent nuclei that haven't been frozen. B) Confocal fluorescence microscope image produced from nuclei that were freeze thawed prior to combing. C) displays an image of combed DNA from nuclei that were not frozen prior to purification of DNA.

The isolation of nuclei without snap freezing appears to increase the length of DNA as visualised by DNA combing, consistent with the shearing of the DNA during the freeze-thaw step. In addition, DNA combing of DNA from *in vitro* DNA replication assays is possible with modification of the procedures to isolate nuclei. However, omitting the freezing step prevents characterisation of the nuclei in cell free DNA replication experiments to identify batches that initiate DNA replication *in vitro*. Furthermore, repeat experiments using the same nuclei could not be performed. Additionally, isolating nuclei directly prior to DNA purification and combing adds significant time to an experiment as each will have to be preceded by days of cell synchrony and nuclei isolation. Whilst a simple solution had yielded better results, it was far from an ideal solution long term.

To allow long-term storage of nuclei, the damage incurred by freeze thawing must be mitigated. Increased fragmentation of the DNA results in an increased concentration of short DNA, preventing quantitative analysis of DNA replication events. To overcome this issue, it may be feasible to remove the fragmented DNA by electrophoresis. As nuclei are encapsulated in agarose plugs, application of a current to the plugs containing DNA could remove the smaller DNA leaving a higher proportion of longer DNA preventing surface binding being outcompeted by the smaller DNA.

To test this, cell free DNA replication reactions were prepared, nuclei were embedded in agarose and naked DNA produced by proteinase K digestion. Agarose plugs were placed in an electrophoresis tank and run at 100 V for 15 minutes. Agarose Plugs were retrieved, washed and prepared for DNA combing (Section 2.3) (Figure 3.18).

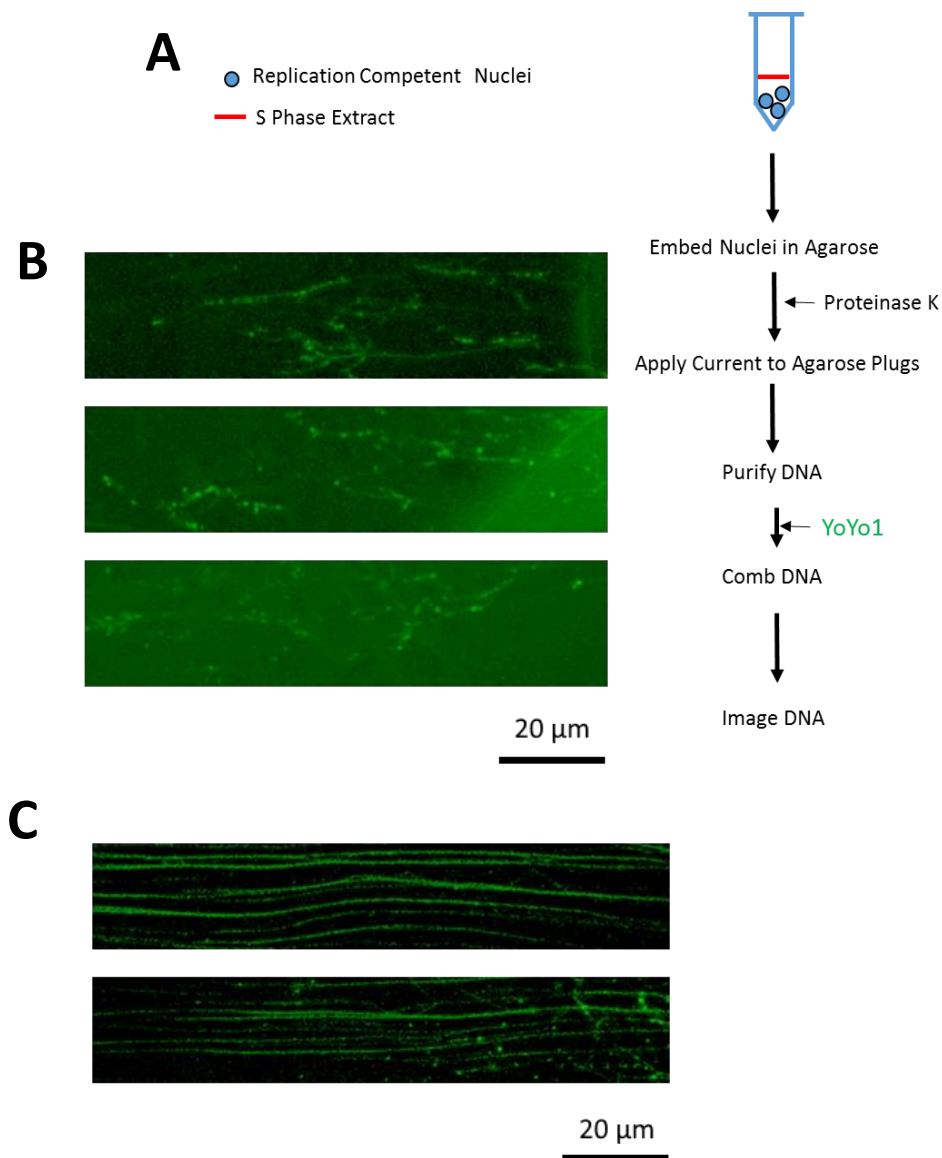


Figure 3.18 - Enriching Long DNA Fibres by Electrophoresis. Schematic for removing smaller DNA from agarose plugs using gel electrophoresis. DNA is purified as normal. However, prior to agarose digestion a 100 V current is applied to samples in TBE buffer for 15 minutes. DNA is then stained with Yoyo1 and combed. b) Confocal microscopy images of YoYo1 stained DNA fibres before electrophoresis. c) As b except for DNA fibres underwent electrophoresis at 100 V for 15 minutes prior to isolation of DNA to remove fragmented DNA.

The application of a current to remove short DNA fragments allowed more efficient alignment and length of DNA during DNA combing (Figure 3.19b/c). This demonstrates that it is feasible to isolate and validate nuclei that have been snap frozen prior to analysis. It remains to be addressed whether DNA replication fork rates are consistent with an

unperturbed, cell-based analysis of DNA replication rates. Having established techniques that can be used to isolate DNA from *in vitro* cell free DNA replication assays, the 2 strategies will enable measurement of DNA replication fork dynamics *in vitro*.

3.3.3. *in vitro* labelling methods

The use of *in vitro* DNA replication assays provides an opportunity to use modified nucleotides as opposed to halogenated pyrimidine analogues (Marheineke et al., 2005; Bianco et al., 2012). Candidates include EdU, biotin-16-dUTP and digoxigenin 11 dUTP. Biotin 16 UTP is used already in *in vitro* reactions (Chapter 5) and produces a sufficient signal to noise ratio on nuclei from *in vitro* reactions. However, biotin-dUTP has not yet been used to label nascent DNA by DNA combing. EdU has been shown to be labelled effectively in DNA combing experiments (Figure 3.11), however it has not been used for *in vitro* experiments. The third candidate is digoxigenin 11 dUTP. Digoxigenin has been used for combing previously (Marheineke et al., 2009). If the use of bulky modified nucleotides are not suitable the other option would be to use IdU and CldU as before for dual labelling. To test the viability for this BrdU was used. The viability of each nucleotide for labelling was verified in *in vitro* DNA replication assays with S phase extract and each modified nucleotide was performed (Figure 3.19).

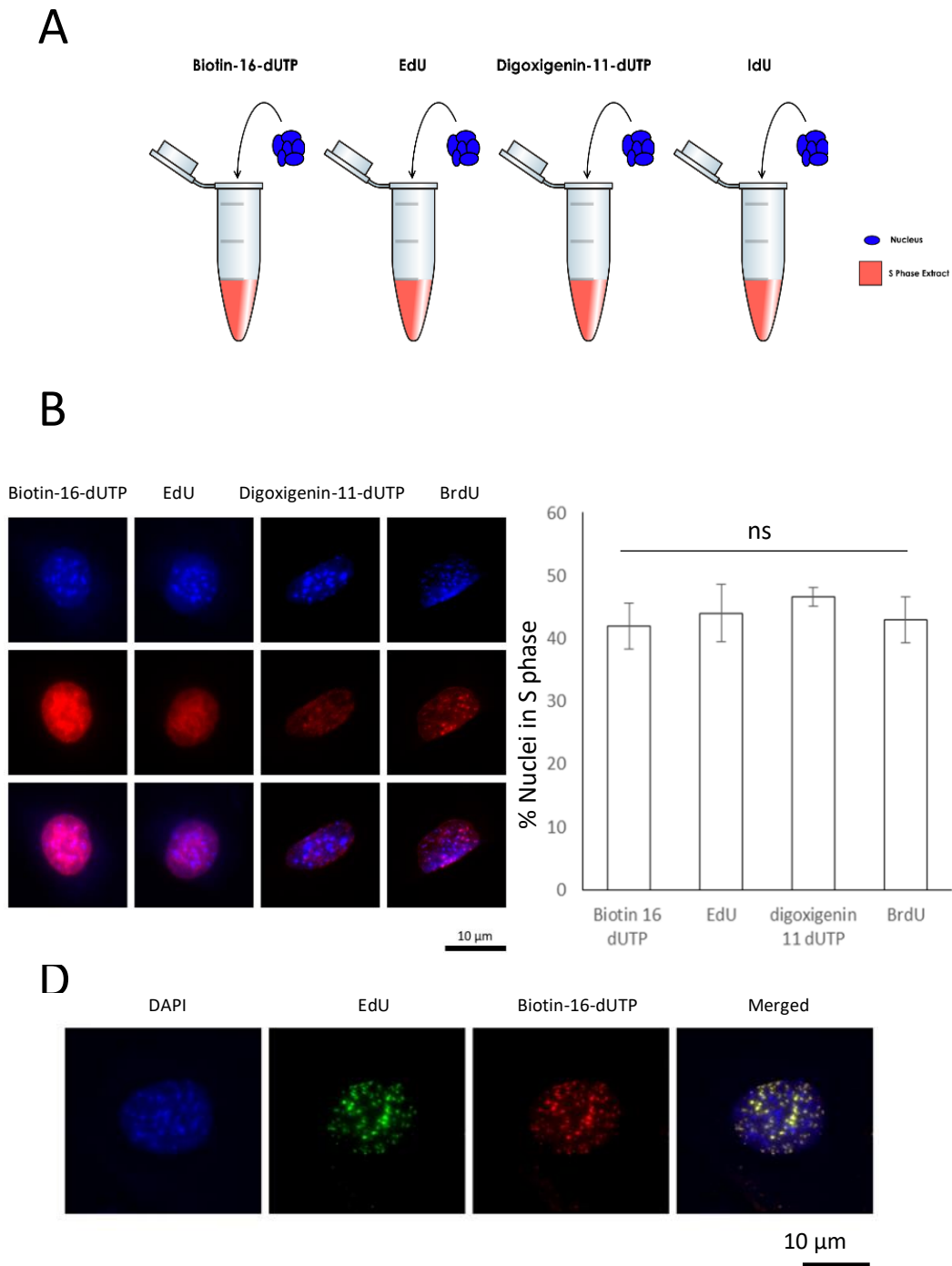


Figure 3.19. Labelling of *in vitro* reactions with multiple nucleotides. A) A graphical schematic of the experiment. B) Representative images of positively labelled nuclei for each nucleotide used. C) The mean proportion of nuclei in S phase did not vary significantly between conditions (one-way ANOVA $P > 0.05$, $n = 3$ for each condition, error bars represent standard deviation). D) Representative image of the positively labelled dual nucleotide labelled nuclei.

Fluorescence microscopy allowed discrimination between labelled, and unlabelled nuclei and there was a high signal to noise ratio for all nucleosides tested. Importantly, there was no significant difference in the percentage of S-phase nuclei, with Biotin 16 dUTP, EdU, and digoxigenin 11 dUTP showing 42%, 44% and 47 % of nuclei in S phase, respectively. This compares with 43% for BrdU. There were no significant differences to mean S phase entry between any of the nucleotides used. In addition, dual labelling with EdU and biotin-UTP showed strong colocalization of biotin 16 dUTP and EdU on the dual labelled nuclei, suggesting that this combination would be appropriate in DNA combing *in vitro* replication experiments. This suggests that modified nucleotides used here had no adverse effects on replication suggesting that they may be used to label DNA replication in DNA combing experiments.

3.3.4. Labelling of Nucleotides of DNA from *in vitro* Replication Experiments

Having successfully labelled nascent DNA replication *in vitro*, this approach was combined with DNA combing to determine the rate of DNA synthesis. The use of *in vitro* replication assays are a powerful tool for analysis of replication dynamics in multiple conditions. The addition of DNA combing to this approach would greatly enhance the quantitative analyses that could be performed beyond a binary G1 or S-phase score that is used currently. To determine if modified nucleotides provided sufficient sensitivity to label nascent DNA synthesis in DNA combing using an *in vitro* system, EdU, biotin -16-dUTP and digoxigenin-11-UTP were used in 50 µl S phase *in vitro* reactions (Figure 3.20).

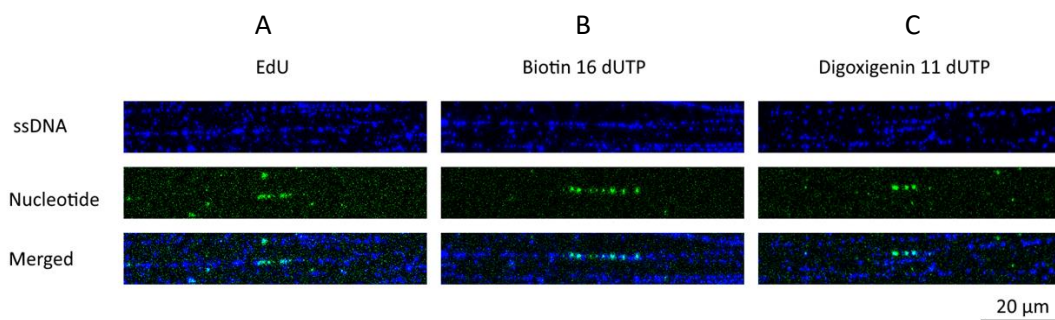


Figure 3.20- Labelling of Replication on Combed DNA From *in vitro* Replication Experiments. Blue shows DNA, green shows the modified nucleotide (A: EdU, B: Biotin-16-dUTP, C: Digoxigenin-11-dUTP) incorporated into DNA during replication. Scale bar shows 20 μm .

The labelling of DNA with YoYo-1 and visualisation of nascent DNA replication was achieved using EdU (Figure 3.21A), biotin-16-dUTP (Figure 3.21B) and digoxigenin (Figure 3.21C) each of the nucleotides had a visible signal, and a sufficient signal to noise ratio to make accurate measurements. Signalling from antibody derived labelling methods (IdU, CldU, and digoxigenin 11 dUTP) resulted in non-contiguous (dotty) labelling. This same effect was observed in labelling of DNA from cell-based experiments. The non-contiguousness still allows for data analysis as clear labelling regions are shown. This result confirmed that these labelling methods were viable to perform experiments with modified nucleotides (Biotin or digoxigenin-dUTP) and EdU. Together these data suggest that any of these nucleotides could be viable for performing DNA combing experiment from *in vitro* replication reactions.

3.4. Chapter Discussion

This chapter establishes the use of DNA combing for analysis of DNA replication in cell based and cell free DNA replication analyses. The results from this chapter have verified the DNA combing technique to be used in later chapters (Chapter 6). Early experiments utilized labelling of DNA in both double stranded and single stranded states. dsDNA was labelled using DNA intercalating dye yoyo 1. ssDNA was labelled using fluorescent antibody conjugated immune-labelling. Early experiment used viral (Lambda phage) DNA to confirm DNA aligning and DNA stretching factor. Together these results would verify the efficacy of the coverslip trimethoxy silane coating (Labit et al., 2008).

Using λ DNA enabled verification of the basic parameters of DNA combing. The DNA fibres were shown to be both straight and parallel and observed DNA length was consistent with published values of $2\text{kb}/\mu\text{m}$ (Lebofsky & Bensimon, 2003). The average ratio between the length of fibres, and DNA fibre straightness was within expected parameters which is essential for accurate measurements of DNA replication. In addition, dual labelling experiments revealed that their antibodies could discriminate between IdU and CldU with 2 separate tracks identified. Additionally, tracks could be identified that represented each of the replication patterns (Figure 3.21).

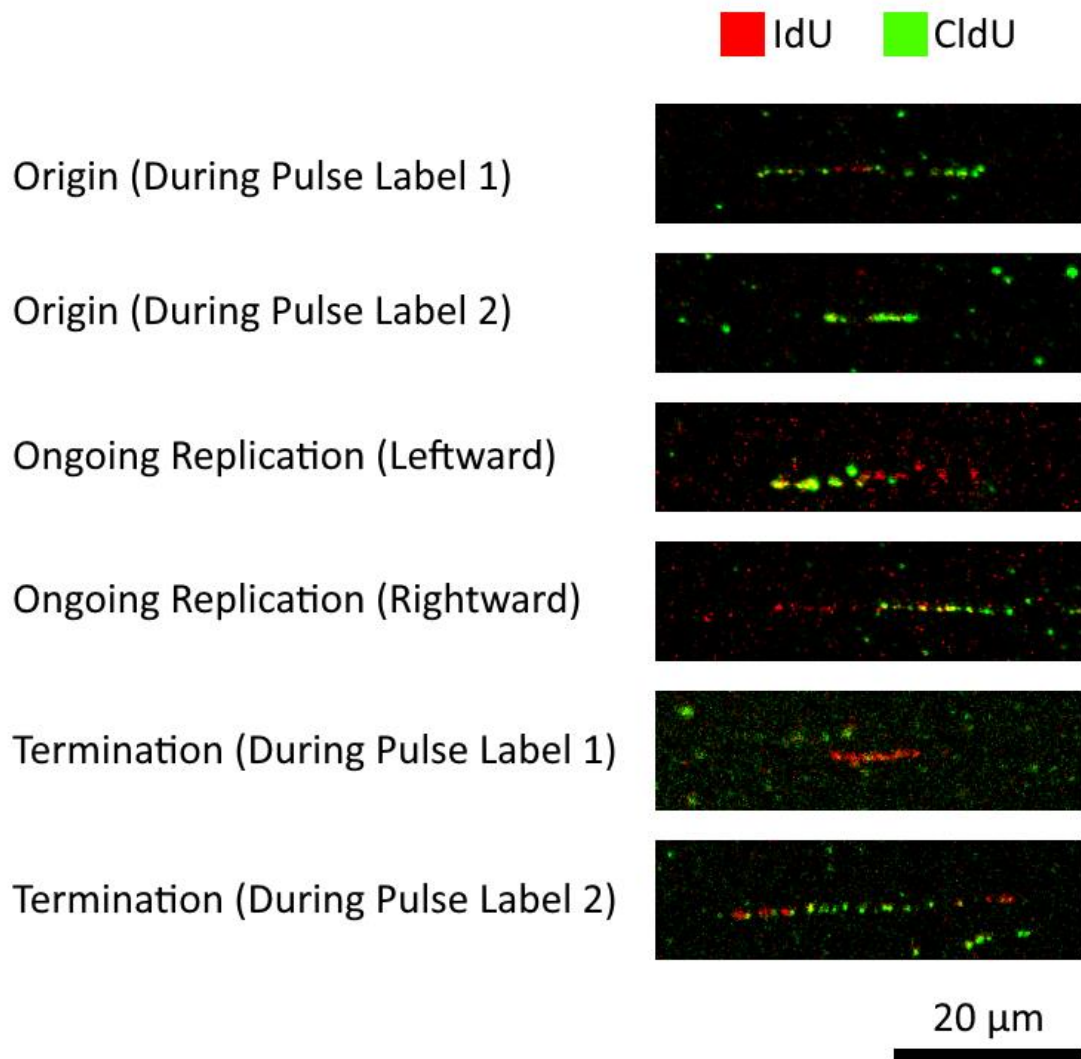


Figure 3.21. Patterns of DNA replication. Replication patterns derived from a sequential pulse labelling with IdU and CldU. Each of the replication patterns shown is characteristic of a specific replication event and timing. The replication event and timing for each observed pattern is described on the left. A scale bar is included.

Resolution of all major replication patterns (Initiation, elongation, termination) was achieved. Additionally, the quality of imaging was comparable to previously published DNA combing and DNA fibre analysis (Bianco et al., 2012). Resolution of these patterns would allow measurements of changes in replication dynamics in experiments throughout this study. Additionally, to ensure that the nucleotides were not interfering with replication in these cells the replication rates needed to be measured. If this measurement were to reveal

that replication rates were largely different between published replication rates for other cell lines, then the nucleotides and concentrations used would have to be addressed.

Measurements taken from a total of 150 replication events revealed that the median replication rate was 1.4 kbp/min. This rate was comparable to the rates identified for unstressed cells of a wide variety of different cell lines and species including DT40 cells, HeLa cells present with lower replication fork velocities than the cells used in this report, likely due to oncogenic mutations (Petermann et al., 2006; Petermann et al., 2008). Specifically, this replication fork rate was comparable to published rates from NIH 3T3 cells (Bhaskara et al., 2013; Zhao et al., 2018). The range of DNA replication fork rates displayed here showed a large variation from 0.4 kbp/min to 8 kbp/min. It has been observed in several published works from a variety of different cell lines and species, although typically between 0.4 kbp/min – 5 kbp/min (Petermann et al., 2006; Petermann et al., 2008). This large range is likely due to the variation of DNA replication rates within a cell (Yurov et al., 1980; Rhind et al., 2013). Additionally, the length of individual combed fibres is a limit for large replication fork rates as breaks are more likely to occur in longer replication tracks (Kaykov et al., 2015).

Analysis of DNA replication using synchronised nuclei has previously utilised mimosine to arrest cells in early S-phase (Marheineke et al., 2005). Here DNA combing has been achieved using the physiologically relevant synchronisation using G0 arrest for the first time. DNA combing experiments using mimosine synchronised nuclei labelled with digoxigenin dUTP and Biotin dUTP. These studies demonstrated that new replication origins fired bi-directionally in these *in vitro* replication assays, and similarly to cell-based experiments fork rates *in vitro* were highly variable. Additionally, this study identified that replication forks from mimosine arrested nuclei proceeded less rapidly than from whole cells of the same cell type. This shows the advantage of DNA combing, which allows measurement of each

datapoint, whereas other methods of measuring fork progression rate measure averaged out data losing some fidelity (Nazari et al., 2013).

This report marks the first example of late G1 nuclei promoted into S phase via incubation with an S phase extract being used for DNA combing. Additionally, this study has demonstrated that other nucleotides beyond digoxigenin dUTP and biotin 11 dUTP could be used for cell free DNA combing such as including BrdU, CldU, IdU and EdU. Successful BrdU labelling implies that IdU and CldU would be successful, which could allow a more direct comparison between cell based and cell free DNA combing experiments. The major advantage of using post quiescent nuclei is the reduced use of chemical synchrony which may have aberrant effects on results (Krude et al., 2006). Together the combination of these two techniques will allow for the high-fidelity measurement of replication kinetics *in vitro*. This will allow measurements of how individual molecular factors affect replication dynamics. For example, these techniques will be used to investigate the effect of CDK levels on DNA replication dynamics, how this is modulated by CIZ1, and the effect of replication inhibitors on DNA replication, as this is a cell free system, inclusion of these factors into cell cycle specific stage extracts is simple (Chapter 5). This bypasses complex genetic manipulation, or nonspecific chemical inhibition/activation allowing a more rapid measurement of DNA replication. When coupled with cell-based data this will provide deeper insight on a single event resolution into how replication initiation is controlled.

The optimisation of DNA combing labelling methods for both cell based and cell free experiments has enabled this approach to be used to measure replication dynamics at altered levels of CIZ1 (Chapter 5 and 6) and altered levels of Cyclin/CDK signalling (Chapter 5). CIZ1 has been shown to have a role in multiple cancers (Higgins et al., 2012; Chen et al. 2019), and a specific role at co-ordinating CDK signalling around the nuclear matrix during the G1/S transition (Coverley et al., 2005; Copeland et al., 2010; Copeland et al., 2015). If

altered CIZ1 levels affect DNA replication dynamics, this could induce DRS which could drive a mutator phenotype directly explaining the link between CIZ1 and cancer.

Chapter 4.

Cell Cycle Analysis of CIZ1 Null Murine Fibroblasts

4.1. Introduction

4.1.1 Introduction to CRISPR Cas9

In this chapter, the potential role for CIZ1 in cell cycle regulation will be assessed. This will be achieved utilizing CRISPR Cas9 techniques to produce CIZ1 null fibroblasts to aid evaluation of its function in cell cycle regulation and begin to assess its potential role in tumourigenesis. Previous reports have demonstrated a role for CIZ1 in regulation of the G1/S transition and cooperative activity with cyclin A-CDK2 to promote replication initiation, an activity inhibited by CDK2 mediated phosphorylations (Copeland et al., 2010; Copeland et al., 2015), and in the DDR to HU (Nishibe et al., 2013). Experiments were performed to measure changes to cell cycle profile, and replication protein assembly, in this chapter the effect of loss of CIZ1 was determined. This provides a framework for future Chapters to investigate the specific changes that were observed in a targeted detailed manner.

4.1.2. CRISPR Cas9

To further investigate the role of the protein CIZ1 within the context of how its cellular levels effect cell cycle progression, DNA replication, and response to replicative stress, this section aims to produce a CIZ1 knockout cell line to aid functional analysis. Phenotypic analysis of CIZ1^{-/-} cells may elucidate its role in a number of common cancers (Higgins et al., 2012) as well as its activity surround the G1/ S-phase transition (Copeland et al., 2010; Copeland et al., 2015; Pauzaite et al, 2017). CIZ1 is typically overexpressed in cancer (Rahman et al., 2010; Higgins et al., 2012, Swarts et al., 2018) but CIZ1 null mice have revealed that CIZ1 may have a tumour suppressor role that has not been characterised (Nishibe et al., 2013). To generate CIZ1 knockout NIH 3T3 cells, CRISPR Cas9 was used to produce a double strand break which, when incorrectly repaired by NHEJ promotes frameshifts that introduce stop codons in an early codon, effectively knocking out the CIZ1 gene.

The clustered regularly interspaced short palindromic repeats/CRISPR associated system (CRISPR/CAS system) is a key component of the adaptive prokaryotic immune systems defence against viral infection (Barrangou, 2015). In bacterial DNA there are spacer sequences separated by palindromic repeat, these encode crRNA (crRNA) sequences, these crRNA bind to invading viral bacteriophage DNA targeting it for destruction by CAS endonucleases (Barrangou et al., 2007, Brouns et al., 2008, Marraffini & Sontheimer, 2008). Additionally, after viral infection bacteria incorporate new spacers in their CRISPR arrays to provide a memory response to provide resistance to viral infection (Barrangou et al., 2007).

The ability to target specific sequences within DNA provides a useful tool for mammalian genome editing. The most commonly used CAS for genome editing is Cas9 which binds after a protospacer adjacent motif (PAM) with sequence 5' – NGG – 3'. crRNAs can be generated with a 20 bp specific sequence, these coupled with a trans activating CRISPR RNA (tracrRNA) recruit the Cas9 to the PAM sequence which then cuts the DNA leaving blunt ends (Tsai et al., 2016). This is interpreted by eukaryotic cells as a double strand break (DSB), activating the DNA damage response (DDR). The DSB can be repaired by two mechanisms: non-homologous end joining (NHEJ) or by homologous repair (Zaboikin et al., 2017). NHEJ is an imprecise method for repairing DNA prone to DNA insertions and deletions (Chang et al., 2017). DNA insertion or deletion mutations mediated during NHEJ may produce a frame shift where the number is not divisible by 3 and therefore inserts a nonsense mutation terminating transcription. This effectively knocks out specific genes and this technique was used in this project to generate CIZ1 knockout mouse fibroblast cells.

For more precise genome editing the homologous recombination (HR) pathway is used.

Briefly, HR utilizes homologous DNA as a template for DNA repair this limits repair by HR to G2/M making it a rarer event than NHEJ (approximately 25% of the time) (Mao et al., 2008). This repair pathway can be manipulated by concurrently transfecting cells with the tools for the CRISPR/Cas9 system along with a sequence of DNA containing the desired point mutation, insertion, or deletion flanked by regions of homologous DNA. HR uses this modified template to incorporate the desired gene manipulation into the genome. Since mammalian cells are diploid, both chromosomes must be edited, reducing the proportion of cells that are successfully modified (Figure 4.1).

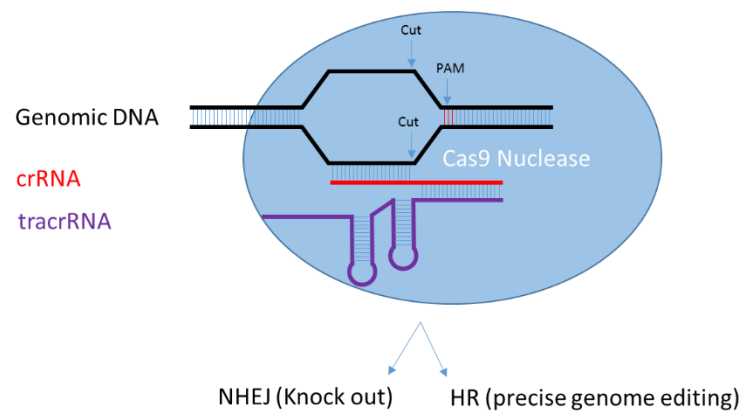


Figure 4.1 – CRISPR CAS9 mediated genome editing A) Schematic of the CRISPR Cas9 mechanism used to edit eukaryotic genomes. crRNA binds complimentary sequence onto genomic DNA adjacent to a PAM sequence, together with tracrRNA this complex recruits the nuclease Cas9, which nicks the genomic DNA proximal to the PAM sequence. The DSB is then repaired by either NHEJ or HR. These repair pathways can be exploited to modify DNA either through truncations or by genome editing.

4.1.2. Chapter Aims

- Generate 2 distinct CIZ1 KO NIH 3T3 clones (KO1 and KO2)
- Generate CIZ1 add back cell lines that express GFP-CIZ1 (CIZ1^{AB}) NIH 3T3 Cells.
- Analyse and compare cell cycle profiles for parental WT fibroblasts and CIZ1 null fibroblast cell lines.
- Determine cell cycle re-entry kinetics upon loss in WT and CIZ1 null fibroblasts
- Evaluate the response to DNA Damage in CIZ1 null fibroblasts.

4.2. Generating CIZ1 Null Cells using CRISPR-Cas9

To functionally knockout the CIZ1 gene, oligonucleotides were designed that would target the second exon of the mouse CIZ1 gene. The second exon was chosen because of differential splicing of the CIZ1 gene leads to 2 major transcripts that are developmentally regulated. The full length CIZ1 gene utilises Exon 1 and the embryonic CIZ1 (ECIZ1) splice variant does not express exon 1 (Higgins et al., 2012). Targeting of exon 2 would inactivate both splice variants. To ensure that the effects of targeting the CIZ1 gene with CRISPR-CAS9 results in a phenotype associated with CIZ1 knockout, two different crRNA oligonucleotide templates were designed for distinct PAM sequences within the same exon. This approach was used as CRISPR-Cas9 may have significant off target effects (Cradick et al., 2013), although there is disagreement regarding how significant off target effects are (Cenci et al., 2014). Production of two CIZ1 knockout cell lines through targeting of distinct sites enables comparison of any phenotype changes with independent clones. Consequently, a consistent phenotype in both CIZ1 knockout clones would suggest that it is related to the loss of CIZ1 than from off-target effects.

The complementary sequences for crRNA uses 20 nucleotides 5' to a PAM sequence (Figure 4.2). PAM sequences for Cas9 have a conserved sequence of 5' – NGG – 3'. Two PAM sequences were identified: one at position 1137 with sequence 5' – AGG – 3', and one at position 1155 with sequence 5' – TGG – 3'. Oligonucleotides for the guide RNA sequence were designed, inserted into the linearized gene art CD4 CRISPR plasmid (as described in Section 2). The oligonucleotides and structure of the dimerised oligonucleotides for PAM 1137 (named KO1) and PAM 1154 (named KO2) is shown in Figure 4.2b.

A

Ciz1 KO1 Guide Sequence: (position 1116 genomic)

...CAAAGAGCTTTGCTCCTACAGCAGTTGCAAGGACTGGACCA...

Ciz1 KO1 For: TTGCTCCTACAGCAGTTGCAGTTTT

Ciz1 KO1 Rev: TGCAACTGCTGTAGGAGCAACGGTG

```

      5'-TTGCTCCTACAGCAGTTGCAGTTTT-3'
      |||
      3'-GTGGCAACGAGGATGTCGTCAACGT-5'

```

B

Ciz1 KO2 Guide Sequence: (position 1134 genomic)

...CAGCAGTTGCAAGGTATGGCAGTTCCCCGTGGTAACCCATT...

Ciz1 KO2 For: CAAGGTATGGCAGTTCCCCGGTTTT

Ciz1 KO2 Rev: CGGGGAACGCCATACCTTGCGGTG

```

      5'-CAAGGTATGGCAGTTCCCCGGTTTT-3'
      |||
      3'-GTGGCGTTCCATACCGTCAAGGGGC-5'

```

Figure 4.2 – crRNA Sequences targeting CIZ1 A) The target sequence for generating CIZ1 knockouts at the KO1 site (A) and KO2 (B) showing the PAM site (red) and target sequence (green). The structure of the annealed oligonucleotide for inserting into plasmid GeneART plasmids to be transfected into cells to generate knockouts is also shown.

Cells were transfected with the CRISPR-Cas9 plasmid, enriched, and plated in a 96 well plate diluted to single cells and verified by microscopy. Clonal populations were expanded from single cells up to 6 well plates and screened for CIZ1 knockouts by western blotting using plate of wild type NIH 3T3 cells as positive control. CIZ1 knockouts were confirmed by the disappearance of the CIZ1 band for CIZ1 PAM 1116 (hereafter called CIZ1-KO1) and CIZ1 Pam 1134, hereafter called CIZ1 KO2). Both clones were DNA sequenced to ensure the presence of a nonsense mutation in both chromosomes (Figure 4.3). Together, this data suggested that CIZ1 null cell lines had been successfully been generated utilizing both PAM sites.

Due to non-specificity of the lab made polyclonal CIZ1 antibody bands were present on the CIZ1 KO western blot. To ensure that these bands were not due to alternative truncations of

CIZ1 a titration of CIZ1-N471 was added to blocking buffer. This did not promote disappearance of bands present exclusively in CIZ KO. The conclusion was bands were not from CIZ1 but were nonspecific bands. As the antibody is raised against CIZ1-N471 there was a possibility of C-terminal only truncations, however these lack the important binding regions so would be unlikely to be functional.

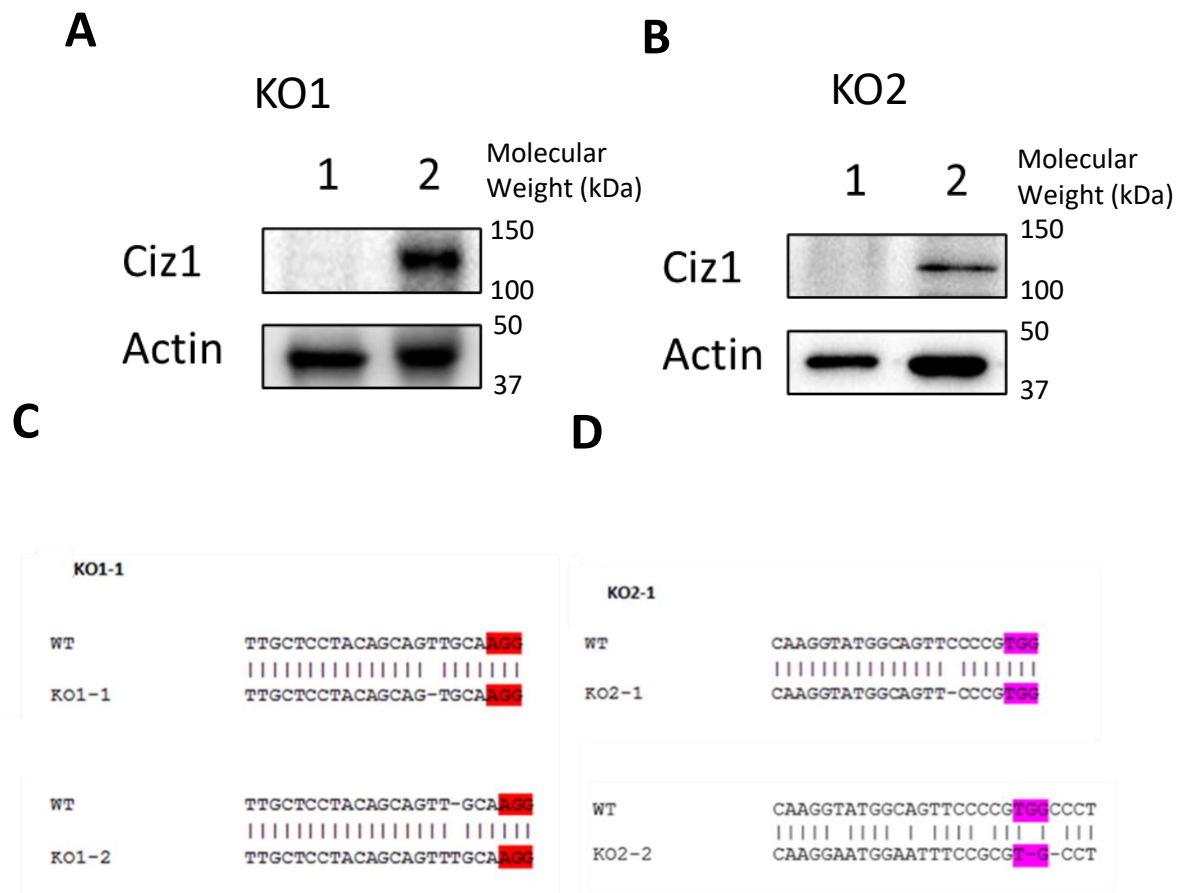


Figure 4.3-Generation of CIZ1 null NIH 3T3 cells A/B) Western blots of successful CRISPR CAS9 mediated CIZ1 knockout cells. Both CIZ1 KO1 (A) and CIZ1 KO2 (B) PAM sites resulted in the knocking out of CIZ1. Lane 1 displays the candidate for KO, lane 2 displays untreated cells. Blots were probed with antibodies for CIZ1 and actin. C/D) Sequencing of the PAM sites of the successful CRISPR CAS9 mediated CIZ1 knockout cells. Both CIZ1 KO1 (C) and CIZ1 KO2 (D) PAM sites resulted truncation of the CIZ1 gene prior to the PAM sites. The 2 KOS are displayed showing the 2 sequences from the 2 strands of DNA.

4.3. Characterisation of CIZ1 Null Cells

4.3.1. Loss of CIZ1 Does Not Affect the Asynchronous Cell Cycle Profile of NIH 3T3 Cells

Previous work has implicated a cell cycle role for CIZ1. CIZ1 levels accumulate as cells re-enter the cell cycle from quiescence (Pauzaite et al., 2017). CIZ1 has additionally been shown to interact with the G1/S cyclins: Cyclin A-CDK2 and Cyclin E-CDK2 (Copeland et al., 2010). This work led to the proposal that CIZ1 contributed to localisation of cyclin-CDK activity to putative replication origins suggesting that CIZ1 null cells may have altered cell cycle kinetics. However, no cell cycle or developmental defects in CIZ1 null mice have been identified (Nishibe et al., 2013; Ridings-Figueroa et al., 2017). To investigate the role of CIZ1 in cell cycle regulation and control of DNA replication timing, cell cycle characteristics of asynchronous cells were determined by EdU labelling and fluorescence microscopy, and EdU labelling and flow cytometry. Experiments were performed using WT NIH 3T3 cells, CIZ1 KO1, and CIZ1 KO2 (Figure 4.4).

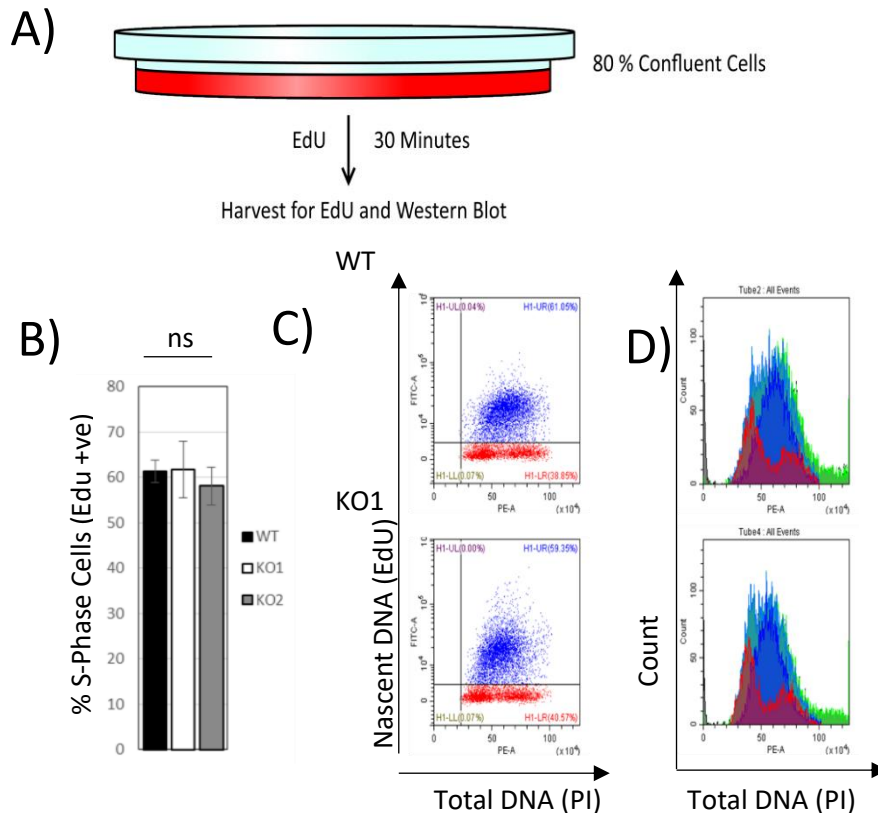


Figure 4.4 – Analysis of Cell Cycle Profiles of WT and CIZ1 KO Cell lines A) Schematic of the experimental design. B) The proportion of cells in S-phase (EdU +ve) measured using fluorescence microscopy ($N = 3 \pm S.D.$). No significant differences in the proportion of S phase cells was observed across cell lines (One Way ANOVA, $p > 0.05$) C) Displays flow cytometry profiles of cells of WT, and KO1, measuring nascent DNA synthesis (EdU incorporation) and total DNA content (PI). D) Flow cytometry profiles of WT and CIZ1 KO1 cells. EdU negative cells are red (G1 or G2/M), EdU positive cells are blue (S-phase). All data collected is displayed in green.

There was no significant difference between the proportion of cells in S-phase, as determined by EdU labelling and fluorescence microscopy with 61 % of asynchronous WT cells were in S-phase compared to 62 % of CIZ1 KO1 cells, and 57 % of CIZ1 KO2 (Figure 4.4B). Further analysis of WT and CIZ1 KO1 cells using flow cytometry is consistent with fluorescence microscopy and show that between 50 % and 70 % of cells are in S-phase. Additionally, analysis of EdU positive cells by flow cytometry reveals similar proportions of WT and CIZ1 KO cells in early, mid and late S-phase (Figure 4.4C). This suggests that unperturbed asynchronous cells have no significant changes to cell cycle kinetics. Furthermore, analysis of the G1 and G2/M populations reveals similar proportions of cells in each phase (Figure 4.4D).

This data suggests that CIZ1 deletion does not grossly affect cell cycle progression in asynchronous mouse fibroblast cells. This observation is consistent with murine CIZ1 null mice that displayed no defects in cell cycle status, or cell growth (Nishibe et al., 2013; Riding-Figueroa et al., 2017). Interestingly, loss of CIZ1 did cause increased aberrant cell cycle progression and DNA damage in aged mice (Khan et al., 2018), but this was not apparent in either CIZ1 KO cell line at low passage number. These results, together with previous work suggest that deletion of CIZ1 does not result in gross cell cycle defects in unstressed cycling cells.

4.3.2. CIZ1 KO Cells display Altered Cell Cycle Profiles During Cell Cycle Re-entry Post Quiescence.

Much of the work on CIZ1 suggests that it contributes to cell cycle progression in post-quiescent cells (Coverley et al., 2005; Copeland et al., 2010). Cell free DNA replication assays that have evaluated CIZ1 function are isolated from post-quiescence nuclei and in this context CIZ1 cooperates with cyclin A-CDK2 to promote initiation of DNA replication. CIZ1 accumulates as cells re-enter the cell cycle post-quiescence, and phosphorylation status is linked to activities of the G1/S cyclin CDK complexes (Copeland et al., 2015; Pauzaite et al., 2017). To investigate whether CIZ1 has a role in controlling S-phase entry timing post-quiescence WT, CIZ1 KO1, and CIZ1 KO2 cells were synchronised in G₀ through contact inhibition and serum depletion (Section 2.4.5). Cell cycle kinetics and levels of DNA

replication factors MCM2, CDC6, and PCNA were assessed for WT and CIZ1 KO1 cell lines (Figure 4.5).

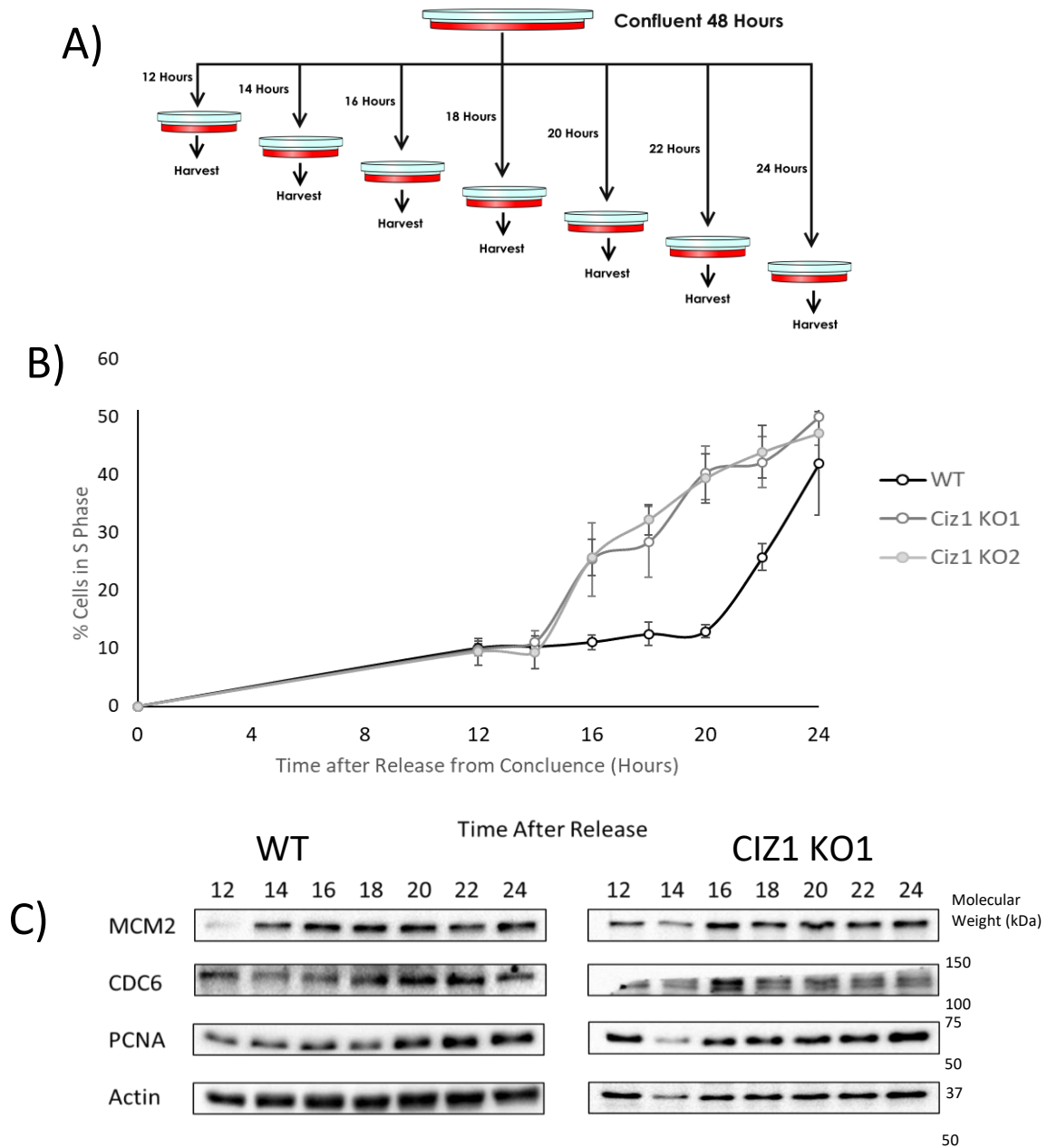
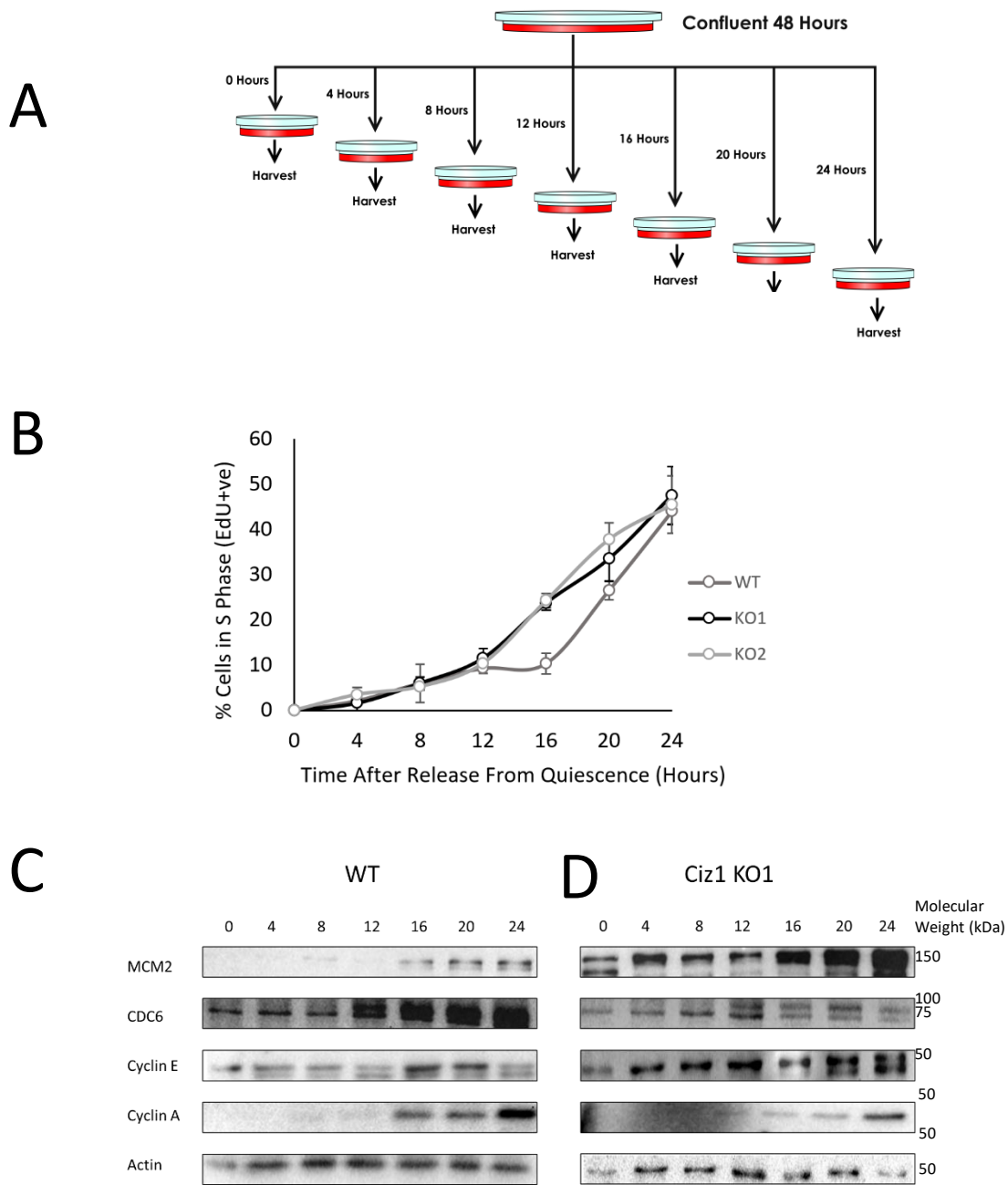


Figure 4.5 – Cell Cycle re-entry Profiles of WT and CIZ1 null cells A) a Schematic of the experimental design. WT, CIZ1 KO1 and CIZ1 KO2 cells were synchronised in G_0 and released into S-phase. Samples were harvested at 2 hourly time points. B) The proportion of cells in S-phase measured by EdU incorporation. The proportion of cells in S phase at each time point ($n = 3$ repeats) for each cell line was compared using a two-way ANOVA with time and cell line as factors (P (time) < 0.01 , P (cell line) < 0.01 , P (interaction) < 0.01). Pairwise comparisons were made by simple main effects analysis: no significant differences were observed between KO1/KO2 cells at any timepoint, or WT/KO1 and WT/KO2 cells at 12, 14, and 24 ($P > 0.05$ at each timepoint). Significant differences were observed between WT/KO1 and WT/KO2 cells at all remaining timepoints ($P < 0.001$ for all timepoints). Error bars in B = standard deviation. C) Western blots of whole cell extracts displaying MCM2, CDC6, PCNA and Actin.

To determine the effect on CIZ1 deletion on cells re-entering the cell cycle post-quiescence, the percentage of S-phase cells was determined for WT and CIZ1 KO1 and KO2 cell lines between 12-24 hours post-release from G₀. The low percentage of cells in S-phase at 12 hours and the rise in proportion of cells in S-phase after 16 hours is consistent with effective synchronisation and cell cycle re-entry for both WT and CIZ1 KO cell lines. However, there is a marked difference in G1 length as the CIZ1 KO cell lines entered S-phase 4 hours earlier than WT cells (Figure 4.5B). Both KO cell lines show an increase in S-phase cells at 16 hours, whereas the WT cell line enters S-phase later at ~20 hours post-release from quiescence. Between 16 – 20 hours significantly fewer WT cells are in S phase compared to both KO cell lines.

A two way ANOVA revealed significant interaction between cell line and time after release from quiescence on the proportion of cells entering S phase. Simple mains effects analysis revealed that this difference was significant between WT and KO1, WT and KO2, but not KO1 and KO2 cells between 16-22 hours post quiescence.

As CIZ1 KO cell lines showed differences in G1 length after release from quiescence, pre-RC proteins CDC6 and MCM2 and the replisome protein PCNA were monitored using western blotting of whole cell extracts (Figure 4.6). Western blots showed that there is an accumulation of PCNA and MCM2 in both WT And CIZ1 KO cell lines. Importantly, in WT cells increased MCM2 levels was observed between 12-14 hours that was not observed in CIZ1 KO1 cells. Broadly, there are no gross changes in the protein accumulation for CDC6 or PCNA for WT and CIZ1 KO cells. As the protein levels are comparable, the accumulation of replication proteins as well as Cyclin A and Cyclin E was determined in a more comprehensive time course from 0-24 hours to capture potential differences in early G1 phase (Figure 4.6).



37

Figure 4.6 – Loss of CIZ1 changed the timing of cell cycle re-entry A) A schematic of the experimental design. B) Cell cycle re-entry post quiescence showing proportion of cells in S-phase at each time point for WT and CIZ1 KO cell lines. The proportion of cells in S phase at each time point ($n = 3$ repeats) for each cell line was compared using a two-way ANOVA with time and cell line as factors (P (time) < 0.001 , P (cell line) < 0.001 , P (interaction) < 0.001 . Pairwise comparisons were made by simple main effects analysis: no significant differences were observed between KO1/KO2 cells at any timepoint, or WT/KO1 and WT/KO2 cells at 0, 4, 8, 12 and 24 ($P > 0.05$ at each timepoint). Significant differences were observed between WT/KO1 and WT/KO2 cells at all remaining timepoints (20 Hours $P < 0.05$ for both comparisons, $P < 0.001$ for all remaining timepoints). Error bars in B = standard deviation D) Western blots showing the levels of MCM2, CDC6 cyclin A and Cyclin E in WT (C) and KO1 cells (D).

Both WT and CIZ KO cell lines efficiently synchronised in G₀ and re-entered the cell cycle. The very low S populations of S-phase cells are early timepoints and increasing S-population indicate that both WT and CIZ1 KO cells are effectively synchronised at G₀ and effectively re-enter the cell cycle. Between 0 to 12 hours, there are no differences in the percentage of WT, KO1 and KO2 cells in S-phase. However, CIZ1 KO cell lines entered S-phase more rapidly than WT cells. Both CIZ1 KO cell lines show an increase in S-phase cells at 16 hours, whereas the WT cell line enters S-phase later at 20 hours post-release from quiescence, consistent with Figure 4.5.

A two way ANOVA revealed significant interaction between cell line and time after release from quiescence on the proportion of cells entering S phase. Simple main effect analysis revealed that this difference was significant between WT and KO1, WT and KO2, but not KO1 and KO2 cells between 16-20 hours.

As CIZ1 KO cell lines showed differences in G₁ length after release from quiescence, pre-RC proteins CDC6 and MCM2 as well as the G₁/S phase cyclins, Cyclin A and Cyclin E were determined (Figure 4.6C,D). Accumulation of CDC6 in WT cells was more apparent than in CIZ1 KO cells at late time points. Conversely, MCM2 levels were increased at early time points in CIZ1 KO cells compared to WT cells. Importantly, cyclin E and A are detectable at earlier time points for CIZ1 KO cell lines relative to WT 3T3 cells. This suggests that CIZ1 null cells may express Cyclins E and A earlier to overcome the loss of CIZ1 function that enhances their activity at the G₁/S transition (Copeland et al., 2010) and suggests that CIZ1 contributes to the mechanisms that maintain cell cycle timing and progression at the G₁/S transition in post-quiescent cells.

4.3.3. Analysis of cell cycle exit into quiescence in WT and CIZ1 KO murine fibroblasts

The difference in G1 length observed in post quiescent WT NIH 3T3 and CIZ1 KO cells is accompanied by a change in G1 and S-phase cyclin levels. As cyclin expression is driven through mitogenic signals, changes in cyclin E and cyclin A accumulation in CIZ1 null cells may be due to a difference in the degree of synchrony achieved by contact inhibition or changes in the restriction point. The levels of cyclin expression also regulate G1 length after quiescence, as Cyclin E overexpression changes cell cycle re-entry kinetics post-quiescence (Macheret & Halozonetis, 2018). To validate that differences in results seen between WT, and CIZ1 KO cells re-entering the cell cycle effective synchrony at G_0 , exiting the cell cycle needed to be confirmed. To determine the effect of CIZ1 deletion on cells exiting the cell cycle, the proportion of WT, CIZ1 KO1, and CIZ1 KO2 cells exiting the cell cycle was determined in confluent cells on day 0 (day of confluence), 24 hours after reaching confluence, and 48 hours after reaching confluence. (Figure 4.7).

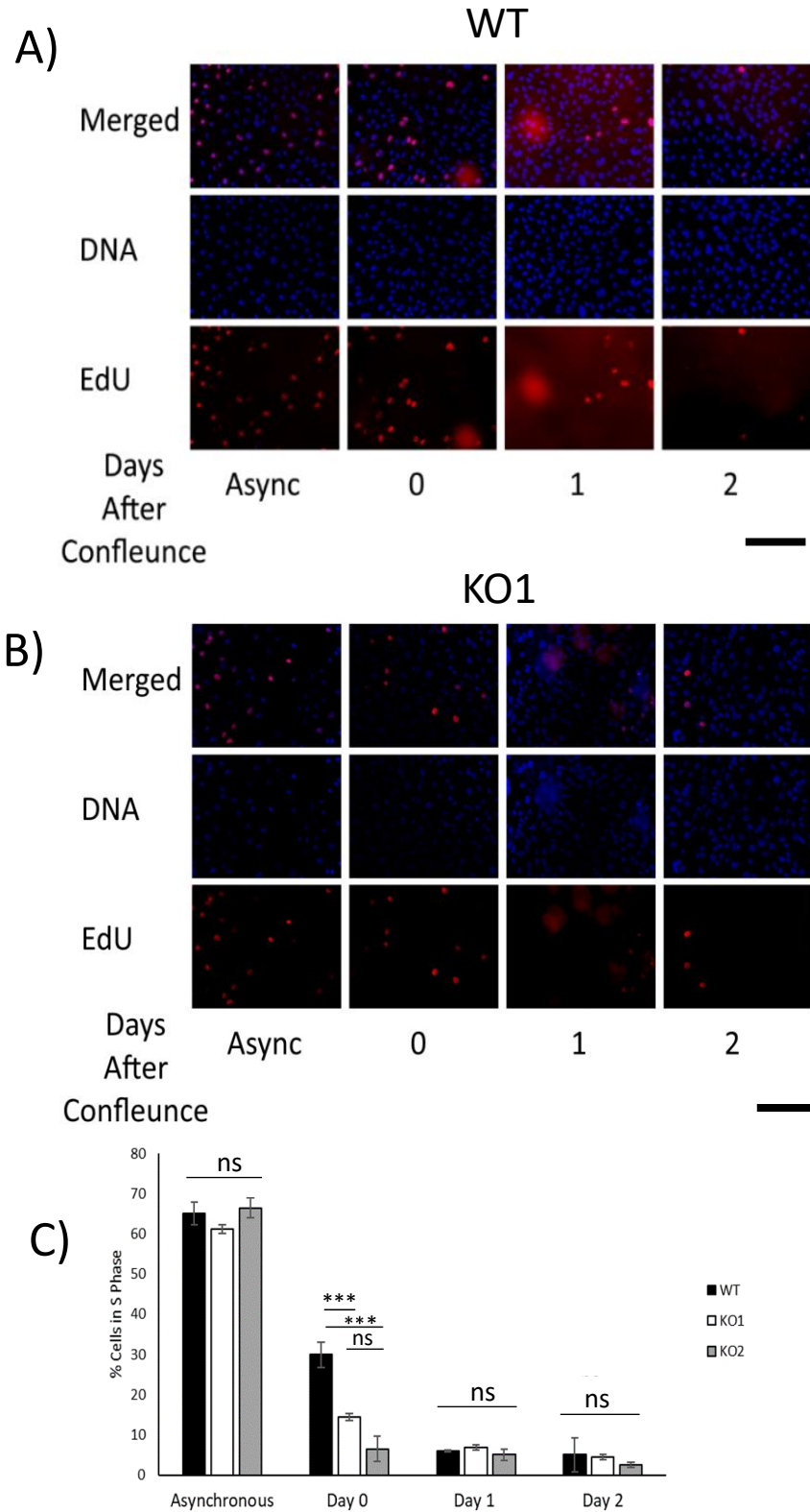


Figure 4.7 – *CIZ1* KO cells exit cell cycle more rapidly than WT cells A/B) Representative images of WT and KO1 cells asynchronous, at quiescence, and each day after quiescence release. Blue represents DAPI, and red represents EdU. Scale bars represent 200 μm . C) The proportion of cells in S phase at each time point for each cell line. Measured by fluorescence microscopy of cells that incorporated EdU. The proportion of cells in S phase at each time point ($n = 3$ repeats) for each cell line was compared using a two-way ANOVA with time and cell line as factors (P (time) < 0.001, P (cell line) < 0.001, P (interaction) < 0.001. Pairwise comparisons were made by simple main effects analysis, significance is highlighted on C. ns = non-significant * = $p < 0.05$, ** = $p < 0.01$, *** $p < 0.001$. Error bars in C = standard deviation

Analysis of asynchronous cell cultures between 60 -70 % of each cell line (WT, CIZ1 KO1, and CIZ1 KO2) were in S-phase, and no large differences were observed between the cell lines. However, at the day of 100 % confluence (day 0), fewer WT cells had exited the cell cycle than either of the CIZ1 KO cell lines, with 32 % of WT cells were in S-phase, compared to 12 % and 10 % of CIZ1 KO1 and CIZ1 KO2 cell lines respectively. A two way ANOVA revealed significant interaction between time point and cell line. Simple main effects analysis revealed significant differences between WT cells, and both KO1 and KO2 cells on the day of confluence (day 0), no significant differences were observed between KO1 and KO2 cells at any timepoint. This suggested both KO cells lines exited the cell cycle faster than WT cells. 24 hours after reaching confluence, all cell lines had fewer than 10 % of cells in S-phase and 2 days after confluence all cell lines had <5% of cells in S-phase.

The reduction in the proportion of cells in S-phase by two days after reaching confluence show that both WT, and CIZ1 KO cells are effectively synchronised at G₀ by contact inhibition and serum starvation. This result confirms that differences observed in cell cycle re-entry were not due to an inefficiency in cell cycle exit caused by loss of CIZ1. The decrease in the number of both KO cells in S-phase at earlier time points suggest that CIZ1 KO cells exit the cell cycle faster than WT cells and that differences in cyclin E and A expression are not due to asynchrony in the CIZ1 KO cell lines. This data supports the potential for CIZ1 in regulation of the restriction point. The kinetics of cell cycle exit is linked to intracellular kinase levels carried over from the previous cell cycle (Moser et al., 2018). This is consistent with the CIZ1's proposed role as a kinase sensor that regulates the G1/S transition through with Cyclin A and Cyclin E interactions (Copeland et al., 2015). These data further support observations that implicate CIZ1 as a kinase sensor and modulator of cyclin-CDK activity. These data suggest that CIZ1 affects the efficiency of cells exiting of the cell cycle at quiescence, and also influences cell cycle re-entry from quiescence.

4.3.4. Analysis of the timing for Restriction point in WT and CIZ1 null fibroblasts.

Results up to this point have revealed that CIZ1 null cells have different cell cycle re-entry kinetics when compared to WT cells. There is some evidence indicating this result was due to changes in response to external growth signals. CIZ1 null cells display a more rapid cyclin expression profile and exit the cell cycle more rapidly when growth signals are depleted. If cells are responding differently to growth signals, a change in the timing of the restriction point may be observed. The restriction point describes the point in G1 at which cells no longer require mitogenic signal to complete the cell cycle. Post-restriction point cells are 'committed' to completing the cell cycle and to dividing.

To determine the timing of restriction point in WT and CIZ1 KO cell lines, synchronised cells were released and cultured in media with serum. Cells were synchronised in G₀ released into fresh media and grown on coverslips for analysis of the proportion of cells at each time point in S-phase. Subsequently, at time points media was removed, cells washed and serum free media plus EdU added to define the time point where cells become independent of mitogens for cell cycle progression (Figure 4.8).

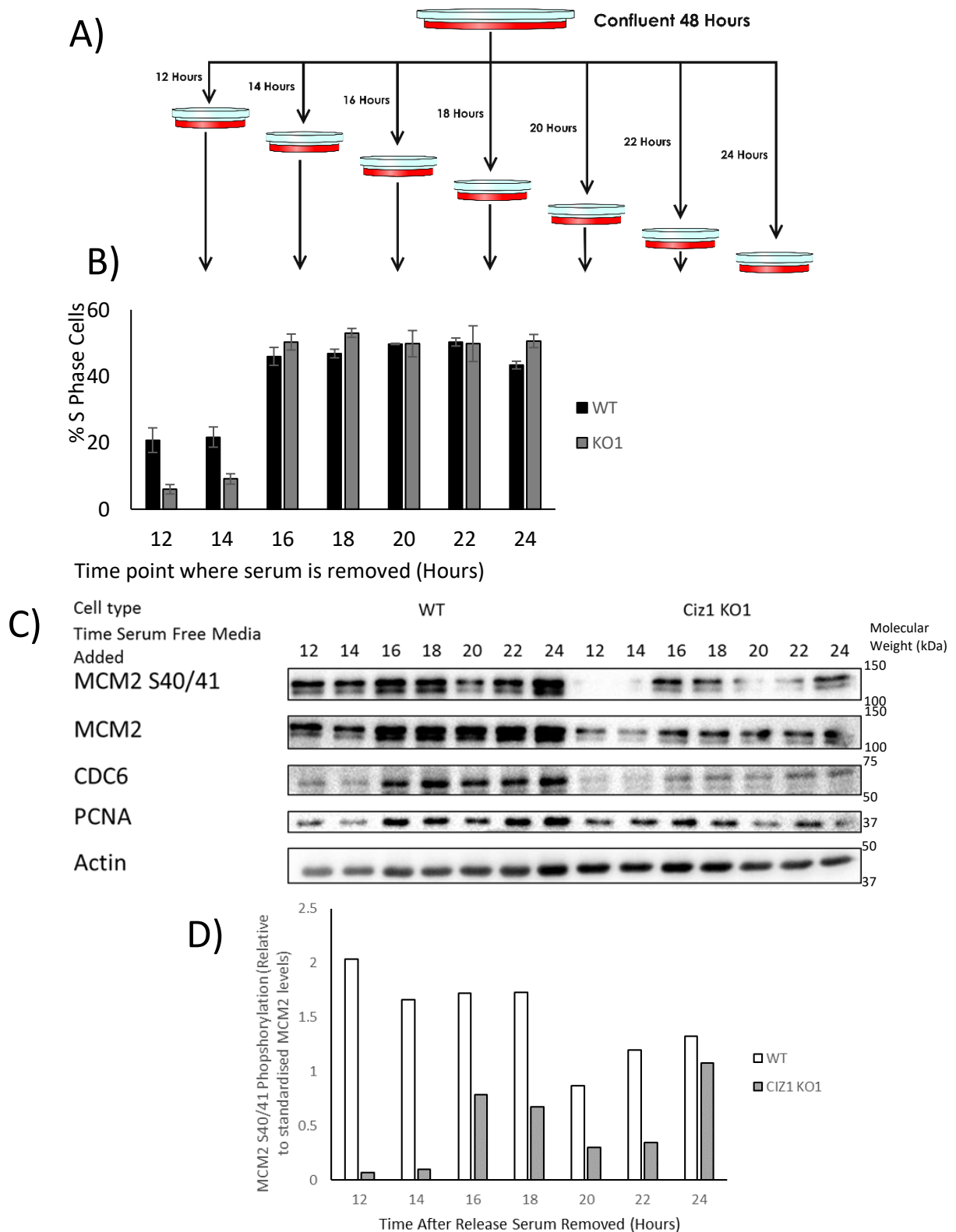


Figure 4.8-Loss of CIZ1 altered serum dependence A) A graphical schematic of the experimental design. B) The percentage of cells that were EdU positive, measured by fluorescence microscopy ($N = 3 \pm S.D.$). C) Western blots of a number of replication factors at each time point for WT and CIZ1 KO1 cells. D) Quantification of MCM2 S40/41 phosphorylation relative to MCM2 levels standardised to actin

To determine the effect of CIZ1 knockout on the timing of the restriction point after cells are synchronously released from G₀, the percentage of S-phase cells was determined 24 hours after release. The removal of serum is indicated for each time point for WT and CIZ1 KO1. To establish if any changes observed were associated with differences in accumulation of replication licensing factors western blots of whole cell extracts were performed with DNA replication licensing factors and PCNA.

In contrast to cell cycle re-entry in a complete medium, WT cells appear to be less dependent on serum for cell cycle re-entry than CIZ1 KO cells, pre-restriction point. For CIZ1 KO1 cells, less than 10 % of cells enter S-phase before 14 hours but from the 16 hour time point onward between 45 – 55 % of cells had reached S-phase by 24 hours, comparable to the WT cells. As CIZ1 KO cell lines showed reduced numbers of cells in S-phase levels before the 16 hour time point, we monitored the Pre-RC proteins CDC6 and MCM2, pS40/41 MCM2 and PCNA. The phosphospecific anti-MCM2 phosphoserine 40/41 monitor DDK and CDK mediated phosphorylation (Fei et al., 2018). Western blots showed a reduction in MCM2, and CDC6 in CIZ1 KO cells relative to WT controls at each time points. PCNA accumulation seemed less affected in CIZ1 KO1 cells, relative to controls PCNA levels increase from 16 hours onwards was observed in WT cells. Reduced pre-RC (Cdc6, MCM2) protein levels are observed in CIZ1 null cells after the restriction point implying a deficiency in the cellular signalling that results in their accumulation. PCNA levels are largely unchanged implying that this deficiency is linked to replication licensing and initiation rather than replisome assembly. MCM2 phosphorylation was higher at all timepoints in WT cells. MCM2 Phosphorylation was unaffected by passing the restriction point in WT cells. In CIZ1 KO cells before the restriction point there was a large decrease in MCM2 s40/41 phosphorylation (4.8D). Together this indicates a greater reliance on growth signals in CIZ1 KO cells pre-restriction point. However, post restriction point replication is allowed to continue with reduced accumulation of

licensing and initiation factors. This could result in DRS due to under licensed DNA in conditions with low levels of growth signals.

The rise in proportion of cells in S-phase for both WT, and CIZ1 KO1 cells from 16 hours post release suggests cells were effectively synchronised at G_0 , meaning differences were due to loss of serum. The increase in number of both WT, and CIZ1 KO1 cells in S-phase between 14 hours and 16 hours indicates that the restriction is between 14 and 16 hours post release from quiescence. The reduced proportion of CIZ1 KO1 cells in S-phase prior to this implied restriction point suggests that before the restriction point, CIZ1 KO1 cells have an increased dependence on exterior signalling than WT cells. This coupled with increased cell cycle re-entry rate suggesting a role for CIZ1 both before and after the restriction point.

4.3.5. Loss of CIZ1 Causes a Moderate Shift in the Restriction Point in Post Quiescence Cells

To further investigate if there was any difference in the restriction point experiments from 4.6. were repeated at hourly intervals surrounding 14-16 hours. The proportion of cells in S-phase at 24 hours were determined from 15-17 hours (Figure 4.9).

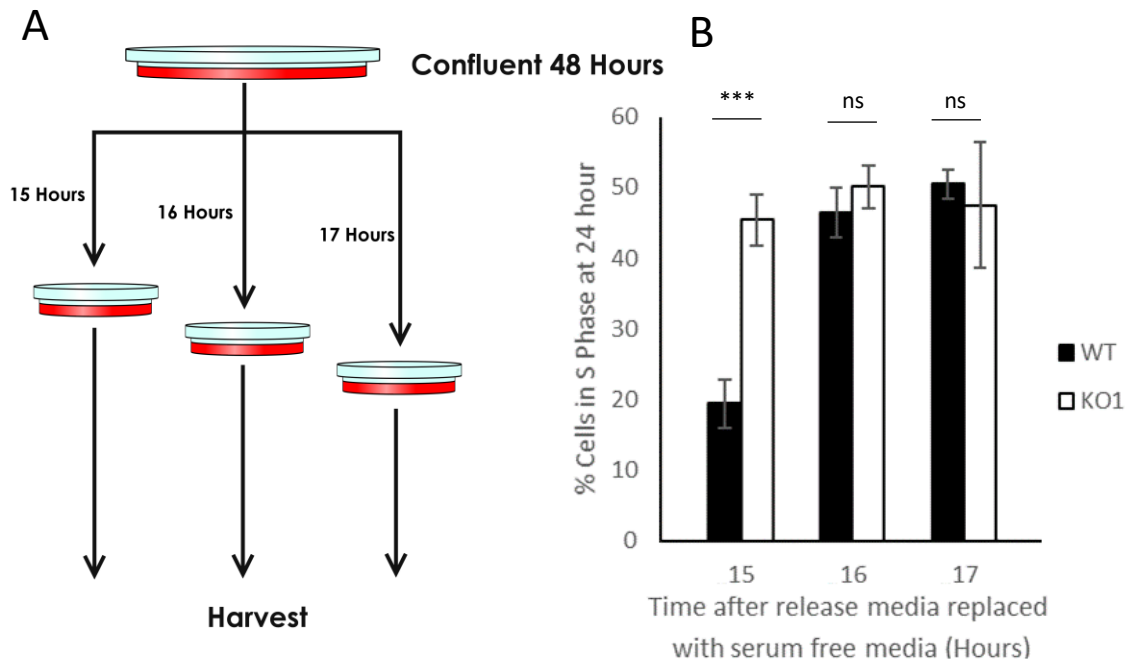


Figure 4.9-Loss of CIZ1 altered the restriction point A) A graphical schematic of the experimental design. B) The proportion of cells that were EdU positive, measured by fluorescence microscopy. The proportion of cells in S phase at each time point ($n = 3$ repeats) for each cell line was compared using a two-way ANOVA with time and cell line as factors (P (time) < 0.001 , P (cell line) < 0.01 , P (interaction) < 0.01). Pairwise comparisons were made by simple main effects analysis, significance is highlighted on C. ns = $p > 0.05$, * = $p < 0.05$, ** = $p < 0.01$, *** $p < 0.001$ Error bars in B= standard deviation

A low proportion of WT cells were in S-phase at 15 hours post-release, consistent with Figure 4.8. However, there is an increase in the percentage of S-phase cells 15 hours post release from quiescence in CIZ1 KO cell lines. This was significantly difference from WT cells. The difference is short lived as at the 16 hour time point 40-50 % of both WT and CIZ1 KO cells are in S-phase, consistent with earlier results (Figure 4.8), no significant differences were observed between cell lines at either the 16 or 17 hour timepoints.

The data presented here suggests that at early time points before 14 hours after release, WT cells are more likely to enter S-phase after removal of serum but that CIZ1 KO cell lines have

an earlier restriction point. In WT cells the restriction point lies between 15-16 hours post release from quiescence, where as in CIZ1 KO1 cells it lies between 14- 15 hours post release from quiescence. Coupled with earlier data, this indicates that CIZ1 may contribute to the mechanisms that regulate the timing of restriction point.

4.3.6. Loss of CIZ1 Results in a Prolonged DDR to Hydroxyurea

In fibroblasts isolated from murine CIZ1 knockout models, CIZ1 null cells were sensitive to DNA damaging agent Hydroxyurea (HU) (Nishibe et al., 2013). Hydroxyurea is frequently used to increase DRS through the depletion of nucleotide pools leading to stalled DNA replication forks. To investigate the effect of HU treatment in CIZ1 KO cells, WT, CIZ1 KO1, and CIZ1 KO2 cells were treated with hydroxyurea for 2 hours, HU removed and cell incubated in fresh media. To investigate the impact on DNA replication the proportion of cells in S-phase was determined and activation of the DDR by phosphorylation of H2AX was determined at each time point by western blot for WT, and CIZ1 KO1 cells (Figure 4.10).

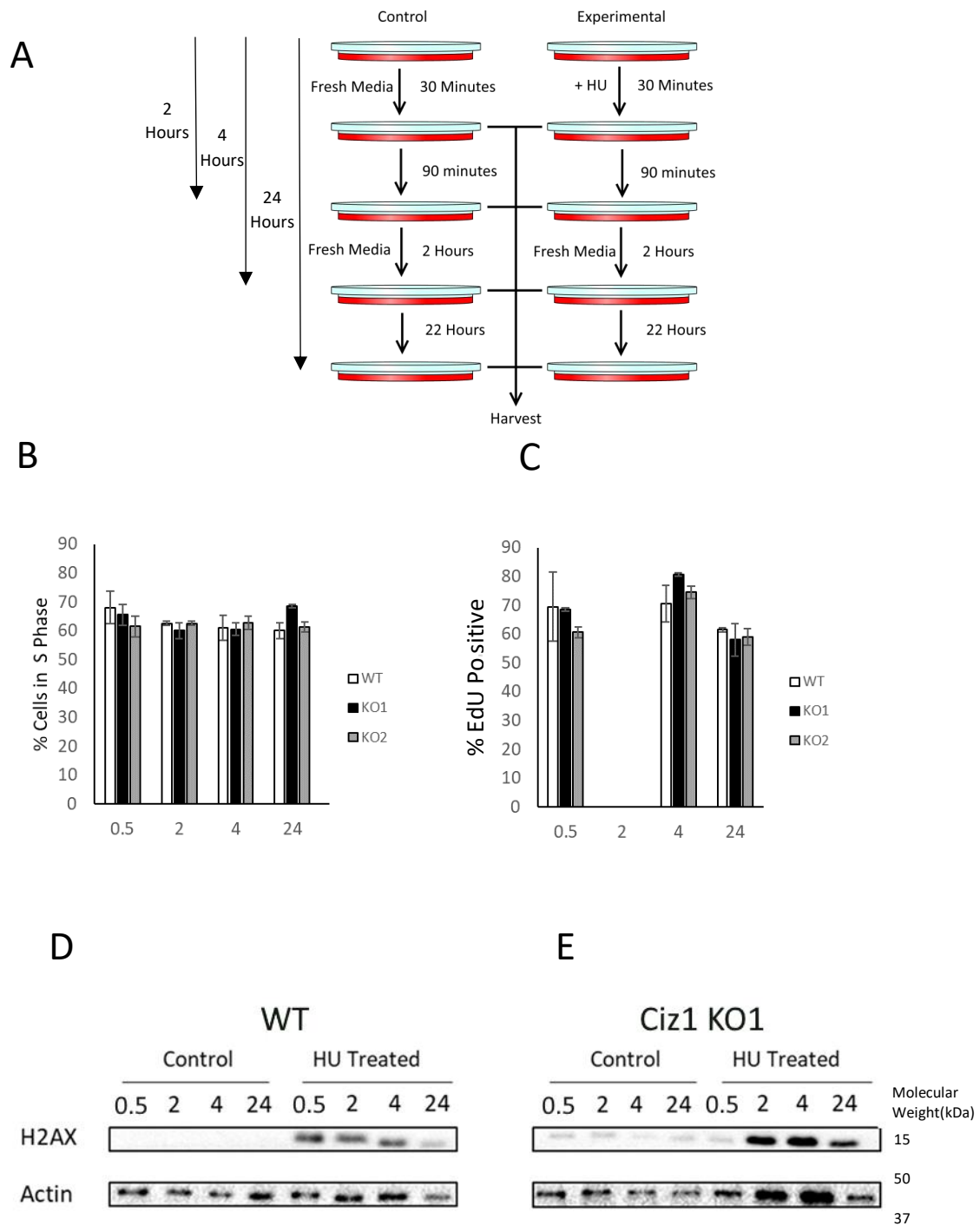


Figure 4.10 – Loss of CIZ1 moderates the DDR to HU Cells were treated with HU and then HU was removed. A) A graphical schematic of the experimental design. B) The proportion of cells in S-phase at each time point for negative controls with no HU C) The proportion of cells in S-phase at each time point for experimental samples ($N = 3 \pm S.D.$) D) The levels of γ H2aX phosphorylation at each time point for WT cells. E) The level of γ H2aX phosphorylation at each time point for KO1 cells

For both WT, CIZ1 KO1, and CIZ1 KO2 cells there were small variations in the proportion of cells in S-phase at time points, however all remained between 50 – 70 %. This provides a base level of cells in S-phase, that is corroborated by earlier data. Treatment with HU resulted in no change in the percentage of S-phase cells 30 minutes after treatment. However, 2 hours after treatment with HU there was complete ablation of the S-phase population of cells for WT and CIZ1 KO cell lines. Controls were included in which media changes occurred, but no HU was included (Figure 4.10 b). After removal of HU WT and CIZ1 KO1 and 2 cells rapidly entered the cell cycle within 2 hours (Figure 4.10C).

CIZ1 KO cell lines showed no differences in cellular responses to HU and cell cycle re-entry at these time points, but previous reports had indicated loss of CIZ1 results in a disrupted DDR. Next the phosphorylation status of Histone H2 was monitored at each time point for WT, and CIZ1 KO1 cells. In untreated control samples, no H2AX phosphorylation was observed at any time point. For WT cells (Figure 4.10D), a H2AX response was observed 30 minutes after HU treatment, which was sustained for the length of HU treatment (2 hours), and 2 hours after removal of the HU challenge. 24 hours after HU treatment H2AX phosphorylation had returned to baseline levels.

In CIZ1 KO1 cells (Figure 4.10E), there was a delay in H2AX phosphorylation relative to WT cells. There was a low H2AX phosphorylation signal, similar to those of negative controls after 30 minutes HU treatment. However, the phosphorylation of H2AX increased after 2 hours and this signal was maintained for 24 hours after treatment HU in CIZ1 KO1 cells. This prolonged intense H2AX signal suggests that CIZ1 null cells are deficient in fork restart or in the repair of damaged cells relative to WT cells (Figure 4.10D).

The drop, and subsequent resumption of the proportion of cells in S-phase show in response to HU treatment and removal implies that both WT, and CIZ1 KO cells effectively halt and restart S-phase in response to HU challenge. HU depletes nucleotide pools causing a stalling

in DNA replication. Efficient fork restart following this HU challenge indicates that the DDR is functional in CIZ1 KO cells. H2AX signalling changes in CIZ1 KO1 cells implies that loss of CIZ1 reduces the efficiency of the DDR, leading to prolonged phosphorylation of H2AX. This failure may cause increased DNA damage in response to DNA replication stress, leading to the prolonged H2AX response observed in CIZ1 KO1 cells. The prolonged response may also be due to a de-regulation of the DDR upon loss of CIZ1. This implicates CIZ1 as having a role in the efficiency of the DDR in response to replication stress. It has been proposed that CIZ1 deregulation may lead to DRS, this may be linked to the alternative DDR observed in response to HU (Chapter 6.).

4.4. Generating and Characterising CIZ1^{AB} Cells

4.4.1. Ectopic Expression of CIZ1 in CIZ1 KO1 NIH 3T3 Cells

To ensure that differences in cell behaviour observed between WT and CIZ1 KO NIH 3T3 cells were due to loss of CIZ1 and not an off-target effect introduced during the CRISPR Cas9 process, a GFP-CIZ1 addback cell line was produced. A GFP-CIZ1 construct was produced that contained a selection cassette to ensure stable transfection. CIZ1 KO1 cells were used to generate stably expressing GFP-CIZ1. The GFP-CIZ1 plasmid was linearized using ApaLI, and cells transfected with the linearized plasmid. After 24 hours 400 µg/ml geneticin (G-418) was added to the plate as a selection agent for 14 days, with media changes every 3 days. After selection, to validate that cells were expressing GFP-CIZ1, CIZ1 KO1 cell were harvested for western blot (Figure 4.11 e) and fluorescence microscopy analysis (Figure 4.11D). This stable transfection was performed in the CIZ1 KO1 cell line, which expressed the mouse WT ECIZ1 gene fused to GFP and will be referred to CIZ1^{AB} hereafter.

After 2 weeks of selection, fluorescence microscopy and western blotting were used to confirm GFP-CIZ1 expression. (Figure 4.11c/d/e). Fluorescence microscopy revealed a predominantly nuclear GFP fluorescence (Figure 4.11) demonstrating that selected cells expressed GFP-CIZ1. In addition, western blots showed the appearance of a GFP band at in transfected cells at the expected size (140 kDa), and CIZ1 was not present in untransfected CIZ1 KO1 cells. This data demonstrates successful stable expression of GFP-CIZ1 in the CIZ1^{AB} cell line. This cell line was used to investigate if CIZ1^{AB} cells would reverse the CIZ1 KO phenotypes observed in this chapter.

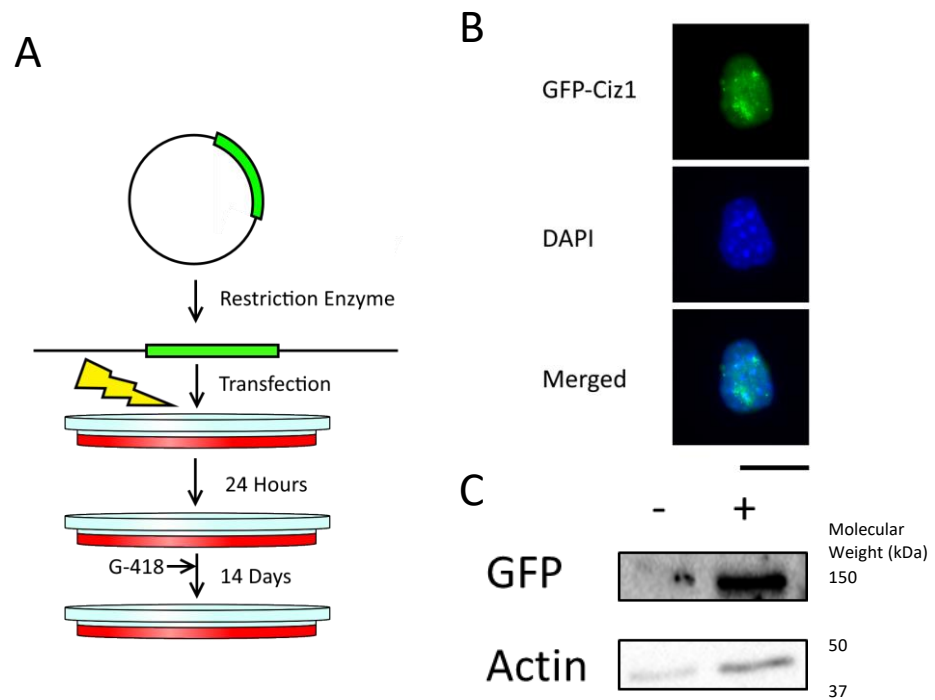


Figure 4.11-Generation of stably transfected CIZ1^{AB} Cell line A) Displays a Graphical Schematic of the process for generation of stably transfected GFP-CIZ1 expressing cells B) Displays representative images of cells expressing GFP-CIZ1 2 weeks after transfection and selection C) Western blot showing expression of GFP-CIZ1 in positive cells.

4.4.2. Asynchronous Cell Cycle Profiles of GFP-CIZ1 Addback Cells

Earlier experiments revealed that loss of CIZ1 caused no changes to the cell cycle profile of cells in S-phase (4.3.1). To validate the viability of CIZ1^{AB} cells and ensure that the addition had no effect on the proportion of cells in S-phase these experiments were to be repeated with CIZ1^{AB} cells. Again, asynchronous plates of WT, KO1, and CIZ1^{AB} cells were EdU labelled, samples were analysed by flow cytometry and scoring of the proportion of cells in S-phase, protein samples from whole cell extracts were also taken for analysis by western blotting (Figure 4.12).

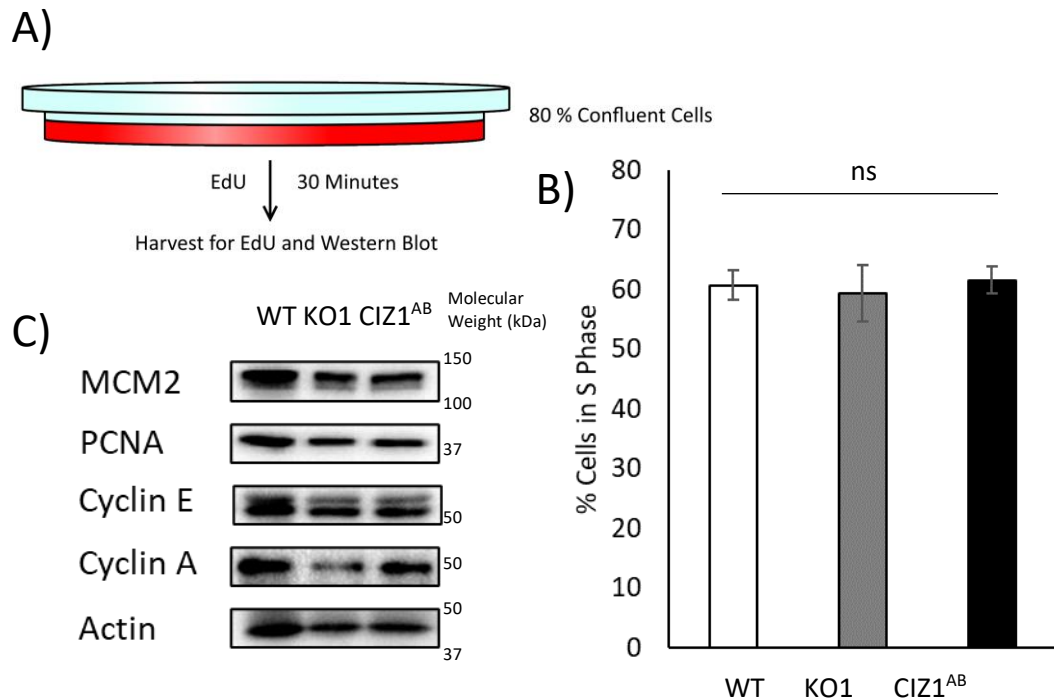


Figure 4.12-Analysis of asynchronous CIZ1^{AB} cell lines A) Displays a graphical schematic of the experimental design. B) Displays the proportion of each cell line in S-phase counted through fluorescence microscopy of positively Edu labelled cells. The mean proportion of cells in S phase did not vary significantly between conditions (one-way ANOVA $P > 0.05$, $n = 3$ for each condition), Error bars represent S.D. C) Displays western blot analysis of whole cell extracts of asynchronous cultures of the 3 cell lines.

To determine the viability of CIZ1^{AB} cells the proportion of WT, CIZ1 KO1 and CIZ1^{AB} cells was determined for asynchronous cell cultures. No significant differences were observed in the proportion of cells in S-phase for cells in WT, CIZ1 KO and CIZ1^{AB} cell lines in asynchronous

culture (Figure 4.12b). For each cell line an average of ~60 % of cells were in S-phase any observed differences were insignificant.

Western blots analysis of WT, CIZ1 KO and CIZ1^{AB} cell lines for pre RC protein MCM2, replisome protein PCNA, G1 cyclin: Cyclin E, and S-phase cyclin: Cyclin A (Figure 4.12c). No differences in the levels of MCM2, PCNA or Cyclin E were observed across cell lines. No differences in proportion of cells in S-phase between WT, and CIZ1 KO cells corroborated earlier data (Figure 4.3). In addition, genetic add back of CIZ1 did not affect cell cycle progression in asynchronous cells.

However, a reduction of Cyclin A levels was observed in CIZ1 KO1 cells compared to WT cells. This effect was reversed in CIZ1^{AB} cells that showed Cyclin A levels comparable to WT cells. This provides a key link between Cyclin A, and CIZ1. Previous studies have shown that CIZ1 interacts with Cyclin A at the nuclear matrix (Coverley et al., 2005; Copeland et al., 2010; Copeland et al., 2015), but no study has identified a link between CIZ1 and Cyclin A levels. This effect could be caused through disruption of the cellular signals that promote the expression of Cyclin A, or through disruption to the proteolytic pathways that result in the degradation of Cyclin A. The lower level of Cyclin A was not accompanied by a reduction in the proportion of cells in S-phase a direct link between CIZ1 and Cyclin A has interesting implications for its role in the G1/S transition (Chapter 5).

4.4.3. CIZ1^{AB} cells display WT cell cycle re-entry kinetics.

CIZ1 KO cells displayed a more rapid entry to S-phase from G₀ than WT cells (Figure 4.4-4.6). To provide additional support for the role of CIZ1 contributing to mechanisms that regulate the G1/S transition CIZ1^{AB} cells were used to demonstrate that this effect was reversible. If no effect is observed, this would suggest that this effect was likely mediated by off target effects.

To evaluate the effect of CIZ1 add back on cell-cycle re-entry kinetics post quiescence CIZ1^{AB} cells were compared to WT cells. Cells were synchronised in quiescence, released and cells were harvested as indicated. Cells were analysed by EdU labelling and fluorescence microscopy (Figure 4.13).

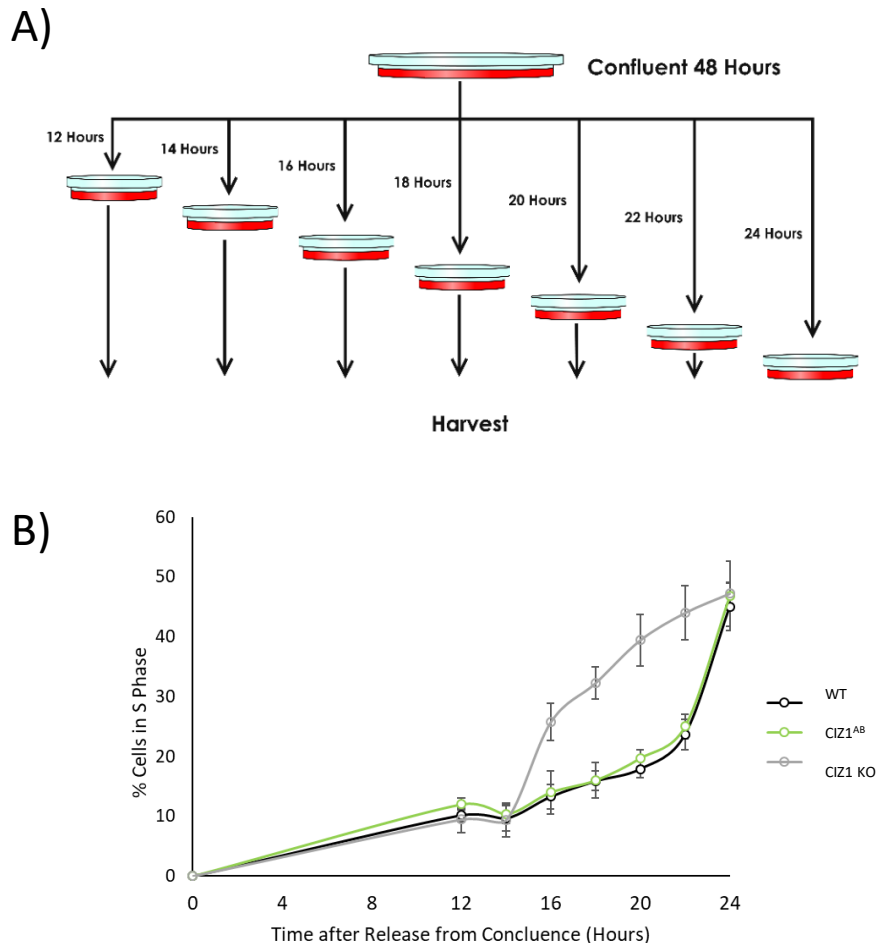


Figure 4.13. CIZ1^{AB} cell cycle re-entry post-quiescence mirrors WT cells. A) An overview of the experimental design B) Cell cycle progression was determined by EdU incorporation in S-phase, showing the percentage of cells at each time point. KO1 data is superimposed from Figure 4.5. The proportion of cells in S phase at each time point ($n = 3$ repeats) for each cell line was compared using a two-way ANOVA with time and cell line as factors (P (time) < 0.001 , P (cell line) < 0.001 , P (interaction) < 0.001). Pairwise comparisons were made by simple main effects analysis: no significant differences were observed between WT/CIZ1^{AB} cells at any timepoint, or WT/KO1 and KO1/CIZ1^{AB} cells at 12, 14, and 24 ($P > 0.05$ at each timepoint). Significant differences were observed between WT/KO1 and KO1/CIZ1^{AB} cells at all remaining timepoints ($P < 0.001$ for all timepoints). Error bars in B = standard deviation.

WT cells re-entered the cell cycle with increasing EdU incorporation from 20 hours and this was mirrored in CIZ1^{AB} cells. Both cell lines had consistent percentages of cells in S-phase at all time points. These data were notably different from results from CIZ1 KO1 that showed an increase in EdU positive cells from 16 hours after release from quiescence (Figure 4.4,

data also shown in Figure 4.13). In contrast, there were no large differences between WT and CIZ1^{AB} cell lines at any time point.

A two way ANOVA with revealed significant interaction between cell line and time after release from quiescence on the proportion of cells entering S phase. Simple main effect analysis revealed that this difference was significant between 16-20 hours between WT and KO1, KO1 and CIZ1^{AB}, but not WT and CIZ1^{AB} cells.

Earlier experiments revealed that the rapid entry of CIZ1 KO cells into the cell cycle after G₀ arrest occurred after 12 hours. To confirm this and validate the synchrony of CIZ1^{AB} cells, parallel experiments were designed to monitor cell cycle re-entry between WT and CIZ1^{AB} (Figure 4.14).

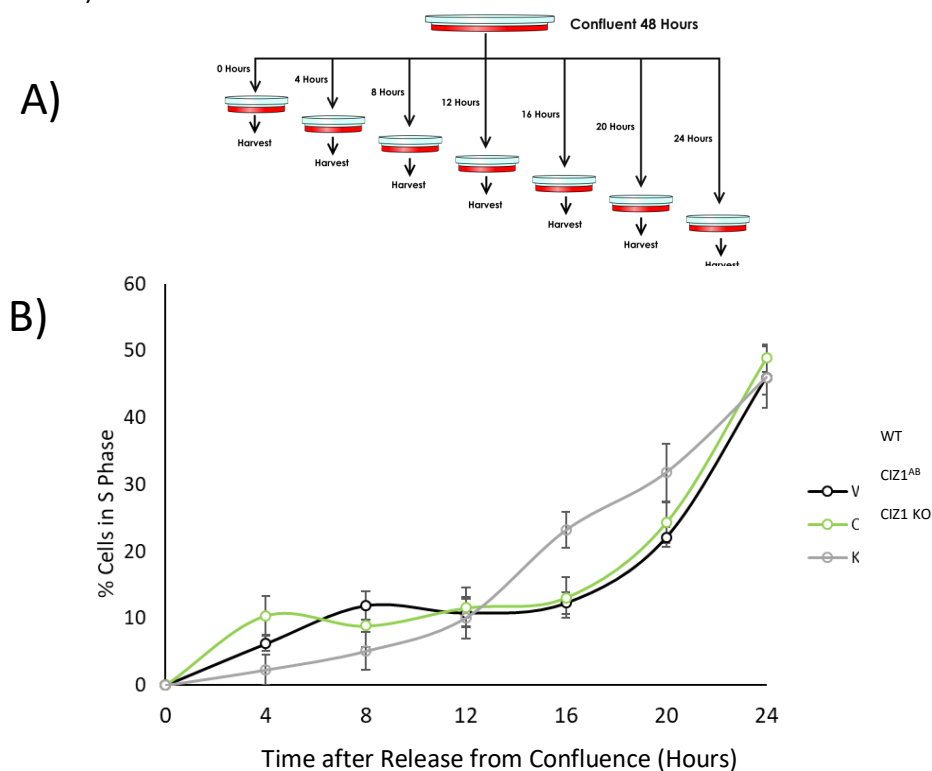


Figure 4.14 – 24 hour monitoring of a release of CIZ1^{AB} cells into S-phase A) Displays a graphical schematic of the experimental design B) The proportion of cells in S-phase for each time point measured by fluorescence microscopy of positively labelled cells. KO1 data is superimposed from Figure 4.6 . The proportion of cells in S phase at each time point (n = 3) for each cell line was compared using a two-way ANOVA with time and cell line as factors (P (time) < 0.001, P (cell line) < 0.001, P (interaction) < 0.001. Pairwise comparisons were made by simple main effects analysis: no significant differences were observed between WT/CIZ1^{AB} cells at any timepoint, or WT/KO1 and KO1/CIZ1^{AB} cells at 0, 4, 8, 12 and 24 hours (P > 0.05 at each timepoint). Significant differences were observed between WT/KO1 and KO1/CIZ1^{AB} cells at all remaining timepoints (P < 0.01 for all comparisons). Error bars in B = standard deviation

Comparison of 0-24 time courses revealed that WT and CIZ1^{AB} have similar re-entry kinetics that are not significantly different. This contrasts with CIZ1 KO1 that showed significant differences at time points 16-20 hours post release (Figure 4.6, data also shown in Figure 4.14). These differences were reversed by in CIZ1^{AB} cells.

A two way ANOVA with revealed significant interaction between cell line and time after release from quiescence on the proportion of cells entering S phase. Simple main effects analysis revealed that this difference was significant between WT and KO1, KO1 and CIZ1^{AB}, but not WT and CIZ1^{AB} cells between 16-20 hours. This suggested ectopic CIZ1 expression reversed the increased quiescence rate phenotype observed in CIZ1 KO.

As there were no significant differences between WT and CIZ1^{AB} cells at any timepoint. This confirmed G₀ synchrony of CIZ1^{AB} cells and marked another observable difference upon loss of CIZ1 that was rescued by ectopic expression of the GFP-CIZ1 fusion protein.

4.4.4. Altered 'Restriction Point' of CIZ1 KO cells is rescued by Ectopic Expression of GFP CIZ1

Earlier experiments revealed that loss of CIZ1 KO resulted in a shift in the timing of the restriction point by approximately 1 hour (Figure 4.9). This subtle, yet significant shift, may explain how CIZ1 null cells have altered cell cycle kinetics. Next to see if this effect was reversed in CIZ1^{AB} cells, restriction point was determined by adding serum free media between 15-17 hours post quiescence, the percentage of cells in S-phase determined (Figure 4.15).

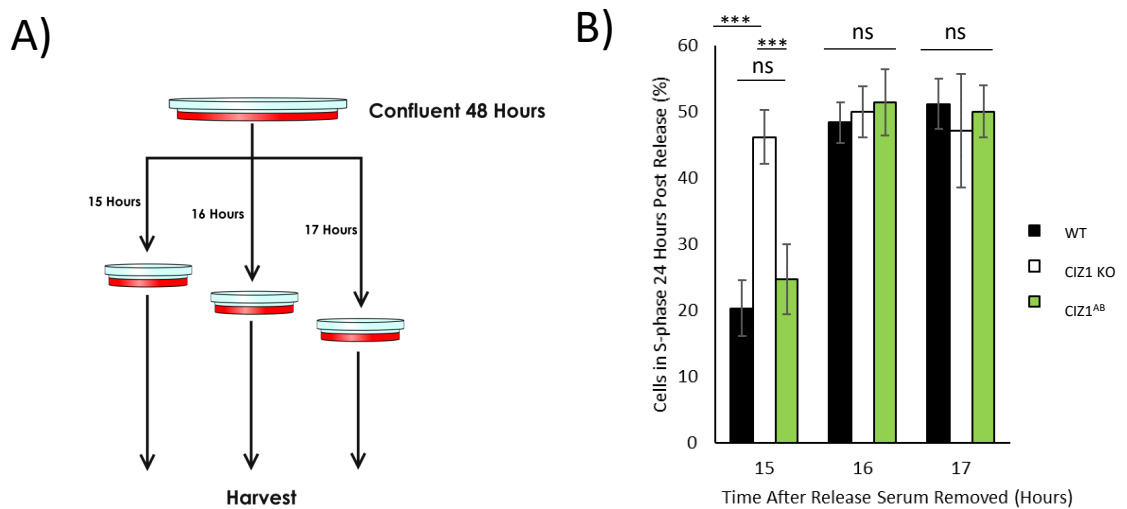


Figure 4.15-Analysis of the restriction of the CIZ1^{AB} cells. A) Displays a graphical schematic of the experimental design. B) Displays the proportion of cells in S-phase at 24 hours post release for each of the media change time points, measured through fluorescence microscopy of the positively EdU labelled cells. The proportion of cells in S phase at each time point ($n = 3$) for each cell line was compared using a two-way ANOVA with time and cell line as factors (P (time) < 0.001 , P (cell line) < 0.001 , P (interaction) < 0.001). Pairwise comparisons were made by simple main effects analysis, significance is highlighted on C. $ns = p > 0.05$, $* = p < 0.05$, $** = p < 0.01$, $*** p < 0.001$ Error bars in B= standard deviation. KO1 data is superimposed from Figure 4.9.

Removing serum at 15 hours showed 20 – 30 % of cells in S-phase for both cell lines. that increased for 16 hours to 40 – 50 % of cells were in S-phase, this is comparable to controls with no media change and suggests that the restriction point is between 15 and 16 hours for WT and CIZ1^{AB} cell lines. Comparison with CIZ1 KO1 cell line (From Figure 4.9, also shown in Figure 4.15) shows that restriction point was before 15 hours, showing that the CIZ1^{AB} cell line reversed differences in restriction point.

A two way ANOVA revealed significant interaction between cell line and time after release from quiescence on the proportion of cells entering S phase. Simple main effects analysis revealed that this difference at the 15 hour timepoint was significant between WT and KO1, and KO1 and CIZ1^{AB}, but not WT and CIZ1^{AB} cells. This indicated that ectopic CIZ1 expression could rescue the altered restriction point phenotype. This data suggests that CIZ1 plays a role in establishing the timing of restriction point in murine fibroblasts.

4.4.5. CIZ1^{AB} cells reverse defects in cellular response to Hydroxyurea

Earlier results demonstrated that loss of CIZ1 results in an altered DDR in response to DRS caused by HU. This was characterised by a delayed, yet prolonged phosphorylation of histone H2AX. To evaluate the effect of genetic add back of CIZ1, parallel experiments were performed to compare responses to HU in WT and CIZ1^{AB} cells. Cells were treated with 1 mM HU for 2 hours. The experiment mirrored the experiment in Figure 4.10. Briefly, for experimental cells, media was replaced with media containing 1 mM HU, samples were harvested after 30 minute and 2 hours HU treatment. After 2 hours HU media was replaced with fresh media – HU. Control plates were harvested without addition of HU. At time points cells were harvested for EdU labelling and western blot analysis (Figure 4.16).

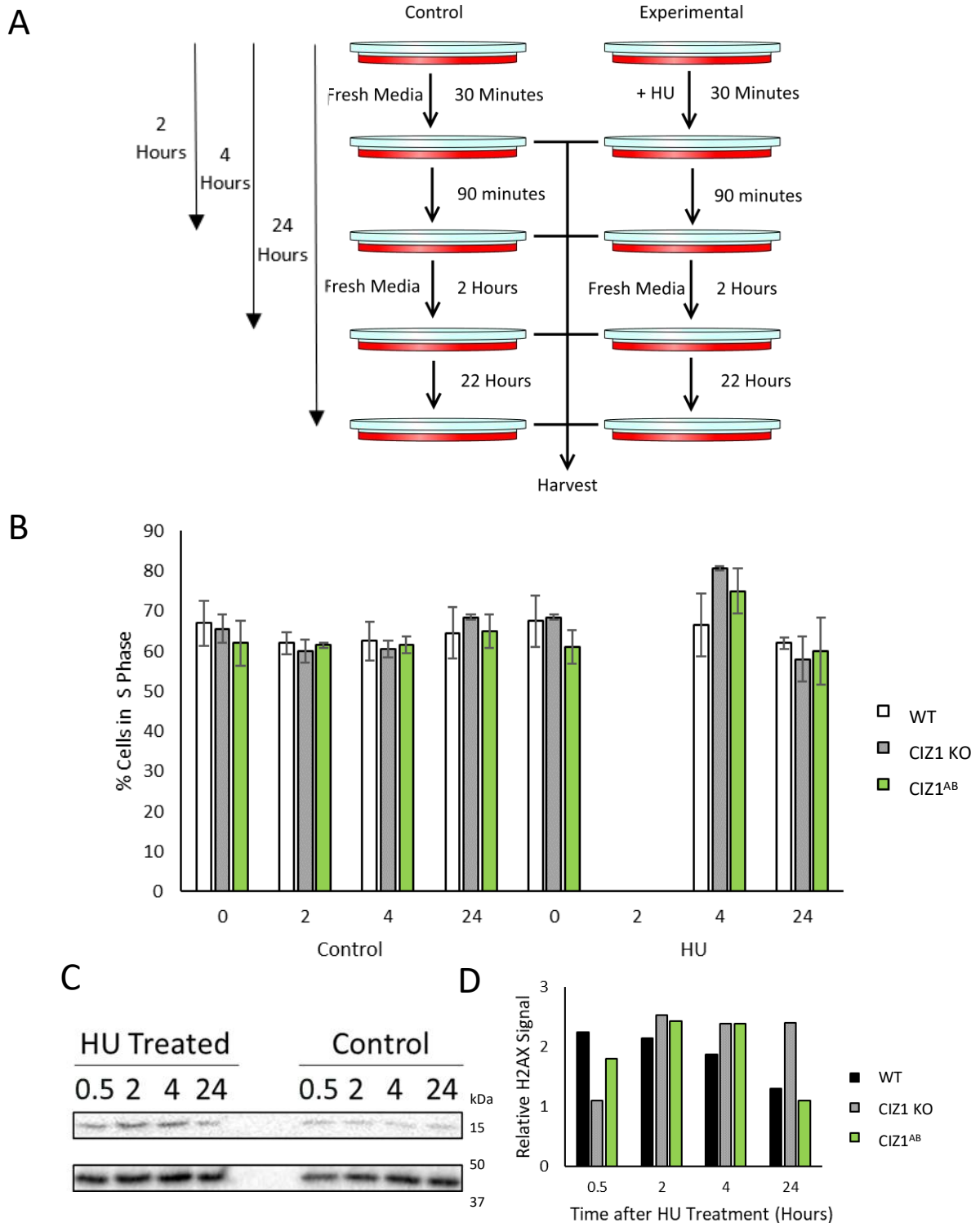


Figure 4.16-Response to HU treatment in CIZ1^{AB} cells A) Displays a graphical schematic of the experimental design. B) Displays the proportion of cells in S-phase at each time point. Measured by counting the positively EdU labelled cells using fluorescence microscopy. The proportion of cells in S phase at each time point ($n = 3$) for each cell line was compared using a two-way ANOVA with time and cell line as factors (P (time) < 0.05 , P (cell line) > 0.05 , P (interaction) > 0.05). C) Displays western blots of H2AX phosphorylation in CIZ1^{AB} cells. D) Relative intensity of H2AX signal for each cell line (WT and KO1 data from Figure 4.10) Each sample is standardised to actin intensity and compared to the untreated control (0.5 hour sample) ($N = 3$).

For both WT, and CIZ1^{AB} control cells no differences were seen in the proportion of cells in S-phase at any time point. Both WT and CIZ1^{AB} induced the same effect in the proportion of actively replicating cells, 2 hours after treatment a complete ablation of the population of S-phase cells was observed, this was resolved 2 hours later, returning to control levels. This remained 24 hours after treatment. This confirmed that HU mediated replication stress resulted in the halting of the cell cycle. A Two way ANOVA confirmed there was no significant difference between cell lines.

Western blots revealed that CIZ1^{AB} cells responded similarly to WT cells from Figure 4.10. an increase in gamma H2AX was observed 30 minutes after HU treatment. This signal was maintained through the HU treatment, and 2 hours after removal. 24 hours after treatment the gamma H2AX levels had returned to untreated control levels (Figure 4.16C). Relative intensities of the blots presented here and in Figure 4.10, confirmed that ectopic CIZ1 expression partially restored the WT phenotype of H2AX phosphorylation, although the initial response (0.5 hours) was lower in CIZ1^{AB} cells (Figure 4.16d). Critically the sustained response observed in CIZ1 KO1 cells 24 hours after treatment with HU was lost in CIZ1^{AB} cells. This implied that the defect in response to HU caused by loss of CIZ1 was rescued by returning GFP-CIZ1, CIZ1^{AB} respond to HU more similarly to WT NIH 3T3 cells. Together this implies that ectopic expression of GFP-CIZ1 partially restores the altered DDR to HU observed in CIZ1 null cells.

No differences in proportion of cells in S-phase between WT, and CIZ1^{AB} cells implies that ectopic expression of GFP-CIZ1 didn't result in gross changes in response to HU mediated DNA replication stress. Ablation of S-phase population confirmed that HU resulted in a stalling of the cell cycle through DDR activation. As the pattern of H2AX was more similar to WT cells than CIZ1 KO1 cells (Figure 4.10) this implied that ectopic expression of GFP-CIZ1 was sufficient to reduce sensitivity to DNA replication stress. This further implies a role for

CIZ1 in modulating the DDR in response to replication stress. This will be further explored in Chapter 6.

Critically, all of the subtle changes in cell cycle re-entry and response to DRS observed in CIZ1 KO cells was either resolved or partially resolved by GFP-CIZ1 expression. Future Chapters will investigate the link between CDK networks and cell cycle re-entry (Chapter 5) and investigate the effect CIZ1 levels have on replication initiation, and DRS, using DNA combing (Chapter 6).

4.5. Chapter Discussion

Discovery of CRISPR Cas9 heralded a new age of rapid, cheap, efficient genome editing. The ability to simply modify the DNA sequence within cells had wide felt implications for research, and disease treatment. CRISPR CAS9 is being actively developed as a treatment for cystic fibrosis, mutation has been achieved *in vitro* in cultured cystic fibrosis epithelia cells (Maule et al., 2019). However, more recently problems have arisen for CRISPR Cas9 as a genome editing tool. Primarily this is focussed on the observed high frequency of off target mutation in cells that have been undergone the CRISPR CAS9 genome editing programme. Zhang et al. (2015) observed that there was a greater than 50 % rate of off target mutations. This could be problematic if mutations result in a phenotype change that incorrectly interpreted as being due to the loss of the target. In this study, this has been mitigated in 3 ways. Firstly, a genome wide search of the complementary guide sequence revealed no repeats, this should prevent off target effects caused directly by a repeating PAM. Secondly, two neighbouring PAM sites in the CIZ1 sequence were targeted: CIZ1 KO1 and CIZ1 KO2. The use of 2 unique PAM sites should minimise the likelihood of common off target effects. Finally, the return of genetic addback CIZ1 to the KO1 cells to produce CIZ1^{AB} cells reverses the phenotypes observed with respect to cell cycle regulation and responses to HU.

All phenotypes in CIZ1 KO clones 1 and 2 were consistent. In addition, the observed differences were consistently statistically significantly between WT and KO1 and KO2, whereas there were no significant differences between CIZ1 KO1 and KO2. Similarly, analysis of the CIZ1^{AB} cell line showed a partial or full reversal to the WT phenotype. This was borne out in mean results returning to WT levels whilst remaining disparate from results observed in KO1 & KO2 cells. Using multiple levels of redundancy, the results observed in this Chapter & future Chapters are highly likely to be due to the deletion of CIZ1 in the cells.

In this chapter, it has been demonstrated that CIZ1 directly plays a role on cell cycle. Loss of CIZ1 dysregulates timing of S-phase entry in cells exiting quiescence and alters the timing of restriction point. The timing of the G1 to S-phase transition is critical for maintenance of genome integrity through the fidelity of DNA replication. DNA replicated early can be “under licenced” this would result in insufficient origins firing resulting in S-phase not concluding before the onset of mitosis (Limas & Cook, 2019). From the data presented here, it is unclear whether CIZ1 KO increases the potential for mitosis before completion of DNA synthesis. Whilst cell-cycle re-entry is accelerated it remains to be addressed whether the early entry into S-phase has an effect on DNA replication fidelity.

Importantly, cell synchronisation revealed a difference in the expression pattern of the G1 and S-phase cyclins between the WT and CIZ1 KO cells. Cells without CIZ1 appeared to show earlier expression of Cyclin A, although consistent Cyclin E. As the driving forces of cell cycle entry, more rapid cyclin expression would explain an early entry into S-phase. Previous reports have demonstrated that, during the G1/ S-phase transition CIZ1 anchors both Cyclin E/CDK2 and Cyclin A/CDK2 to the nuclear matrix (Copeland et al., 2010) promoting a switch between which cyclin is active during S-phase. Additionally, phosphorylation status of CIZ1 drives the binding of cyclins to the nuclear matrix (Copeland et al., 2015). Localisation of both cyclin A and Cyclin E is key to their function; both are shuttled between the nucleus and

cytoplasm during the cell cycle depending on whether they are driving genome replication or cytoplasmic regulation (Jackman et al., 2002). Loss of CIZ1 may therefore cause a change in localisation of cyclins that could change their activity.

Additionally, production of the G1/S cyclins occurs in a positive feedback loop. The initial signal is provided by the binding of exterior growth signals. These promote synthesis of Cyclin D. Cyclin D/CDK 4/6 phosphorylates tumour suppressor pRB which initiates a signal transduction pathway resulting in the activation of the E2F transcription factor which promotes production of Cyclins A and E (Lukas et al., 1997; Zarkowska et al., 1999). These cyclins dimerise with CDK2 promoting full phosphorylation of RB fully activating E2F resulting in the synthesis of more cyclin E, and cyclin A as well as a number of replication proteins including MCM2, CDC6, and PCNA.

Changes in levels of replication factors can also partially be explained through increased cyclin E and cyclin A signalling. In cells, re-entering the cell cycle, CDK2 mediated phosphorylation of these replication factors regulate their stability and regulation by the UPS. For example, in G1 phosphorylation of CDC6 by Cyclin E/CDK2 protects it from proteolysis mediated by the APC/C^{CDH1}, the major E3 ligase active from anaphase to early G1 (Mailand & Diffley, 2005).

Results in this Chapter predominantly stemmed from observing cells re-entering the cell cycle. A consistent, repeatable, average increase in the proportion of cells entering S-phase at earlier time points was observed in CIZ1 KO1 and KO2 cell lines. This result could be interpreted in multiple ways. The first is that CIZ1 null cells re-enter the cell cycle more rapidly than their WT counterparts. However, re-entry into the cell cycle is not homogenous, as a number of cells within the quiescent population will remain quiescent and will simply not enter the cell cycle (Wang et al., 2017). Because of this, a second interpretation of this result could be that simply, more CIZ1 null cells re-enter the cell cycle and S-phase following

quiescence. This seems less likely than the former option, as 24 hours after release from quiescence there are similar levels of WT and CIZ1 KO cells in S-phase. If simply more cells were entering S-phase, following the same 'replication programme' the expected result would be a greater proportion of cells in S-phase. Additionally, the shift in the restriction point observed in these experiments would not be expected.

The data presented imply that CIZ1 contributes to regulation of G1 length specifically in cells re-entering the cell cycle from quiescence. This is of particular interest for genetic stability. It is long established that overexpression of oncogenic proteins Cyclin E and Cyclin D result in a shortened G1 in cells re-entering the cell cycle, Cyclin E also having this effect on cycling cells. Expression of these proteins also results in a delayed entry into quiescence phenotype (Resnitzky et al., 1994) It is not clear if this explains how altered CIZ1 expression effects this phenotype, Cyclin E is a known interacting partner (Coverley et al., 2005; Copeland et al., 2010), although this has not been observed with Cyclin D. However, it is clear that shortened G1 phenotype results in increased DRS (Ahuja et al., 2016).

G1 length and replication licensing is linked to genetic instability. Cells of different age, development and cell type present with varying length G1 phases (Matson et al., 2017). Additionally, the initial G1 phase after cell cycle re-entry is longer than in actively cycling cells. To ensure replication occurs unimpeded, cells with shorter G1 phase licence replication origins more rapidly than cells with slower G1 phases. Critically overexpression of Cyclin A or Cyclin E separates the G1 length from the replication licensing process resulting in early S phase and DRS, driving genome instability. CIZ1 has been shown to play a role in coordinating the activity of Cyclin A and Cyclin E surrounding the G1/S transition (Copeland et al., 2010; Copeland et al., 2015). Interestingly, increasing the length of G1 following quiescence synchrony allows increased replication licensing to levels more comparable with cycling cells (Matson et al., 2019). Results in this chapter demonstrated that loss of CIZ1

resulted in a shorter G1 following quiescence perhaps due to changes in replication licensing through altered Cyclin levels. If this shortened G1 phase is coupled with decreased replication licensing, then this may act as a source of genome instability, potentially explaining the Tumour suppressor function of CIZ1 that has been reported (Nishibe et al., 2013; Ridings-Figueroa et al., 2017). Future Chapters will investigate responses to Cyclin/CDKs in post-quiescent nuclei with and without CIZ1, as well as investigating if loss of CIZ1, and altered CDK levels results in a stressed phenotype.

Other factors that regulate the G1 length include co-drivers of the cell cycle with the cyclin CDK networks. Cell cycle regulation is associated with temporally regulated activation of E3 ligases that degrade Cyclin subunits inactivating CDKs, resetting the cell cycle, and regulatory factors allowing cell cycle progression. CDH1 is a co-activator of APC, APC^{CDH1} is an E3 ligase active from anaphase to the onset of S-phase. One target of APC^{CDH1} is SKP2, SKP2 is a component of another cell cycle relevant E3 ligase SCF^{SKP2}. SCF^{SKP2} is active from S-phase onset till degradation during mitosis by APC^{CDH1}. Critically, SCF^{SKP2} degrades CDKi proteins p21 and p27 (Rizzardi et al., 2012). P21 is a CIZ1 interacting partner (Mitsui et al., 1999). p21 and p27 inhibit CDK2 activity in G1, Depletion of CDH results in reduced levels of p21 and p27 in G1. Typically, CDK inhibition is overcome through CDK2 activity, allowing a molecular switch for cell cycle entry. In CDH1 deficient cells the positive feedback loop is weakened resulting in a lower CDK activity required to overcome p27 activity. This resulted in reduced G1 length (Yuan et al., 2014). CDH1 depletion leads to DRS, misregulated cyclin localisation, DNA damage and mitotic defects (Griel et al., 2016). CDH1, also promotes inhibition of origin firing after cells experience severe replication stress, this occurs in a p21 and p53 dependent manner. The effect of CIZ1 levels on the CDK activity level required for S-phase entry is investigated in Chapter 5.

Activation of oncogenes shorten G1 phase, resulting in the activation of replication origins independently of both constitutive origins, and dormant replication origins. These oncogene induced origins are localised in heavily transcribed genomic regions. These same origins are typically suppressed by transcription, and reduced G1 length may result in firing of origins before the transcriptional suppression has taken effect. Replication from these oncogene induced origins results in transcriptional collision and DNA replication stress, resulting in an increase in DSBs near these origins (Macheret & Halazonetis, 2018). Critically, this chapter has uncovered 2 major phenotype changes, which could be explained through deregulated cyclin/CDK networks.

This chapter has demonstrated subtle changes in cell cycle and DDR regulation in response to loss of CIZ1. Many of these effects may be attributed to a change in the expression patterns of the G1/S cyclins during cell cycle re-entry. This is summarised in Figure 4.17 Future chapters will investigate further the effect of changes in cyclin signalling effects DNA replication in a CIZ1 context, and how these changes effects DNA replication fidelity.

Loss of Ciz1

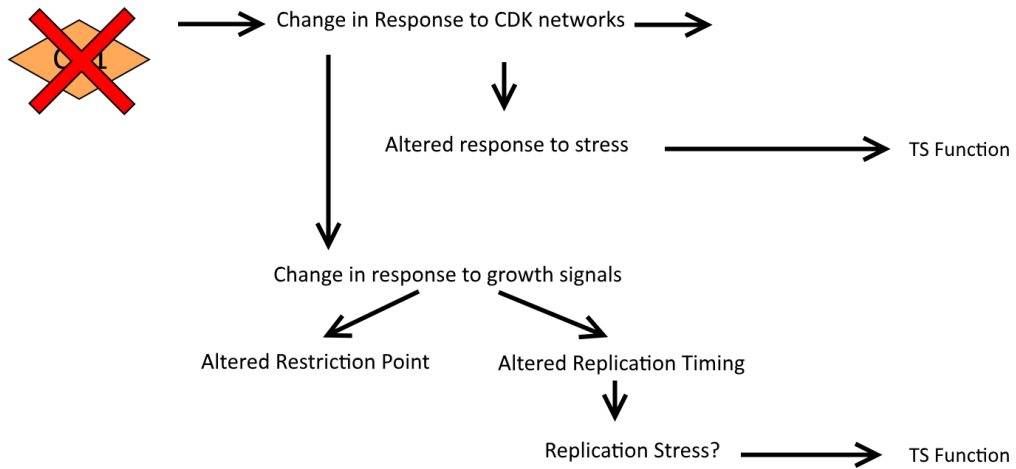


Figure 4.17-A model for how loss of CIZ1 induces cellular changes Results in this Chapter have demonstrated that CIZ1 null cells display altered cell cycle re-entry kinetics. It can be hypothesised that this is linked to the observed tumour suppressor function of CIZ1. CIZ1 is involved in co-ordinating CDK2 activity during the G1/S transition. Changes in responses to CDK signalling could explain both altered cell cycle re-entry timing and altered response to stress. Both would result in DNA replication stress, which could drive a mutator phenotype in cells that have lost CIZ1 function. The interplay between CDK signalling and CIZ1 at the G1/S transition and replication kinetics of CIZ1 null cells will be investigated in future Chapters.

Chapter 5.

**CIZ1 defines the CDK activity
thresholds for the initiation of DNA
replication *in vitro***

5.1. Introduction to *in vitro* Replication Experiments

Cell free *in vitro* replication systems recapitulate the events of DNA replication initiation and synthesis of nascent DNA outside the cell. Variations of these reactions have taken many forms and have been used to identify the regulatory mechanisms that control DNA replication for decades. These experiments have progressed in complexity, and precision from merging cell extracts, to the use of defined recombinant proteins that recapitulate the events and stoichiometry of eukaryotic DNA replication. The cell free approaches used to study cell cycle regulation beginning with cell fusion experiments through to the latest *in vitro* systems will be evaluated here.

5.1.1. Cell Fusion Experiments.

The earliest *in vitro* experiments were performed by fusing cells. In a classical experiment, Rao & Johnson (1970) fused HeLa cells creating multinucleate cells. This approach established that soluble factors were able to induce mitosis (Maturation promoting factor, MPF), or induce DNA replication (S phase promoting factor, SPF). Critically, they found that DNA replication could be induced by fusing an S phase cells with G1 cells, however the same was not true when G2 multinucleate cells were fused with S phase cells. As well as demonstrating the unidirectional nature of the cell cycle, these experiments provided some of the earliest evidence for the quantitative model of CDK activity as the major regulator of the cell cycle (discussed in Chapter 1.8).

5.1.2. Identification of Replication Origins and Fork Dynamics *in vitro*.

The earliest *in vitro* replication systems were developed in yeast. In these experiments yeast plasmids (typically the yeast 2 μ m plasmid), were initiated to replicate by crude enzyme extracts prepared from yeast cell extracts (Jazwinski & Edelman, 1979). This technique was modified to increase activity providing a useful tool for measuring eukaryotic DNA replication

(Kojo et al., 1981). These experiments demonstrated that replication proceeded bidirectionally from the origin and recapitulated the order of replication events determined in *in vivo* experimentation. This system identified the autonomous replicating sequences (ARS), the specific sequences within the yeast genome that specify putative origins of replication through the recruitment of the origin recognition complex (ORC) (Celniker & Campbell, 1982). This highlighted how *in vitro* experiments could be used to learn about the *in vivo* process of DNA replication.

5.1.3. Metazoan Cell Free DNA Replication Assays

Following on from yeast experiments of the 1970s, the earliest animal *in vitro* replication experiments used eggs from the frog genus *Xenopus*, these experiments focussed largely on methods for isolating cell cycle competent S phase extracts. After roughly a decade of refinement of cell extract isolation, Blow & Laskey (1986) modified the extract isolation method developed by Lohka & Masui (1983, 1984, 1984). Using this new technique, they were able to demonstrate for the first time *Xenopus* DNA initiation in a cell free *in vitro* replication assay. These early experiments paved the way for the use of cell free DNA replication experiments using mammalian nuclei and extracts to probe the events of DNA replication initiation (Krude et al., 1997).

In these experiments, isolated egg extracts promote DNA replication of sperm DNA. This methodology was used to identify many proteins involved in the DNA replication-licensing phase of replication initiation. These include the hexameric DNA helicase proteins of the MCM complex (Chong et al., 1995). Experiments performed using this system have also identified the activity of various cyclin/CDK proteins. Critically, the *Xenopus* system was used to demonstrate that Cyclin A/CDK2 and Cyclin E/CDK2 can both promote S phase entry (Strausfeld et al., 1996). These experiments implicated Cyclin E in the earliest events of DNA replication initiation; whereas Cyclin A would function later on.

More recently, *xenopus in vitro* replication systems have been used to demonstrate that the Chk1 response inhibits late firing origins, and that precise levels of Chk1 are required during stressed and normal S phase to maintain the DNA replication programme (Platel et al., 2015). Additionally, *Xenopus* systems were used to demonstrate that MCM10, a replication factor, is not required for DNA replication initiation; however, reduction of MCM10 levels can result in reduced fork rate, a replication stress phenotype (Chadha et al., 2016).

Mammalian *in vitro* replication assays were developed later than their frog and yeast counterparts. These experiments utilized the same nucleotide mix and energy regeneration system developed in frog *in vitro* replication assays (Blow & Laskey, 1986). As mammalian cells lack the ARS found in yeast, mammalian DNA replication systems utilised intact nuclei isolated in late G1 phase, supplemented by S-phase cytosolic extracts (Krude et al., 1997; Coverley 2002, Copeland 2015). To achieve this the cells needed to be efficiently synchronised. While this is achieved very efficiently with yeast, mammalian cells are more difficult to synchronise. The common methods used to generate the cell cycle stage specific cell extracts are: double thymidine block (S-phase cells), contact inhibition (Chapter 2) and serum starvation (G1 cells), and chemical synchronisation using mimosine (Late G1) (Krude et al., 1999).

Culturing cells in an excess of thymidine blocks the production of nucleotides by overwhelming ribonucleotide reductase that depletes the dNTP pool. This stalls DNA replication forks in early S-phase and dilution of thymidine allows fork restart and progression through S phase. By repeating thymidine incubations, a high proportion of cells can be arrested in early S-phase (Copeland et al., 2010; Copeland et al., 2015; Chen et al., 2018). The other common method used for cell synchronisation for cell free experiments is mimosine arrest. Mimosine is a plant derived amino acid that halts cell cycle progression in G1 through inhibition of CTF4 binding to chromatin, release from this block allows nuclei to enter S phase (Park et al., 2012). A schematic displaying the two methods used for cell cycle synchronisation in this report displayed in Figure 5.1.

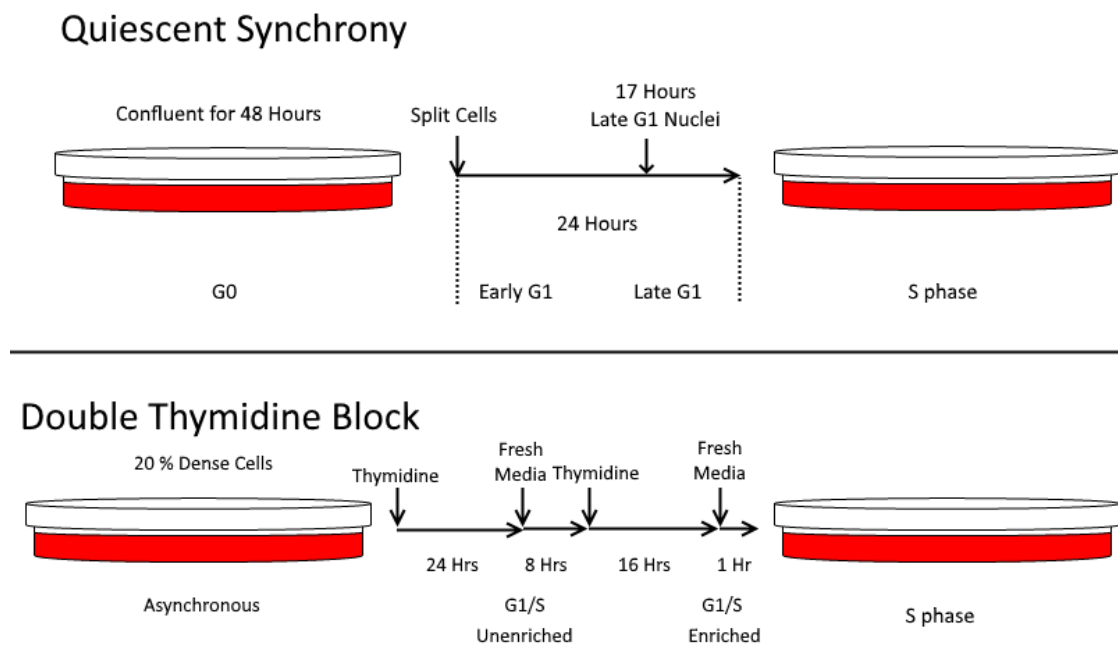


Figure 5.1 - Overview of approaches used for mammalian cell cycle synchronisation A) Synchronous release of cells from quiescence into S phase using contact inhibition and serum starvation. B) Synchronous release of cells into S phase using inhibition of nucleotide synthesis by a double thymidine block.

The use of mammalian cell free DNA replication assays demonstrated that Cyclin A-CDK2 is sufficient to initiate mammalian DNA replication *in vitro* (Coverley et al., 2005) Mammalian cell free DNA replication assays identified that CIZ1 promotes DNA replication with cyclin A-CDK2 (Coverley et al., 2005; Copeland et al., 2010) and that noncoding Y RNAs are required for efficient DNA replication initiation (Krude, 2000; Driedonks et al., 2018). Critically, when combined with DNA combing, they have demonstrated that depletion of these Y RNAs prevent the initiation of new replication forks, but not the elongation of ongoing replication forks (Krude et al., 2009). These results demonstrated a novel regulator of DNA replication, but also demonstrated the power of combining the two techniques of *in vitro* replication assays and DNA combing.

More recently, *in vitro* replication assays were further developed from studies using cell cycle stage specific cell extracts and nuclei, to the recapitulation of DNA replication using entirely recombinant proteins to define the minimal replication machinery in yeast. Yeeles et al. (2015) identified the minimal protein toolkit required for recapitulation of origin specification, origin licensing and firing on DNA by the addition of 16 replication factors. Using this technique both the loading of preRC, conversion to preIC, and finally DNA replication were achieved (Yeeles et al., 2015). This technique was further developed to demonstrate that Mrc1 and Csm3/Tof1 are required to achieve optimal DNA replication rates *in vitro*. These experiments also revealed that DNA pol delta primarily used for lagging strand synthesis may be required for priming of leading strand synthesis to achieve optimal replication rate (Yeeles et al., 2017).

This review demonstrates the power of *in vitro* replication assays to measure parameters about replication across multiple species. These experiments allow analysis of how individual factors can affect replication at both the assembly, and elongation level, which is difficult to isolate within a cell, due to downstream effects of genetic alteration, or non-specificity of

inhibitors. Cell free approaches allow analysis of the fundamental events that underpin DNA replication. Allowing identification of effectors of DNA replication and provide mechanistic insight if specific factors can alter replication and potentially drive tumorigenesis.

5.1.4. Chapter Aims

- Validate the replication competence of nuclei from post-quiescent WT, CIZ1 KO1 and CIZ1^{AB} nuclei
- Measure the replication initiation kinase thresholds in nuclei
- Investigate how recombinant CIZ1 modulates kinase thresholds
- Investigate the effect of CIZ1 and Cyclin A/CDK2 on replication kinetics

5.2 Expression of Recombinant CIZ1 and Cyclin A-CDK2 for use in Cell Free DNA Replication Assays.

Full length CIZ1 has proven to be challenging to purify in the past due to a natively disordered C terminal resulting in degradation. To overcome this issue, other fragments and splice variants have been used which are more stable including ECIZ1 an embryonic splice variant and ECIZ1 N471 a variant lacking the C terminus. (Copeland et al., 2010). Purified ECIZ1 N471 at a high concentration was already available in the lab from previous work (Tollitt, 2017).

Purification of recombinant cyclin A/CDK2 is more challenging than expressing and purifying a single protein as the proteins need to be dimerised at stoichiometric levels. To achieve this the protein purification is staggered. A 3:1 culture ratio of cyclin A to CDK2 is used. GST-cyclin A is purified, the GST tag removed by 3C cleavage. The purified cyclin A is added to GST-CDK2 that is immobilised on glutathione sepharose beads. The beads are washed to remove unbound cyclin A and stoichiometric cyclin A-CDK2 released by 3C cleavage of the

GST tag (Coverley et al., 2012). An SDS-PAGE gel showing each purification step is displayed in Figure 5.2.

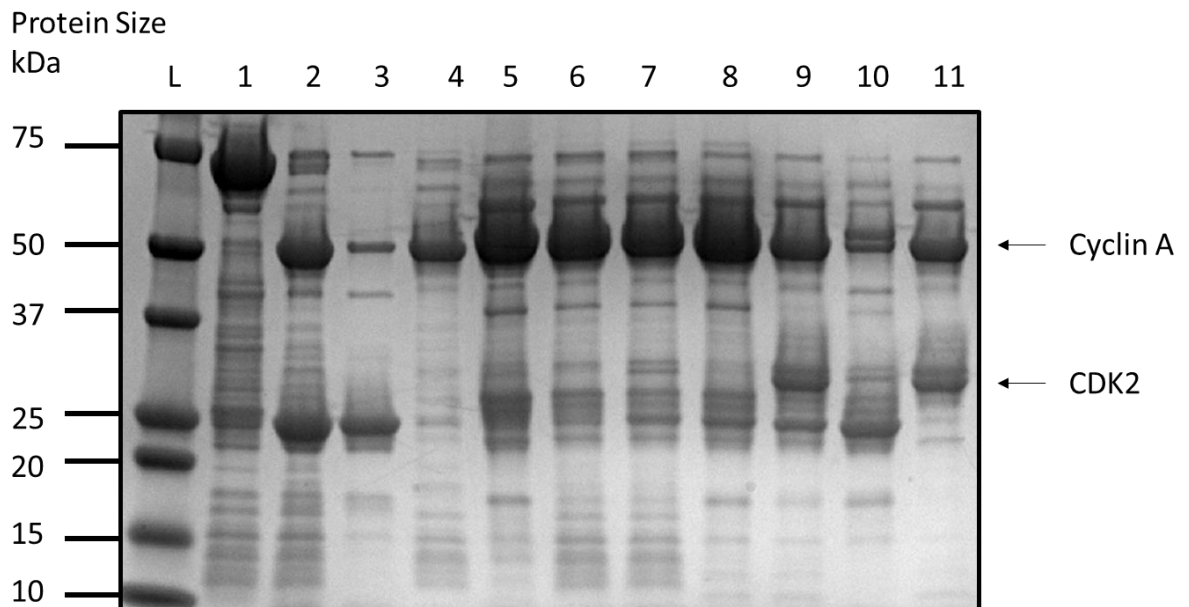


Figure 5.2 – Purification of Cyclin A-CDK2: Cyclin A-GST and CDK2-GST were expressed. Cyclin A was purified: Lane 1, Cyclin A Lysate on glutathione sepharose beads, Lane 2, Cyclin A bound glutathione sepharose beads after 3c cleavage, Lane 3, Glutathione sepharose beads after elution of cleaved protein. Lane 4, purified Cyclin A. Lane 5, CDK-GST bound to glutathione sepharose beads and incubated with Cyclin A (from lane 4) (Lane 6). Lane 7, shows beads bound protein after overnight digestion, and after washing (Lane 8). Samples were then digested overnight with 3C protease, Lane 9 shows all protein after digestion. Lane 10 shows Glutathione sepharose beads after elution of non-bound protein after digestion. Lane 11 shows final eluted protein after overnight 3c digestion and purification.

Lane 1 displays a strong band at roughly 70 kDa representing the Cyclin A-GST fusion protein (~25 kDa for GST and ~47 kDa cyclin A). Following 3c cleavage Lane 2 displays 2 strong bands at roughly 50 kDa (cyclin A) and 25 kDa (GST). These bands remain in Lane 3 which indicates not all cyclin A had been eluted. Lane 4 shows cyclin A at 50 kDa. In lane 5 the CDK2 GST fusion protein is shown at 50 kDa (both are ~25kDa). Lanes 6, 7, and 8 show an intense band at 50 kDa representing both cyclin A and CDK2-GST during the binding and washing stages. Lane 9 shows intense bands at 50 kDa, 30 kDa, and 25 kDa representing Cyclin A, CDK2, and

GST respectively. Lane 10 shows bands at 25 kDa and 50 kDa representing GST and CDK2-GST, potentially indicating incomplete 3c cleavage. Following purification, the eluted protein bands for cyclin A (50 kDa) and CDK2 (30 kDa) (Lane 11) were of similar intensity suggesting a 1:1 stoichiometry. The recombinant cyclin A-CDK2 complex was then functionally assessed using the cell free DNA replication assay to ensure quality of preparation.

5.3 Using *in vitro* Reactions to Investigate Interplay Between CIZ1-N471 and Cyclin A/CDK2

5.3.1 Cell Free Analysis of the Initiation Phase of DNA Replication.

The initiation of DNA replication can be studied using replication licensed G1 nuclei that are stimulated by S-phase cell extracts or G1 extracts supplemented with cyclin A-CDK2 (Figure 5.3). S phase extracts have the optimal amount of kinase activity to promote DNA replication initiation as they lie between the S phase threshold, and the S phase inhibitory threshold (Chapter 1.8). If CIZ1 plays a role in defining these thresholds, addition of recombinant CIZ1-N471 may influence the concentration dependent activation of DNA replication. Cell free DNA replication assays with late G1 nuclei (From Chapter 3), and G1 cytosolic extracts supplemented with 0.1 ng/ μ l Cyclin A/CDK2 (From Figure 5.2), or an S phase extract (Figure 5.3a/b). To determine the effect of increasing CIZ1 concentrations, cell free assays were prepared using 0.1 to 100 nM CIZ1 in S-phase extracts and G1 Extracts supplemented 0.1 ng/ μ l cyclin A-CDK2 concentration (Figure 5.3c-f). For both sets of reactions the proportion of nuclei in S-phase was determined.

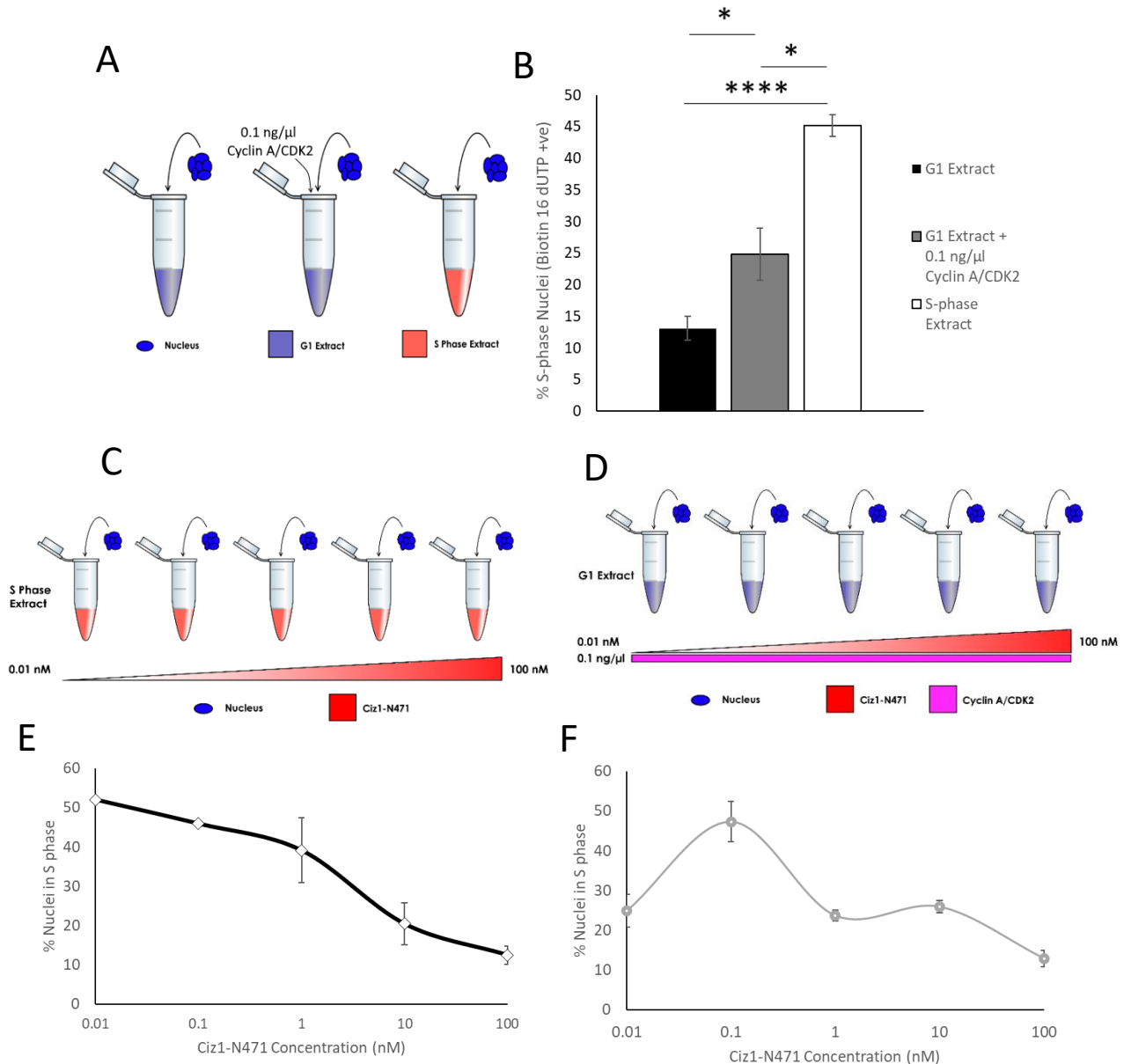


Figure 5.3-High concentrations of CIZ1-N471 block DNA replication initiation. A) A schematic of the experimental design of simple *in vitro* reactions. B) Demonstration that 0.1 ng/μl Cyclin A/CDK2 promotes replication initiation, but not to the level of an S-phase extract. The proportion of S-phase nuclei is shown after a 30 minute incubation in each extract. N=3 showing mean ± standard deviation. Significant differences were observed across the three conditions (One Way ANOVA, $p < 0.001$) Pairwise comparisons were conducted by Tukey's HSD test, significance is indicated on the graph: ns = $p > 0.05$ * = $p < 0.05$, ** = $p < 0.01$, *** $p < 0.001$. C) Schematic for titration of CIZ1-N471 into S phase extract (result in E) D) Schematic for titration of CIZ1-N471 into a G1 extract supplemented with 0.1ng/μl Cyclin A/CDK2 (Result in F) E) The percentage of nuclei in S phase when different concentrations of CIZ1-N471 were added to an S phase extract. F) The percentage of nuclei in S phase when different concentrations of CIZ1-N471 were added to a G1 extract with 0.1 ng/μl Cyclin A-CDK2. N=3 showing mean ± standard deviation.

A one way ANOVA revealed significant differences between the three conditions, and significant differences between each condition. Addition of Cyclin A/CDK2 promoted replication initiation twofold over a G1 extract alone from 13.1 % to 24.8 % of nuclei in S phase after S phase (Figure 5.3B). Addition of an S phase extract resulted in an increase to 45.1 %, approximately three-fold more nuclei in S phase after incubation when compared to a G1 extract and 1.8 times more nuclei in S phase than a G1 extract supplemented with 0.1 ng/ μ l Cyclin A/CDK2. This data is consistent with results from Coverley et al. (2005) and demonstrated that Cyclin A/CDK2 alone promoted DNA replication initiation *in vitro* but not to the same level as an S phase extract. This indicated that Cyclin A/CDK2 could promote replication initiation *in vitro*.

Addition of CIZ1-N471 to S-phase extracts (Figure 5.3E) initially has little effect on the percentage of nuclei in S phase. However, there is a slight concentration dependent reduction in the percentage of cells in S-phase at 0.01 ng/ μ l, 0.1 ng/ μ l, or 1 ng/ μ l of CIZ1-N471, with an average of 51 %, 45 %, and 40 % of nuclei respectively. At 10 ng/ μ l of CIZ1-N471 22% of nuclei were in S phase and at 100 ng/ μ l an average of 13 % of nuclei were in S phase. This was comparable to the G1 control. This indicated that high levels of CIZ1 inhibit replication initiation by an S-phase extract *in vitro*.

The titration of CIZ1-N471 into a G1 extract with optimal cyclin A/CDK (Figure 5.3F), shows a concentration dependent increase in initiation of DNA replication. The most efficient initiation occurs at 0.1 nM CIZ1 and there is a general decrease in activity at higher concentrations. At high concentrations of CIZ1-N471 (1 and 10 ng/ μ l) an average of between 22 – 26 % of nuclei were in S phase, comparable to cyclin A-CDK2 alone. This suggests that the replication initiation promoting activity of CIZ1 is concentration dependent and is inhibitory at high levels in both S phase extracts and with recombinant cyclin A-CDK2.

5.3.2 In vitro analysis of CIZ1 null fibroblasts during the initiation phase of DNA replication.

The observation that CIZ1 is required for initiation of DNA replication in murine fibroblasts (Coverley et al., 2005, Copeland et al., 2010) suggested that CIZ1 may be an essential gene. However, murine knock out models demonstrated that this was not the case. Although, CIZ1 may play a role in the maintenance of genomic stability as CIZ1 KO mice are predisposed to lymphoblastic tumours (Ridings-Figueroa et al., 2017) and viral oncogenic transformation (Nishibe et al., 2013). These observations suggest that CIZ1 knockout mice may have subtle defects in the regulation of DNA replication.

Here the parental WT NIH 3T3 cell, the CIZ1 KO1 cell line and the CIZ1^{AB} cell line were used to evaluate if there are any phenotypic differences between wild type (WT) and CIZ1 KO cell lines. To begin to characterise the role of CIZ1 in the regulation of DNA replication in vitro DNA replication assays using replication competent nuclei were harvested from WT, CIZ1 KO1 and CIZ1^{AB} NIH 3T3 cells. The initiation kinetics and replication dynamics of these nuclei were determined in parallel reactions were set up comparing the effects of a G1 extract with an S phase extract. In addition, to probe changes in chromatin loading, nuclear fractionation was performed and analysed by western blot (Figure 5.4).

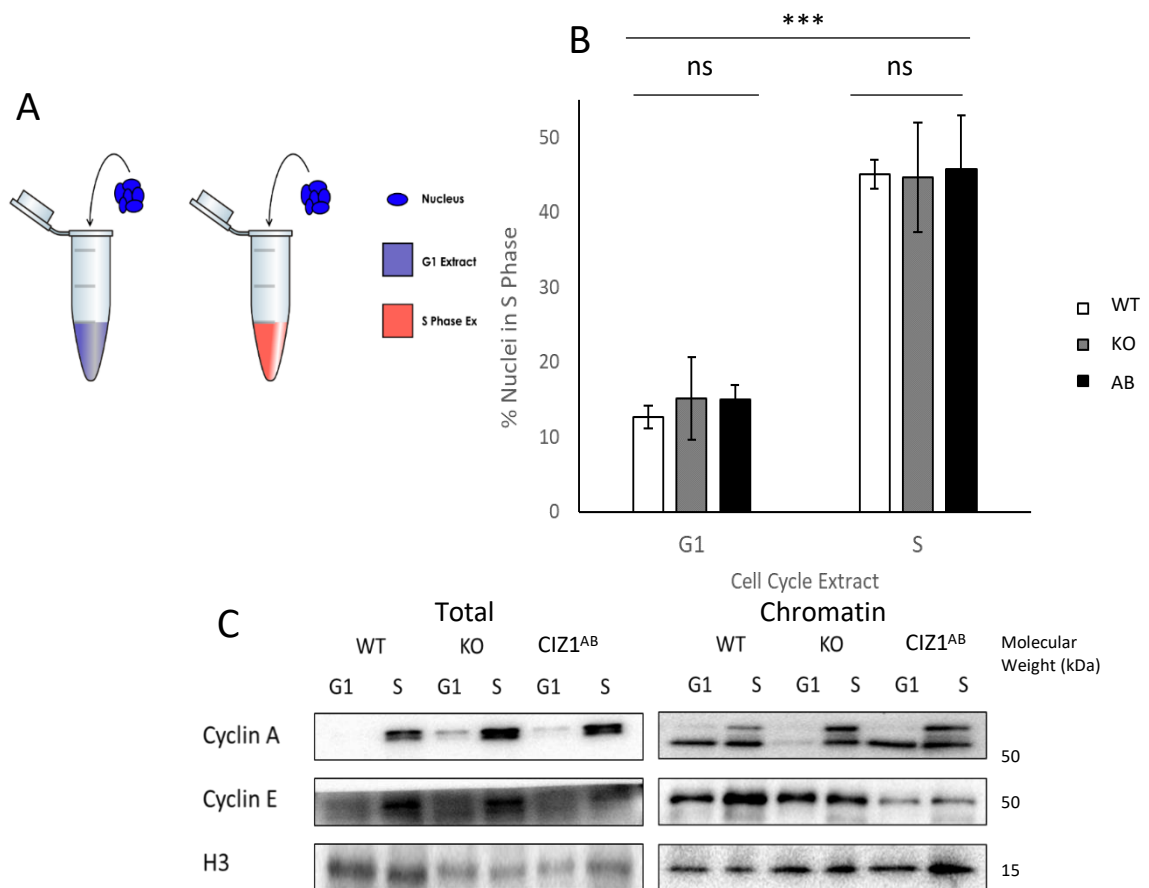


Figure 5.4 – Comparison of WT, CIZ1 KO and CIZ1^{AB} Nuclei S Phase Entry in vitro A) A schematic of the experimental design. B) Bar chart showing the percentage of S-phase nuclei for WT, CIZ1 KO, & CIZ1^{AB} in a G1 and S phase extracts. (N=3 ± S.D.) The proportion of nuclei in S phase in each extract (n = 3 repeats) for each cell line was compared using a two-way ANOVA with extract and cell line as factors (P (extract) < 0.0001, P (cell line) > 0.05, P (interaction) > 0.05). C/D) Total protein (C) and chromatin protein (D) fractions probed with G1/S cyclins: Cyclin A & Cyclin E, and Histone H3 as a load control.

A two way ANOVA revealed no significant interaction between cell line and extract. All three nuclei batches prepared from WT, CIZ1 KO and CIZ1^{AB} cell lines displayed a similarly low level of nuclei in S phase between 10 – 15 % (Figure 5.4b) and there were no significant differences in the level of S-phase nuclei in G1 extracts. The percentage of nuclei that initiated DNA replication when incubated in an S-phase extract was between 40-50 % for WT, CIZ1 KO and CIZ1^{AB} nuclei. There were no significant differences in the number of replicating nuclei in S-phase extracts. Importantly, when comparing the increase in S-phase

nuclei after incubation with S-phase extracts all of the nuclei tested show a significant increase relative to G1 extracts.

Western blot analysis revealed differences in the localisation of cyclin A. In total protein fractions there is a low level of cyclin A in G1 extracts for CIZ1 KO and AB, but less protein is detected in WT nuclei and extracts. However, isolation of the chromatin fraction showed similar levels of cyclin A on chromatin in the WT and CIZ1^{AB} nuclei. However, there is a clear reduction in cyclin A in CIZ1 KO cells relative to WT and CIZ1^{AB} nuclei. Loss of cyclin A chromatin localisation in KO nuclei, suggests that CIZ1 KO cells have impaired cyclin A localisation during the G1/S phase transition. Importantly, genetic addback of CIZ1 (CIZ1^{AB}) reversed this effect. This further implicates CIZ1 in recruiting cyclin A to insoluble nuclear structures, as CIZ1 promotes chromatin association of Cyclin A and Cyclin E during the G1/S phase transition (Copeland et al., 2010).

This reduction in cyclin A recruitment may be related to the observation that CIZ1 aids localisation of cyclin A to chromatin (Copeland et al., 2010) and that this facilitates initiation of DNA replication. The use of S-phase extracts that contain high levels of cyclin A-CDK2 from HeLa cells enabled efficient loading of cyclin A in all contexts. It should be noted that S-phase HeLa cytosolic extracts have CIZ1 protein that may be able to promote cyclin A binding *in vitro*. In G1 extracts, no differences were seen in chromatin localisation of cyclin E between WT, and CIZ1 KO nuclei. This suggests loss of CIZ1 does not affect the localisation of cyclin E *in vitro* (Figure 5.4d).

5.3.3. CIZ1 is required for efficient Cyclin A chromatin association *in vitro*

In G1 extracts prepared from CIZ1 KO cells, there is a cytosolic pool of cyclin A that fails to load onto chromatin (Figure 5.4C). The reduction in cyclin A chromatin binding in G1 phase in CIZ1 KO cells suggests that CIZ1 may act as a molecular scaffold, enabling efficient cyclin A recruitment. Titration of recombinant CIZ1 promotes cyclin A loading onto chromatin in DNA

replication assays in vitro (Copeland et al., 2010). To determine if biochemical add back of CIZ1 influences cyclin A localisation in CIZ1 KO cells, in vitro reactions were prepared with CIZ1 KO Nuclei, G1 cytosolic extracts and recombinant CIZ1-N471 concentrations were increased from 0 to 1 nM. This experiment was performed for two goals, firstly to investigate the effect recombinant CIZ1 had on the proportion of CIZ1 KO nuclei in a G1 extract. Secondly, to see if CIZ1 could promote chromatin localisation of Cyclin A that was lost when CIZ1 KO nuclei were incubated in a G1 extract. (Figure 5.5)

Addition of recombinant CIZ1-N471 had no effect on S phase entry KO nuclei, with 10 – 15 % of cells in S phase at all CIZ1 concentrations tested (Figure 5.5B). Western blotting of the chromatin fraction showed that cyclin E chromatin loading is unaffected by addition of CIZ1-N471. (Figure 5.5C). However, cyclin A chromatin localisation mirrored the increasing concentration of CIZ1-N471.

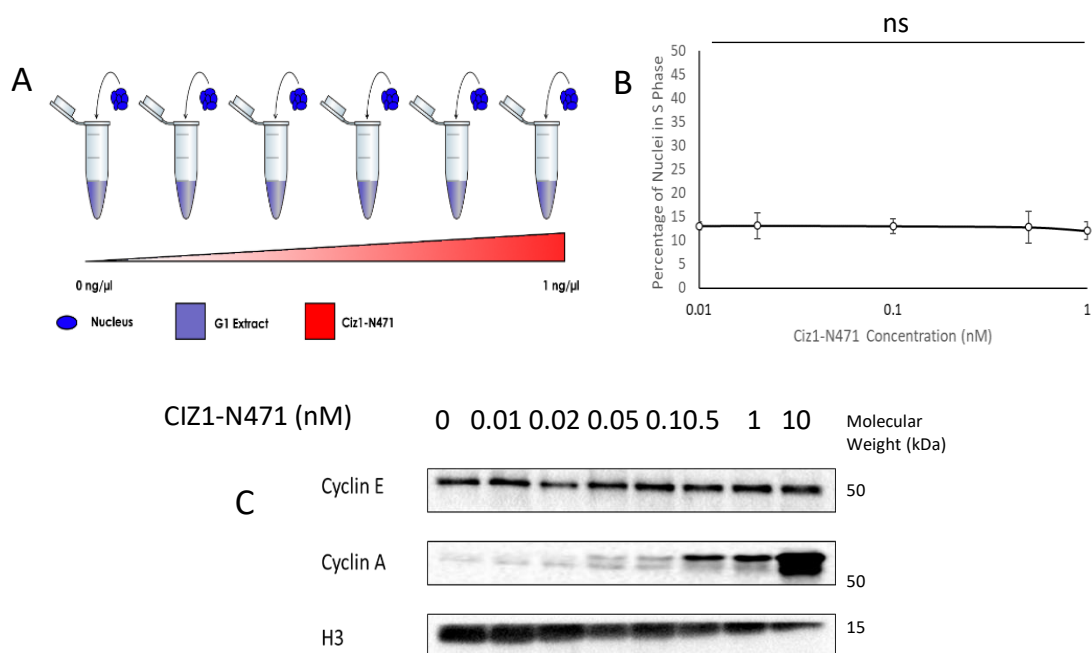


Figure 5.5. CIZ1 Titration promotes cyclin A loading onto CIZ1 KO nuclei in vitro. A) Experimental design. B) The proportion of nuclei in S phase for each of the concentrations ($n = 3 \pm$ standard deviation). No significant difference in S phase entry was observed across the range of CIZ1-N471 concentrations (One Way ANOVA, $p > 0.05$). C) Loading of G1/S cyclins onto chromatin at each of the CIZ1-N471 concentrations.

Titration of CIZ1 alone into in vitro reactions using G1 nuclei and G1 cytosolic extracts did not promote initiation of DNA replication, demonstrating that CIZ1 alone is insufficient to trigger this signal in a G1 context. A one way ANOVA revealed no significant differences between means. This is consistent with a molecular scaffold, as it requires either S-phase extracts or recombinant cyclin A-CDK2 to enhance initiation of DNA replication (Coverley et al., 2005; Copeland et al., 2010; Copeland 2015). The biochemical add back of CIZ1 is consistent with results from the genetic addback of CIZ1 (CIZ1^{AB} nuclei) (Figure 5.4c./5.5c and Figure 4.12) where chromatin recruitment of Cyclin A in a G1 extract lost upon loss of CIZ1 was restored. Taken together, these observations demonstrate that CIZ1 plays a role in the chromatin localisation of cyclin A in replication licensed nuclei, consistent with the cooperative activity of CIZ1 and cyclin A-CDK2 that promotes the G1/S transition (Copeland et al., 2010).

5.2.4 Cyclin A/CDK2 promotes initiation of DNA replication in a narrow concentration range.

The initiation of DNA replication occurs within a narrow concentration range (around 0.1 ng/ μ l). This threshold is maintained by the opposing activities of cyclin dependent kinases and ubiquitin proteasome system that induces an unstable irreversible switch, key phosphorylations by CDKs promote degradation of replication licensing proteins by the UPS. (Rizzardi et al., 2012; Moser et al., 2018; Heldt et al., 2018). CIZ1 influences this threshold and enables initiation of DNA replication at a wide range of cyclin A-CDK2 activities (Copeland et al., 2010). The data presented here suggests that CIZ1 KO cells are inefficient for the recruitment of cyclin A-CDK2 to chromatin. Therefore, this suggested that CIZ1 KO nuclei may have altered cyclin A-CDK2 activity thresholds to promote initiation of DNA replication as a consequence of the reduction in cyclin A-CDK2 chromatin recruitment.

To determine the optimal cyclin A-CDK2 activity to promote initiation of DNA replication, cell free DNA replication assays were prepared with replication licensed nuclei prepared from

WT, CIZ1 KO and CIZ1^{AB} cell lines. Recombinant cyclin A/CDK2 was titrated from 0 to 1 ng/μl and the percentage S-phase nuclei determined for each concentration (Figure 5.6).

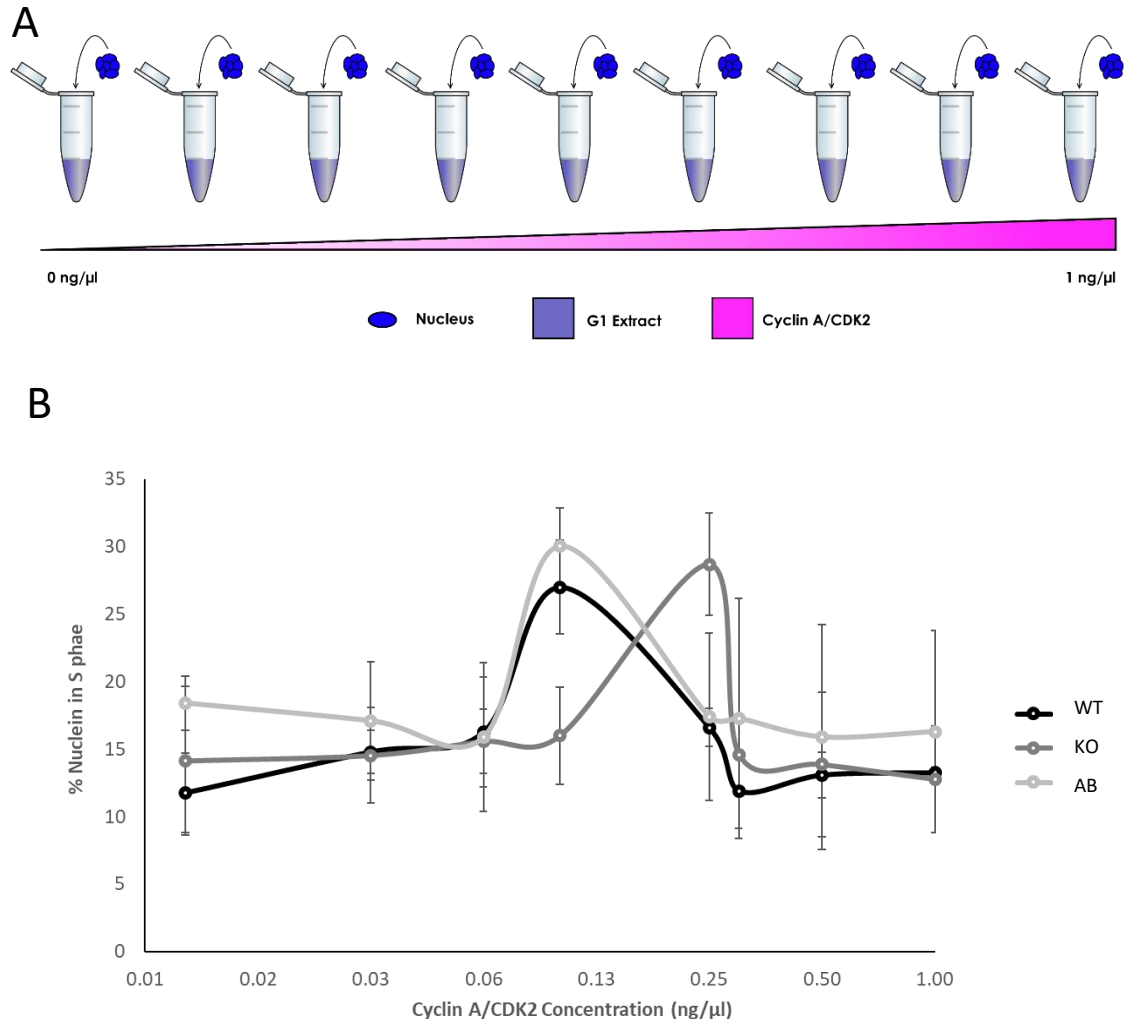


Figure 5.6 – Titration of Cyclin A into G1 extracts promotes replication initiation at a narrow range of concentrations A) A schematic design of the experiment. B) mean proportion of nuclei in S phase at each concentration ($n = 3 \pm$ standard deviation). The proportion of nuclei in S phase at each Cyclin A/CDK2 concentration for each cell line was compared using a two-way ANOVA with cyclin A/CDK2 concentration and cell line as factors (Cyclin A/CDK2 concentration) < 0.05 , P (cell line) < 0.05 , P (interaction) < 0.05 . Pairwise comparisons were made by simple main effects analysis WT and CIZ1^{AB} nuclei were not significantly different at any Cyclin A/CDK2 concentration ($p > 0.05$). CIZ1 KO nuclei were significantly different from WT and CIZ1^{AB} nuclei at 0.1 and 0.25 ng/μl Cyclin A/CDK2 ($p < 0.05$ for all comparisons). CIZ1 KO nuclei were not significantly different from WT or CIZ1 nuclei at any other concentrations. Error bars in B = standard deviation.

This cell free DNA replication system allows precise titration Cyclin A-CDK2 activity. This allows precise control of CDK activity and provides a useful tool to study the quantitative model of CDK activity for regulation of the cell cycle, mimicking both the S phase kinase

threshold and the S phase inhibitory threshold (Chapter 1). This approach showed that cyclin A-CDK2 promotes initiation of DNA replication at 0.1 ng/ μ l and is consistent in several studies (Coverley et al., 2002; Copeland et al., 2010). As expected for WT nuclei, cyclin A-CDK2 promotes initiation of DNA replication in a concentration dependent manner peaking at 0.1 ng/ μ l (Figure 5.6B). Significantly, CIZ1 KO nuclei do not initiate at 0.1 ng/ μ l and required a 2 fold increase in cyclin A-CDK2 to initiate DNA replication (Figure 5.5). The optimal cyclin A-CDK2 shifted to a higher concentration, suggesting that CIZ1 can influence the threshold of kinase activity that is required for initiation of DNA replication.

A two-way ANOVA was conducted which identified significant differences across cell line and Cyclin A/CDK2 levels. Simple main effects analysis tests showed that WT and CIZ1^{AB} nuclei did not respond differently. Whereas CIZ1 KO nuclei responded significantly differently to both, and CIZ1^{AB} nuclei. The shift in peak initiating concentration of Cyclin A/CDK upon CIZ1 KO was significant, and rescuable through ectopic expression of GFP-CIZ1.

These results lead to two main conclusions. Firstly, cyclin A/CDK2 can initiate DNA replication in a G1 nuclei at a specific concentration. At low cyclin A-CDK2 levels this signal is insufficient to initiate replication, peaking at a characteristic concentration and above this DNA replication initiation is blocked. Secondly, the cyclin A-CDK2 threshold required to optimally initiate DNA is determined in part by CIZ1. Deletion of the CIZ1 gene (CIZ1 KO) reveals that the kinase activity threshold is increased ~2-fold and this effect can be reversed by CIZ1^{AB}.

5.3.5. Recombinant CIZ1 can promote WT like DNA replication initiation kinetics in CIZ1 null nuclei.

The previous experiment identified that loss of CIZ1 promoted a change in the activating concentration of CDK2 signal and that the optimal concentration for initiation of DNA replication could be restored through genetic addback of GFP-CIZ1. To investigate whether a biochemical add back of CIZ1 could influence the kinase threshold that regulates initiation of

DNA replication, recombinant CIZ1- N471 was added to WT and CIZ1 KO nuclei in cell free DNA replication assays (Figure 5.7).

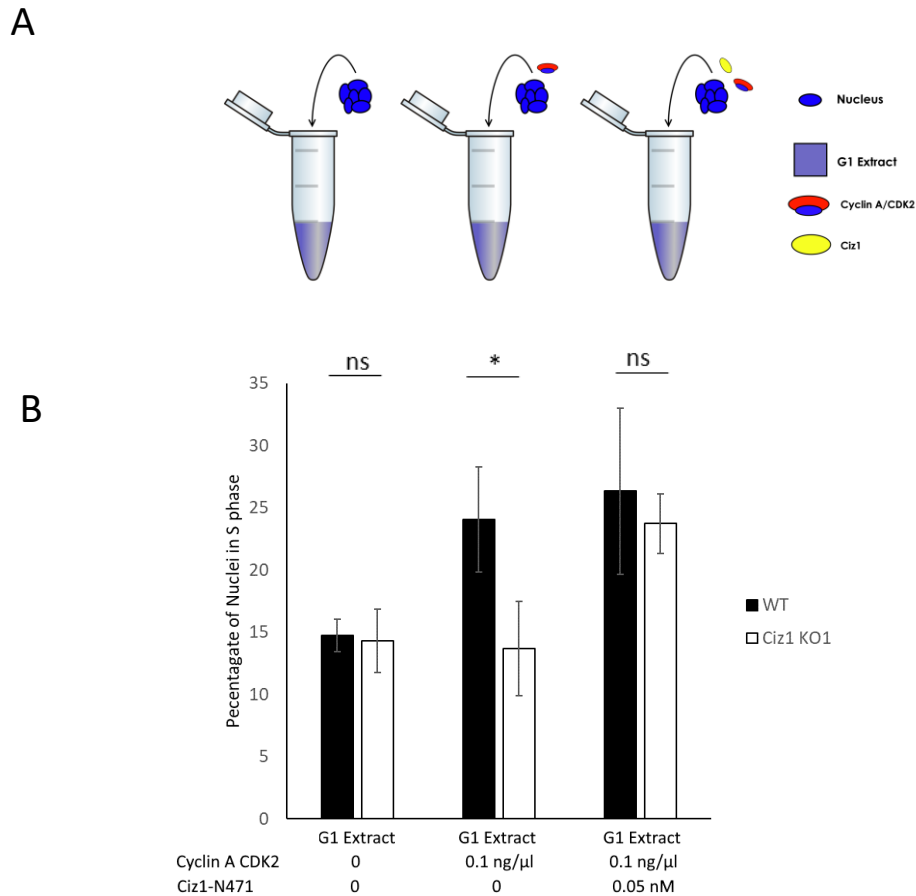


Figure 5.7 – Recombinant CIZ1 rescues CIZ1 KO nuclei, and restores optimal CDK thresholds *in vitro* A) Experimental overview. WT, and CIZ1 KO nuclei were incubated in G1 extracts with or without CIZ1-N471 and Cyclin A/CDK2. B) Bar chart showing the percentage (where $N = 3$, showing mean \pm standard deviation) of WT (Black) and CIZ1 KO1 (White) nuclei in S phase. The proportion of nuclei in S phase in each extract ($n = 3$ repeats) for each cell line was compared using a two-way ANOVA with extract and cell line as factors (P (extract) < 0.01 , P (cell line) < 0.05 , P (interaction) < 0.05). Pairwise comparisons were made by simple main effects analysis, significance is highlighted on C. ns = $p > 0.05$ * = $p < 0.05$, ** = $p < 0.01$, *** $p < 0.001$

To determine if the CDK threshold that promoted DNA replication *in vitro* could be restored to WT levels in CIZ1 KO nuclei, nuclei were incubated in G1 extracts, G1 extracts supplemented with 0.1 ng/μl Cyclin A CDK2, and G1 extracts supplemented with 0.1 ng/μl Cyclin A CDK2 and 0.05 nM CIZ1 N471 (Figure 5.7a). This is around half the level of CIZ1 to promote optimal initiation of DNA replication *in vitro*. To determine the effect on DNA

replication initiation the proportion of nuclei were in S phase was determined by measuring incorporation of Biotin-11-dUTP by fluorescence microscopy.

A two way ANOVA revealed significant interaction between cell line and extract. In G1 extracts, WT and CIZ1 KO nuclei displayed similar levels of nuclei in S-phase (WT: 14.7 %, CIZ1 KO: 14.3) that were not significantly different. When incubated in G1 extracts supplement with 0.1 ng/ μ l Cyclin A/CDK2, there is an increase in S-phase nuclei to 24 % that is absent for CIZ1 KO nuclei (13.7%), that showed a significant difference in the percentage of S phase nuclei. However, the addition of 0.05 nM CIZ1-N471 with 0.1 ng/ μ l Cyclin A/CDK2 the percentage of S-phase nuclei was increased to a similar level in both WT and CIZ1KO, that were not significantly different, yet significantly different from both G1 extract control sample and G1 extracts supplemented with Cyclin A/CDK2 samples. Results here reiterated earlier results that in the absence of CIZ1 the CDK threshold required to promote initiation of DNA replication is increased. This result demonstrated that recombinant CIZ1-N471 recapitulates the lower Cyclin A/CDK2 threshold replication in CIZ1 KO nuclei and phenocopy wild type nuclei. These data support the hypothesis that CIZ1 contributes to mechanisms that establish the kinase thresholds that regulate the G1/S phase transition and DNA replication initiation *in vitro*.

5.3.6. CIZ1 Expands the range of concentrations of Cyclin A/CDK2 that promote DNA replication initiation.

Previous experiments have demonstrated that the interplay between CIZ1 and Cyclin A/CDK2 alter when nuclei enter S phase *in vitro*. The cyclin A-CDK2 activity required to promote initiation altered upon loss of CIZ1. This can be restored through addback of CIZ1 through either biochemical or genetic means (Figure 5.7). Next, experiments were designed to investigate how CIZ1 affects the range of concentrations of cyclin A/CDK2 that promote DNA replication initiation.

Cell free DNA reactions were prepared WT, CIZ1 KO and CIZ1^{AB} nuclei, with a mid G₁ extract. The concentration of Cyclin A/CDK2 was titrated between 0.01 and 1 ng/μl in parallel reactions with 0.1 nM CIZ1-N471 and the percentage of nuclei in S-phase determined (Figure 5.8).

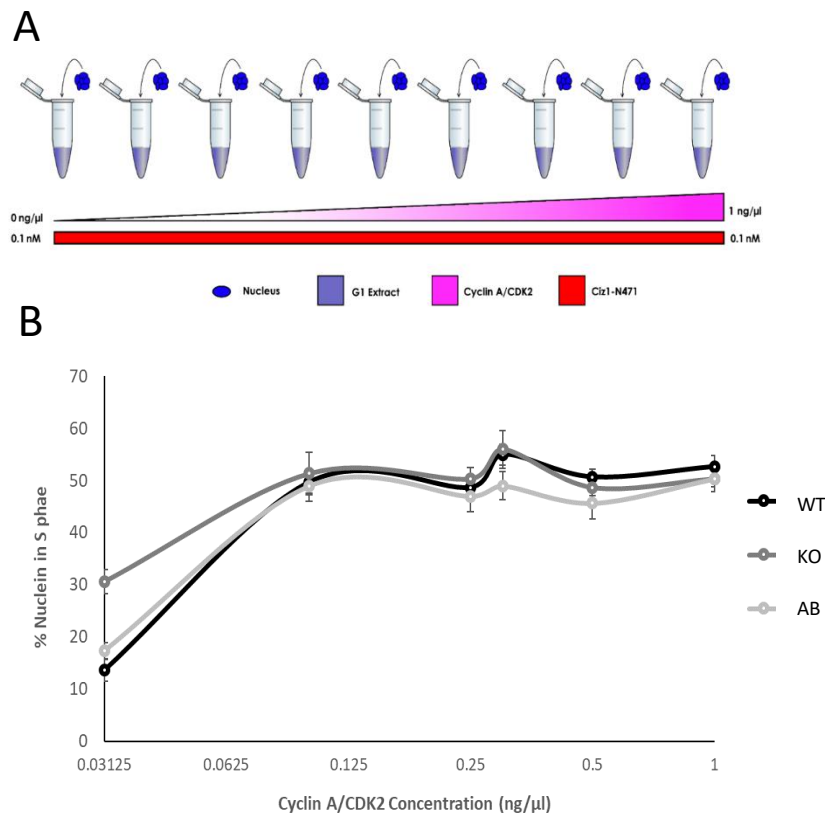


Figure 5.8. CIZ1-N471 Expands concentrations of Cyclin A/CDK2 that can promote DNA replication initiation A) Schematic diagram of the experimental design. B) mean proportion of nuclei in S phase for each reaction ($n = 3 \pm$ standard deviation). The proportion of nuclei in S phase at each Cyclin A/CDK2 concentration for each cell line was compared using a two-way ANOVA with cyclin A/CDK2 concentration and cell line as factors P (Cyclin A/CDK2 concentration) < 0.05 , P (cell line) > 0.05 , P (interaction) > 0.05 .

A two way ANOVA revealed there were no significant interaction between the three cell lines and Cyclin A-CDK2 concentration in the presence of 0.1 nM CIZ1-N471. For WT, CIZ1 KO and CIZ1^{AB} nuclei, addition of 0.1 nM CIZ1-N471 expanded the range of concentrations of Cyclin A/CDK2 that could promote DNA replication initiation *in vitro*. Addition of CIZ1-N471 promoted DNA replication at concentrations 10-fold higher than reactions without exogenous CIZ1 (Figure 5.8).

For the majority of concentrations of Cyclin A/CDK2 added there were no significant differences between the proportion of nuclei in S phase across nuclei, and each nuclei type displayed significantly more nuclei in S-phase upon addition of CIZ1-N471 (when compared to data from Figure 5.6). Notably at low concentrations of Cyclin A/CDK2 (0.03ng/ μ l), WT and CIZ1^{AB} nuclei displayed a proportion of nuclei in S phase that was not different from the same concentration in the absence of CIZ1 (data from Figure 5.6). However, at the same concentration, KO nuclei showed a significant increase in the proportion of nuclei in S phase from 14.5 % to 30.6 % upon addition of CIZ1-N471. Next, the replication kinetics of each of the nuclei was determined.

5.3.7. Recombinant CIZ1 can enhances activity of Cyclin A/CDK2 *in vitro*.

The data are consistent with CIZ1 contributing to mechanisms that establish the cyclin A/CDK2 activity threshold that triggers DNA replication initiation *in vitro*. To investigate whether addition of recombinant CIZ1 can alters the optimal concentration of cyclin A/CDK2 for initiation of DNA replication, cell free DNA replication assays were performed. The assays used G1 extracts containing the optimal concentration of cyclin A/CDK2 and increasing CIZ1-N471 concentrations. from 0.03 to 1 nM. The effect was determined in WT, CIZ1 KO and CIZ1^{AB} nuclei and the percentage of S-phase nuclei determined (Figure 5.9).

Additionally, reactions for CIZ1 KO nuclei were performed at both 0.1 ng/ μ l and 0.2 ng/ μ l cyclin A/CDK2. This was to determine if the WT Cyclin A/CDK2 replication initiation activating concentration could be restored through chemical addback of recombinant CIZ1-N471. As well as observing the effects of recombinant CIZ1-N471 at CIZ1 KO nuclei activating concentration. The data for CIZ1 KO nuclei at 0.2 ng/ μ l Cyclin A-CDK2 is shown in Figure 5.10.

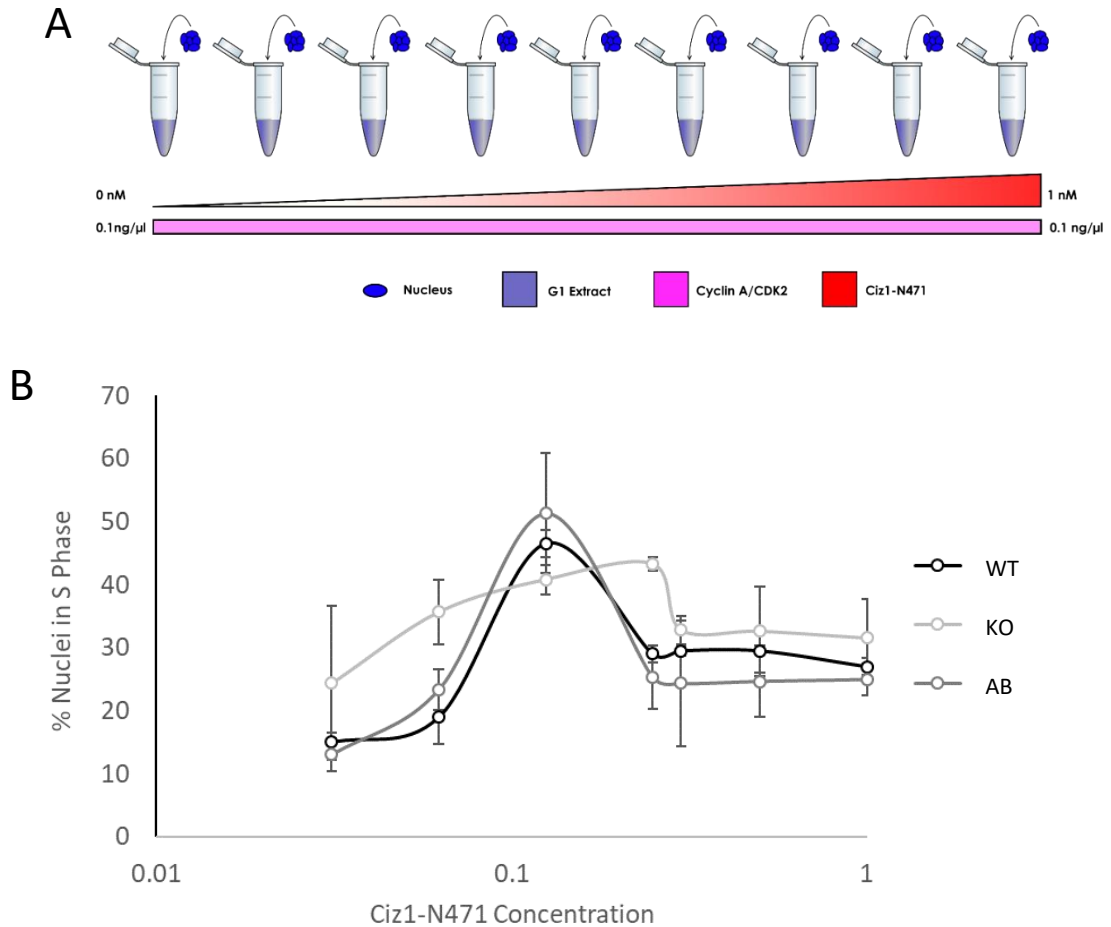


Figure 5.9 – CIZ1-N471 increases the activity of cyclin A-CDK2 and enhances initiation of DNA replication. A) Experimental overview. B) The mean percentage of nuclei in S phase at each CIZ1-N471 concentration in G1 extracts, with 0.1 ng/μl ($n = 3 \pm$ standard deviation).

This experiment was performed to investigate how CIZ1 levels affect DNA replication at the optimal level of Cyclin A/CDK2 for WT, and CIZ1^{AB} nuclei. The aim was to identify if CIZ1 levels altered the ability of recombinant Cyclin A/CDK2 to promote replication. Without addition of recombinant CIZ1-N471, 0.1 ng/μl Cyclin A/CDK2 promoted an increase in initiation of DNA replication by a factor of 2 for the WT, CIZ1 KO and GFP CIZ1 nuclei. The increase in initiation of DNA replication was comparable between the nuclei, any observed differences were non-significant.

Addition of CIZ1-N471 at low concentrations (<0.1 nM) did not promote any change in rates of DNA replication initiation compared to the cyclin A/CDK2 alone in WT, CIZ1 KO and CIZ1^{AB} nuclei. However, CIZ1-N471 promoted an increase in DNA replication initiation at

concentrations >0.1 nM in WT, CIZ1 KO, and GFP-CIZ1 KO nuclei. Comparison of the WT and CIZ1 KO nuclei revealed a 2-fold increase in cyclin A-CDK2 levels to reach peak activity. This may reflect the difference in CIZ1 levels in CIZ1 KO cells relative to WT and CIZ1^{KI} cells.

Interestingly at 0.2 nM CIZ1-N471, more CIZ1 KO nuclei were in S phase: 44.2 % of CIZ1 KO nuclei were in S phase compared to 28.1 % of WT nuclei, and 25.3 % of CIZ1^{AB}. This could be due to loss of endogenous CIZ1 in CIZ1 KO nuclei, resulting in a greater requirement of CIZ1-N471 to promote optimal replication initiation. This effect was reversed in CIZ1^{AB} nuclei, that peaked at 0.1 nM CIZ1-N471.

The data presented in Figure 5.9 utilise the optimal cyclin A-CDK2 concentration for WT nuclei. However, the optimal concentration for CIZ1 KO cells is 0.2 ng/μl. This change in cyclin A-CDK2 activity may affect the concentration of CIZ1 that is optimal for initiation of DNA replication. To investigate how this effects replication initiation a CIZ1 titration in CIZ1 KO nuclei supplemented with 0.2 ng/μl cyclin A-CDK2, cell free DNA replication assays were performed (Figure 5.10).

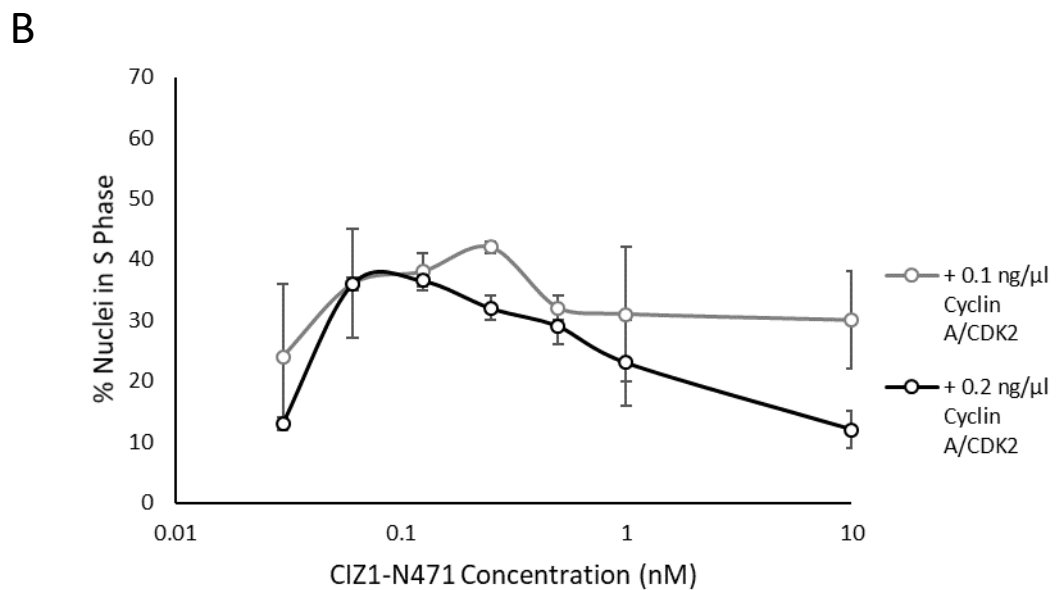
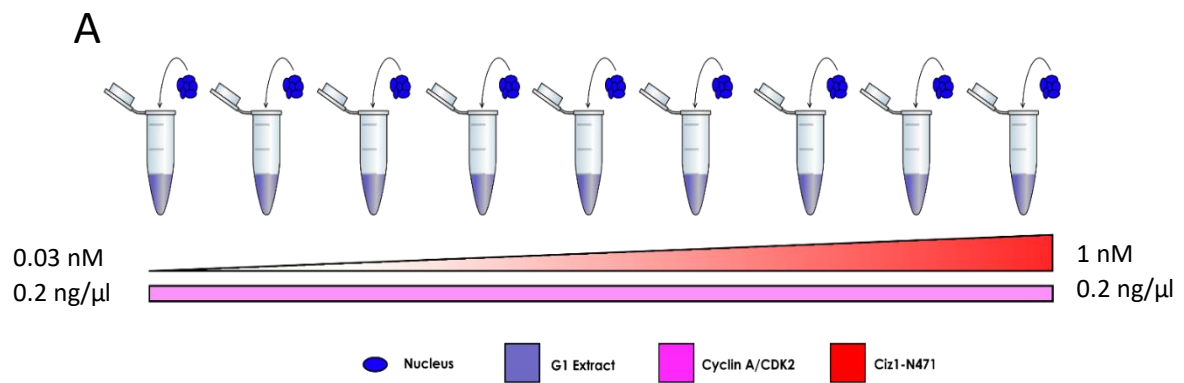


Figure 5.10 – Increased cyclin A-CDK2 concentration changes optimal CIZ1 levels for CIZ1 KO Nuclei A) Experimental overview. B) mean roportion of nuclei in S phase at each concentration superimposed over data at 0.1 ng/μl from Figure 5.9 ($n = 3 \pm$ standard deviation).

The data show that there is a concentration dependent initiation of DNA replication, with a peak at 0.1 nM CIZ1. There are 2 phases of activity at concentrations less than 0.1 nM increasing CIZ1 enhances initiation of DNA replication, and above 0.1 nM the activity of CIZ1 does not promote such an increase in replication initiation. This is consistent with earlier results showing that there is both an activating and inhibitory effect when increasing CIZ1 concentrations (Figure 5.2). The data presented here shows that the optimal CIZ1 concentration is dependent on the cyclin A-CDK2 activity present in cell free DNA replication

assays. At low cyclin A-CDK2 (0.1 ng/μl) CIZ1 KO nuclei require additional CIZ1 (0.25nM) for optimal activity (Figure 5.10). Increasing the concentration of Cyclin A-CDK2 to 0.2 ng/μl reduces the requirement for CIZ1 and shifts the optimal peak to 0.1 nM CIZ1-N471.

Additionally, increasing Cyclin A/CDK2 concentrations reduces the increase in nuclei in S phase at 0.03 nM CIZ1-N471, indicating an importance on the ratio of Cyclin A-CDK2:Ciz1 levels in promoting replication initiation. Critically, using optimal Cyclin A/CDK2 levels returned the observed peak to a distribution more similar to WT, and CIZ1^{AB} nuclei.

Taken with the other data presented here, there is a cooperativity between cyclin A-CDK2 activity and the levels of CIZ1 that contribute to the kinase activity threshold that regulates the initiation phase of DNA replication. Changing the concentration of either factors affects the optimal concentrations required for efficient initiation of DNA replication. This adds to data that indicates that CIZ1 could be acting as a kinase sensor. Levels of CIZ1, alter the concentration at which Cyclin CDK networks promote the onset of S phase. Genetic loss of CIZ1 increases the amount of signal required to promote S phase initiation. CIZ1 addback, through both genetic and chemical methods, can restore the concentration at which cyclin A/CDK2 can promote replication initiation.

5.4. DNA combing of Cell free DNA replication assays *in vitro*

5.4.1. Replication fork velocities are reduced in CIZ1 KO nuclei in cell free DNA replication assays

In vitro DNA replication assays revealed that CIZ1-N471 modulates the response to increasing cyclin A-CDK signalling in vitro. To test how changes in CIZ1 levels and cyclin A-CDK2 activity alter the DNA replication programme, DNA replication fork velocities were determined using DNA combing in cell free DNA replication assays.

Firstly, differences in fork progression rates were estimated in WT, CIZ1 KO and CIZ1^{AB} nuclei.

A measure of this would be achieved through the single labelling technique developed in

Chapter 3. Reactions were performed using replication competent WT, CIZ1 KO and CIZ1^{AB} nuclei incubated in an S phase extract for 30 minutes and nascent DNA labelled with EdU. The nuclei were harvested, DNA was purified, combed and the EdU labelled. A measure of replication rate was determined using the length of EdU tracks (Figure 5.11).

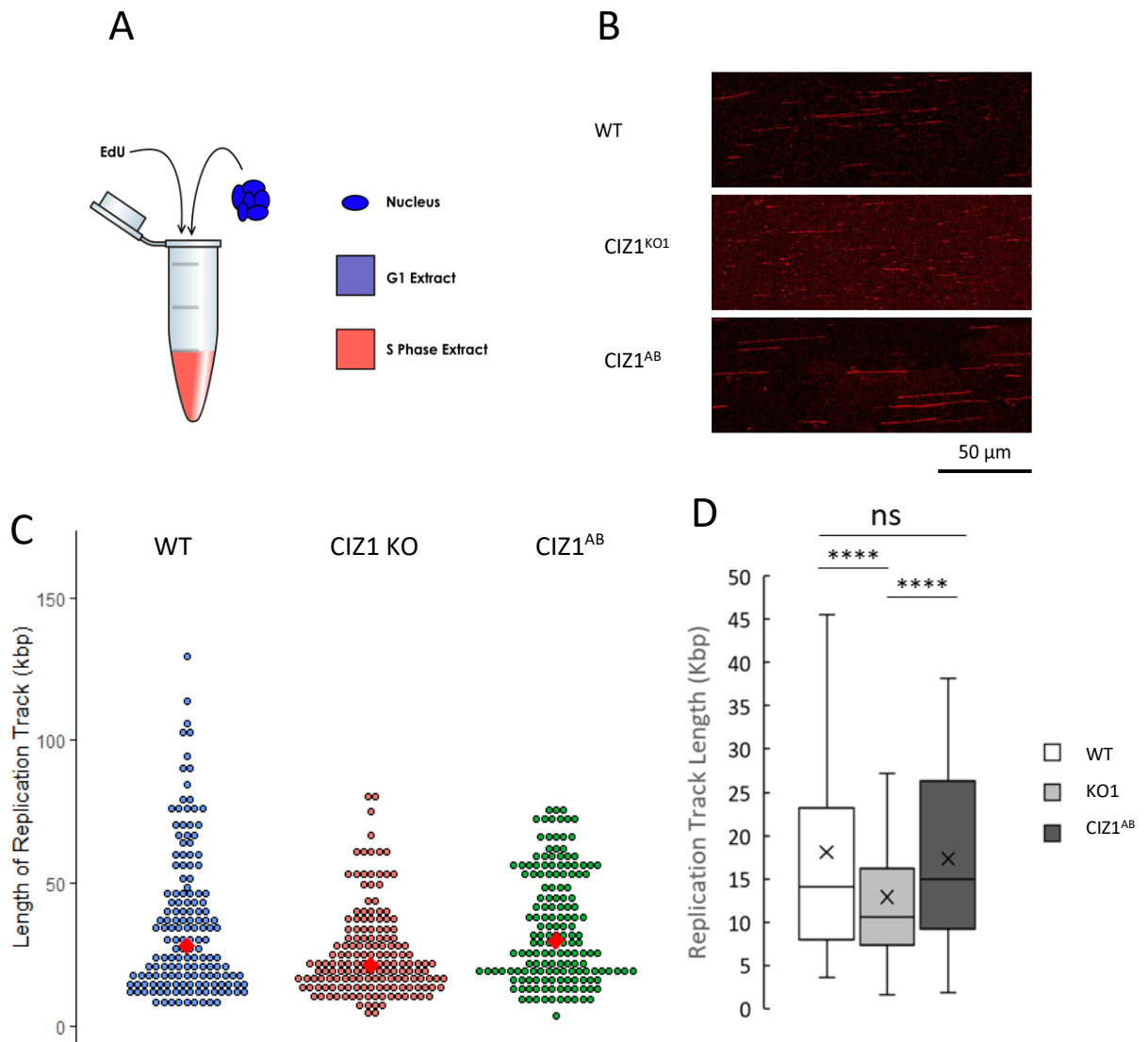


Figure 5.11- Measuring Replication Kinetics in in vitro reactions. A) Displays a schematic of the experimental design. B) Representative confocal fluorescence microscopy images of positively labelled DNA. C) Displays swarm plots of replication track lengths for DNA from nuclei of each cell line: WT (Blue), CIZ1 KO1 (Red), CIZ1^{AB} (Green) (n = 150). Red dots represent the median for each dataset. D) Displays box and whisker charts displaying the distribution of replication track lengths for each cell line: WT (White), CIZ1 KO1 (Light grey), CIZ1^{AB} (Dark grey). The crosses represent the mean value for each dataset (N = 150). Significant differences between the replication track lengths were observed across the three cell line (One Way ANOVA, $p < 0.0001$). Pairwise comparisons were conducted by Tukey's HSD test, significance is indicated on the graph: ns = $p > 0.05$, * = $p < 0.05$, ** = $p < 0.01$, *** = $p < 0.001$, **** = $p < 0.0001$

A one way ANOVA was conducted that indicated there were significant differences in mean replication track lengths across the three nuclei types. Analysis of the DNA replication track length showed that WT nuclei had higher replication track lengths than CIZ1 KO nuclei, and that was reversed by CIZ1^{AB} (median track length of 14 kbp, 10.6 kbp and 15 kbp respectively). Furthermore, the drop in replication track length between WT and CIZ1 KO and also CIZ1 KO and CIZ1^{AB} were found to be statistically significant. The CIZ1^{AB} nuclei had a median track length of 15.01 kbp and comparison with WT nuclei (14 kbp) showed they were not statistically significantly different. This implied that CIZ1 KO caused an alteration in the replication programme, if this is consistent in cell based experiments this may indicate a DRS phenotype, this is further explored in Chapter 6 through determination of replication kinetics in WT, CIZ1 KO and CIZ1^{AB} cells.

5.4.2. Cyclin A and CDK2 Co-operate to Promote Optimal DNA Replication *in vitro*

Earlier experiments have demonstrated that loss of CIZ1 in nuclei resulted in reduced fork rate, a phenotype that is consistent with DNA replication stress. This data demonstrated that CIZ1 plays a role in maintaining DNA replication. With the tools at disposal this could not be uncovered in cell-based experiments. Fortunately using the *in vitro* replication experiments an *in vitro* model of this could be developed.

Earlier experiments demonstrated (for WT nuclei) an optimal concentration at which cyclin A/CDK2 initiated DNA replication (0.1 ng/ μ l), above and below this level DNA replication was not initiated at a level above baseline. Secondly, addition of an optimal concentration of recombinant CIZ1-N471 (0.1 nM for WT cells) resulted in an increase in the proportion of cells in S phase, as well as a widening of the concentrations of Cyclin A/CDK2 that allowed a significant increase in the proportion of nuclei entering S phase. These levels shifted with genetic loss of CIZ1 but could be returned by addback of recombinant CIZ1-N471.

Experiments were designed to analyse the effects of increased CIZ1 levels on DNA replication initiation. Four Reactions were set up, all reactions were performed in a G1 extract. For the first, a final concentration of 0.1 ng/ μ l recombinant cyclin A/CDK2 was added to the reaction. For the second, 0.1 nM CIZ1-N471, and 0.1 ng Cyclin A/CDK2 was added (This represented optimal replication). For the third, 0.02 ng/ μ l and 0.1 nM CIZ1-N471 was added to the reaction (This represented replication that at a low CDK level only permissible upon addition of CIZ1-N471). For the fourth and final reaction 0.1 nM CIZ1-N471 and 1 ng/ μ l of cyclin A/CDK2 was added to the reaction (This represented replication that at a high CDK level only permissible upon addition of CIZ1-N471). After, incubation the nuclei were isolated, DNA purified, combed, labelled, and imaged. The results from this experiment are displayed in Figure 5.12.

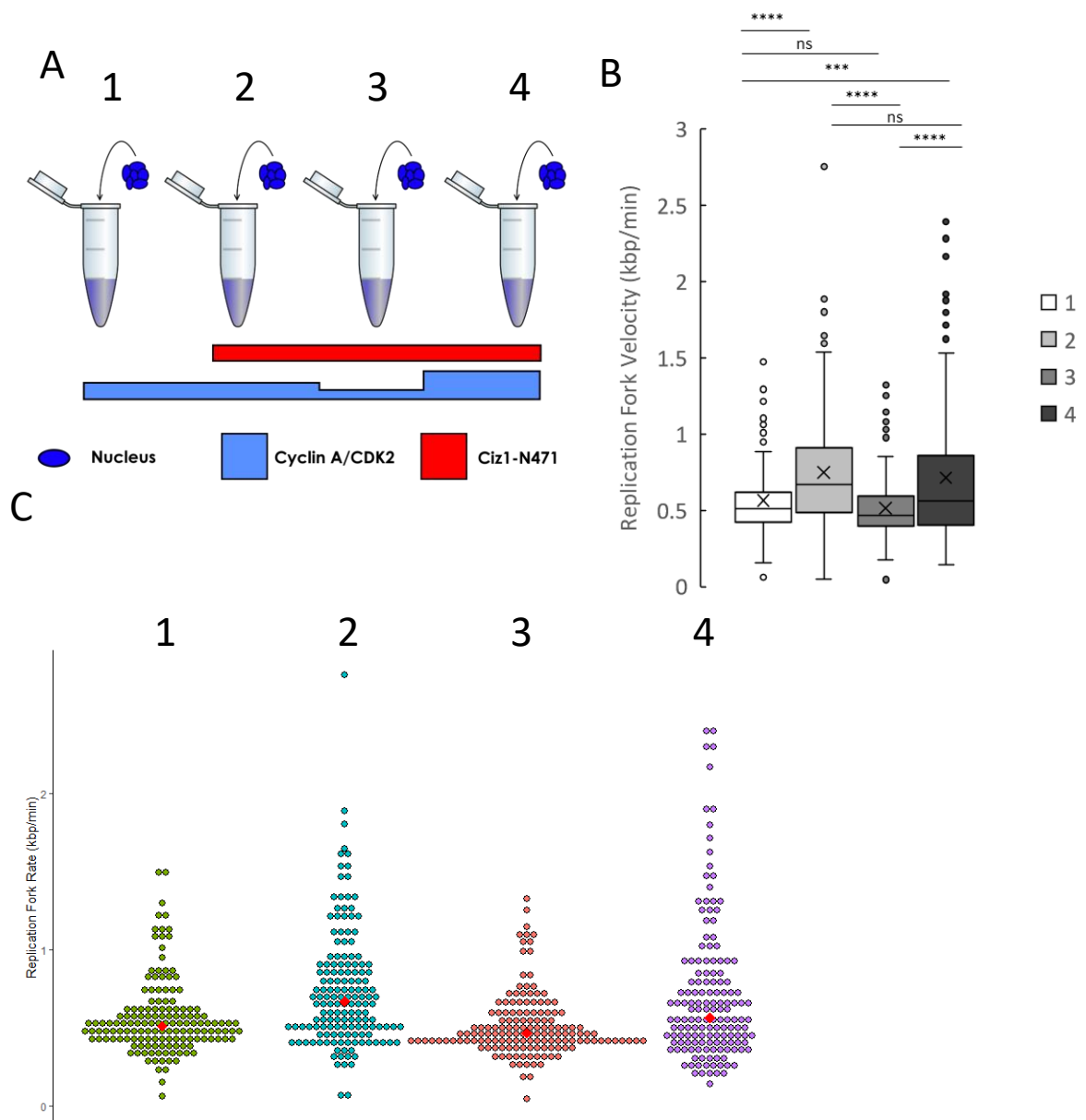


Figure 5.12. The effect of adding recombinant CIZ1 to a range of cyclin A/CDK2 concentrations in vitro A) Displays a graphical schematic of the design of the experiment. Using data from Chapter 5 an optimal (0.1 ng/ μ l), high (1 ng/ μ l) and low (0.02 ng/ μ l) cyclin A/CDK2 concentration was assigned, and optimal CIZ1 concentration (0.1 nM). B) displays box and whisker plots showing the distribution of fork rates from nuclei in each experimental condition ($n = 150$). (1=optimal Cyclin A/CDK2, 2=Optimal Cyclin A/CDK2 and optimal CIZ1-N471, 3=Low Cyclin A/CDK2 and optimal CIZ1, 4=High Cyclin A/CDK2 and optimal CIZ1-N471). Significant differences in fork rate were observed between the conditions (One Way ANOVA, $p < 0.0001$). Pairwise comparisons were conducted by Tukey's HSD test, significance is indicated on the graph: ns = $p > 0.05$, * = $p < 0.05$, ** = $p < 0.01$, *** = $p < 0.001$, **** = $p < 0.0001$ C) displays a swarm plot of fork rates of each of the experimental conditions (green = 1, blue = 2, red = 3, purple = 4). Red diamonds represent median values ($n = 150$).

Figure 5.12b and 5.12c displays the replication fork rate of each of the reactions.

Interestingly, all observed replication fork velocities were lower than what was observed in cell based experiments (Chapter 3). A one way ANOVA was conducted that indicated there were significant differences in mean fork rate across the four samples. For reaction 1 (0.1 ng/ μ l Cyclin A/CDK2) a median replication fork rate of 0.51 kbp/min was observed. This was lower than the observed rate when nuclei were stimulated with an S phase extract (0.83 kbp/min, Figure 5.11). This is unsurprising, experiments in Chapter 6 revealed that S phase entry was less efficient with addition of cyclin A/CDK2 in a G1 extract compared to an S phase extract.

The second reaction (0.1 ng/ μ l cyclin A/CDK2 and 0.1 nM CIZ1-N471) Displayed a median replication rate of 0.75 kbp/min. This was higher than in reaction 1, and additionally, the difference between the two was significant. This indicated that addition of CIZ1-N471 at optimal concentrations prompted a change in replication dynamics. The fork rate was lower than in an S phase extract, representing an intermediate value.

Reaction 3 (low Cyclin A/CDK2 and 0.1 nM CIZ1-N471) displayed a median replication fork velocity of 0.52 kbp/min. This replication fork rate was comparable to the rate seen in reaction 1. The difference between the two values was not significant. The value was significantly different from reaction 2. This indicated that low CIZ1 levels allow replication to occur, but the replication programme is altered.

Reaction 4 (High Cyclin A/CDK2 and 0.1 nM CIZ1-N471) displayed a median replication fork velocity of 0.72 kbp/min. This value was comparable to reaction 2. The 2 datasets were not significantly different. The value was significantly higher than reaction 1, and reaction 3, and lower than an S phase extract. This indicates that high levels of CIZ1 results in a comparable replication programme to optimal levels, approaching the phenotype observed in an S phase extract.

A number of implications can be inferred from this data. Firstly, *in vitro*, replication initiated in a G1 extract is inefficient, and results in a reduced replication fork rate compared to S phase extracts. This could be due to a number of reasons; many replication factors present in S phase extracts will not be present. This replicates the effect of replicating DNA early, due to oncogenic activation, which can result in mitotic issues. Critically, addition of CIZ1-N471 allows replication to occur at lower cyclin A/CDK2 concentrations. This resulted in a reduced replication fork velocity. This could indicate that increased CIZ1 allows DNA replication to occur at lower cyclin A/CDK2 levels, and critically replication that occurs results in a stressed phenotype.

At optimal kinases levels for replication, addition of CIZ1 results in promoting replication kinetics more similar to those seen by addition of an S phase extract (although remaining significantly lower). This could indicate that CIZ1 at optimal levels promotes a healthier replication programme in these *in vitro* conditions. This could indicate that CIZ1 is one of the factors missing from the G1 extract that results in reduced replication efficiency. At high cyclin A/CDK2 concentrations a similar phenotype was observed, an intermediate phenotype between no CIZ1 and an S phase extract. Again, indicating that increased CIZ1 levels may promote a healthy replication programme at higher CDK levels.

5.5. Chapter Discussion

5.5.1. CIZ1 Shifting Kinase Thresholds May Induce DRS

The results presented here provide evidence that CIZ1 contributes to mechanisms that control the kinase thresholds that underpin both S phase entry and prevent re-replication of chromosomes. Cancer cells have disrupted Cyclin/CDK signalling networks through mutations and disruption of these networks leads to DNA replication stress (Gailard et al., 2015). There are a number of ways that the cell cycle and CDK activity can be perturbed

including oncogenic signalling, TSG inactivation obfuscating the requirement of external growth signals (Hanahan and Weinberg, 2000).

Firstly, there is clear evidence that loss of CIZ1 caused a change in the concentration of cyclin A/CDK2 that promotes DNA replication initiation. The data presented in this chapter show that there is cooperativity between CIZ1 and cyclin A-CDK2 activity and here for the first time evidence suggests an interdependence for their activity. The data has demonstrated that the concentration of cyclin A-CDK2 that promotes initiation of DNA replication can be modulated by CIZ1 levels, and conversely, loading of Cyclin A to DNA in a G1 extract can be modulated by CIZ1 levels (Figure 5.5/5.5). The deletion of CIZ1 and cell free DNA replication assays have revealed that loss of endogenous CIZ1 increases the concentration of cyclin A-CDK2 that is required to promote initiation of DNA replication (Figure 5.6). This effect is reversible by either addition of recombinant CIZ1 or by genetic add back of GFP-CIZ1 in CIZ1^{AB} nuclei.

Significantly, addition of exogenous CIZ1 increases the range of cyclin A-CDK2 activity that can promote initiation of DNA replication *in vitro*. However, this effect is concentration dependent as that addition of CIZ1 to cell free replication assays at very high concentrations can block DNA replication initiation *in vitro*. This observation was observed in cell free assays using both an S phase extract, or G1 extracted supplemented with the optimal concentration of Cyclin A/CDK2 to promote initiation.

Data from this chapter can be applied to the quantitative cell cycle model (Discussed in detail in Section 1.8). Briefly, this model attributes cell cycle progression to oscillating kinase levels driven by increasing levels of Cyclin proteins as cells progress from G1 through to Mitosis. The kinase level is “reset” during anaphase due to the activity of the APC/C (Uhlmann et al., 2011; Swaffer et al., 2016; Alfieri et al., 2017). Surrounding S phase there are two kinase thresholds: a lower kinase activity which must be passed to allow DNA replication initiation (T_s), and a higher kinase activity above which replication licensing, and initiation is prevented

(iT_s). These two thresholds can be directly observed in cell free DNA replication assays using cyclin A-CDK2 titrations (Figure 5.6).

Data in this chapter has demonstrated that the addition of recombinant CIZ1 can allow replication at kinase levels that are either below or above the thresholds that typically allow DNA synthesis (T_s and iT_s). This narrow range of CDK activity that facilitates initiation of DNA replication is termed the permissive CDK activity range. A proposed model for the effect of CIZ1 levels on kinase thresholds is summarised in Figure 5.13.

Loss or gain of CIZ1 altered T_s, additional of recombinant CIZ1-N471 promoted DNA replication initiation at lower kinase levels, accompanied by a chromatin localisation of Cyclin A (Figure 5.13b). Genetic loss of CIZ1 (CIZ1 KO) shifted T_s to higher Cyclin A/CDK2 concentrations than observed in WT nuclei (Figure 5.13c). Loss of control of the T_s through loss or gain of CIZ1 may result in replication occurring earlier than in healthy cells. Often, oncogenic activation results in a shortening of G1, which results in DNA replication stress, and increased replication/transcription machinery collisions (Macheret & Halazonetis, 2015; Macheret & Halazonetis, 2018). Loss of control over the T_s will result in an erosion of genome, and regulation integrity (Técher et al., 2017).

Experiments in this chapter demonstrated that loss of CIZ1 alters iT_s, addition of recombinant CIZ1 promoted replication initiation at previously non permissible kinase level (Figure 5.13b) and genetic loss of CIZ1 (CIZ1 KO) shifted T_s above the iT_s observed in WT nuclei (Figure 5.13c). Deregulation of the iT_s in these manners could result in re-replication promoting genome amplification, aneuploidy and aberrant chromosomal structures (Hook et al., 2007). Re-replication is observed in tumour cells (Melixetian et al., 2004). Furthermore, as well as inducing chromosome level alterations DNA re-replication leads to mutation. In yeast, re-replication can induce 30 fold increases in frameshift rates, as well as inducing base substitutions (Bui & Li, 2019). Clearly, the iT_s is important for maintenance of genome, and

replication integrity. Critically, if dysregulation of CIZ1 results in erosion of control of S-phase thresholds this has implications for the role that CIZ1 may play in cancers (Higgins et al., 2012; Nishibe et al., 2013; Xhou et al., 2018).

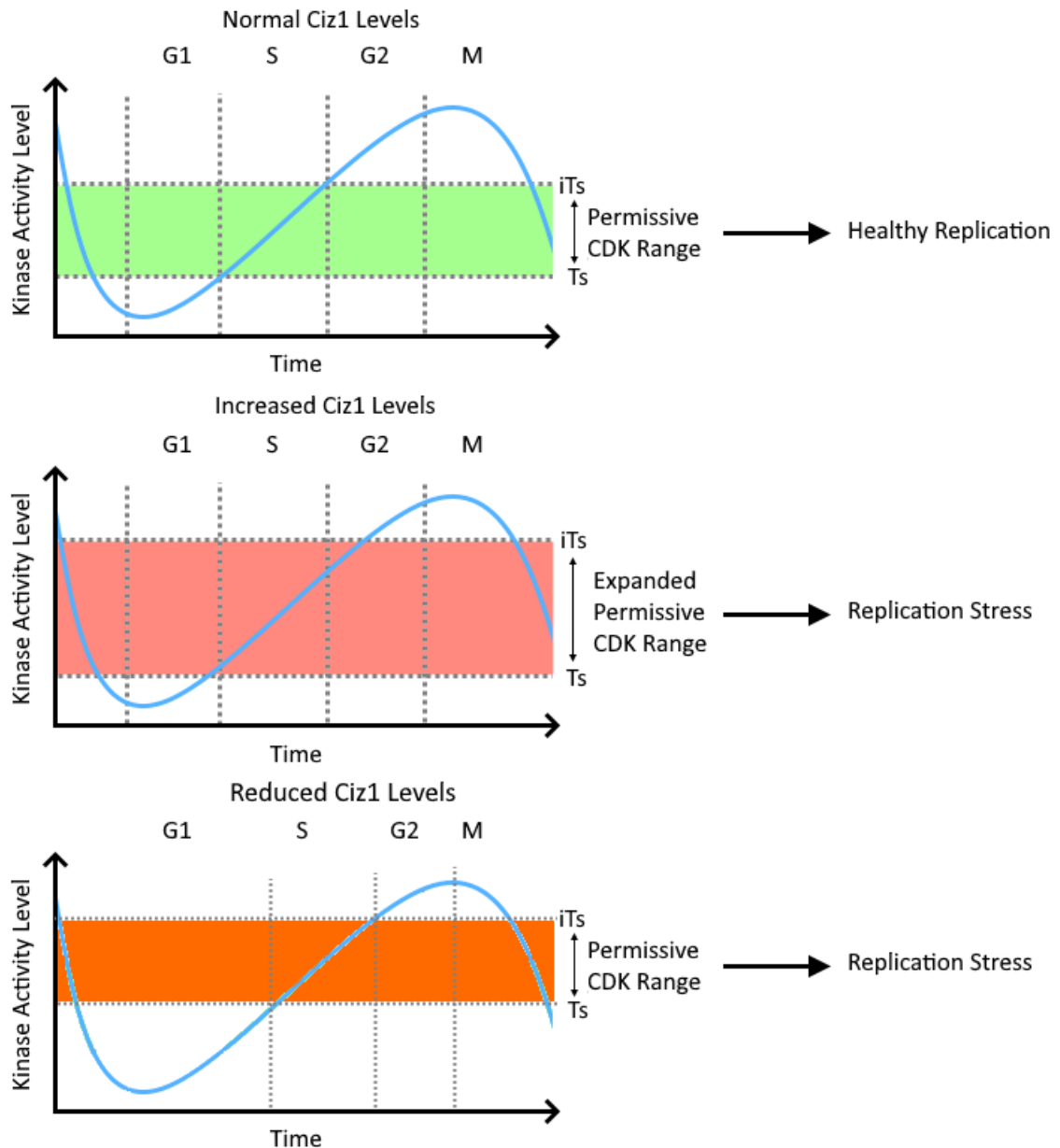


Figure 5.13 – Model for the effect of CIZ1 levels and thresholds for initiation of DNA replication A) Displays the kinase thresholds for normal cells. B) Displays a proposed model wherein CIZ1 expands kinase thresholds resulting in mistimed replication, this may be measurable by inducing DNA replication stress. C) Displays a proposed model wherein loss of CIZ1 shifts kinase thresholds resulting in mistimed replication, again this may be measurable by inducing DNA replication stress.

5.5.2. CIZ1 Disruption of Kinase Thresholds may be Linked to its Role in Cancers

Together these data provide a model for how CIZ1 could be involved in tumorigenesis; both with its apparent oncogenic and tumorigenesis activity (Higgins et al., 2012; Nishibe et al., 2013; Riding-Figueroa et al., 2017). Altered responses to CDK signalling at the G1/S transition could promote mistimed replication, this could induce replication stress, driving genome instability and promoting a mutator phenotype promoting tumourigenesis. Uncoupling of kinase activity and replication initiation control has been shown to induce DNA replication stress. (Matson et al., 2019). Oncogenic mutations that promote increased kinase activities have also demonstrated replication stress (Srinivasan et al., 2013; Llobet et al., 2019). CIZ1 disruption of kinase thresholds may induce DRS

Loss of CIZ1 increases the S phase kinase threshold, this would promote S phase occurring later than appropriate timing. Intriguingly this was not observed in cells in Chapter 4. Conversely, S phase occurred more rapidly in cell re-entering the cell cycle. Although, CIZ1 null cells did more rapidly exit the cell cycle upon contact inhibition and serum starvation. This could perhaps be explained by a more rapid increase in Cyclin A accumulation following quiescence in CIZ1 null cells (Figure 4.6), which may compensate for the increased CDK2 threshold required to initiate DNA replication that was observed *in vitro*. Additionally, CIZ1 levels accumulate as cells re-enter the cell cycle from quiescence (Pauzaite et al., 2017), the levels of CIZ1 may be low enough during cell-cycle re-entry that the threshold manipulation of CIZ1 observed in this Chapter may not be the major effector on G1 length stemming from CIZ1 loss observed in cells (Chapter 4).

Some evidence of replication stress was provided in DNA combing results from this Chapter *In vitro* data provides evidence for what happens to cells when they gain excess CIZ1. This is important as it could explain CIZ1's dual role as both a tumour suppressor and as an oncogene (Higgins et al., 2012; Nishibe et al., 2013). In this chapter, it was revealed in Figure

5.12. that addition of CIZ1-N471 to low cyclin A/CDK2 concentrations allows replication. However, this replication is inefficient, characterised by a low replication fork velocity. This is consistent with DRS, that could result in genome instability (Figure 6.13). At higher cyclin A/CDK2 concentrations addition of CIZ1 promotes a replication dynamic more similar to S phase cells. This indicates healthy replication could occur at these levels. This could provide another clue as to why overexpressed CIZ1 is observed in cancers. This provides a model where cells with higher CIZ1 levels can replicate more readily, due to the expanded permissible kinase window. This model is summarised in Figure 5.14.

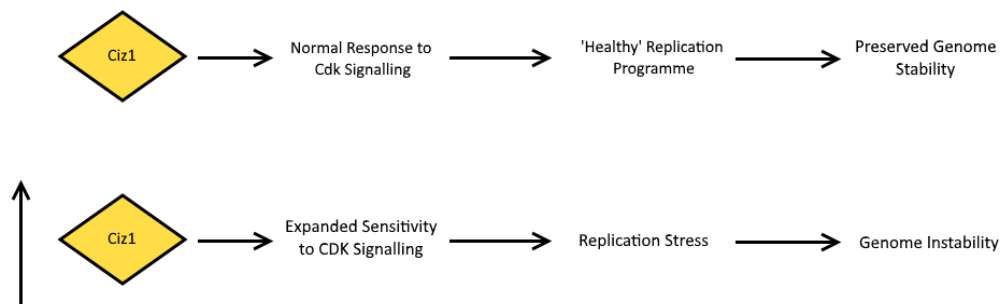


Figure-5.14- Model for the effect of increased CIZ1- Summary of a potential model for why high CIZ1 levels are observed in certain cancers. In this model genome instability is triggered by replication stress caused by CIZ1 allowing DNA replication to occur at lower CDK2 activity levels than 'healthy cells'.

A second hypothesis can be derived from these results. The overexpression of CIZ1 increases the permissive range of cyclin A-CDK2 activities that can promote DNA replication. This may provide a growth advantage in cancers with a perturbed cell cycle or persistent oncogenic signalling. Cancer cells often have oncogenic mutations that promote increased kinase activity and deranged replication dynamics, many of these are proposed cancer therapeutic targets (Chen et al., 2018; Caruso et al., 2018). A potential role for CIZ1 is that it may be overproduced to allow cancerous cells to grow in non-favourable conditions, such as where there is deregulation of cyclin-CDK activity as a result of oncogenic activation.

In this role, CIZ1 may be a subject of “non oncogene gene addiction”, this phenomenon describes how cancer cells become dependent on a non-oncogenic (or oncogenic) gene as a result of phenotypes derived from cancerous mutations. An example of this is Heat shock factor 1 (HSF1), a heat shock protein involved in protein refolding. Loss of HSF1 results in a decrease in viability of numerous human tumour cells, whilst having no effect on non-cancerous cells. It is hypothesised that HSF1 relieves the stress present in cancer cells (Dai et al., 2007; Solimini et al., 2007). Targeting gene addiction has been proposed as a novel cancer therapeutic strategy (Torti & Trusolino, 2011). Future research should focus on the dependence of various cancer on CIZ1 to observe whether CIZ1 becomes a gene addiction and identify the efficacy of targeting CIZ1 as a personalised cancer therapeutic.

5.5.3. Analysis of Cell Free DNA Replication Kinetics

Interestingly, Marheineke et al. (2005) have performed DNA combing experiments on nuclei synchronised through mimosine arrest. Using this method human bladder carcinoma EJ30 cells were used. These cells are treated for 24 hours with mimosine which halts their cell cycle progression at late G1. These can be signalled to enter S phase by addition of a cytosolic extract from asynchronous cells. S phase nuclei in this report were generated using thymidine inhibition. In this report nuclei displayed lower replication rates than would be expected from similar cell-based experiments. 0.3 kb/min, similar to the 0.5 kb/min displayed in this report. Intriguingly comparable replication rates in these nuclei were found from G1 to S phase nuclei, increases in replication were due to an increase replication origin firing characterised by an increase in replication density.

The observed reduction in replication fork rate for *in vitro* DNA replication assays relative to cell-based experiments suggests that there are limiting factors that reduce fork progression. For example, addition of CIZ1 and Cyclin A/CDK2 can modulate replication rates *in vitro*. For the nuclei in this report, nuclei may be under additional stress, Replication origins, after cell

cycle restart, are under licensed in the first S phase this would lead to a hypersensitivity to DNA replication stress (Matson et al., 2019). It is unclear if mimosine mediated cell cycle arrest would have a similar effect, there are no published reports measuring the efficiency of replication licensing in S phase following mimosine arrest. It is unlikely that the synchronisation method used would have this effect on DNA fork rate, as both methods (Mimosine/Contact inhibition + serum starvation) produced the similar fork rates compared to cell-based experiments.

The effect that was observed in this report could be similar to what is observed when generating the minimal toolkit required to promote DNA replication *in vitro*. In these experiments the minimum proteins required for DNA replication were generated. Nascent DNA could be synthesised simply using a mixture of eukaryotic proteins from yeast. Replication could be achieved with a minimum of 16 replication factors including replication licensing, replication initiation and DNA polymerase proteins (Yeeles et al., 2015). However, this minimal toolkit achieved replication but at a lower than *in vivo* replication rate. Further replication factors were required to be added to achieve optimal replication rates. These included mrc1, Csm3/Tof1, PCNA and DNA Pol δ . As these replication factors were added replication fork rates steadily increased to optimal levels (Yeeles et al., 2017). This is strikingly similar to the effect of adding CIZ1 to G1 extracts containing Cyclin A/CDK2. Perhaps, CIZ1 promotes optimal DNA replication through co-ordination of CDK signalling. In a cancer context. This may provide a growth advantage to cells with deranged CDK networks.

These methods were used to identify yeast origin dynamics showing that yeast leading strand occurs adjacent to the origin, originating from a lagging strand primer (removing the need to prime leading strand synthesis) then replicating through the origin (Aria & Yeeles, 2019). These effects were observed using yeast proteins on yeast DNA, it would be difficult to incorporate CIZ1 in these experiments as there is no Yeast CIZ1 homolog. The minimal

toolkit for mammalian DNA replication would have to be identified to utilize CIZ1 in this type of experiment, a significant challenge. Future experiments should use *in vitro* techniques from this report to establish other factors required for optimal DNA replication in a G1 extract.

Perhaps, the reduced fork rate observed in the *in vitro* experiments in this report, and earlier reports is due to a similar effect. CIZ1 can increase the fork rate (in the presence of Cyclin A-CDK2). From this result there are 2 major possibilities. 1: CIZ1 is a replication factor lacking from G1 extracts that is required to achieve efficient replication *in vitro*. 2: If the effect observed here is not similar to the effect from Yeeles et al. (2017), then CIZ1 actively promotes DNA replication fork rate increase (to S phase like levels) in the presence of Cyclin A/CDK2. Both implicate CIZ1 strongly in the link between CDK signalling and replication initiation and could explain how deregulation of CIZ1 can lead to deregulation of replication initiation.

Experiments in this Chapter showed that CIZ1 can promote more optimal replication kinetics when added in conjunction with Cyclin A-CDK2. This implies that CIZ1 may play a role at the replication fork. Future experiments should aim to identify the role of CIZ1 in the replisome. Previous studies have demonstrated that CIZ1 co-localizes to both nascent DNA and replication factor PCNA (Coverley et al., 2005). However how CDK activity effects this is unclear. Using iPOND techniques to identify replisome proteins could shed light on the role CIZ1 plays in DNA replication, and identify any post translational modifications on CIZ1 (Dungrawala & Cortez, 2016).

This chapter has built on data from Chapter 4, in that chapter CIZ1 KO caused altered cell cycle re-entry kinetics that were accompanied by altered Cyclin accumulation. This chapter has demonstrated that CIZ1 KO alters how post quiescent nuclei respond to CDK signalling. Additionally, data in this Chapter highlighted that CIZ1 KO nuclei may have an altered

replication programme to WT nuclei. Next, the tumour suppressor function of CIZ1 can be assessed using CIZ1 KO cell lines to evaluate DNA replication stress *in vivo*. DNA combing will be used to determine the effects of CIZ1 KO on DNA replication kinetics that could underpin its dual role as a tumour suppressor and potential oncogene.

Chapter 6

Analysis of DNA Replication Kinetics in CIZ1 KO by DNA Combing

6.1. Introduction

CIZ1 has been implicated to have both a tumour suppressor (Nishibe et al., 2013), and oncogenic activity (Chen et al., 2019; Higgins et al., 2012; Wang et al., 2014; Yu et al., 2014). Increased CIZ1 expression promotes tumour growth and tumorigenicity in lung, colon, prostate, breast and bladder cancers (Chen et al., 2019; Higgins et al., 2012; Wang et al., 2014; Yu et al., 2014; Den Hollander 2006). However, in CIZ1 knock out mice, there is an increased sensitivity to DNA damage, and these mice develop lymphoproliferative disorders (Nishibe et al., 2013; Ridings-Figueroa et al., 2017). As yet, there are no mechanisms that could explain both phenotypes. CIZ1 is proposed to influence the epigenetic landscape and contribute to mechanisms that control DNA replication initiation. In addition, CIZ1 has also been implicated in regulation of transcriptional responses in oestrogen responsive (Den Hollander 2006) and YAP/TAZ regulated genes (Lei et al., 2016). Defects in epigenetics, transcription and DNA replication regulation are all associated with DNA replication stress (DRS). This phenomenon could potentially provide a mechanism for the tumorigenic transformation of cells with deregulated CIZ1 levels.

Oncogene activation or inactivation of tumour suppressors promote DRS, which is characterised by reduced DNA replication forks rates and fork stalling during S phase (Gailard et al., 2015). Prolonged DNA replication stress results in genome instability, a traditional cancer hallmark (Hanahan & Weinberg, 2000). Replication stress itself has been proposed as an additional hallmark of cancer (Macheret & Halazonetis, 2015). Other sources of replication stress include bulky DNA lesions introduced by UV irradiation, collisions with the transcription machinery, and premature S phase entry (Ahuja et al., 2016; Gottipati et al., 2008; Yajima et al., 2009). Importantly, premature S phase entry was observed in CIZ1 null cells re-entering the cell cycle (Chapter 4), and this may be a cause of DRS in CIZ1 null mice.

Stalling or slowing replication forks introduces a disparity between the rate that DNA polymerases and DNA helicases progress along DNA, this unwinding of DNA exposes long stretches of single stranded DNA (ssDNA) (Byun et al., 2005). This decoupling primarily occurs on leading strand synthesis upon the stalling of DNA pol δ or DNA pol ϵ (Taylor & Yeeles, 2019). RPA binds to and stabilises exposed ssDNA and accumulation of RPA can activate the DNA damage response (DDR). Prolonged accumulation of RPA results in activation of p53, halting of the cell cycle, and cells are either repaired, enter senescence, or in cases of serious damage become apoptotic (Maréchal & Zou, 2015). In most cases activation of the DDR and halting of the cell cycle acts as a tumorigenesis barrier (Priour & Peeper, 2008). Suppression of RPA in ATR deficient cells results in increased rates of replication fork stalling (Toledo et al., 2013).

In cases of severe replication stress, replication forks stall because of collision with bulky DNA damage (UV), or the transcription machinery (Gottipati et al., 2008). In this situation, cells usually restart replication forks through activation of the ATR and Chk1 pathway (Mazouzi et al., 2014). If cells are deficient in this pathway it can lead to replication fork collapse, where proteins dissociate from the DNA and DSB can occur which if not repaired can lead to under replicated DNA and chromosome abnormalities following mitosis (Burrell et al., 2013; Gaillard et al., 2015). Secondly, collision with transcription machinery induces replication stress. Collisions with DNA:RNA hybrid loops induce replication fork stalling, occurring primarily in highly transcriptionally active common fragile sites (Kotsantis et al., 2018). Head on collisions are resolved less easily than co-directional collisions. DNA damage induced by transcriptional machinery has been recorded across all domains of life (Gómez-González et al., 2019). Transcription is upregulated in cancer cells, due to the requirements of accelerated cell growth, further exacerbating this increase in genomic instability. As such, inhibition of transcription has been proposed as a novel way to treat cancers (Laham-Karam et al., 2020). Clinical trials demonstrated in humans (phase 1) that treatment with CX-5461,

an RNA Polymerase I Transcription Inhibitor, had some anticancer effect, although strong side effects (Khot et al., 2019). Nevertheless, this validates targeting these pathways in cancer

Additionally, DNA methylation is linked to replication stress (Prado & Aguilera, 2005).

Recently it was demonstrated that methylation of DNA in active transcription zones slows DNA replication to prevent collisions between replication and transcription machinery (Chong et al., 2018). This could be of particular interest here, as CIZ1 has been shown to play a role in X chromosome activation through colocalization with Xist RNA (Ridings-Figueroa et al., 2017; Sunwoo et al., 2017).

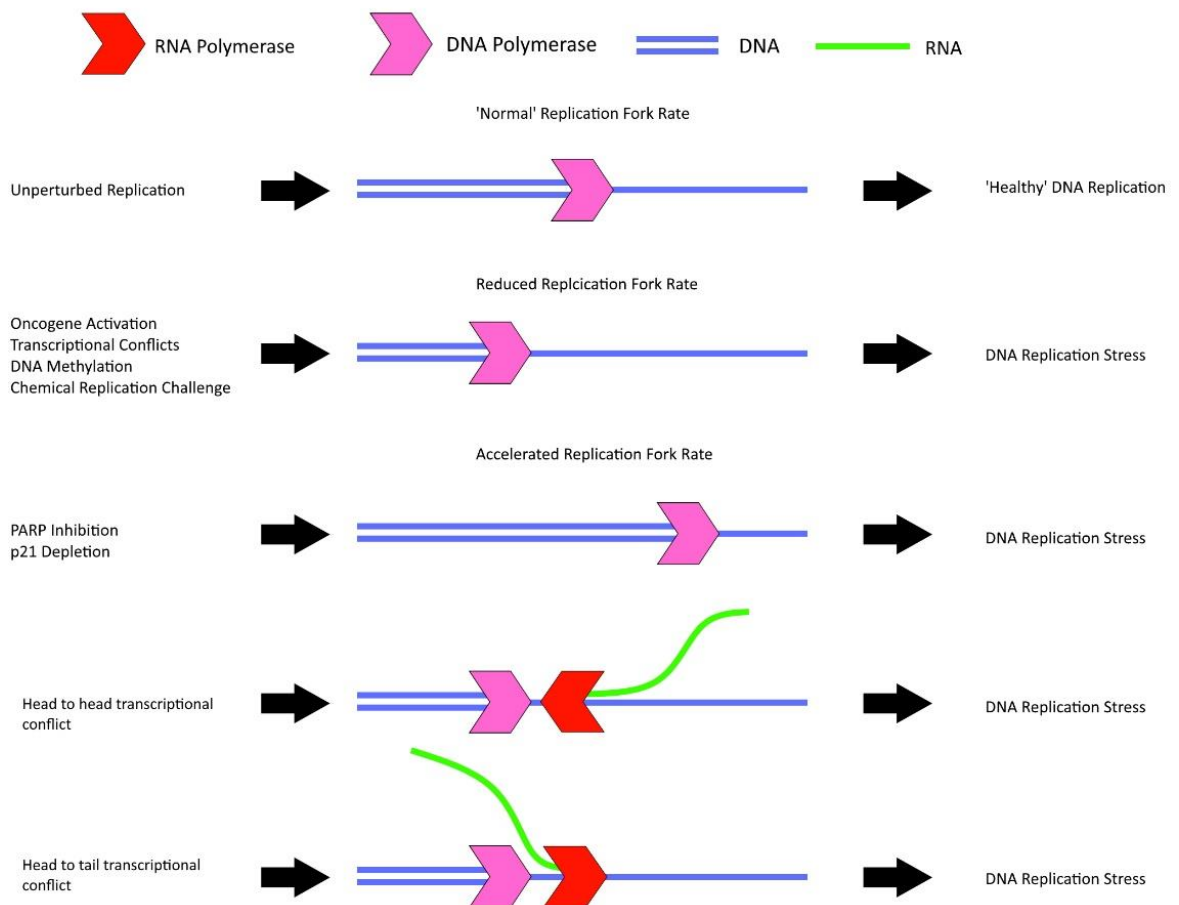


Figure 6.1 - Sources of DNA Replication Stress Replication stress can be induced through changes in DNA replication dynamics, and transcriptional collisions. These changes can be resolved by either the slowing or stalling of DNA replication forks. The factors that induces these changes are briefly summarised in this Figure. Oncogene Activation, and changes in DNA methylation often induce a shortening of fork rate. PARPi and p21 can result in a fork rate acceleration replication stress phenotype. Head on, and head to tail collisions between replication and transcription machinery results in fork stalling and DNA replication stress.

6.1.2 Aims

This chapter will use the tools developed here to investigate the role of CIZ1 in establishing DNA replication kinetics in parental and CIZ1 KO cell lines. In addition, the CIZ^{AB} cell line will be used to investigate if effects are reversible through genetic add back. In addition, the effect of increased DRS using hydroxyurea will be determined in parental, CIZ1 KO and CIZ1^{AB} cell lines. In this chapter DNA combing is used to:

- Observe changes in DNA replication kinetics in CIZ1 null cells
- Evaluate the changes in response to HU at the single replication event level
- Assess how observed changes can be linked to the tumour suppressor function of CIZ1

6.2. Results

6.2.1. Using DNA Combing to Measure Changes in DNA Replication Dynamics.

Data from this report suggests that aberrant CIZ1 expression could induce replication stress via perturbations in the activating threshold of CDK activity required to initiate DNA replication. Deregulation of CDK activity by over-expression of cyclin D, or E can reduce G1 length and promote oncogenesis (Lange et al., 2010; Dong et al., 2018). This suggests that CIZ1 may contribute to genome stability through contributing to the mechanisms that control timely activation of replication origins.

In Chapter 5, the activating concentration of cyclin A-CDK2 to promote initiation of DNA replication was altered depending on the level of CIZ1 expression. In CIZ1 KO nuclei, 2-fold higher levels of cyclin A-CDK2 were required to promote initiation of DNA replication than in WT nuclei (Figure 5.6). In addition, cell free DNA replication assays with additional recombinant CIZ1, which may be consistent with CIZ1 overexpression in vivo, showed that cells could initiate DNA replication at both aberrantly high and low CDK levels. The CDK

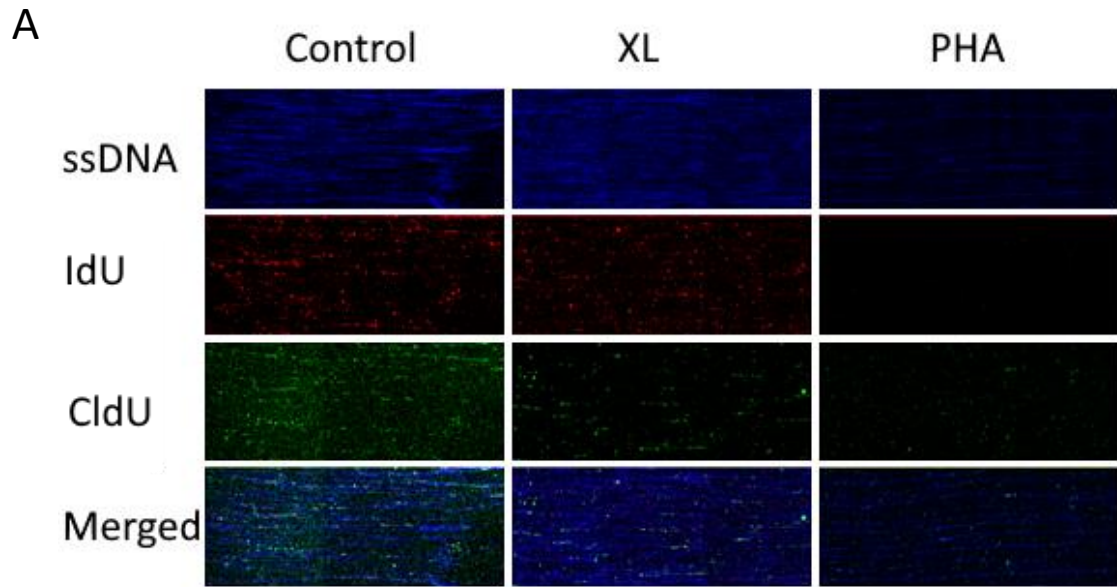
thresholds that regulate the G1/S transitions are precisely controlled and the data show that CIZ1 levels can influence the permissive CDK activity range at the G1/S transition.

Perturbations to CIZ1 levels may lead to replication stress, which promotes a mutator phenotype that underpins both the tumour suppressor and oncogenic effects observed in CIZ1 knockout cells and overexpressing cells.

Analysis of the timing of restriction point and the G1/S transition using parental WT, CIZ1 KO and CIZ1^{AB} cell lines (Chapter 4) demonstrated that CIZ1 deficiency can change the timing of the cell cycle, specifically in G1 phase. Following synchronisation and release from quiescence, CIZ1 KO cells entered S phase more rapidly than both WT and CIZ1^{AB} cells.

Additionally, in CIZ1 KO cells loss of CIZ1 changed the timing at which cells relied on the presence of exterior growth signals to enter the S phase. These experiments also revealed a defect in the DDR in response to agents that promote the stalling of DNA replication forks, characterised by prolonged H2AX phosphorylation. Together this data demonstrated that changes in CIZ1 levels caused changes to cell cycle control. It is not yet clear if this results in alterations in replication dynamics which could help to explain why CIZ1 is linked to cancer development.

First to ensure that changes in DNA replication dynamics could be measured using DNA combing CDK/DDK inhibitor drugs PHA-767491 (PHA) and XL-413 hydrochloride (XL) were used. Published reports on PHA and XL have demonstrated that they both inhibit Dbf4 dependent kinase (Dbf4-Cdc7, DDK) signalling through inhibition of CDC7 kinase. However, PHA has demonstrated off target signalling, specifically for CDK2 (Montagnoli et al., 2008) Due to the different off target effects for PHA and XL they inhibit entry into S phase by different mechanisms which effects DNA replication fork progression, this may result in a change in the effect on DNA replication dynamics. To measure the effects on DNA replication kinetics DNA combing was use. NIH 3T3 cells were treated with 10 μ M of PHA or 10 μ M of



75 μ m

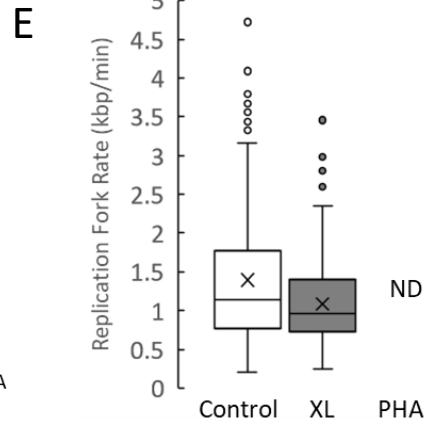
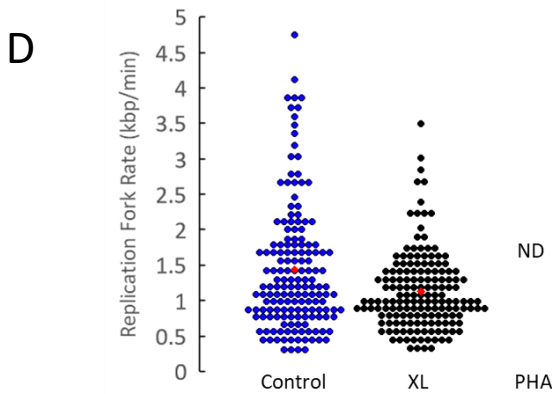
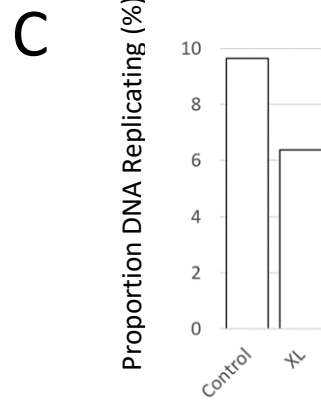
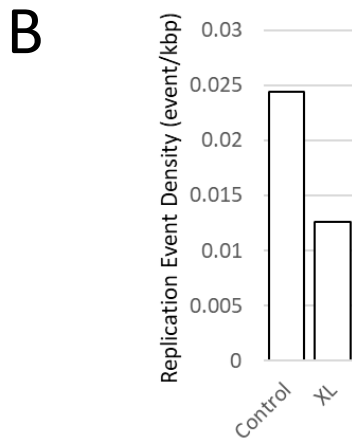


Figure 6.2. Replication dynamics of cell treated with CDC7 inhibitors PHA-767491 or XL-413. A) DNA combing analysis of DNA replication kinetics showing ssDNA (Blue), IdU (Green) and CldU (Red) B) Displays replication event density for untreated and XL-413 treated cells. C) Displays the proportion of DNA co-labelled with either IdU or CldU, this forms a measure of the proportion of total DNA replicating for untreated and XL-413 treated cells. D) Replication fork velocities for untreated (Blue) and XL-413 treated (Black) cells. Red spots show the median value for each dataset (N =150). E) Replication fork velocities for untreated (white) and XL-413 treated (grey) cells. Displaying the quartile values from the data. X represents the mean value. The mean fork rate of XL treated nuclei was significantly lower than control (T test $P < 0.001$, $n=150$ for each condition). ND references data that was not detected due to insufficient numbers of replication forks.

XL. Control cells were compared with DDK inhibitor treated cells after sequential pulse labelled with IdU and CldU (Chapter 3). Cells were harvested, combed and labelled for analysis by fluorescence microscopy. Parameters measured from imaged fibres were fork rate, replication density and the proportion of total measured DNA in S phase (Figure 6.2).

Cells that were treated with PHA displayed so few replication forks that it was not possible to acquire sufficient events to measure replication kinetics, due to potent inhibition of DNA replication. Comparison of control cells and XL413 treated cells revealed a significant difference in fork velocities for untreated cells and with median replication fork rates of 1.14 kbp/min and had a 0.96 kb/min, respectively (Figure 6.2D,E). The significant reduction in replication fork velocity in cells treated with XL 413 was accompanied by a reduction in replication event density by a factor of 2 (Figure 6.2B) identifying a reduction in the number of replication origins firing in the XL-413 treated cells. Additionally, a drop in the proportion of DNA replicating was observed, a reduction by $\sim 40\%$ after 24 hours treatment with XL-413 (Figure 6.2c).

Together, this data reveals that the DDK inhibitors, PHA-767491 and XL 413, cause 2 distinct phenotypes. PHA causes a complete block into S phase entry, this has been previously observed (Pauzaitė, 2019). Whereas, XL 413 reduces efficiency of replication origin activation and reduces replication fork efficiency during S phase. This indicates that XL 413 may have a more selective effect than PHA, potentially due to off target inhibition of CDK2 eliciting a more potent response. This result also demonstrates that XL-413 mediated inhibition of DDK signalling at the G1/S transition induces a replication stress like phenotype. This was characterised by a global reduction in the amount of DNA being replicated caused by a reduction in both replication fork rate and the number of replication origins that fired. This data has verified that the DNA combing technique optimised in Chapter 3 can be used to measure changes in replication kinetics.

6.2.2. CIZ1 KO Induces a DNA Replication Stress Phenotype

Cells under constitutive replication stress show a reduced replication fork rate, and decreased IOD due to activation of cryptic origin sites. To determine the effects of CIZ1 KO on DNA replication kinetics, CIZ1 KO1 and CIZ1 KO2 cell lines were compared to parental WT cells. Asynchronous cultures of WT NIH 3T3 cells, CIZ1 KO1 cells, and CIZ1 KO2 cells were sequentially pulse labelled (20 minutes) with IdU and CldU, cellular DNA harvested, combed and imaged

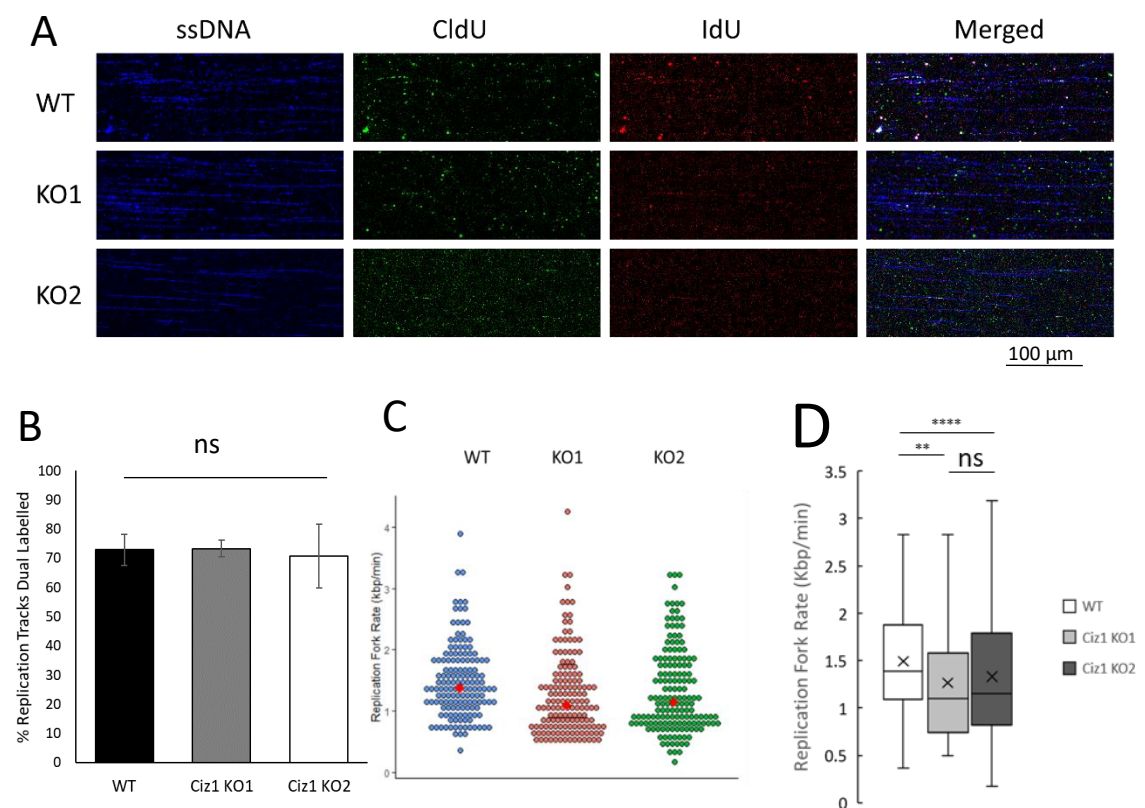


Figure 6.3-Replication dynamics of parental WT NIH 3T3 and CIZ1 KO Cells Cells were labelled for DNA combing analysis by sequential 20 minutes IdU and CldU labelling. A) Representative DNA combing tracks B) Bar chart of WT and CIZ1 KO cell lines displaying mean percentage of dual labelled tracks for WT, KO1 and KO2 cell lines ($n = 150$). C) Swarm plot showing replication fork velocities for WT, KO1 and KO2 cell lines. The red dot represents the median of each dataset. ($N = 150$), no significant differences were observed across cell lines (One Way ANOVA, $P > 0.05$). D) Box and whisker plots showing the distribution of replication fork velocities for WT, and CIZ1 KO cell lines. Cross represents the mean value. Significant differences are indicated by significance bars. There was a significant difference in fork rates across cell lines (One Way ANOVA, $P < 0.001$, $N = 150$). Pairwise comparisons were conducted by Tukey's HSD test, significance is indicated on the graph: ns = $p > 0.05$ * = $p < 0.05$, ** = $p < 0.01$, *** = $p < 0.001$, **** = $p < 0.0001$ C

Firstly, the proportion of dual labelled replication tracks was calculated. Changes in the number of dual labelled tracks could indicate increased fork stalling, origin firing, and termination events. There were no significant differences in the mean proportion of dual labelled replication tracks from Wild type parental cell line (WT), and 2 independent CIZ1 clones CIZ1 KO1 and KO2.

Next dual labelled replication tracks were selected and lengths of the second track (CldU) were measured to determine fork progression rates and single track kinetics displayed in swarm plots and box and whisker charts. For WT cells the median velocity was 1.4 kb/min, this value is comparable to published rates from NIH 3T3 cells (between 1.25 – 1.5 kbp/min) (Bhaskara et al., 2013). This indicates that WT cells are efficiently progressing through S phase. Both KO cells displayed decreased replication fork velocities at approximately 1.1 kb/min. Significant differences were observed between the mean rates across the 3 samples, specifically between the WT and KO cell lines. There was no significant difference between the two KO cell lines. This observation suggests that CIZ1 KO is responsible for the reduction in fork rate, as the KO cell lines used independent PAM sites within the CIZ1 sequence. This data suggests that CIZ1 KO alters the DNA replication programme, reducing fork velocities consistent with DNA replication stress.

6.2.3. CIZ1^{AB} reverses the DNA replication stress phenotype observed in CIZ1 KO Cells.

Changes in replication fork dynamics were observed between WT and CIZ1 KO cells. To evaluate the reversibility of the DRS in CIZ1 KO cell lines, replication fork dynamics were monitored using DNA combing (Figure 6.3). WT cells, CIZ1 KO1 and CIZ1^{AB} cells were grown to 80 % density, treated sequentially for 20 minutes with IdU, and CldU. Cells were harvested, DNA was purified, combed, labelled and imaged (Figure 6.4).

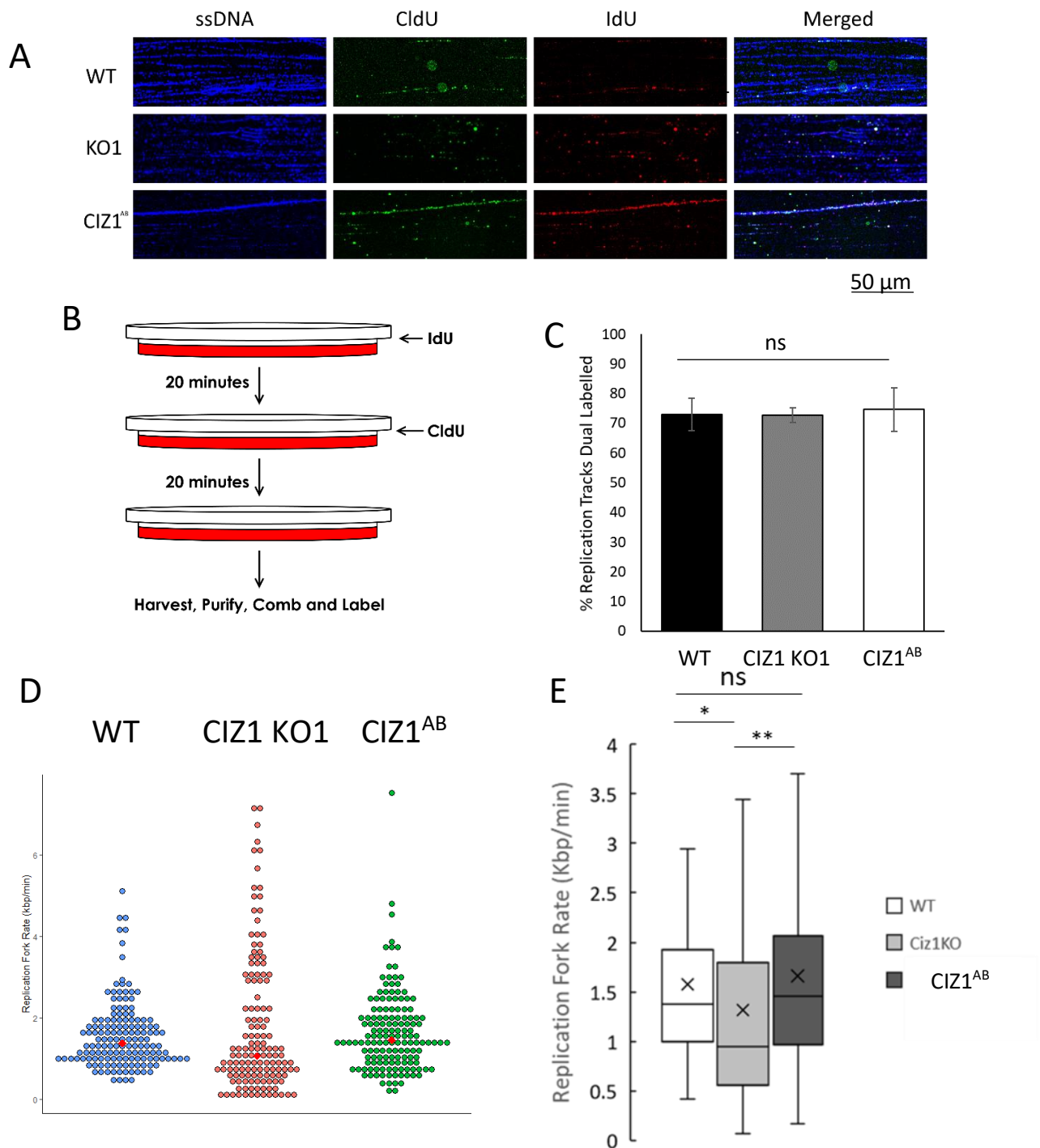


Figure 6.4. CIZ1^{AB} reverses the DRS phenotype in CIZ1KO cells Cells were labelled for DNA combing analysis by sequential 20 minutes IdU and CldU labelling. A) Displays a representative image of combed DNA from each of the samples. B) Displays a Graphical schematic of the experimental design. C) displays the mean proportion of each cell that is dual labelled ($n = 150$), no significant differences were observed across cell lines (One Way ANOVA, $P > 0.05$). D) Displays replication fork rate of each of the samples. Red dots represent the median value for each data set. E) Displays box and whisker charts displaying the distribution of fork rates for WT, CIZ1 KO1, and CIZ1^{AB} cell lines. The cross represents the mean for each data set. There was a significant difference in fork rates across cell lines (One Way ANOVA, $P < 0.01$, $N = 150$) Pairwise comparisons were conducted by Tukey's HSD test, significance is indicated of the graph: $ns = p > 0.05$, $* = p < 0.05$, $** = p < 0.01$, $*** = p < 0.001$, $**** = p < 0.0001$.

For WT cells, 76 % of counted replication tracks were dual labelled. CIZ1 KO1 cells and CIZ1^{AB} cells showed no significant differences relative to parental cell lines with 73% and 75% of scored replication forks dual labelled (Figure 6.4C). Together this data confirms consistent replication dynamics between experiments and between the cell lines.

The median replication fork velocity was 1.4 kbp/minute for WT cells, consistent with earlier data (1.4 kbp/min, Figure 6.3). In contrast, the median fork rate for CIZ1 KO cells was 1 kbp/min, consistent with earlier data for CIZ1 KO1 and 2 (1.1 kbp/min vs 1 kbp/min). Significantly, the reduced median fork progression rate was reversed in CIZ1^{AB} cells, which had a median replication fork velocity of 1.45 kbp/minute. A one way ANOVA revealed that there were significant differences between the means across the 3 cell lines. Critically, Tukey's HSD tests showed the difference in fork rate was statistically significant between WT and CIZ1 KO1 cells, and between KO1 and CIZ1^{AB}. However, the WT and CIZ1^{AB} fork rates were not significantly different. Together, these data demonstrated CIZ1 KO cells have reduced fork rates, an effect that can be rescued by CIZ1^{AB}, reversing the replication stress like phenotype observed in CIZ1 KO cells. These data suggest that CIZ1 contributes to mechanisms that prevent DNA replication stress and promote efficient DNA replication.

6.2.4. CIZ1 KO Results in Increased Origin Activation, consistent with DRS.

When cells are put under replication stress (e.g. chemically, or physically) the replication fork velocities slow. To compensate this reduced replication rate, cells activate 'cryptic origins' to ensure that DNA replication is completed within a suitable time frame (McIntosh & Blow, 2012). This is seen as a decrease in inter-origin distance (IOD), that is revealed by an increase in replication origin firing events per micrometre of DNA. To test if there are changes in origin activation in CIZ1 KO cells, the number of replication events were determined using EdU. The use of a single label allows 2 variables to be determined (i) the proportion of labelled DNA as a ratio with total DNA provides an estimate for the global amount of DNA

synthesis, and (ii) The number of replication events per micron provides an estimate of origin activation (Figure 6.5).

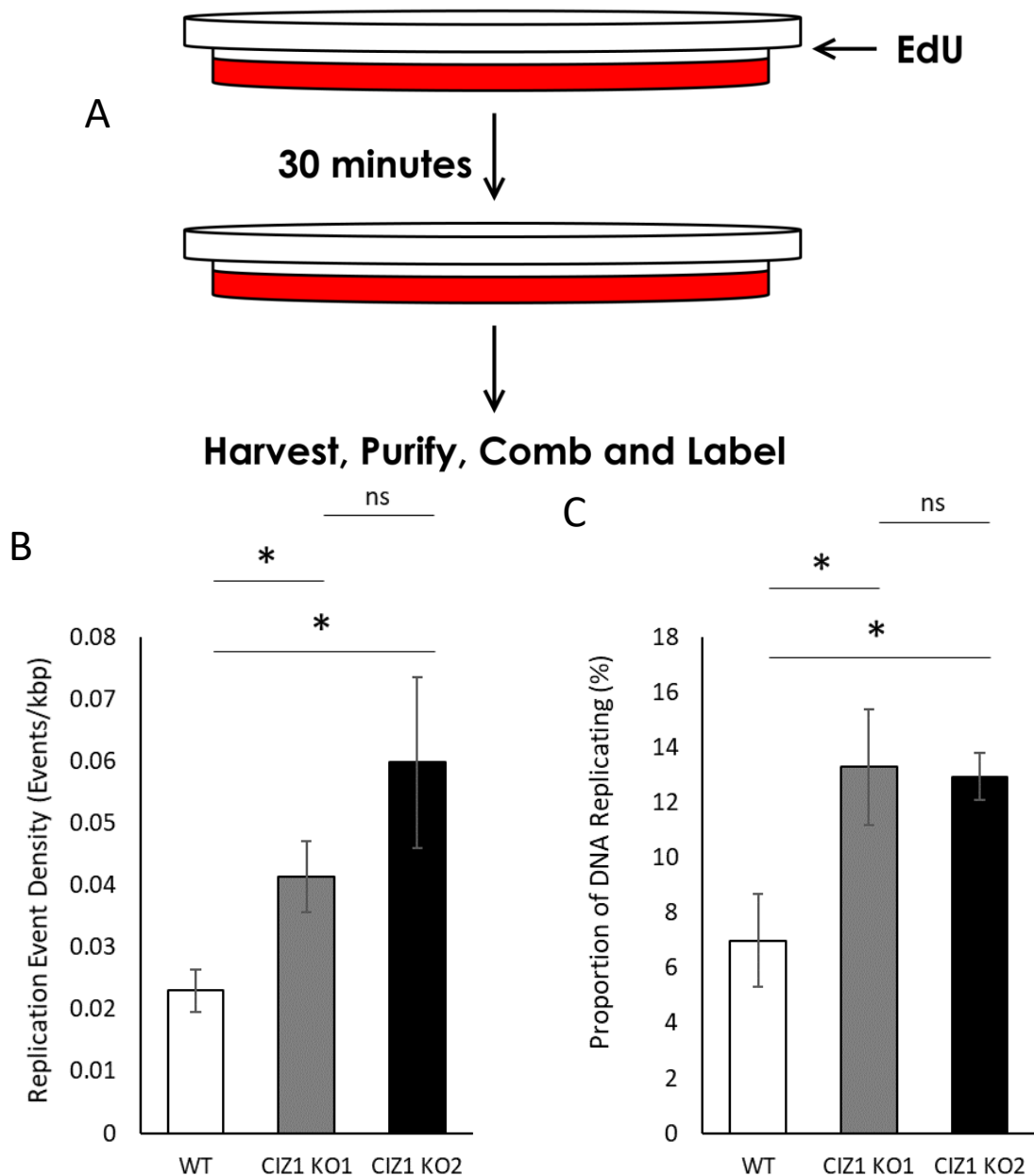


Figure 6.5. CIZ1 KO increases activation of cryptic replication origins A) A schematic of the experimental design. Cells were treated with EdU for 30 minutes before harvesting for DNA combing. B) Displays the replication event density (replication events per kbp DNA). There was a significant difference in replication density across cell lines (One Way ANOVA, $P < 0.01$, $N = 3$), Tukey's HSD test demonstrated KO1 and KO2 results were significantly different from WT cells (WT:KO1, $P < 0.05$, WT:KO2 $P < 0.01$) but KO1 and KO2 cells did not have significantly different replication densities ($p > 0.05$). C) Displays the proportion of DNA replicating (percentage of DNA positively labelled). There was a significant difference in proportion of replicating DNA across cell lines (One Way ANOVA, $P < 0.0001$, $N = 3$). Pairwise comparisons were conducted by Tukey's HSD test, significance is indicated of the graph: ns = $p > 0.05$ * = $p < 0.05$, ** = $p < 0.01$, *** = $p < 0.001$, **** = $p < 0.0001$.

WT NIH 3T3 cells have 0.023 events/kbp, which translated to one replication event every 43 kbp of DNA. For CIZ1 KO1 and CIZ1 KO2, there was a significant increase in replication events by a factor of 1.98 and 2.6 respectively relative to WT. The difference between KO1 and KO2 cells was not significant.

For WT NIH 3T3 cells, an average of 8 % of DNA was being replicated during the 30 minute EdU incubation, this was comparable to results observed in an enriched S phase nuclei population (Marheineke et al., 2005). For both CIZ1 KO cells an increase in the proportion of DNA that was being replicated during the 30 minute EdU incubation increased by a factor of 1.9 and 1.85 respectively compared to WT cells. A one way ANOVA revealed that there were significant differences between the means across the 3 cell lines. A Tukey's HSD post hoc test revealed that the averages were significantly different from WT cells. The average values for KO1 and KO2 cells was not significantly different. This indicated that upon loss of CIZ1 there is an increase in the proportion of DNA actively replicated, consistent with an increase in origin usage to compensate for reduced fork rate. This represents a further difference in the DNA replication programmed in NIH 3T3 cells upon genetic ablation of CIZ1. The data show that CIZ1 KO NIH 3T3 cells have an altered replication programme compared to WT NIH 3T3 cells, with increased origin firing, a higher percentage of DNA undergoing replication but with reduced replication fork velocity.

To determine if the activation of cryptic origins was as a consequence of CIZ1 KO, the origin density was determined for WT, CIZ1 KO1 and CIZ1^{AB} (Figure 6.6). A one way ANOVA revealed significant differences between the means across the three cell lines. CIZ1 KO cells displayed an increase in replication event density by a factor of 2.3 compared to WT cells. Importantly, this effect is reversed in CIZ1^{AB} cells, which displayed an increase by a factor of 1.1 compared to WT cells. The CIZ1 KO was significantly higher than WT cells, but not CIZ1^{AB}

cells ($P = 0.063$) suggesting ectopic CIZ1 addback could only partially rescue the CIZ1 KO phenotype.

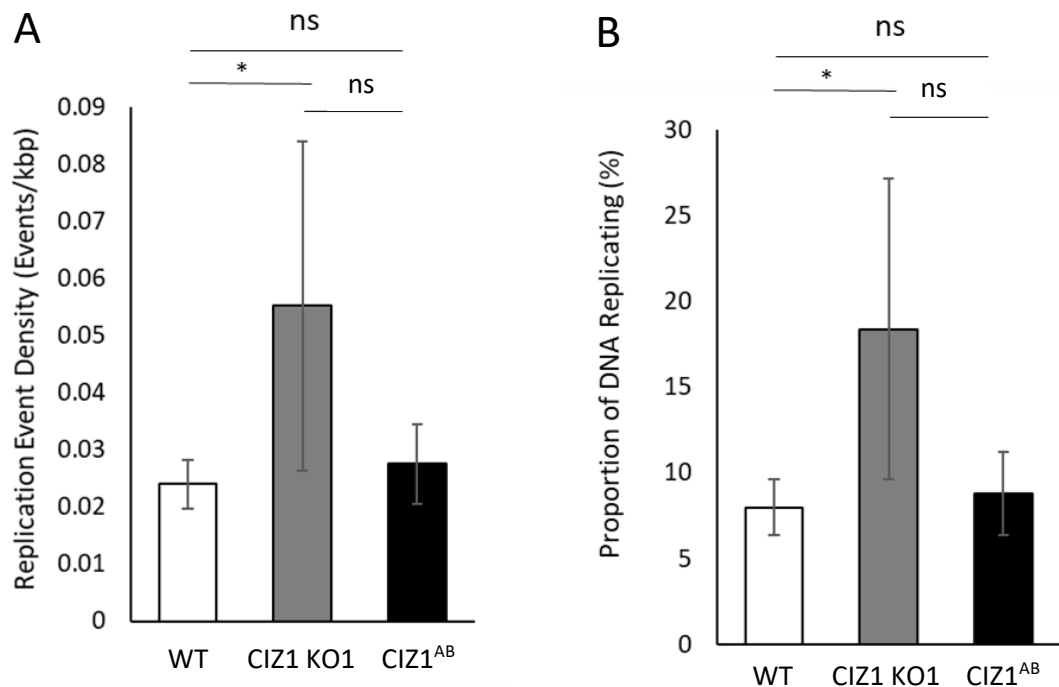


Figure 6.6. CIZ1^{AB} reverses the activation of cryptic replication origins in CIZ1 KO cells. A) Displays the replication event density (replication events per kbp) (showing mean \pm S.D.). There was a significant difference in replication density across cell lines (One Way ANOVA, $P < 0.01$, $N = 3$), Tukey's HSD test demonstrated WT replication densities were significantly different from KO1 cells ($P < 0.05$) but there were no significant differences between WT and CIZ1^{AB} ($p > 0.05$), or KO1 and CIZ1^{AB} cells ($P > 0.05$) B) Displays the proportion of DNA replicating (percentage of DNA positively labelled) (showing mean \pm S.D.). There was a significant difference in the proportion of replicating DNA across cell lines (One Way ANOVA, $P < 0.05$, $N = 3$). Pairwise comparisons were conducted by Tukey's HSD test, significance is indicated of the graph: ns = $p > 0.05$, * = $p < 0.05$, ** = $p < 0.01$, *** = $p < 0.001$, **** = $p < 0.0001$.

In addition, there is an increase in the percentage of nascent DNA in CIZ1 KO cells with respect to WT NIH 3T3 cells. A one way ANOVA revealed significant differences between the means across the three cell lines. For WT cell lines, an average of 8 % of DNA was undergoing DNA replication, compared to 18% for CIZ1 KO NIH 3T3 cells. In contrast, in CIZ1^{AB} cells showed similar level of nascent DNA compared to WT cells, to 8.8 %. There was no significant difference between CIZ1 KO and CIZ1^{AB} cell lines. This demonstrates that the increased origin

activation seen in CIZ1 KO cell lines is only partially reversed by genetic add back of CIZ1 (CIZ1^{AB}). Together these results indicate that CIZ1 KO induces DNA replication stress, and that this effect can be partially rescued by CIZ1^{AB}.

6.2.5. Evaluation of the role of CIZ1 in cellular responses to increased DRS.

In Chapter 4, experiments revealed that loss of CIZ1 altered the response to replication stress inducing agents HU. This was characterised by prolonged H2AX phosphorylation after HU treatment in CIZ1 KO cells relative to WT cells (Figure 4.10). However, the proportion of cells in S phase remained consistent between WT, CIZ1 KO and CIZ1^{AB} cell lines. As a difference in DDR was observed, the phosphorylation status of H2AX will be monitored to detect dsDNA breaks. In addition, DNA combing or DNA fibre analysis are commonly used tools to detect how cells change their response to replication stress or DNA damage.

Cells with chronic DNA replication stress often display increased sensitivity to agents that induce DRS and have defects in replication fork restart. Fork restart efficiency can be determined by sequential incubations in IdU, HU and then restart determined with a second incubation with CldU (Nieminuszczy et al., 2016). In this context, fork restart is efficiently determined by the presence of both labels. This contrasts with stalled forks that cannot efficiently restart and are labelled with IdU only. Similarly, origins that fire after HU treatment will be labelled solely with a CldU track. This allows discrimination of both events and aids their exclusion from analyses. Termination events during the 1st pulse labelling stage will also be labelled as a single IdU track, however these should form such a minority that they can be ignored.

To measure changes in fork restart rates upon loss of CIZ1: WT, KO1, KO2, and CIZ1^{AB} were labelled with IdU for 2 hours, treated with HU for 2 hours, then released from HU block into fresh media supplemented with CldU for 30 minutes and control cells were left in media supplemented with CldU and HU for 30 minutes (Figure 6.7).

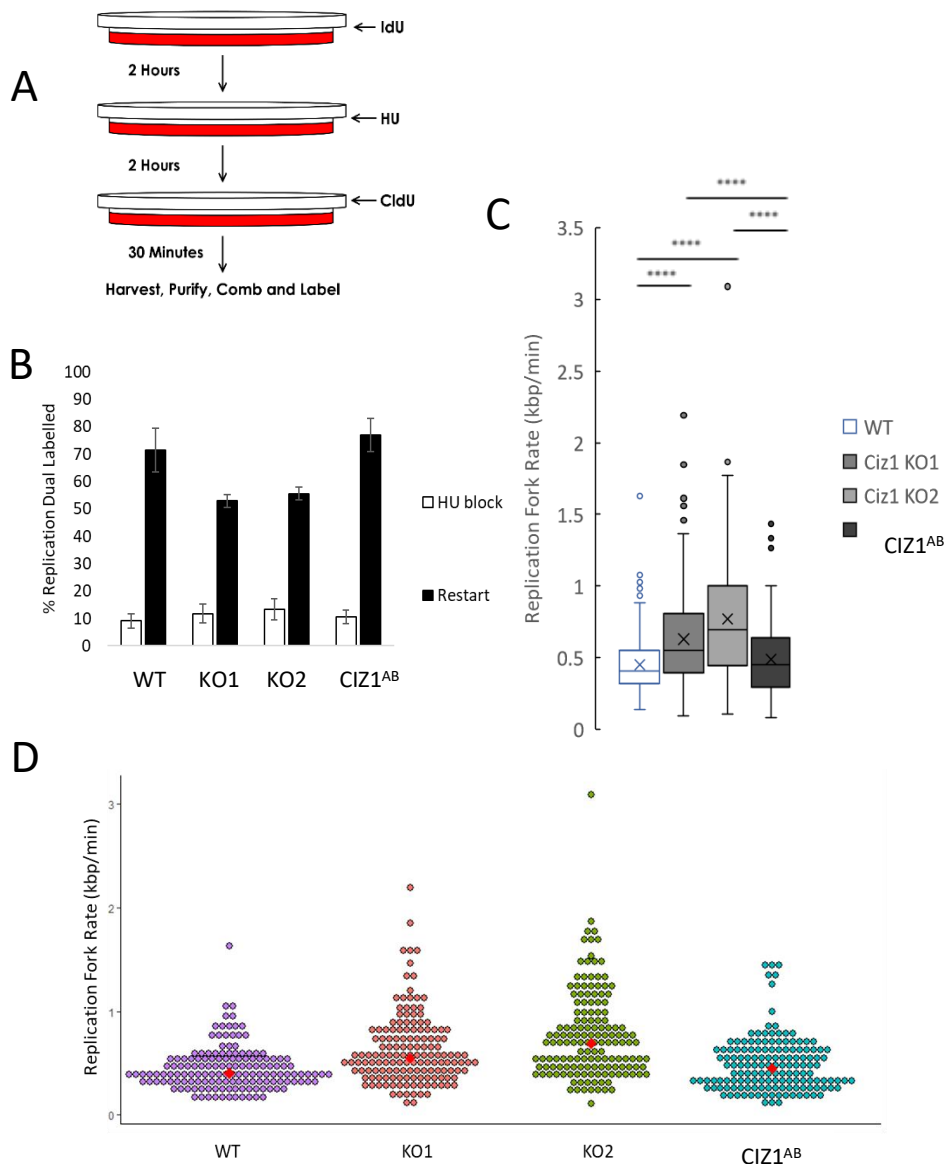


Figure 6.7. CIZ1 KO cells have impaired ability to restart forks after replication challenge with HU. WT, CIZ1 KO1, CIZ1 KO2, and CIZ1^{AB} were treated sequentially with IdU (2 hours, HU 2 hours, and CldU for 30 minutes, control cells were co-incubated with HU and CldU. A) Displays a schematic of the design of the experiment. B) displays the proportion of replication tracks labelled with both IdU and CldU for both the HU treated (black) and control (white) cells. This is a measure of fork restart efficiency. The proportion of replication forks dual labelled in each condition ($n = 3$) for each cell line was compared using a two-way ANOVA with treatment and cell line as factors (P (treatment) < 0.0001 , P (cell line) < 0.01 , P (interaction) < 0.01 . Pairwise comparisons were made by simple main effects analysis. No significant differences were observed for cells not released from HU ($p > 0.05$ for all comparisons). No significant differences were observed between WT/CIZ1^{AB} cells or KO1/KO2 cells released from HU ($P > 0.05$ for all comparisons). Significant differences were observed between either KO cell line and WT or CIZ1^{AB} cells ($p < 0.01$ for all comparisons.) C) Displays box and whisker charts showing the distribution of fork rates of restarted forks for experimental samples for each cell line. (WT: White, CIZ1 KO1: Dark grey, CIZ1 KO2: light grey, CIZ1^{AB}: Black). There was significant differences in rates of restarted fork rates across cell lines (One Way ANOVA, $P < 0.0001$, $n = 150$) Pairwise comparisons were conducted by Tukey's HSD test, significance is indicated of the graph: ns = $p > 0.05$, * = $p < 0.05$, ** = $p < 0.01$, *** = $p < 0.001$, **** = $p < 0.0001$. D) displays swarm plots of the fork rates of restarted forks for experimental cells ($n = 150$) (WT: Purple, CIZ1 KO1: red, CIZ1 KO2: green, CIZ1^{AB} blue). Red points highlight median values.

Firstly, WT cells in a HU block an average of 9 % of replication tracks were dual labelled. Similar results were observed in both KO cell lines with an average of 11% and 13 % for KO1 and KO2 respectively. Unsurprisingly, CIZ1^{AB} cells also displayed a low proportion of tracks dual labelled: 10.3 %. There were no significant differences between cell lines for controls. This indicated that H2AX phosphorylation efficiently stalled replication regardless of CIZ1 levels. For each cell line, a minority of replication forks were able to continue. This could be due to cell to cell variation in responses to hydroxyurea.

However, significant differences were observed in the proportion of replication forks that were able to restart after HU challenge. In WT cells, released from the HU block, an average of 72 % of replication tracks were dual labelled, an increase of 61 % from controls. For the CIZ1 KO1 and KO2 cell lines there was a reduction in fork restart with only 53% and 42% dual labelled respectively (Figure 6.7C). The reduced capacity to restart DNA replication after HU treatment was reversed in CIZ1^{AB} cells, that showed an average of 77 % of dual labelled replication tracks. Critically, the proportion of forks that restarted for WT and CIZ1^{AB} cells were both significantly different from both CIZ1 KO cell lines. The proportion of restarted forks was not significantly different when comparing WT and CIZ1^{AB} or KO1 and KO2 cell lines.

Interestingly, for WT and CIZ1^{AB} cell lines, the proportion of dual labelled restarted forks was comparable to untreated cells where 69 % and 70 % of replication forks were dual labelled for WT and CIZ1^{AB} cells respectively (Figure 6.4). This indicates that recovery from HU challenge in these cells was a result of restarting stalled forks, rather than an increase in replication origin firing from dormant origins. For CIZ1 KO cell lines a decrease in the proportion of dual labelled fork was observed, compared to untreated cells (Figure 6.4). This indicates that CIZ1 null cells may be deficient in restarting forks in response to HU challenge and did not compensate by firing dormant origins. This data coupled with data from 4.10

indicated that loss of CIZ1 promotes a deficient recovery from HU mediated replication stress.

All cell lines showed reduced fork rates after HU treatment compared to unchallenged cells (Figure 6.7D, E and Figures 6.3/6.4). A one way ANOVA revealed significant differences between the means across the 4 cell lines. Both CIZ1 KO cell lines showed an increased fork rate after withdrawal of HU compared to WT and CIZ1^{AB} cells. For WT cells, the median replication fork velocity was 0.4 kbp/min after release from HU. CIZ1 KO1 cells displayed a median replication fork velocity of 0.55 kbp/min and KO2 cells showed a median replication fork rate of 0.7 kb/min. The fork rates were significantly higher than WT. Comparison with unperturbed fork rates in KO1 and KO2 cells showed an approximate 2-fold reduction, lower than the observed drop in WT cells. This increase in median fork rate for CIZ1 KO1 cells was reversed in CIZ1^{AB} cells. The median fork rate of the restarted replication forks in CIZ1^{AB} cells was 0.45 kbp/min. This was lower than unstalled forks in CIZ1^{AB} cells by a factor of 3 (Figure 6.4). This dataset was not significantly different from rates of restarted forks observed in WT cells. However, this data was significantly different from restarted fork rates for both KO1 and KO2 cells lines.

Together these results indicate that CIZ1 may contribute to mechanisms that regulate fork restart following DRS induced by a HU block. This manifests as an observed higher replication fork rate in CIZ1 KO cell lines relative to WT and CIZ1^{AB} cell lines. This could be due to either faster fork rates, or a more rapid restart after release from the HU replication challenge. The increase in fork rate observed may be compensation for the reduced proportion of restarted forks that was observed. This could be linked to the phenotype observed in Chapter 4, in which a delayed H2AX activation was observed that resulted in a prolonged response 24 hours after treatment. Perhaps, an inefficient response to HU results in an accumulation of

damage that results in the prolonged H2AX activation. This change in response at the DNA has implications for the fidelity of DNA replication following replication challenge.

6.2.6 CIZ1 KO cell lines show defective origin activation 24 Hours after HU Treatment.

Analysis of DNA replication kinetics after an acute period after HU treatment revealed evidence of defects around fork restart in CIZ1 KO cells. Previously, CIZ1 KO cells displayed prolonged H2AX gamma phosphorylation 24 hours post release from HU block, where WT cells did not. However, there was no significant difference in the proportion of cells in S-phase at the 24 hour time point in WT, CIZ1 KO and CIZ1^{AB} cells. To investigate if there is a difference in fork rates after HU treatment after 24 hours DNA combing was used. WT, CIZ1 KO1, and CIZ1^{AB} cells were each treated for 2 hours with 2 mM HU and released for 24 hours. Fork rates were determined as well as the proportion of replication forks that were dual labelled (Figure 6.8).

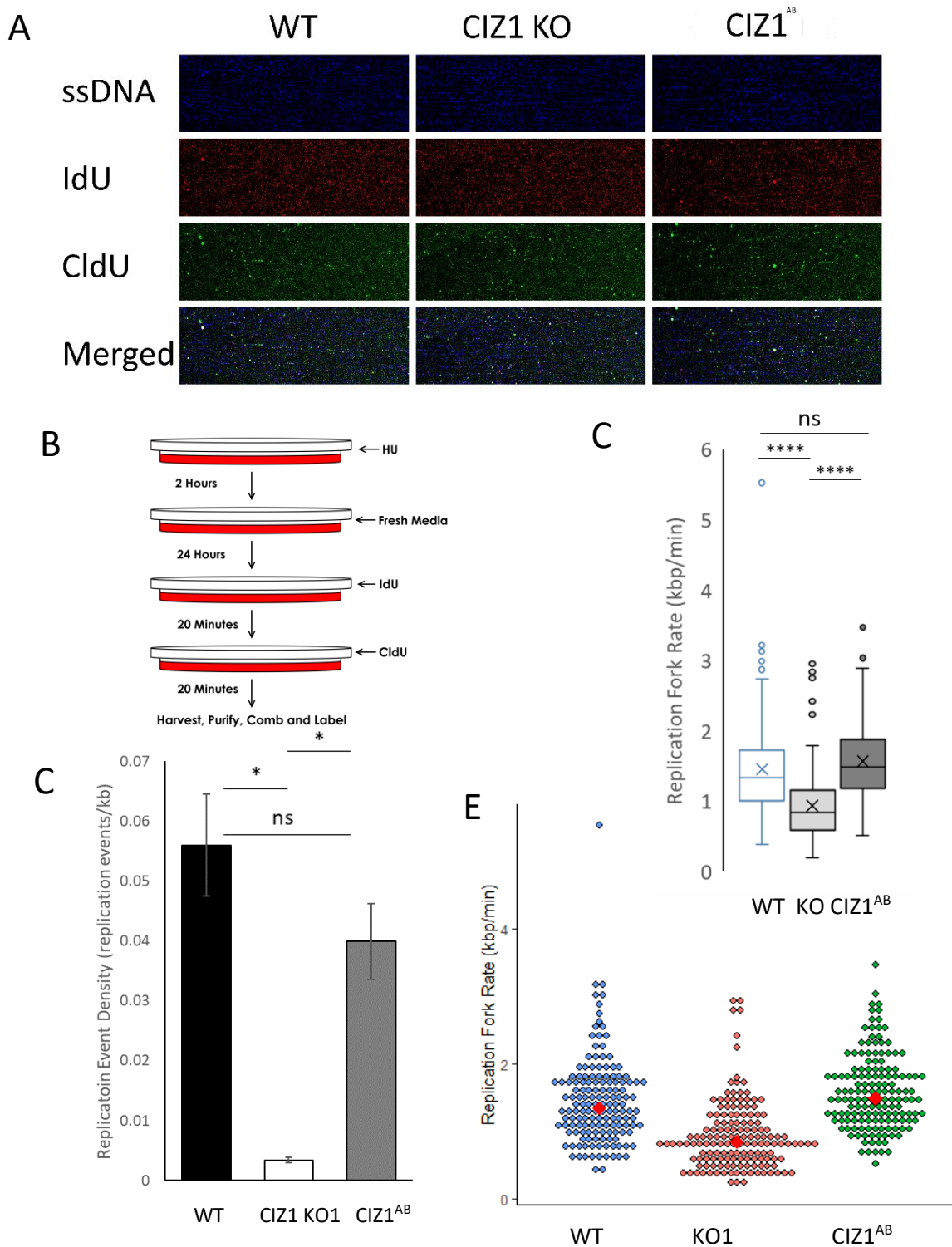


Figure 6.8 Measuring Replication Dynamics 24 hours after HU Mediated Replication Stress. A) Representative images of combed fibres displaying ssDNA (Blue), IdU (Red), CldU (Green). B) A schematic of the design of the experiment. C) Replication Event densities of the three cell lines used. Calculated by measuring replication events (non-contiguous replication tracks) as a proportion of total length of DNA measured. There were significant differences in replication density across cell lines (One Way ANOVA, $P < 0.05$). Pairwise comparisons were conducted by Tukey's HSD test, significance is indicated of the graph: ns = $p > 0.05$, * = $p < 0.05$, ** = $p < 0.01$, *** = $p < 0.001$, **** = $p < 0.0001$. D) Box and whisker chart showing the distribution of fork rates for each cell line: WT (White), CIZ1 KO1 (Light grey), CIZ1^{AB} (Dark Grey). The cross represents the mean value. There were significant differences in fork rate across cell lines (One Way ANOVA, $P < 0.0001$, $n = 150$). Pairwise comparisons were conducted by Tukey's HSD test, significance is indicated of the graph: ns = $p > 0.05$, * = $p < 0.05$, ** = $p < 0.01$, *** = $p < 0.001$, **** = $p < 0.0001$. E) Swarm plots displaying the replication fork rates for each cell line: WT (Blue), CIZ1 KO1 (Red), and CIZ1^{AB} (Green). Red point represents the median for each data set. ($N = 150$)

In contrast to DNA replication rates 2 hours after release from HU (Figure 6.7), median fork progression rates for WT and CIZ1^{AB} were consistent with unperturbed rates (Figure 6.4). WT cells displayed an average replication fork rate of 1.5 kbp/min, and CIZ1^{AB} cells 1.6 kbp/min consistent with fork rates in unperturbed cells (Figure 6.3/6.4). CIZ1 KO cells had a median fork rate of 0.9 kb/min, lower than in unperturbed CIZ1 KO cells (Figure 6.3/6.4). This suggested after increased DRS CIZ1 KO developed increased DRS. A one way ANOVA revealed significant differences across the means for the 3 cell lines. Importantly, the mean fork rates for WT and CIZ1 KO were significantly different, an effect that was reversed in CIZ1^{AB} cells (Figure 6.8 D,E).

When comparing replication fork density, a measure of the origin activation, there is a significant difference in replication origin usage. A one way ANOVA revealed significant differences between the means across the 3 cell lines. Parental WT cells have more active DNA replication origins per kb of DNA and this is reduced in CIZ1 KO cells (0.05 and 0.002 origins/kb DNA) consistent with a reduction in origin firing in CIZ1 KO cells. This effect is mostly reversed in CIZ1^{AB} cells (0.04 origins/kb) suggesting that expression of CIZ1 is required for efficient origin activation after increased DRS. CIZ1 KO replication density was significantly different from both WT, and CIZ1^{AB} cells; whereas, mean values for WT and CIZ1^{AB} samples were not significantly different from each other (Figure 6.8 C). This indicated ectopic CIZ1 could rescue the DRS phenotype.

This effect is distinct from the typical response to origin activation, where cryptic origins are activated to ensure timely completion of S-phase and the precise mechanism that underpins this response has yet to be identified. However, this experiment revealed that after 24 hours release from a HU mediated replication block CIZ1 KO1 cells display a significantly lower fork progression rate and a reduction in origin activation than untreated WT and CIZ1^{AB} cells. This data shows that CIZ1 KO cells have a reduced ability to recover from a HU mediated

replication block, compared to WT cells, and this can be rescued by the genetic addback of GFP-CIZ1.

6.3. Chapter Discussion

Together, data from this chapter has linked CIZ1 function and regulation of DNA replication dynamics. Loss of CIZ1 induces a change in replication dynamics that is consistent with DNA replication stress. Together with data from previous chapters, this has demonstrated the link between CIZ1 levels and replication fidelity. In addition, the data demonstrates that the loss of CIZ1 results in a DRS phenotype and a hypersensitivity to further replication stress such as HU treatments. Taken together the data suggest that CIZ1 potentially plays a tumour suppressor role by acting to regulate fork dynamics and reduce potential for DRS. These observations will be discussed with implications for the potential mechanisms that promote genetic instability and tumour formation in the absence of CIZ1.

6.3.1. CIZ1 Null cells undergo DRS and have increased sensitivity to DRS inducing agents

Comparison of WT and CIZ1 KO cell lines has revealed that CIZ1 cells have a DRS phenotype. Typically, replication stress results in an increased origin activation and decreased replication fork. (Zhong et al., 2013). CIZ1 KO cell lines show typical DRS characteristics with a drop in DNA replication fork rates (Figure 6.3) and an increase in active replication origins (Figure 6.5). This result was consistent with synchronised nuclei in *in vitro* DNA replication assays (Chapter 5.4.). The results presented in this chapter demonstrated that loss of CIZ1 results in an impaired DDR, both in regards to replication fork restart (fewer forks restarted 2 hours after HU treatment), and replication kinetics 24 hours after exposure to the DNA replication stress agent HU (Fork progression was impaired 24 hours after HU exclusively in CIZ1 null cells). Erosion of an effective DDR coupled with induction of replication stress may help provide CIZ1 null cells the ability to bypass the tumourigenesis barrier.

In CIZ1 KO cells, when cells were further stressed by HU treatment a reduction in both fork velocity and origin usage was observed (Figure 6.8). A similar phenotype is observed upon MCM depletion, reduced origin firing and fork progression due to a reduced ability to fire dormant origins (Ge et al., 2007). These cells were unable to respond to increased damage as a result of HU treatment. A similar result was observed in pancreatic cancer cells treated with MEK inhibitor GSK212, this blocked both HR and NHEJ repair, these cells displayed delayed resolution of DSBs from radiotherapy resulting in a prolonged H2AX response. This was used to radio-sensitise the pancreatic cancer cells (Estrada-Bernal et al., 2015).

This could implicate a role for CIZ1 in the replisome during fork restart, and this is supported by results from Chapter 4 showing that CIZ1 KO cells experienced a sustained H2AX response after treatment with HU. If CIZ1 null cells are deficient in fork restart this may result in an inability to repair DNA introducing more complex damage resulting in a sustained DDR (Huang et al., 2020).

6.3.2 A potential model for the role of DRS in tumorigenesis in CIZ1 KO mice

Replication stress is crucially important at the early stages of tumorigenesis. Pre-cancerous and early tumour cells have stressed replication, resulting in incomplete or low fidelity replication. This erodes the stability of the genome, expediting the mismatches, and mutations. When these occur in key tumour suppressor and oncogenic genes pre-cancerous cells can become cancerous, or cancerous cells can become more aggressively proliferative (Macheret & Halazonetis, 2015).

Severe replication stress will result in the exposure of ssDNA promoting a DDR. ssDNA is protected by RPA coating, which activates ATR triggering the DDR. The DDR provides a 'tumorigenesis barrier' that functions in 2 ways. Firstly, the cell cycle can be stalled at the S phase checkpoint allowing resolution of stalled forks, DNA damage repair to allow S phase to reach completion before the cell divides at mitosis. After this stage, mutations will become

permanent and increase the likelihood of mutations within proto-oncogenes or tumour suppressors that underpin cancer development. Secondly, in cases of severe DNA damage or irretrievable DNA replication blockage the DDR can inhibit cell cycle progression and division, safeguarding from mutation (Turgeon et al., 2018). This can occur through committing the cell into an irreversible cell cycle exit known as senescence, a major barrier to tumorigenesis. The other option, in severe cases is apoptosis (Bartkova et al., 2006). Apoptosis is programmed safe cell death. This removes any dangerously damaged cells preventing mutations. If this barrier fails to function, mutation rate will increase, and cancer could develop (Childs et al., 2014).

Cancers have multiple mechanisms to bypass the tumorigenesis barrier. The most common method to bypass this barrier is to erode the S phase checkpoint by weakening the DDR. One of the most common mutations found in cancer is the 'guardian of the genome' p53 encoded for by gene TP53. p53 is the most frequently mutated gene in cancers (Shajani-Yi et al., 2018). p53 has a range of functions that allow it to function as a tumour suppressor, most inactivate the protein (Rivlin et al., 2011). Some mutations allow the p53 protein to gain an oncogenic function (Brosh & Rotter, 2009; Oren & Rotter, 2010).

The inactivation of CIZ1 promotes lymphoblastic tumours suggesting that it may function as a tumour suppressor (Nishibe et al., 2013). One model that could be constructed from data presented here is that loss of CIZ1 induces DNA replication stress that underpins tumour formation in CIZ1 null mice (Figure 6.9).

Changes in the DNA replication programme may cause constitutive replication stress and drive a mutator phenotype. A reduction in replication fork progression rate is typical with a replication stress phenotype. This suggests that cells with reduced CIZ1 are under a replication stress like phenotype. As CIZ1 is known to act as a tumour suppressor gene this could help explain that role (Nishibe et al., 2013). It is likely that increased CIZ1 expression

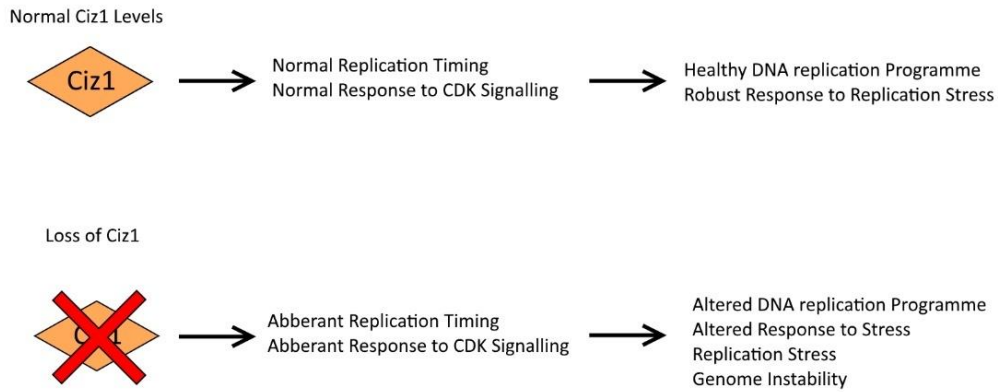


Figure 6.9 A Model for the Tumour Suppressor Function of CIZ1. Summary of phenotypes observed when Cells lose CIZ1, and how this could potentially lead to a mutator phenotype.

also causes a change in replication dynamics, which was observed in Chapter 5. This forms a model in which CIZ1 levels are required to be precisely controlled. Cell free DNA replication assays have revealed that modulation of CIZ1 levels can cause a change in response to cyclin/CDK networks and alter the kinase thresholds that regulate the initiation phase of DNA replication. In addition, DNA combing experiments have revealed that CIZ1 KO changes replication dynamics and responses to hydroxyurea induced replication stress.

Taken together the data demonstrated the importance of CIZ1 in maintaining genomic stability. The CIZ1 KO and CIZ1^{KI} cell lines have demonstrated that CIZ1 contributes to regulation of DNA replication fork rates, replication origin usage and fork restart following HU induced DRS. These observations support a role for CIZ1 at the replisome, where it maintains replication fork integrity. Significantly, the deletion of CIZ1 promotes DRS, and this perturbation to the DNA replication program is proposed to induce a mutator phenotype and underpin tumorigenesis.

Chapter 7.

General Discussion

7.1. Summary of Results

Through a combination of cell free DNA replication assays, cell cycle analysis and DNA combing, this work has demonstrated a role for CIZ1 in genome stability. CIZ1 null fibroblasts have identified key phenotypes, including a shortened G1 phase, an alteration in restriction point timing and sensitivity to growth signals present in serum following quiescence.

Intriguingly, these experiments also identified reduced Cyclin A chromatin loading, which has previously been found to be an important step in the initiation process (Copeland et al., 2010) could link to each observed phenotypic change.

Cell free replication assays demonstrated an interdependence between CIZ1 and Cyclin A/CDK2, where CIZ1 levels modulated the Cyclin A/CDK2 concentration that promoted initiation of DNA replication. In a G1 context, cyclin A recruitment to chromatin was reduced in CIZ1 KO cells and this effect was reversed by titration of increasing concentrations of exogenous CIZ1-N471. Significantly, the interdependence between CIZ1 and cyclin A-CDK2 activity was associated with a reduced fork rate and increase origin activation in CIZ1 KO cells, consistent with DRS. Importantly, the stoichiometry of CIZ1 and cyclin A-CDK2 appeared to be a crucial factor. Addition of CIZ1 with low cyclin A-CDK2 levels induced a DRS like effect on fork rate and origin usage, yet at optimal or high cyclin A-CDK2 levels, CIZ1 facilitated replication fork rates more typical of a complete S-phase extract. These results suggest that CIZ1 and cyclin A-CDK2 cooperate to ensure that fork progression is optimal, and that activation of replication origins is maintained at sufficient levels for duplication of the genome in a timely manner.

Consistent with data from cell free experiments, data generated using CIZ1 null fibroblasts displayed a DRS phenotype: reduced fork rate, and increased origin usage. This phenotype was specific to the loss of CIZ1, as two independent PAM sites were used and generated similar replication kinetics. In addition, this phenotype was rescued by ectopic expression of

GFP-CIZ1 (CIZ1^{AB}). Finally, results demonstrated that CIZ1 null cells display an aberrant DDR to HU, this was characterised by a delayed, and sustained H2AX response. At a cellular level no changes in fork stalling/restart rate were observed. However, DNA combing revealed that fork restart after removal of HU CIZ1 KO cells occurred at fewer forks, and that restarted replication forks proceeded more rapidly than in WT, and CIZ^{KI} cells. Yet at 24 hours after HU treatment, CIZ1 null cells had significantly slower replication forks, and reduced origin usage. This implied an inability to recover from heightened DRS. These data collectively support a role for CIZ1 in recovery from DRS, an effect that requires further mechanistic analysis.

Results presented in this report have not fully identified the role that CIZ1 plays during DNA replication initiation. However, the novel findings presented here have provided clues that can direct future research to answer these questions. As the majority of the results observed in this report have implications for genome stability, this Chapter will focus on findings in this report and previous studies identifying how results here can be explained and enrich previous work in that context. Additionally, proposals will be made to direct future research to elucidate the role of CIZ1.

7.2. Loss of CIZ1 Alters the kinetics of cell cycle re-entry from Quiescence

The initial findings presented in this report demonstrated no significant cell cycle profile deviations in asynchronous fibroblasts (Figure 4.4). Interestingly, later findings revealed that DNA replication dynamics were altered in these cells (Chapter 6). However, numerous changes were observed in cells entering, and exiting quiescence, additionally, a change in sensitivity to serum, and the restriction point was observed. The main CIZ1 interacting partners that play a role in controlling quiescence entry and exit are: Cyclin E, Cyclin A, and p21.

The link between p21^{Cip1/Waf1} is long established. The initial discovery of CIZ1 reported that CIZ1 was a p21 binding partner. Thus, CIZ1 was named p21^{Cip1} interacting zinc finger protein

1. This paper reported competition of the CDK binding site on p21, between CIZ1 and CDK2, with a preference for binding CDK2. Co-expression of CIZ1 increased p21 levels suggesting CIZ1 may have a protective effect of p21 levels. The conclusion of the report was that when expressed alone, both CIZ1 and p21 localised to the nucleus. However, co-expression of CIZ1 and p21 promoted cytoplasmic localisation (Mitsui et al., 1999).

Little has been reported exploring the interaction of p21 and CIZ1. Coverley et al. (2005) demonstrated that the replication initiation promoting activity of CIZ1 was independent of p21, remaining functional in a p21 null background. The conclusion made here was that CIZ1 did not promote replication initiation through alleviation of the p21 mediated CDKi, instead acting directly promoting the activity of the replisome. Since then the link between p21 and CIZ1 has largely been unexplored. Zhou et al. (2017) identified increased CIZ1 levels in SLCC cells compared to normal tissue, correlating with the cancer stage. In the same tumour samples the opposite was seen in P21 levels, P21 levels were lower in cancer cells compared to normal cells (Li et al., 1994; Rodriguez & Meuth, 2006; Georgakilas et al., 2017).

The restriction point marks the point where CDK activity overcomes CDK inhibition from p27/p21 (Zetterberg et al., 1995). p21 plays a role in setting the restriction point in cycling cells. Cells with low CDK2 (due to high p21) enter a pre-restriction point stage, not entering the cell cycle until triggered. Whereas cells with higher CDK2 activity (due to low p21 in G2 and M phase) continue replicating entering the cell cycle in a hyperphosphorylated RB state (Moser et al., 2018). Since CIZ1 binds p21 (Mitsui et al., 1999) it may be bringing p21 to the nuclear matrix, increasing the local concentration and potentially reducing its CDK inhibitory activity. Loss of CIZ1 may therefore result in lower interactions between Cyclin- CDK complexes and p21 which could explain the increased cell cycle re-entry observed here and may also have implications for the altered CDK threshold that promotes initiation of DNA replication in CIZ1 KO cells.

Alternatively, the altered quiescence phenotype could be due to a compensatory mechanism. Cyclin A levels on chromatin in CIZ1 KO1 cells were reduced, additionally *in vitro* data suggested that higher kinase activities were required to promote S-phase onset. Taken together these data would imply that CIZ1 null cells should require more time to re-enter the cell cycle. However, data from Chapter 4 implied that Cyclin E and Cyclin A levels accumulated faster in CIZ1 KO1 cells re-entering the cell cycle and previous reports show that suppression of Cyclin E during cell cycle re-entry results in delayed S phase entry (Léger et al., 2016). An unknown compensatory mechanism may be active in CIZ1 null cells compensating for reduced chromatin Cyclin A. As both Cyclin A and Cyclin E are E2F regulated proteins (Dimova et al., 2005), the regulation of the E2F pathways, and RB phosphorylation should be assessed in CIZ1 null fibroblasts re-entering the cell cycle.

Critically, the timing of G1 in cells re-entering the cell cycle has implications for genome stability. Shortening of G1 in cycling cells results in DRS (Macheret & Halazonetis, 2018). Replication origins in the first cell cycle are under licensed, with reduced MCM levels compared to cycling cells and become hypersensitive to replication stress due to a reduced ability to activate cryptic origins, a similar effect to Cyclin E overexpression. Interestingly lengthening the first G1 phase after quiescence through p21 accumulation, promoted increased origin licensing, which reduced the inherent instability of cell cycle re-entry. (Matson et al., 2018). Loss of CIZ1 reduced the length of the first G1 after cell cycle re-entry through an unknown mechanism (Chapter 4). This could result in an erosion of genome stability. Future work should analyse DNA replication licensing in CIZ1 null cells re-entering the cell cycle from quiescence.

7.3. Loss of CIZ1 Alters Replication Dynamics which Could Result in Genome Instability

Loss of CIZ1 induced a change in replication programme characteristic of DRS. DRS can be caused through DNA lesions blocking replication, or oncogenic activation promoting

mistimed DNA replication, resulting in an increase in collisions between replication and transcriptional machinery. This results in increased DRS in certain cancers, and DRS is a proposed therapeutic target in triple negative breast cancer (Jones et al., 2013; Fragkos et al., 2015; Llobet et al., 2020). The effect of replication stress by oncogene activation is an erosion in genome integrity, increased p53 mutations, aneuploidy, and increases tumour size are all observed in Cyclin E overexpressing cancers (Lindahl et al., 2004).

Linking CIZ1 levels to genome stability has clear links to its role in cancers (Higgins et al., 2012; Chen et al., 2019). However, the effect of increased CIZ1 levels on replication remains unclear. *In vitro* experiments demonstrated that addition of increased CIZ1-N471 at low (typically non permissible) Cyclin A/CDK2 concentrations promoted replication initiation with increased DRS to an S phase extract. Whereas adding CIZ1 to optimal and high (typically non permissible) concentrations of Cyclin A/CDK2 promoted replication more comparable to an S phase extract (Figure 5.12). If this is extrapolated to a cell based system, then increased CIZ1 could promote early replication at low CDK2 activities with increased DRS reducing genome stability. This effect could support a potential mechanism where overexpression of CIZ1 promotes genome stability as a precursor to tumour formation. Further work is required to confirm this.

There are indications that the increase in DRS has been observed elsewhere. CIZ1 null MEFs exposed to γ irradiation displayed increased DNA breaks, and sustained phosphorylation of γ -H2AX (Khan et al., 2019). These results could indicate a sensitivity due to a decrease in genome stability from the increased DRS phenotype. Alternatively, this result could be as a result of a defect in activating the DDR as upregulated DDR due to constitutive replication stress results in radioresistance in glioblastoma cells (Carruthers et al., 2018).

7.4. Loss of CIZ1 Promotes an altered DDR

Data from this report has expanded on work from Nishibe et al. (2013) regarding CIZ1 null cells sensitivity to HU. CIZ1 KO resulted in a delayed H2AX response, leading a prolonged activation of DDR (Chapter 4). This Response manifested as reduced fork restart within 2 hours of removal of HU, and faster replication from the reduced restarted replication forks. 24 hours after removal of HU a collapse in replication dynamics was observed in CIZ1 KO1 cells, whereas WT and CIZ1^{AB} cells displayed a return (or partial return) to replication kinetics comparable with untreated cells. These results identified another scenario where removal of CIZ1 resulted in a reduction in genome stability.

It remains unclear what role CIZ1 performs in response to DRS induced by HU, but predictions can be made. Firstly, CIZ1 KO promoted a prolonged DRS. An ineffective initial response to HU in CIZ1 null cells may result in more complex DNA damage, hence the prolonged H2AX phosphorylation and deranged replication kinetics. The delayed H2AX phosphorylation could indicate a delayed DDR. In response to ionising radiation a delayed DDR can result in complex DNA damage that cells cannot repair (Eccles et al., 2011).

A second hypothesis is that CIZ1 plays a direct role in the replisome during fork stalling and fork restart as well as the G1/S transition. CIZ1 co-ordinates the localisation of Cyclin A/CDK2 to Cyclin E rich regions of the nuclear matrix during the G1/S transition in a CDK2 phosphorylation regulated manner (Copeland et al., 2010; Copeland et al., 2015). Perhaps CIZ1 plays a similar role during replication fork stalling and restart. Reduction of Cyclin E degradation results in a delay in the onset of S-phase (Bi et al., 2015). Blocking of replication fork progression through treatment with mitomycin C results in a stabilisation of Cyclin E/CDK2 through inhibition of its degradation by the UPS. This is thought to inhibit S phase progression by blocking Cyclin A associating with CDK2 impairing its ability to promote origin firing (Lu et al., 2009). Additionally, prevention of inhibitory phosphorylation of CDK2 after

HU treatment prevents cyclin E accumulation, promotes p21 accumulation, increases DNA damage, and results in defects restarting S phase (Hughes et al., 2013). Therefore, CIZ1 KO may alter the phosphorylation or localisation of Cyclin E following heightened DRS.

CIZ1 overexpressing cancers have displayed altered DDR, or sensitivity to DNA damage. Removal of exon 5 of CIZ1 in mice resulted in sensitivity to gamma irradiation (Khan et al., 2018). Knockdown of CIZ1 in bladder cancer cells induced tumour apoptosis and upregulation of p21, p53 and caspase 3. This implied CIZ1 was suppressing the DDR, potentially adapting cells to growth in cancer conditions (Chen et al., 2019). Critically, some cancers become dependent on an intact DDR, that can be exploited through therapeutic approaches to induce synthetic lethality (Beijersbergen et al., 2017). This has provided a platform for development of new therapeutics that exploit this weakness to selectively treat specific cancers, most famously, PARPi in BRCA1/2 mutant cancers (Yi et al., 2019). Future work should endeavour to assess the feasibility of targeting the DDR in CIZ1 overexpressing cancers.

An aberrant DDR (observed in this report) may be linked to other conditions associated with CIZ1. DDR defects result in neurodevelopment disorders, such as Xeroderma Pigmentosum, and age-related neurodegenerative disorders such as Alzheimer's disease (Madabhushi et al., 2017). CIZ1 null mice display developmental abnormalities, as CIZ1 null mice age motor defects become more pronounced: increased DNA damage, and oxidative stress. (Khan et al., 2018; Xiao et al., 2018). Mirroring the role of the DDR in neurodegenerative disorders. This may suggest a physiologically relevant role for CIZ1 in the DDR. Future work should identify whether CIZ1 plays a direct role during fork restart. Additionally, the physiological relevance of the DDR role in CIZ1 overexpressing cancers should be assessed. This could help elucidate the activity of CIZ1 during increased DRS, as well as provide therapeutic targets in cancers with altered CIZ1 expression.

7.5. The Quantitative Model: CIZ1 as a Kinase Sensor at G1/S Phase Transition

The quantitative model of the cell cycle was discussed in detail in Chapters 1 and 5. Briefly, this model simplifies control of cell cycle progression to oscillating kinase gradients. Critical cell cycle events (S phase, and Mitosis) are regulated by kinase thresholds, driven through differentially phosphorylated populations of proteins (Spencer et al., 2013; Gutierrez-Escribano & Nurse, 2015; Swaffer et al., 2016; Moser et al., 2019; Ord et al., 2019).

There is compelling evidence presented in this report that suggests that CIZ1 may play a role in 'setting' the kinase levels at which the T_s and the iT_s are found. Increasing CIZ1 levels altered the kinase levels required to promote S phase entry *in vitro*. Importantly, the modulation of CIZ1 levels, either through CIZ1 KO, or addition of recombinant CIZ1-N471, promoted initiation of DNA replication above the iT_s and below the T_s , as determined in WT cells without the addition of CIZ1.

The mechanism by which CIZ1 alters thresholds is unclear. This contrasts cell-based experiments where loss of CIZ1 promoted more rapid S-phase entry following quiescence. However, the more rapid cell cycle re-entry in CIZ1 null cells was accompanied by a more rapid accumulation of Cyclin A (Chapter 4). It may be in a cellular context, that the more rapid restriction point required for S phase entry is compensated for by the earlier restriction point. The mechanism of restriction point bypass could be through altered p21 activity, or reduced degradation of Cyclin A in early G1 by the UPS. In a DDR context, Cyclin E accumulation competes with Cyclin A delaying S-phase onset (Bi et al., 2015).

One mechanism by which CIZ1 may play this role is by acting as a kinase sensor. Evidence for this was suggested by Copeland et al. (2015). This paper revealed that CIZ1 had different activities dependent on its phosphorylation state. At low CDK2 levels CIZ1 promotes pre-RC assembly through interactions with CDC6 on the nuclear matrix. As Cyclin A/CDK2 levels increase it binds CIZ1 promoting preIC assembly through phosphorylation of preRC proteins,

Loss of CIZ1 increased concentration of CDK2 required to initiation. CIZ1 localises Cyclin A/CDK2 to the nuclear matrix, this could create a local increase in Cyclin A concentration at preRCs. This may increase the replication promoting effect of Cyclin A-CDK2, by localising activity, it may also sequester Cyclin A from inhibitory phosphorylation similar to how Cyclin D-CDK4/6 sequesters p21 and p27 from Cyclin E-CDK2 (Planas-Silva & Weinberg, 1997), increasing CDK activity. CIZ1 KO may create an environment where increased cyclin A-CDK2 is required to promote equivalent kinase activity without CIZ1 mediated localisation to replication origins.

7.6. CIZ1's Links to Tumorigenesis

Results observed in this report have clear links between CIZ1 and genome stability, which has clear links to cancer development. However, to elucidate CIZ1's DNA replication activity these results have focussed on loss of CIZ1. The tumour suppressor function of CIZ1 has been observed only in engineered CIZ1 null cell lines (Nishibe et al., 2013; Khan et al., 2019). CIZ1 overexpression and splice variation have commonly been associated with a range of common cancer types (Table 7.1) (Higgins et al., 2012; Zhang et al., 2014; Liu et al., 2015; Chen et al., 2019). Surveying published data to unpick the various alterations reported in cancers with altered CIZ1 levels can contextualise the data from this report.

Observed CIZ1 Alteration	Cancer Type	Reference
Overexpression	Colorectal Cancer	Yin et al., 2013
	Prostate Cancer	Liu et al., 2015
	Breast Cancer	Li et al., 2020
	Lung Cancer	Zhou et al., 2017
Splice Variation	Lung Cancer	Higgins et al., 2012
	Colon Cancer	Swarts et al., 2018
	Breast Cancer	

Table 7.1 – CIZ1 alterations observed in cancers. Adapted from Pauzaite et al., 2017

Splice variation of CIZ1 has been associated with cancers. Two splice variants of CIZ1: CIZ1-B and CIZ1-F have both been found to be expressed in tumour samples. Both variants lack the nuclear matrix attachment domain of CIZ1. This CIZ1 variant was found to lack the C terminal

nuclear matrix anchor domain. In mice xenograft experiments loss of the CIZ1-B in tumours resulted in a suppression of tumour growth (Higgins et al., 2012). Interestingly CIZ1-F transcription is suppressed during cell cycle re-entry after quiescence until multiple cycles after cell cycle re-entry. CIZ1-F transcription was also suppressed after treatment with DNA replication inhibitor aphidicolin (Swarts et al., 2018). These are of note due to the role CIZ1 plays during quiescence, and response to DNA replication inhibitor HU that were observed in this report.

In other cancers, CIZ1 expression levels change. Haemangioma of the tongue, bladder cancer, prostate carcinoma, and colon cancer have all been found overexpressing CIZ1. In each of these examples, suppression of CIZ1 reduces cellular proliferation (Chen et al., 2019; Liu et al., 2015; Wang et al., 2019, Yin et al., 2013). This implies a direct role for CIZ1 for maintaining tumorigenicity and proliferation in cancer. This aligns with observations in this report that CIZ1 may adapt tumour cells to altered internal conditions.

Despite the observed TS function of CIZ1 *in vitro* (Nishibe et al., 2013; Khan et al., 2019) no clinical samples have yet been identified. However, in recent years useful tools have been developed that analyse the genomes of multiple cancer types allowing the identification of specific mutations, and copy number variations (CNVs) of thousands of genes. The cancer genome atlas (TCGA), has surveyed genomes across over 30 different cancer types (Weinstein et al., 2014). This allows analysis of mutations in CIZ1 across cancers. Multiple mutations in CIZ1 were identified inserting a stop codon relatively early in the sequence of CIZ1 or introduced a frameshift mutation (Figure 7.1a).

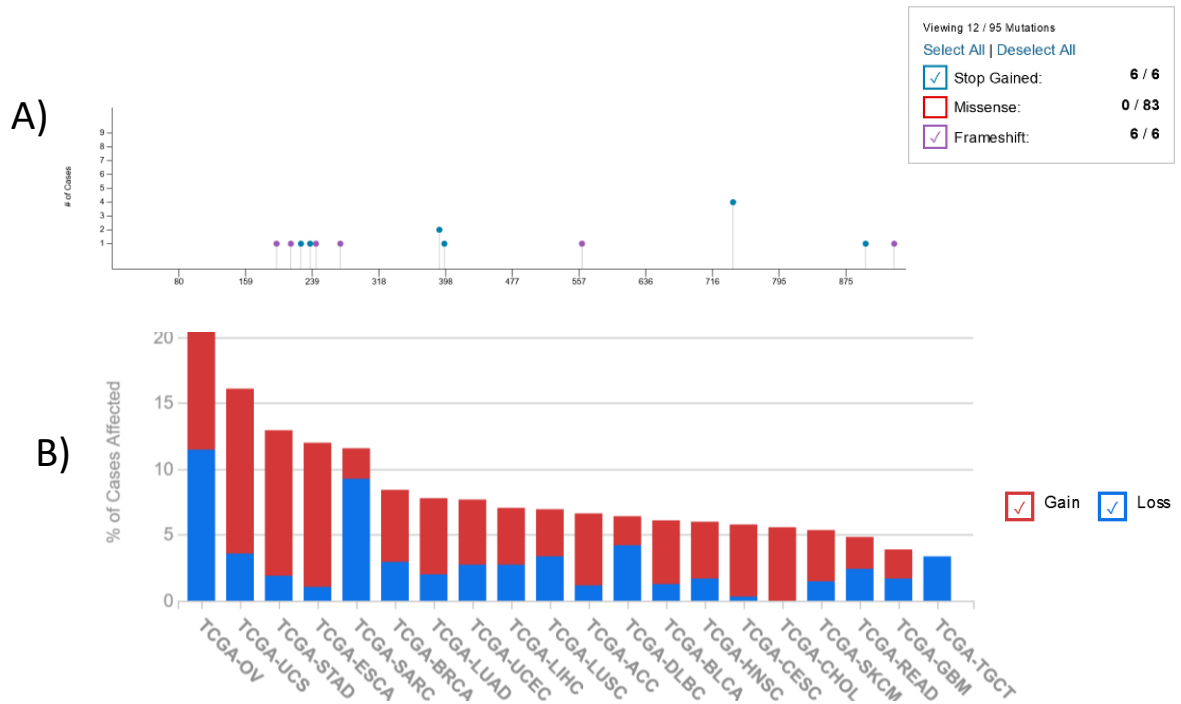


Figure 7.1 – Surveying CIZ1 alterations in cancers in the cancer genome atlas A) The presence of stop codon gained and frameshift mutations in cancers.. Notably there are several loss of function mutations early in the CIZ1 sequence. B) The incidence of CNV changes in CIZ1 in cancers studied in the cancer genome atlas. Red represents gain of CNV, and Blue represents Loss. CNV strongly correlates with mRNA expression. Cancers with CIZ1 mostly present with gain although there are a striking number of cancers with losses. This particularly striking in ovarian cancers, testicular germ cell cancers, sarcomas, and Diffuse Large B-cell Lymphoma. The results shown here are in whole or part based upon data generated by the TCGA Research Network: <https://www.cancer.gov/tcga>.

Additionally, CIZ1 copy number variation (CNV) changes were identified in a number of cancers. CNV is the number of amplifying or decreasing >1kbp DNA segments in the genome. TCGA allows analysis of CNV changes in response to specific genes in cancers. CNV is positively correlated with the mRNA expression levels of the gene (Shao et al., 2019). A search for CIZ1 reveals the presence of both loss and gain of CNV (Figure 7.1B). Certain cancer types such as ovarian have predominantly reduced copies of the CIZ1 gene. This suggests that there may be a clinical relevance to the TS function of CIZ1. Future studies should analyse multiple cancer cell lines that have a reduced CIZ1 copy number to investigate the clinical relevance, if any, of CIZ1 acting as a TS. Data from this report implies

a genome stability role for CIZ1, which could be linked to cancer phenotypes. *In vitro* data from this report implies a model whereby overexpression of CIZ1 could allow replication to occur in the altered environment cancerous cell. Future work should identify the clinical relevance of the tumour suppressor function of CIZ1 and identify strategies for targeting CIZ1 activity in CIZ1 dependent tumours.

7.7. Phenotypes Observed upon Loss of CIZ1 Consistently have Links to Epigenetics

There may be an epigenetic role for CIZ1, linked to the phenotypes observed in CIZ1 null cells. CIZ1 is involved in the localisation of Xi. CIZ1 is recruited by Xist, this is accompanied by methylation and ubiquitylation of Xi histones. Loss of CIZ1 results in a reduction in the methylation (H3K27me3) and ubiquitylation (H2AK119UB1) of Xi histones. (Ridings-Figueroa et al., 2017; Stewart et al., 2019). The link between CIZ1 and epigenetics is unexplored in the context of DNA replication.

The epigenetic landscape of DNA has links to the key observations of this report: Quiescence, replication dynamics, and the DDR. Histone methylation is also altered in quiescent cells. The histone methyltransferase proteins EZH1 and EZH2 that trimethylate histone 3 lysine 27 (H3K27me3) during quiescence in stem cells (Yao, 2014). Quiescent stem cells have reduced H3K27 methylation, until stem cell activation when H3K27 methylation increases (Liu et al., 2014). CIZ1 KO may cause altered H3K27 methylation in quiescence which may explain the altered quiescence kinetics in CIZ1 KO.

H3K27me3 is linked to replication fidelity, and H3K27 methylation is important for protecting against DRS (Yi et al., 2009; Khurana & Oberdoerffer, 2015). In the ciliate *Tetrahymena thermophila*, H3K27 methylation deficiency promotes DRS (Gao et al., 2015). In *Drosophila* Stwl depletion decreased H3K27 methylation increasing HU sensitivity (Yi et al., 2009). There are parallels between these results and CIZ1 KO. However, links between H3K27 methylation

and DNA replication are not understood in mammalian cells. Additionally, limited research has been performed investigating how CIZ1 effects histone methylation of somatic chromosomes.

The link between CIZ1 and epigenetic maintenance remains unclear. No published CIZ1 binding partner plays a direct role in histone methylation. However, CIZ1 interacts with Cyclin E and Cyclin A, both of which activate CDK2 (Coverley et al., 2005; Copeland et al., 2010). Loss of CIZ1 promotes a change in EZH2 solubility (Stewart et al., 2019). EZH2 phosphorylation by CDK1 and CDK2 promotes methylation of H3K27 on nascent DNA, ensuring epigenetic marks are transferred through generations (Zeng et al., 2011). It is feasible that CIZ1 may influence EZH phosphorylation, and CDK2 mediated phosphorylation of EZH2 promoted tumour development in mice (Nie et al., 2019).

7.8. Future Work

There are several areas for future research that have been developed during this project. Firstly, data presented here strengthened the link CIZ1 and replication initiation (Coverley et al., 2005; Copeland et al., 2010; Copeland et al., 2015) However, the full role of CIZ1 during initiation remains unclear. Secondly, CIZ1 has implications for genome stability, loss of CIZ1 promoted DRS, altered replication timing, and HU sensitivity. Thirdly, the physiological relevance of CIZ1 in cancer, and feasibility of using it as therapeutic target, or to inform treatment decisions. And finally, the further elucidation of the role CIZ1 plays in epigenetic maintenance.

Future work should endeavour to identify if kinase thresholds are altered in whole cell context, crucially this should be expanded to cancer cell lines shown to be dependent on CIZ1 for proliferation. One way to achieve this would be the use of fluorescent kinase sensors. Spencer et al. (2013) developed a fluorescent kinase sensor that as it is phosphorylated moves from nuclear to cytosol localisation, the ratio of cytosol: nuclear

fluorescence was used to measure CDK activity. This demonstrated cells bifurcate into low and high CDK activity following mitosis, determining the rate the next cell cycle begins. If changes observed in this report *in vitro* regarding sensitivity to CDK activity are true in cells then introducing this sensor into CIZ1 null cells should show differences in CDK patterns.

Results from this report have identified a potential role for CIZ1 within the replisome as well as during replication initiation. CIZ1 stabilised replication kinetics *in vitro* at both optimal and high CDK concentrations (Chapter 5). Additionally, loss of CIZ1 promoted a reduction in replication fork rate in both cycling cells (Chapter 6), and nuclei re-entering the cell cycle from quiescence (Chapter 5). It is unclear whether this is a by-product of altered origin firing, or a direct role CIZ1 plays during in the replisome during replication elongation.

One technique that could be used to establish this is iPOND (isolation of proteins on nascent DNA). In this technique, nascent DNA is labelled with EdU, a biotin tag is attached to nascent DNA, then proteins bound to nascent DNA are isolated through streptavidin pulldown (Dungrawala & Cortez, 2016). This technique could be used to confirm a role for CIZ1 at the replisome, additionally, other proteins CIZ1 may have an effect on, such as methyltransferases, would be identified which may help elucidate CIZ1 activity. Critically, if CIZ1 does not play a role directly on the replisome, this technique could identify changes to replisome proteins in CIZ1 null cells.

CIZ1 is overexpressed, or alternatively spliced in a number of cancer cell lines and tumour samples, these reports have been low throughput investigating one specific cancer or cell line (Higgins et al., 2012; Swarts et al., 2018; Chen et al., 2019). The prevalence of CIZ1 overexpression, and dependence should be determined across a wide range of cancers.

Cancer biobanks are a tool that is important for developing personalised cancer therapeutics through the ability to screen multiple cancer types (Patil et al., 2018). Cancer biobank samples should be used to measure CIZ1 expression, and mutation. Samples that display

increased or altered CIZ1 should be used to measure replication dynamics before and after depletion of CIZ1. This would identify the efficacy of potentially targeting CIZ1 cancers (either directly or through a separate mechanism), additionally, this approach may identify if there is a physiological relevance to the TS function of CIZ1 (Nishibe et al., 2013).

Finally, changes in epigenetics upon loss of CIZ1 should be measured. Techniques have been developed that allow measurements of histone modifications. Immunoprecipitation of chromatin proteins, immunostaining, next generation sequencing and RT PCR allows for measurements of all major histone methylation (Zhao et al., 2016). Utilizing similar techniques to compare WT, and CIZ1 null cells will allow assessment of the effect of loss of CIZ1 on the epigenome. If an effect is seen this could be measured in CIZ1 dependent cancers before and after suppression of CIZ1. The activity of histone methyltransferases (such as EZH2) by chemical inhibition could be measured in these cancers to investigate any effect on histone methylation, tumour growth and DNA replication (Duan et al., 2020).

7.9. Concluding remarks

Data from this report has implicated CIZ1 in maintenance of genome stability. Loss of CIZ1 results in changes in replication timing, DRS, and hypersensitivity to DRS. These observations can be used to inform the role that CIZ1 plays in cancer. For the oncogenic function CIZ1 overexpression may provide a growth advantage to cells in cancerous conditions. The TS function can be explained by a reduction in genome stability.

Using data from this report, a hypothesis surrounding this can be built around the role CIZ1 plays (Figure 7.3). Firstly, maintenance of G0, loss of CIZ1 resulted in aberrant cell-cycle re-entry, the expected result of this would be heightened genome instability. Secondly CIZ1 may function to determine the CDK activity that will promote replication initiation and inhibition. Disruption of this could result in under licensed replication and DRS, or provide a growth advantage for cells with disrupted CDK networks. Thirdly, this report identified a role for CIZ1 in maintaining the replisome in cell free and cell based experiments. CIZ1 null cells displayed reduced fork rates, and increased origin usage, a phenotype consistent with DRS. Critically, this resulted in a hypersensitivity to increased DRS.

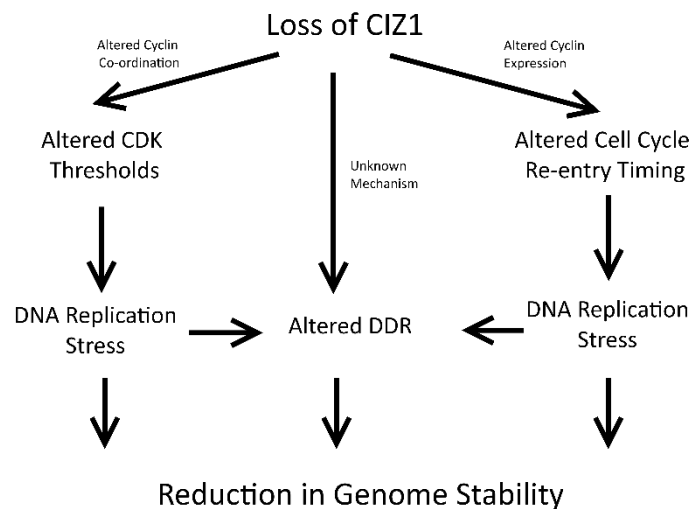


Figure 7.2-A Model for how CIZ1 Loss Reduces Genome Stability. Each of the major phenotypes observed in this report result in a reduction in genome stability. Altered responses to CDK signalling and cell cycle re-entry timing promote DRS. Increased DRS, or another unknown mechanism lead to an altered DDR and hypersensitivity to replication challenge. All these phenotypes lead to a reduction in genome stability.

In conclusion, this report has demonstrated a potential important role for CIZ1 in maintaining genome stability through control over DNA replication. Data presented here has opened many questions as to how CIZ1 is involved in the phenotypes observed, and the physiological relevance of this. Data from this report has informed previous research and provided new avenues to explore in CIZ1 biology. This could provide research avenues for potential treatments, targeting CIZ1 regulatory pathways in CIZ1 overexpressing cancers.

References

- Abbas, T. and Dutta, A., 2009. p21 in cancer: intricate networks and multiple activities. *Nature Reviews Cancer*, 9(6), pp.400-414.
- Abbastabar, M., Kheyrollah, M., Azizian, K., Bagherlou, N., Tehrani, S.S., Maniati, M. and Karimian, A., 2018. Multiple functions of p27 in cell cycle, apoptosis, epigenetic modification and transcriptional regulation for the control of cell growth: A double-edged sword protein. *DNA repair*, 69, pp.63-72.
- Abbotts, R. and Wilson III, D.M., 2017. Coordination of DNA single strand break repair. *Free Radical Biology and Medicine*, 107, pp.228-244.
- Acevedo, J., Yan, S. and Michael, W.M., 2016. Direct binding to replication protein A (RPA)-coated single-stranded DNA allows recruitment of the ATR activator TopBP1 to sites of DNA damage. *Journal of Biological Chemistry*, 291(25), pp.13124-13131.
- Ahuja, A.K., Jodkowska, K., Teloni, F., Bizard, A.H., Zellweger, R., Herrador, R., Ortega, S., Hickson, I.D., Altmeyer, M., Mendez, J. and Lopes, M., 2016. A short G1 phase imposes constitutive replication stress and fork remodelling in mouse embryonic stem cells. *Nature communications*, 7(1), pp.1-11.
- Aldossary, S.A., 2019. Review on pharmacology of cisplatin: clinical use, toxicity and mechanism of resistance of cisplatin. *Biomedical and Pharmacology Journal*, 12(1), pp.7-15.
- Alfieri, C., Zhang, S. and Barford, D., 2017. Visualizing the complex functions and mechanisms of the anaphase promoting complex/cyclosome (APC/C). *Open biology*, 7(11), p.170204.
- Altieri, P., Spallarossa, P., Barisione, C., Garibaldi, S., Garuti, A., Fabbi, P., Ghigliotti, G. and Brunelli, C., 2012. Inhibition of doxorubicin-induced senescence by PPAR δ activation agonists in cardiac muscle cells: cooperation between PPAR δ and Bcl6. *PLoS One*, 7(9), p.e46126.
- Al-Zain, A., Schroeder, L., Sheglov, A. and Ikui, A.E., 2015. Cdc6 degradation requires phosphodegron created by GSK-3 and Cdk1 for SCFCdc4 recognition in *Saccharomyces cerevisiae*. *Molecular biology of the cell*, 26(14), pp.2609-2619.
- Aria, V. and Yeeles, J.T., 2019. Mechanism of bidirectional leading-strand synthesis establishment at eukaryotic DNA replication origins. *Molecular cell*, 73(2), pp.199-211.
- Bageghni, S.A., Frentzou, G.A., Drinkhill, M.J., Mansfield, W., Coverley, D. and Ainscough, J.F., 2017. Cardiomyocyte-specific expression of the nuclear matrix protein, CIZ1, stimulates production of mono-nucleated cells with an extended window of proliferation in the postnatal mouse heart. *Biology open*, 6(1), pp.92-99.
- Barr, A.R., Cooper, S., Heldt, F.S., Butera, F., Stoy, H., Mansfeld, J., Novák, B. and Bakal, C., 2017. DNA damage during S-phase mediates the proliferation-quiescence decision in the subsequent G1 via p21 expression. *Nature communications*, 8(1), pp.1-17.
- Barrangou, R., 2015. Diversity of CRISPR-Cas immune systems and molecular machines. *Genome biology*, 16(1), p.247.

- Barrangou, R., Fremaux, C., Deveau, H., Richards, M., Boyaval, P., Moineau, S., Romero, D.A. and Horvath, P., 2007. CRISPR provides acquired resistance against viruses in prokaryotes. *Science*, 315(5819), pp.1709-1712.
- Bartkova, J., Rezaei, N., Liontos, M., Karakaidos, P., Kletsas, D., Issaeva, N., Vassiliou, L.V.F., Kolettas, E., Niforou, K., Zoumpourlis, V.C. and Takaoka, M., 2006. Oncogene-induced senescence is part of the tumorigenesis barrier imposed by DNA damage checkpoints. *Nature*, 444(7119), pp.633-637.
- Beijersbergen, R.L., Wessels, L.F. and Bernards, R., 2017. Synthetic lethality in cancer therapeutics. *Annual Review of Cancer Biology*, 1, pp.141-161.
- Bensimon, A., Simon, A., Chiffaudel, A., Croquette, V., Heslot, F. and Bensimon, D., 1994. Alignment and sensitive detection of DNA by a moving interface. *Science*, 265(5181), pp.2096-2098.
- Bensimon, D., Simon, A.J., Croquette, V. and Bensimon, A., 1995. Stretching DNA with a receding meniscus: experiments and models. *Physical review letters*, 74(23), p.4754.
- Bétous, R., de Rugy, T.G., Pelegri, A.L., Queille, S., de Villartay, J.P. and Hoffmann, J.S., 2018. DNA replication stress triggers rapid DNA replication fork breakage by Artemis and XPF. *PLoS genetics*, 14(7), p.e1007541.
- Bhaskara, S., Jacques, V., Rusche, J.R., Olson, E.N., Cairns, B.R. and Chandrasekharan, M.B., 2013. Histone deacetylases 1 and 2 maintain S-phase chromatin and DNA replication fork progression. *Epigenetics & chromatin*, 6(1), p.27.
- Bi, H., Li, S., Qu, X., Wang, M., Bai, X., Xu, Z., Ao, X., Jia, Z., Jiang, X., Yang, Y. and Wu, H., 2015. DEC1 regulates breast cancer cell proliferation by stabilizing cyclin E protein and delays the progression of cell cycle S phase. *Cell death & disease*, 6(9), pp.e1891-e1891.
- Bian, X. and Lin, W., 2019. Targeting DNA replication stress and DNA double-strand break repair for optimizing SCLC Treatment. *Cancers*, 11(9), p.1289.
- Bianco, J.N., Poli, J., Saksouk, J., Bacal, J., Silva, M.J., Yoshida, K., Lin, Y.L., Tourrière, H., Lengronne, A. and Pasero, P., 2012. Analysis of DNA replication profiles in budding yeast and mammalian cells using DNA combing. *Methods*, 57(2), pp.149-157.
- Biertümpfel, C., Zhao, Y., Kondo, Y., Ramón-Maiques, S., Gregory, M., Lee, J.Y., Masutani, C., Lehmann, A.R., Hanaoka, F. and Yang, W., 2010. Structure and mechanism of human DNA polymerase η . *Nature*, 465(7301), pp.1044-1048.
- Bishop, A.J. and Schiestl, R.H., 2002. Homologous recombination and its role in carcinogenesis. *Journal of Biomedicine and Biotechnology*, 2(2), p.75.
- Black, J.O., 2016. Xeroderma pigmentosum. *Head and neck pathology*, 10(2), pp.139-144.
- Bleichert, F., Botchan, M.R. and Berger, J.M., 2017. Mechanisms for initiating cellular DNA replication. *Science*, 355(6327).
- Blow, J.J. and Laskey, R.A., 1986. Initiation of DNA replication in nuclei and purified DNA by a cell-free extract of Xenopus eggs. *Cell*, 47(4), pp.577-587.

- Boehm, E.M., Gildenberg, M.S. and Washington, M.T., 2016. The many roles of PCNA in eukaryotic DNA replication. In *The Enzymes* (Vol. 39, pp. 231-254). Academic Press.
- Boopathy, G.T. and Hong, W., 2019. Role of Hippo pathway-YAP/TAZ signaling in angiogenesis. *Frontiers in cell and developmental biology*, 7, p.49.
- Bose, S., Yap, L.F., Fung, M., Starzcynski, J., Saleh, A., Morgan, S., Dawson, C., Chukwuma, M.B., Maina, E., Buettner, M. and Wei, W., 2009. The ATM tumour suppressor gene is down-regulated in EBV-associated nasopharyngeal carcinoma. *The Journal of Pathology: A Journal of the Pathological Society of Great Britain and Ireland*, 217(3), pp.345-352.
- Botezatu, A., Iancu, I.V., Plesa, A., Manda, D., Popa, O., Bostan, M., Mihaila, M., Albulescu, A., Fudulu, A., Vladiou, S.V. and Huica, I., 2019. Methylation of tumour suppressor genes associated with thyroid cancer. *Cancer Biomarkers*, 25(1), pp.53-65.
- Brambati, A., Zardoni, L., Achar, Y.J., Piccini, D., Galanti, L., Colosio, A., Foiani, M. and Liberi, G., 2018. Dormant origins and fork protection mechanisms rescue sister forks arrested by transcription. *Nucleic acids research*, 46(3), pp.1227-1239.
- Broderick, R. and Nasheuer, H.P., 2009. Regulation of Cdc45 in the cell cycle and after DNA damage.
- Brosh, R. and Rotter, V., 2009. When mutants gain new powers: news from the mutant p53 field. *Nature reviews cancer*, 9(10), pp.701-713.
- Brouns, S.J., Jore, M.M., Lundgren, M., Westra, E.R., Slijkhuys, R.J., Snijders, A.P., Dickman, M.J., Makarova, K.S., Koonin, E.V. and Van Der Oost, J., 2008. Small CRISPR RNAs guide antiviral defense in prokaryotes. *Science*, 321(5891), pp.960-964.
- Bui, D.T. and Li, J.J., 2019. DNA rereplication is susceptible to nucleotide-level mutagenesis. *Genetics*, 212(2), pp.445-460.
- Burrell, R.A., McClelland, S.E., Endesfelder, D., Groth, P., Weller, M.C., Shaikh, N., Domingo, E., Kanu, N., Dewhurst, S.M., Gronroos, E. and Chew, S.K., 2013. Replication stress links structural and numerical cancer chromosomal instability. *Nature*, 494(7438), p.492.
- Buscemi, G., Ricci, C., Zannini, L., Fontanella, E., Plevani, P. and Delia, D., 2014. Bimodal regulation of p21waf1 protein as function of DNA damage levels. *Cell cycle*, 13(18), pp.2901-2912.
- Byun, T.S., Pacek, M., Yee, M.C., Walter, J.C. and Cimprich, K.A., 2005. Functional uncoupling of MCM helicase and DNA polymerase activities activates the ATR-dependent checkpoint. *Genes & development*, 19(9), pp.1040-1052.
- Cancer Research UK, 2020, A trial looking at AZD6738 with radiotherapy for advanced solid tumours (PATRIOT), Cancer Research UK, viewed 20 May 2020, <<https://www.cancerresearchuk.org/about-cancer/find-a-clinical-trial/a-trial-looking-AZD6738-radiotherapy-advanced-solid-tumours-patriot#undefined>>.

Carruthers, R.D., Ahmed, S.U., Ramachandran, S., Strathdee, K., Kurian, K.M., Hedley, A., Gomez-Roman, N., Kalna, G., Neilson, M., Gilmour, L. and Stevenson, K.H., 2018. Replication stress drives constitutive activation of the DNA damage response and radioresistance in glioblastoma stem-like cells. *Cancer research*, 78(17), pp.5060-5071.

Caruso, J.A., Duong, M.T., Carey, J.P., Hunt, K.K. and Keyomarsi, K., 2018. Low-molecular-weight cyclin E in human Cancer: cellular consequences and opportunities for targeted therapies. *Cancer research*, 78(19), pp.5481-5491.

Cascales, H.S., Burdova, K., Müllers, E., Stoy, H., von Morgen, P., Macurek, L. and Lindqvist, A., 2017. Cyclin A2 localises in the cytoplasm at the S/G2 transition to activate Plk1. *bioRxiv*, p.191437.

Ceccaldi, R., Sarangi, P. and D'Andrea, A.D., 2016. The Fanconi anaemia pathway: new players and new functions. *Nature reviews Molecular cell biology*, 17(6), p.337.

Celniker, S.E. and Campbell, J.L., 1982. Yeast DNA replication in vitro: initiation and elongation events mimic in vivo processes. *Cell*, 31(1), pp.201-213.

Chadha, G.S., Gambus, A., Gillespie, P.J. and Blow, J.J., 2016. Xenopus Mcm10 is a CDK-substrate required for replication fork stability. *Cell Cycle*, 15(16), pp.2183-2195.

Chang, H.H., Pannunzio, N.R., Adachi, N. and Lieber, M.R., 2017. Non-homologous DNA end joining and alternative pathways to double-strand break repair. *Nature reviews Molecular cell biology*, 18(8), p.495.

Chao, H.X., Poovey, C.E., Privette, A.A., Grant, G.D., Cook, J.G. and Purvis, J.E., 2017. DNA damage checkpoint dynamics drive cell cycle phase transitions. *BioRxiv*, p.137307.

Chatterjee, N. and Walker, G.C., 2017. Mechanisms of DNA damage, repair, and mutagenesis. *Environmental and molecular mutagenesis*, 58(5), pp.235-263.

Chen, G. and Deng, X., 2018. Cell synchronization by double thymidine block. *Bio-protocol*, 8(17).

Chen, H., Liu, H. and Qing, G., 2018. Targeting oncogenic Myc as a strategy for cancer treatment. *Signal transduction and targeted therapy*, 3(1), pp.1-7.

Chen, S. and Parmigiani, G., 2007. Meta-analysis of BRCA1 and BRCA2 penetrance. *Journal of clinical oncology: official journal of the American Society of Clinical Oncology*, 25(11), p.1329.

Chen, S., Chen, X., Gui'e Xie, Y.H., Yan, D., Zheng, D., Li, S., Fu, X., Li, Y., Pang, X., Hu, Z. and Li, H., 2016. Cdc6 contributes to cisplatin-resistance by activation of ATR-Chk1 pathway in bladder cancer cells. *Oncotarget*, 7(26), p.40362.

Chen, Q., Zhang, X., Jiang, Q., Clarke, P.R. and Zhang, C., 2008. Cyclin B1 is localized to unattached kinetochores and contributes to efficient microtubule attachment and proper chromosome alignment during mitosis. *Cell research*, 18(2), pp.268-280.

Chen, X., Wang, P., Wang, S., Li, J., Ou, T. and Zeng, X., 2019. CIZ1 knockdown suppresses the proliferation of bladder cancer cells by inducing apoptosis. *Gene*, 719, p.143946.

- Cheung, T.H. and Rando, T.A., 2013. Molecular regulation of stem cell quiescence. *Nature reviews Molecular cell biology*, 14(6), pp.329-340.
- Child, E.S. and Mann, D.J., 2006. The intricacies of p21 phosphorylation: protein/protein interactions, subcellular localization and stability. *Cell cycle*, 5(12), pp.1313-1319.
- Childs, B.G., Baker, D.J., Kirkland, J.L., Campisi, J. and Van Deursen, J.M., 2014. Senescence and apoptosis: dueling or complementary cell fates?. *EMBO reports*, 15(11), pp.1139-1153.
- Chong, J.P., Mahbubani, H.M., Khoo, C.Y. and Blow, J.J., 1995. Purification of an MCM-containing complex as a component of the DNA replication licensing system. *Nature*, 375(6530), pp.418-421.
- Chong, S.Y., Cutler, S., Lin, J.J., Tsai, C.H., Tsai, H.K., Biggins, S., Tsukiyama, T., Lo, Y.C. and Kao, C.F., 2020. H3K4 methylation at active genes mitigates transcription-replication conflicts during replication stress. *Nature communications*, 11(1), pp.1-16.
- Ciccia, A. and Elledge, S.J., 2010. The DNA damage response: making it safe to play with knives. *Molecular cell*, 40(2), pp.179-204.
- Cicenas, J., Kalyan, K., Sorokinas, A., Stankunas, E., Levy, J., Meskinyte, I., Stankevicius, V., Kaupinis, A. and Valius, M., 2015. Roscovitine in cancer and other diseases. *Annals of translational medicine*, 3(10).
- Coelho, L.M., Cursino-Santos, J.R., Persinoti, G.F., Rossi, A. and Martinez-Rossi, N.M., 2013. The *Microsporium canis* genome is organized into five chromosomes based on evidence from electrophoretic karyotyping and chromosome end mapping. *Medical mycology*, 51(2), pp.208-2013.
- Copeland, N.A., Sercombe, H.E., Ainscough, J.F. and Coverley, D., 2010. CIZ1 cooperates with cyclin-A-CDK2 to activate mammalian DNA replication in vitro. *Journal of cell science*, 123(7), pp.1108-1115.
- Copeland, N.A., Sercombe, H.E., Wilson, R.H. and Coverley, D., 2015. Cyclin-A-CDK2-mediated phosphorylation of CIZ1 blocks replisome formation and initiation of mammalian DNA replication. *Journal of Cell Science*, 128(8), pp.1518-1527.
- Coudreuse, D. and Nurse, P., 2010. Driving the cell cycle with a minimal CDK control network. *Nature*, 468(7327), pp.1074-1079.
- De Falco, M., Ferrari, E., De Felice, M., Rossi, M., Hübscher, U. and Pisani, F.M., 2007. The human GINS complex binds to and specifically stimulates human DNA polymerase α -primase. *EMBO reports*, 8(1), pp.99-103.
- Courtot, L., Hoffmann, J.S. and Bergoglio, V., 2018. The protective role of dormant origins in response to replicative stress. *International journal of molecular sciences*, 19(11), p.3569.
- Coverley, D., Marr, J. and Ainscough, J., 2005. CIZ1 promotes mammalian DNA replication. *Journal of cell science*, 118(1), pp.101-112.
- Cradick, T.J., Fine, E.J., Antico, C.J. and Bao, G., 2013. CRISPR/Cas9 systems targeting β -globin and CCR5 genes have substantial off-target activity. *Nucleic acids research*, 41(20), pp.9584-9592.

- Dahmcke, C.M., Büchmann-Møller, S., Jensen, N.A. and Mitchelmore, C., 2008. Altered splicing in exon 8 of the DNA replication factor CIZ1 affects subnuclear distribution and is associated with Alzheimer's disease. *Molecular and Cellular Neuroscience*, 38(4), pp.589-594.
- Dai, C., Whitesell, L., Rogers, A.B. and Lindquist, S., 2007. Heat shock factor 1 is a powerful multifaceted modifier of carcinogenesis. *Cell*, 130(6), pp.1005-1018.
- Davidson, M.B., Katou, Y., Keszthelyi, A., Sing, T.L., Xia, T., Ou, J., Vaisica, J.A., Thevakumaran, N., Marjavaara, L., Myers, C.L. and Chabes, A., 2012. Endogenous DNA replication stress results in expansion of dNTP pools and a mutator phenotype. *The EMBO journal*, 31(4), pp.895-907.
- Davis, P.K., Ho, A. and Dowdy, S.F., 2001. Biological methods for cell-cycle synchronization of mammalian cells. *Biotechniques*, 30(6), pp.1322-1331.
- de Renty, C., DePamphilis, M.L. and Ullah, Z., 2014. Cytoplasmic localization of p21 protects trophoblast giant cells from DNA damage induced apoptosis. *PloS one*, 9(5), p.e97434.
- Delk, Nikki A., Kelly K. Hunt, and Khandan Keyomarsi. "Altered subcellular localization of tumor-specific cyclin E isoforms affects cyclin-dependent kinase 2 complex formation and proteasomal regulation." *Cancer research* 69, no. 7 (2009): 2817-2825.
- Den Hollander, P., Rayala, S.K., Coverley, D. and Kumar, R., 2006. CIZ1, a novel DNA-binding coactivator of the estrogen receptor α , confers hypersensitivity to estrogen action. *Cancer Research*, 66(22), pp.11021-11029.
- Deng, T., Yan, G., Song, X., Xie, L., Zhou, Y., Li, J., Hu, X., Li, Z., Hu, J., Zhang, Y. and Zhang, H., 2018. Deubiquitylation and stabilization of p21 by USP11 is critical for cell-cycle progression and DNA damage responses. *Proceedings of the National Academy of Sciences*, 115(18), pp.4678-4683.
- Dhar, M.K., Sehgal, S. and Kaul, S., 2012. Structure, replication efficiency and fragility of yeast ARS elements. *Research in microbiology*, 163(4), pp.243-253.
- Dillon, M.T., Barker, H.E., Pedersen, M., Hafsi, H., Bhide, S.A., Newbold, K.L., Nutting, C.M., McLaughlin, M. and Harrington, K.J., 2017. Radiosensitization by the ATR inhibitor AZD6738 through generation of acentric micronuclei. *Molecular cancer therapeutics*, 16(1), pp.25-34.
- Dong, P., Zhang, C., Parker, B.T., You, L. and Mathey-Prevot, B., 2018. Cyclin D/CDK4/6 activity controls G1 length in mammalian cells. *PloS one*, 13(1), p.e0185637.
- Dimova, D.K. and Dyson, N.J., 2005. The E2F transcriptional network: old acquaintances with new faces. *Oncogene*, 24(17), pp.2810-2826.
- Driedonks, T.A., 2019. Circulating Y-RNAs in extracellular vesicles and ribonucleoprotein complexes; implications for the immune system. *Frontiers in immunology*, 9, p.3164.
- Drury, L.S., Perkins, G. and Diffley, J.F., 1997. The Cdc4/34/53 pathway targets Cdc6p for proteolysis in budding yeast. *The EMBO journal*, 16(19), pp.5966-5976.
- Duan, R., Du, W. and Guo, W., 2020. EZH2: a novel target for cancer treatment. *Journal of Hematology & Oncology*, 13, pp.1-12.

- Dufke, C., Hauser, A.K., Sturm, M., Fluhr, S., Wächter, T., Leube, B., Auburger, G., Ott, T., Bauer, P., Gasser, T. and Grundmann, K., 2015. Mutations in *Clz1* are not a major cause for dystonia in Germany. *Movement Disorders*, 30(5), pp.740-743
- Duncker, B.P., 2017. Mechanisms governing DDK regulation of the initiation of DNA replication. *Genes*, 8(1), p.3.
- Dungrawala, H. and Cortez, D., 2015. Purification of proteins on newly synthesized DNA using iPOND. In *The Nucleus* (pp. 123-131). Humana Press, New York, NY.
- Edgell, D.R. and Doolittle, W.F., 1997. Archaea and the origin (s) of DNA replication proteins. *Cell*, 89(7), pp.995-998.
- El-Maouche, D., Merke, D.P., Vogiatzi, M.G., Chang, A.Y., Turcu, A.F., Joyal, E.G., Lin, V.H., Weintraub, L., Plaunt, M.R., Mohideen, P. and Auchus, R.J., 2020. A Phase 2, Multicenter Study of Nevanimibe for the Treatment of Congenital Adrenal Hyperplasia. *The Journal of Clinical Endocrinology & Metabolism*, 105(8), p.dgaa381.
- Engel, S.R., Dietrich, F.S., Fisk, D.G., Binkley, G., Balakrishnan, R., Costanzo, M.C., Dwight, S.S., Hitz, B.C., Karra, K., Nash, R.S. and Weng, S., 2014. The reference genome sequence of *Saccharomyces cerevisiae*: then and now. *G3: Genes, Genomes, Genetics*, 4(3), pp.389-398.
- Estefanía, M.M., Ganier, O., Hernández, P., Schwartzman, J.B., Mechali, M. and Krimer, D.B., 2012. DNA replication fading as proliferating cells advance in their commitment to terminal differentiation. *Scientific Reports*, 2, p.279.
- Estrada-Bernal, A., Chatterjee, M., Haque, S.J., Yang, L., Morgan, M.A., Kotian, S., Morrell, D., Chakravarti, A. and Williams, T.M., 2015. MEK inhibitor GSK1120212-mediated radiosensitization of pancreatic cancer cells involves inhibition of DNA double-strand break repair pathways. *Cell Cycle*, 14(23), pp.3713-3724.
- Fei, L. and Xu, H., 2018. Role of MCM2–7 protein phosphorylation in human cancer cells. *Cell & bioscience*, 8(1), p.43.
- Forment, J.V. and O'Connor, M.J., 2018. Targeting the replication stress response in cancer. *Pharmacology & therapeutics*, 188, pp.155-167.
- Frampton, J.E., 2015. Olaparib: a review of its use as maintenance therapy in patients with ovarian cancer. *BioDrugs*, 29(2), pp.143-150.
- Francica, P. and Rottenberg, S., 2018. Mechanisms of PARP inhibitor resistance in cancer and insights into the DNA damage response. *Genome medicine*, 10(1), pp.1-3.
- Gaillard, H., García-Muse, T. and Aguilera, A., 2015. Replication stress and cancer. *Nature Reviews Cancer*, 15(5), pp.276-289.
- Gandara, D.R., Hammerman, P.S., Sos, M.L., Lara, P.N. and Hirsch, F.R., 2015. Squamous cell lung cancer: from tumor genomics to cancer therapeutics.
- Ganier, O., Prorok, P., Akerman, I. and Méchali, M., 2019. Metazoan DNA replication origins. *Current Opinion in Cell Biology*, 58, pp.134-141.

- Gao, S., Xiong, J., Zhang, C., Berquist, B.R., Yang, R., Zhao, M., Molascon, A.J., Kwiatkowski, S.Y., Yuan, D., Qin, Z. and Wen, J., 2013. Impaired replication elongation in Tetrahymena mutants deficient in histone H3 Lys 27 monomethylation. *Genes & Development*, 27(15), pp.1662-1679.
- Gao, F., 2015. Bacteria may have multiple replication origins. *Frontiers in microbiology*, 6, p.324.
- Ge, X.Q., Jackson, D.A. and Blow, J.J., 2007. Dormant origins licensed by excess Mcm2–7 are required for human cells to survive replicative stress. *Genes & development*, 21(24), pp.3331-3341.
- Georgakilas, A.G., Martin, O.A. and Bonner, W.M., 2017. p21: a two-faced genome guardian. *Trends in molecular medicine*, 23(4), pp.310-319.
- Ghosh, S., Vassilev, A.P., Zhang, J., Zhao, Y. and DePamphilis, M.L., 2011. Assembly of the human origin recognition complex occurs through independent nuclear localization of its components. *Journal of Biological Chemistry*, 286(27), pp.23831-23841.
- Gibson, B., Wilson, D.J., Feil, E. and Eyre-Walker, A., 2018. The distribution of bacterial doubling times in the wild. *Proceedings of the Royal Society B: Biological Sciences*, 285(1880), p.20180789.
- Gladden, A.B. and Diehl, J.A., 2005. Location, location, location: the role of cyclin D1 nuclear localization in cancer. *Journal of cellular biochemistry*, 96(5), pp.906-913.
- Glanzer, J.G., Liu, S., Wang, L., Mosel, A., Peng, A. and Oakley, G.G., 2014. RPA inhibition increases replication stress and suppresses tumor growth. *Cancer research*, 74(18), pp.5165-5172.
- Glover, T.W., Wilson, T.E. and Arlt, M.F., 2017. Fragile sites in cancer: more than meets the eye. *Nature Reviews Cancer*, 17(8), p.489.
- Gómez-González, B. and Aguilera, A., 2019. Transcription-mediated replication hindrance: a major driver of genome instability. *Genes & development*, 33(15-16), pp.1008-1026.
- Gopinathan, L., Tan, S.L.W., Padmakumar, V.C., Coppola, V., Tessarollo, L. and Kaldis, P., 2014. Loss of Cdk2 and cyclin A2 impairs cell proliferation and tumorigenesis. *Cancer research*, 74(14), pp.3870-3879.
- Gottipati, P., Cassel, T.N., Savolainen, L. and Helleday, T., 2008. Transcription-associated recombination is dependent on replication in Mammalian cells. *Molecular and cellular biology*, 28(1), pp.154-164.
- Greaves, E.A., Copeland, N.A., Coverley, D. and Ainscough, J.F., 2012. Cancer-associated variant expression and interaction of CIZ1 with cyclin A1 in differentiating male germ cells. *Journal of cell science*, 125(10), pp.2466-2477.
- Greil, C., Krohs, J., Schnerch, D., Follo, M., Felthaus, J., Engelhardt, M. and Wäsch, R., 2016. The role of APC/C Cdh1 in replication stress and origin of genomic instability. *Oncogene*, 35(23), pp.3062-3070.

- Guo, H., Tian, T., Nan, K. and Wang, W., 2010. p57: A multifunctional protein in cancer. *International journal of oncology*, 36(6), pp.1321-1329.
- Gutiérrez-Escribano, P. and Nurse, P., 2015. A single cyclin–CDK complex is sufficient for both mitotic and meiotic progression in fission yeast. *Nature communications*, 6(1), pp.1-13.
- Hanahan, D. and Weinberg, R.A., 2000. The hallmarks of cancer. *cell*, 100(1), pp.57-70.
- Hégarat, N., Crncec, A., Suarez Peredo Rodriguez, M.F., Echegaray Iturra, F., Gu, Y., Busby, O., Lang, P.F., Barr, A.R., Bakal, C., Kanemaki, M.T. and Lamond, A.I., 2020. Cyclin A triggers Mitosis either via the Greatwall kinase pathway or Cyclin B. *The EMBO journal*, p.e104419.
- Heldt, F.S., Barr, A.R., Cooper, S., Bakal, C. and Novák, B., 2018. A comprehensive model for the proliferation–quiescence decision in response to endogenous DNA damage in human cells. *Proceedings of the National Academy of Sciences*, 115(10), pp.2532-2537.
- Higgins, G., Roper, K.M., Watson, I.J., Blackhall, F.H., Rom, W.N., Pass, H.I., Ainscough, J.F. and Coverley, D., 2012. Variant CIZ1 is a circulating biomarker for early-stage lung cancer. *Proceedings of the National Academy of Sciences*, 109(45), pp.E3128-E3135.
- Hinz, N. and Jücker, M., 2019. Distinct functions of AKT isoforms in breast cancer: a comprehensive review. *Cell Communication and Signaling*, 17(1), p.154.
- Hiraga, S.I., Monerawela, C., Katou, Y., Shaw, S., Clark, K.R., Shirahige, K. and Donaldson, A.D., 2018. Budding yeast Rif1 binds to replication origins and protects DNA at blocked replication forks. *EMBO reports*, 19(9), p.e46222.
- Hirao, A., Cheung, A., Duncan, G., Girard, P.M., Elia, A.J., Wakeham, A., Okada, H., Sarkissian, T., Wong, J.A., Sakai, T. and De Stanchina, E., 2002. Chk2 is a tumor suppressor that regulates apoptosis in both an ataxia telangiectasia mutated (ATM)-dependent and an ATM-independent manner. *Molecular and cellular biology*, 22(18), pp.6521-6532.
- Hoege, C., Pfander, B., Moldovan, G.L., Pyrowolakis, G. and Jentsch, S., 2002. RAD6-dependent DNA repair is linked to modification of PCNA by ubiquitin and SUMO. *Nature*, 419(6903), pp.135-141.
- Hook, S.S., Lin, J.J. and Dutta, A., 2007. Mechanisms to control rereplication and implications for cancer. *Current opinion in cell biology*, 19(6), pp.663-671.
- Hopkins, T.A., Ainsworth, W.B., Ellis, P.A., Donawho, C.K., DiGiammarino, E.L., Panchal, S.C., Abraham, V.C., Algire, M.A., Shi, Y., Olson, A.M. and Johnson, E.F., 2019. PARP1 trapping by PARP inhibitors drives cytotoxicity in both cancer cells and healthy bone marrow. *Molecular Cancer Research*, 17(2), pp.409-419.
- Huang, R.X. and Zhou, P.K., 2020. DNA damage response signaling pathways and targets for radiotherapy sensitization in cancer. *Signal Transduction and Targeted Therapy*, 5(1), pp.1-27.
- Hughes, B.T., Sidorova, J., Swanger, J., Monnat, R.J. and Clurman, B.E., 2013. Essential role for Cdk2 inhibitory phosphorylation during replication stress revealed by a human Cdk2 knockin mutation. *Proceedings of the National Academy of Sciences*, 110(22), pp.8954-8959.

- Jackman, M., Kubota, Y., Den Elzen, N., Hagting, A. and Pines, J., 2002. Cyclin A-and cyclin E-Cdk complexes shuttle between the nucleus and the cytoplasm. *Molecular biology of the cell*, 13(3), pp.1030-1045.
- Jackson, D.A. and Pombo, A., 1998. Replicon clusters are stable units of chromosome structure: evidence that nuclear organization contributes to the efficient activation and propagation of S phase in human cells. *The Journal of cell biology*, 140(6), pp.1285-1295.
- Jang, S.W., Jung, J.K. and Kim, J.M., 2016. Replication Protein A (RPA) deficiency activates the Fanconi anemia DNA repair pathway. *Cell Cycle*, 15(17), pp.2336-2345.
- Japaridze, A., Gogou, C., Kerssemakers, J.W., Nguyen, H.M. and Dekker, C., 2020. Direct observation of independently moving replisomes in Escherichia coli. *Nature communications*, 11(1), pp.1-10.
- Jazwinski, S.M. and Edelman, G.M., 1979. Replication in vitro of the 2-micrometer DNA plasmid of yeast. *Proceedings of the National Academy of Sciences*, 76(3), pp.1223-1227.
- Jones, R.M., Mortusewicz, O., Afzal, I., Lorvellec, M., Garcia, P., Helleday, T. and Petermann, E., 2013. Increased replication initiation and conflicts with transcription underlie Cyclin E-induced replication stress. *Oncogene*, 32(32), pp.3744-3753.
- Kalaszczynska, I., Geng, Y., Iino, T., Mizuno, S.I., Choi, Y., Kondratiuk, I., Silver, D.P., Wolgemuth, D.J., Akashi, K. and Sicinski, P., 2009. Cyclin A is redundant in fibroblasts but essential in hematopoietic and embryonic stem cells. *Cell*, 138(2), pp.352-365.
- Kawakami, H., Ohashi, E., Kanamoto, S., Tsurimoto, T. and Katayama, T., 2015. Specific binding of eukaryotic ORC to DNA replication origins depends on highly conserved basic residues. *Scientific reports*, 5, p.14929.
- Kaykov, A., Taillefumier, T., Bensimon, A. and Nurse, P., 2016. Molecular combing of single DNA molecules on the 10 megabase scale. *Scientific reports*, 6(1), pp.1-9.
- Keck, J.M., Summers, M.K., Tedesco, D., Ekholm-Reed, S., Chuang, L.C., Jackson, P.K. and Reed, S.I., 2007. Cyclin E overexpression impairs progression through mitosis by inhibiting APCdh1. *The Journal of cell biology*, 178(3), pp.371-385.
- Kelly, T. and Callegari, A.J., 2019. Dynamics of DNA replication in a eukaryotic cell. *Proceedings of the National Academy of Sciences*, 116(11), pp.4973-4982.
- Kelman, L.M. and Kelman, Z., 2018. Do archaea need an origin of replication?. *Trends in microbiology*, 26(3), pp.172-174.
- Khan, M.M., Xiao, J., Patel, D. and LeDoux, M.S., 2018. DNA damage and neurodegenerative phenotypes in aged CIZ1 null mice. *Neurobiology of aging*, 62, pp.180-190.
- Khot, A., Brajanovski, N., Cameron, D.P., Hein, N., Maclachlan, K.H., Sanij, E., Lim, J., Soong, J., Link, E., Blombery, P. and Thompson, E.R., 2019. First-in-human RNA polymerase I transcription inhibitor CX-5461 in patients with advanced hematologic cancers: Results of a phase I dose-escalation study. *Cancer discovery*, 9(8), pp.1036-1049.

- Khurana, S. and Oberdoerffer, P., 2015. Replication stress: a lifetime of epigenetic change. *Genes*, 6(3), pp.858-877.
- Kojo, H., Greenberg, B.D. and Sugino, A., 1981. Yeast 2-micrometer plasmid DNA replication in vitro: origin and direction. *Proceedings of the National Academy of Sciences*, 78(12), pp.7261-7265.
- Kotsantis, P., Silva, L.M., Irmscher, S., Jones, R.M., Folkes, L., Gromak, N. and Petermann, E., 2016. Increased global transcription activity as a mechanism of replication stress in cancer. *Nature communications*, 7(1), pp.1-13.
- Krude, T., Jackman, M., Pines, J. and Laskey, R.A., 1997. Cyclin/Cdk-dependent initiation of DNA replication in a human cell-free system. *Cell*, 88(1), pp.109-119.
- Krude, T., 1999. Mimosine arrests proliferating human cells before onset of DNA replication in a dose-dependent manner. *Experimental cell research*, 247(1), pp.148-159.
- Krude, T., 2000. Initiation of human DNA replication in vitro using nuclei from cells arrested at an initiation-competent state. *Journal of Biological Chemistry*, 275(18), pp.13699-13707.
- Krude, T., Christov, C.P., Hyrien, O. and Marheineke, K., 2009. Y RNA functions at the initiation step of mammalian chromosomal DNA replication. *Journal of cell science*, 122(16), pp.2836-2845.
- Kumar, R., Nagpal, G., Kumar, V., Usmani, S.S., Agrawal, P. and Raghava, G.P., 2019. HumCFS: a database of fragile sites in human chromosomes. *BMC genomics*, 19(9), p.985.
- Kushwaha, P.P., Rapalli, K.C. and Kumar, S., 2016. Geminin a multi task protein involved in cancer pathophysiology and developmental process: A review. *Biochimie*, 131, pp.115-127.
- Labit, H., Goldar, A., Guilbaud, G., Douarche, C., Hyrien, O. and Marheineke, K., 2008. A simple and optimized method of producing silanized surfaces for FISH and replication mapping on combed DNA fibers. *Biotechniques*, 45(6), pp.649-658.
- Laham-Karam, N., Pinto, G.P., Poso, A. and Kokkonen, P., 2020. Transcription and Translation Inhibitors in Cancer Treatment. *Frontiers in Chemistry*, 8.
- Lange, C. and Calegari, F., 2010. Cdks and cyclins link G1 length and differentiation of embryonic, neural and hematopoietic stem cells. *Cell cycle*, 9(10), pp.1893-1900.
- Laptenko, O., Beckerman, R., Freulich, E. and Prives, C., 2011. p53 binding to nucleosomes within the p21 promoter in vivo leads to nucleosome loss and transcriptional activation. *Proceedings of the National Academy of Sciences*, 108(26), pp.10385-10390.
- Laugesen, A., Højfeldt, J.W. and Helin, K., 2016. Role of the polycomb repressive complex 2 (PRC2) in transcriptional regulation and cancer. *Cold Spring Harbor perspectives in medicine*, 6(9), p.a026575.
- Lavado, A., Park, J.Y., Paré, J., Finkelstein, D., Pan, H., Xu, B., Fan, Y., Kumar, R.P., Neale, G., Kwak, Y.D. and McKinnon, P.J., 2018. The Hippo pathway prevents YAP/TAZ-driven

hypertranscription and controls neural progenitor number. *Developmental cell*, 47(5), pp.576-591.

Le Beau, M.M., Rassool, F.V., Neilly, M.E., Espinosa III, R., Glover, T.W., Smith, D.I. and McKeithan, T.W., 1998. Replication of a common fragile site, FRA3B, occurs late in S phase and is delayed further upon induction: implications for the mechanism of fragile site induction. *Human molecular genetics*, 7(4), pp.755-761.

Ledermann, J., Harter, P., Gourley, C., Friedlander, M., Vergote, I., Rustin, G., Scott, C.L., Meier, W., Shapira-Frommer, R., Safra, T. and Matei, D., 2014. Olaparib maintenance therapy in patients with platinum-sensitive relapsed serous ovarian cancer: a preplanned retrospective analysis of outcomes by BRCA status in a randomised phase 2 trial. *The lancet oncology*, 15(8), pp.852-861.

Lee, M.J., Byun, M.R., Furutani-Seiki, M., Hong, J.H. and Jung, H.S., 2014. YAP and TAZ regulate skin wound healing. *Journal of Investigative Dermatology*, 134(2), pp.518-525.

Lee, M.Y., Wang, X., Zhang, S., Zhang, Z. and Lee, E.Y., 2017. Regulation and modulation of human DNA polymerase δ activity and function. *Genes*, 8(7), p.190.

Léger, K., Hopp, A.K., Fey, M. and Hottiger, M.O., 2016. ARTD1 regulates cyclin E expression and consequently cell-cycle re-entry and G1/S progression in T24 bladder carcinoma cells. *Cell Cycle*, 15(15), pp.2042-2052.

Lei, L., Wu, J., Gu, D., Liu, H. and Wang, S., 2016. CIZ1 interacts with YAP and activates its transcriptional activity in hepatocellular carcinoma cells. *Tumor Biology*, 37(8), pp.11073-11079.

Leonard, A.C. and Méchali, M., 2013. DNA replication origins. *Cold Spring Harbor perspectives in biology*, 5(10), p.a010116.

Leslie, M., 2006. Cyclin localization controls activity. *The Journal of Cell Biology*, 172(7), pp.961-961.

Li, R., Waga, S., Hannon, G.J., Beach, D. and Stillman, B., 1994. Differential effects by the p21 CDK inhibitor on PCNA-dependent DNA replication and repair. *Nature*, 371(6497), pp.534-537.

Li, J., Meyer, A.N. and Donoghue, D.J., 1997. Nuclear localization of cyclin B1 mediates its biological activity and is regulated by phosphorylation. *Proceedings of the National Academy of Sciences*, 94(2), pp.502-507.

Li, Z., Zhao, B., Wang, P., Chen, F., Dong, Z., Yang, H., Guan, K.L. and Xu, Y., 2010. Structural insights into the YAP and TEAD complex. *Genes & development*, 24(3), pp.235-240.

Li, J., Deng, M., Wei, Q., Liu, T., Tong, X. and Ye, X., 2011. Phosphorylation of MCM3 protein by cyclin E/cyclin-dependent kinase 2 (Cdk2) regulates its function in cell cycle. *Journal of Biological Chemistry*, 286(46), pp.39776-39785.

Li, Z.F. and Lam, Y.W., 2015. A new rapid method for isolating nucleoli. In *The Nucleus* (pp. 35-42). Humana Press, New York, NY.

- Li, H. and O'Donnell, M.E., 2018. The eukaryotic CMG helicase at the replication fork: emerging architecture reveals an unexpected mechanism. *Bioessays*, 40(3), p.1700208.
- Li, Z., Pinch, B.J., Olson, C.M., Donovan, K.A., Nowak, R.P., Mills, C.E., Scott, D.A., Doctor, Z.M., Eleuteri, N.A., Chung, M. and Sorger, P.K., 2020. Development and characterization of a Wee1 kinase degrader. *Cell chemical biology*, 27(1), pp.57-65.
- Li, Y., Zhou, X., Liu, J., Gao, N., Yang, R., Wang, Q., Ji, J., Ma, L. and He, Q., 2020. Dihydroartemisinin inhibits the tumorigenesis and metastasis of breast cancer via downregulating CIZ1 expression associated with TGF- β 1 signaling. *Life Sciences*, 248, p.117454.
- Limas, J.C. and Cook, J.G., 2019. Preparation for DNA replication: the key to a successful S phase. *FEBS letters*, 593(20), pp.2853-2867.
- Lindahl, T., Landberg, G., Ahlgren, J., Nordgren, H., Norberg, T., Klaar, S., Holmberg, L. and Bergh, J., 2004. Overexpression of cyclin E protein is associated with specific mutation types in the p53 gene and poor survival in human breast cancer. *Carcinogenesis*, 25(3), pp.375-380.
- Lindqvist, A., 2010. Cyclin B–Cdk1 activates its own pump to get into the nucleus. *Journal of Cell Biology*, 189(2), pp.197-199.
- Liu, P., Barkley, L.R., Day, T., Bi, X., Slater, D.M., Alexandrow, M.G., Nasheuer, H.P. and Vaziri, C., 2006. The Chk1-mediated S-phase checkpoint targets initiation factor Cdc45 via a Cdc25A/Cdk2-independent mechanism. *Journal of Biological Chemistry*, 281(41), pp.30631-30644.
- Liu, T., Ren, X., Li, L., Yin, L., Liang, K., Yu, H., Ren, H., Zhou, W., Jing, H. and Kong, C., 2015. CIZ1 promotes tumorigenicity of prostate carcinoma cells. *Frontiers in bioscience (Landmark edition)*, 20, pp.705-715.
- Liu, Q., Niu, N., Wada, Y. and Liu, J., 2016. The role of Cdkn1A-interacting zinc finger protein 1 (CIZ1) in DNA replication and pathophysiology. *International journal of molecular sciences*, 17(2), p.212.
- Liu JC, Granieri L, Shrestha M, Wang DY, Vorobieva I, Rubie EA, Jones R, Ju Y, Pellecchia G, Jiang Z, Palmerini CA. Identification of CDC25 as a common therapeutic target for triple-negative breast cancer. *Cell reports*. 2018 Apr 3;23(1):112-26.
- Liu, J.Y., Souroullas, G.P., Diekman, B.O., Krishnamurthy, J., Hall, B.M., Sorrentino, J.A., Parker, J.S., Sessions, G.A., Gudkov, A.V. and Sharpless, N.E., 2019. Cells exhibiting strong p16INK4a promoter activation in vivo display features of senescence. *Proceedings of the National Academy of Sciences*, 116(7), pp.2603-2611.
- Llobet, S.G., van der Vegt, B., Jongeneel, E., Bense, R.D., Schröder, C.P., Everts, M., de Bock, G.H. and van Vugt, M.A., 2019. Cyclin E expression is associated with high levels of replication stress in triple-negative breast cancer. *bioRxiv*, p.532283.
- Lohka, M.J. and Masui, Y., 1983. Formation in vitro of sperm pronuclei and mitotic chromosomes induced by amphibian ooplasmic components. *Science*, 220(4598), pp.719-721.

- Lohka, M.J. and Masui, Y., 1984. Effects of Ca²⁺ ions on the formation of metaphase chromosomes and sperm pronuclei in cell-free preparations from unactivated *Rana pipiens* eggs. *Developmental biology*, 103(2), pp.434-442.
- Lohka, M.J. and Masui, Y., 1984. Roles of cytosol and cytoplasmic particles in nuclear envelope assembly and sperm pronuclear formation in cell-free preparations from amphibian eggs. *The Journal of cell biology*, 98(4), pp.1222-1230.
- Lopez, P., Philippe, H., Myllykallio, H. and Forterre, P., 1999. Identification of putative chromosomal origins of replication in Archaea. *Molecular microbiology*, 32(4), pp.883-886.
- Lu, X., Liu, J. and Legerski, R.J., 2009. Cyclin E is stabilized in response to replication fork barriers leading to prolonged S phase arrest. *Journal of Biological Chemistry*, 284(51), pp.35325-35337.
- Lukas, J., Herzinger, T., Hansen, K., Moroni, M.C., Resnitzky, D., Helin, K., Reed, S.I. and Bartek, J., 1997. Cyclin E-induced S phase without activation of the pRb/E2F pathway. *Genes & Development*, 11(11), pp.1479-1492.
- Luo, H. and Gao, F., 2019. DoriC 10.0: an updated database of replication origins in prokaryotic genomes including chromosomes and plasmids. *Nucleic acids research*, 47(D1), pp.D74-D77.
- Luo, X., Huang, Y. and Sheikh, M.S., 2003. Cloning and characterization of a novel gene PDRG that is differentially regulated by p53 and ultraviolet radiation. *Oncogene*, 22(46), pp.7247-7257.
- Ma, Y., McKay, D.J. and Buttitta, L., 2018. The coordination of terminal differentiation and cell cycle exit is mediated through the regulation of chromatin accessibility. *bioRxiv*, p.488387.
- Macheret, M. and Halazonetis, T.D., 2015. DNA replication stress as a hallmark of cancer. *Annual Review of Pathology: Mechanisms of Disease*, 10, pp.425-448.
- Macheret, M. and Halazonetis, T.D., 2018. Intragenic origins due to short G1 phases underlie oncogene-induced DNA replication stress. *Nature*, 555(7694), pp.112-116.
- Macip, S., Igarashi, M., Fang, L., Chen, A., Pan, Z.Q., Lee, S.W. and Aaronson, S.A., 2002. Inhibition of p21-mediated ROS accumulation can rescue p21-induced senescence. *The EMBO journal*, 21(9), pp.2180-2188.
- Mackiewicz, P., Zakrzewska-Czerwińska, J., Zawilak, A., Dudek, M.R. and Cebrat, S., 2004. Where does bacterial replication start? Rules for predicting the oriC region. *Nucleic acids research*, 32(13), pp.3781-3791.
- Madabhushi, R., Pan, L. and Tsai, L.H., 2014. DNA damage and its links to neurodegeneration. *Neuron*, 83(2), pp.266-282.
- Mailand, N. and Diffley, J.F., 2005. CDKs promote DNA replication origin licensing in human cells by protecting Cdc6 from APC/C-dependent proteolysis. *Cell*, 122(6), pp.915-926.

- Marraffini, L.A. and Sontheimer, E.J., 2008. CRISPR interference limits horizontal gene transfer in staphylococci by targeting DNA. *science*, 322(5909), pp.1843-1845.
- Maugeri-Saccà, M., Bartucci, M. and De Maria, R., 2013. Checkpoint kinase 1 inhibitors for potentiating systemic anticancer therapy. *Cancer treatment reviews*, 39(5), pp.525-533.
- Mahadevappa, R., Neves, H., Yuen, S.M., Bai, Y., McCrudden, C.M., Yuen, H.F., Wen, Q., Zhang, S.D. and Kwok, H.F., 2017. The prognostic significance of Cdc6 and Cdt1 in breast cancer. *Scientific reports*, 7(1), pp.1-11.
- Mailand, N., Gibbs-Seymour, I. and Bekker-Jensen, S., 2013. Regulation of PCNA–protein interactions for genome stability. *Nature reviews Molecular cell biology*, 14(5), pp.269-282.
- Mao, Z., Bozzella, M., Seluanov, A. and Gorbunova, V., 2008. Comparison of nonhomologous end joining and homologous recombination in human cells. *DNA repair*, 7(10), pp.1765-1771.
- Marcel, V., Catez, F. and Diaz, J.J., 2015. p53, a translational regulator: contribution to its tumour-suppressor activity. *Oncogene*, 34(44), pp.5513-5523.
- Maréchal, A. and Zou, L., 2015. RPA-coated single-stranded DNA as a platform for post-translational modifications in the DNA damage response. *Cell research*, 25(1), pp.9-23.
- Marheineke, K., Hyrien, O. and Krude, T., 2005. Visualization of bidirectional initiation of chromosomal DNA replication in a human cell free system. *Nucleic acids research*, 33(21), pp.6931-6941.
- Marheineke, K., Goldar, A., Krude, T. and Hyrien, O., 2009. Use of DNA Combing to Study DNA Replication in Xenopus and Human Cell-Free Systems. In *DNA Replication* (pp. 575-603). Humana Press.
- Marriott, A.S., Copeland, N.A., Cunningham, R., Wilkinson, M.C., McLennan, A.G. and Jones, N.J., 2015. Diadenosine 5', 5'''-P1, P4-tetraphosphate (Ap4A) is synthesized in response to DNA damage and inhibits the initiation of DNA replication. *DNA repair*, 33, pp.90-100.
- Martín-Caballero, J., Flores, J.M., García-Palencia, P. and Serrano, M., 2001. Tumor susceptibility of p21Waf1/Cip1-deficient mice. *Cancer research*, 61(16), pp.6234-6238.
- Matson, J.P., Dumitru, R., Coryell, P., Baxley, R.M., Chen, W., Twaroski, K., Webber, B.R., Tolar, J., Bielinsky, A.K., Purvis, J.E. and Cook, J.G., 2017. Rapid DNA replication origin licensing protects stem cell pluripotency. *Elife*, 6, p.e30473.
- Matson, J.P., House, A.M., Grant, G.D., Wu, H., Perez, J. and Cook, J.G., 2019. Intrinsic checkpoint deficiency during cell cycle re-entry from quiescence. *Journal of Cell Biology*, 218(7), pp.2169-2184.
- Maule, G., Casini, A., Montagna, C., Ramalho, A.S., De Boeck, K., Debyser, Z., Carlon, M.S., Petris, G. and Cereseto, A., 2019. Allele specific repair of splicing mutations in cystic fibrosis through AsCas12a genome editing. *Nature communications*, 10(1), pp.1-11.
- Maya-Mendoza, A., Ostrakova, J., Kosar, M., Hall, A., Duskova, P., Mistrik, M., Merchut-Maya, J.M., Hodny, Z., Bartkova, J., Christensen, C. and Bartek, J., 2015. Myc and Ras oncogenes

- engage different energy metabolism programs and evoke distinct patterns of oxidative and DNA replication stress. *Molecular oncology*, 9(3), pp.601-616.
- Mazouzi, A., Velimezi, G. and Loizou, J.I., 2014. DNA replication stress: causes, resolution and disease. *Experimental cell research*, 329(1), pp.85-93.
- McCulloch, S.D. and Kunkel, T.A., 2008. The fidelity of DNA synthesis by eukaryotic replicative and translesion synthesis polymerases. *Cell research*, 18(1), pp.148-161.
- McDermott, N., Buechelmaier, E.S. and Powell, S.N., 2019. Capitalizing on Cancer Replication Stress by Preventing PAR Chain Turnover: A New Type of Synthetic Lethality. *Cancer cell*, 35(3), pp.344-346.
- McIntosh, D. and Blow, J.J., 2012. Dormant origins, the licensing checkpoint, and the response to replicative stresses. *Cold Spring Harbor perspectives in biology*, 4(10), p.a012955.
- Méchali, M., 2010. Eukaryotic DNA replication origins: many choices for appropriate answers. *Nature reviews Molecular cell biology*, 11(10), pp.728-738.
- Melixetian, M., Ballabeni, A., Masiero, L., Gasparini, P., Zamponi, R., Bartek, J., Lukas, J. and Helin, K., 2004. Loss of Geminin induces rereplication in the presence of functional p53. *The Journal of cell biology*, 165(4), pp.473-482.
- Merrick, C.J., Jackson, D. and Diffley, J.F., 2004. Visualization of altered replication dynamics after DNA damage in human cells. *Journal of Biological Chemistry*, 279(19), pp.20067-20075.
- Michalet, X., Ekong, R., Fougerousse, F., Rousseaux, S., Schurra, C., Hornigold, N., Van Slegtenhorst, M., Wolfe, J., Povey, S., Beckmann, J.S. and Bensimon, A., 1997. Dynamic molecular combing: stretching the whole human genome for high-resolution studies. *Science*, 277(5331), pp.1518-1523.
- Miki, Y., Swensen, J., Shattuck-Eidens, D., Futreal, P.A., Harshman, K., Tavtigian, S., Liu, Q., Cochran, C., Bennett, L.M. and Ding, W., 1994. A strong candidate for the breast and ovarian cancer susceptibility gene BRCA1. *Science*, 266(5182), pp.66-71.
- Miller, M.S. and Miller, L.D., 2012. RAS mutations and oncogenesis: not all RAS mutations are created equally. *Frontiers in genetics*, 2, p.100.
- Mitsui, K., Matsumoto, A., Ohtsuka, S., Ohtsubo, M. and Yoshimura, A., 1999. Cloning and characterization of a novel p21cip1/waf1-interacting zinc finger protein, CIZ1. *Biochemical and biophysical research communications*, 264(2), pp.457-464.
- Mohanta, T.K. and Bae, H., 2015. The diversity of fungal genome. *Biological procedures online*, 17(1), p.8.
- Moiseeva, T.N., Qian, C., Sugitani, N., Osmanbeyoglu, H.U. and Bakkenist, C.J., 2019. WEE1 kinase inhibitor AZD1775 induces CDK1 kinase-dependent origin firing in unperturbed G1- and S-phase cells. *Proceedings of the National Academy of Sciences*, 116(48), pp.23891-23893.
- Moiseeva, T.N., Yin, Y., Calderon, M.J., Qian, C., Schamus-Haynes, S., Sugitani, N., Osmanbeyoglu, H.U., Rothenberg, E., Watkins, S.C. and Bakkenist, C.J., 2019. An ATR and

CHK1 kinase signaling mechanism that limits origin firing during unperturbed DNA replication. *Proceedings of the National Academy of Sciences*, 116(27), pp.13374-13383.

Mol, P.R. and Balan, A., 2013. Oncogenes as Therapeutic Targets in Cancer: A Review. *IOSR J. Dent. Med. Sci*, 5, pp.46-56.

Montagnoli, A., Valsasina, B., Croci, V., Menichincheri, M., Rainoldi, S., Marchesi, V., Tibolla, M., Tenca, P., Brotherton, D., Albanese, C. and Patton, V., 2008. A Cdc7 kinase inhibitor restricts initiation of DNA replication and has antitumor activity. *Nature chemical biology*, 4(6), pp.357-365.

Morales, J., Li, L., Fattah, F.J., Dong, Y., Bey, E.A., Patel, M., Gao, J. and Boothman, D.A., 2014. Review of poly (ADP-ribose) polymerase (PARP) mechanisms of action and rationale for targeting in cancer and other diseases. *Critical Reviews™ in Eukaryotic Gene Expression*, 24(1).

Moritani, M. and Ishimi, Y., 2013. Inhibition of DNA binding of MCM2-7 complex by phosphorylation with cyclin-dependent kinases. *The Journal of Biochemistry*, 154(4), pp.363-372.

Moroishi, T., Hansen, C.G. and Guan, K.L., 2015. The emerging roles of YAP and TAZ in cancer. *Nature Reviews Cancer*, 15(2), pp.73-79.

Moser, J., Miller, I., Carter, D. and Spencer, S.L., 2018. Control of the Restriction Point by Rb and p21. *Proceedings of the National Academy of Sciences*, 115(35), pp.E8219-E8227.

Murga, M., Campaner, S., Lopez-Contreras, A.J., Toledo, L.I., Soria, R., Montaña, M.F., D'artista, L., Schleker, T., Guerra, C., Garcia, E. and Barbacid, M., 2011. Exploiting oncogene-induced replicative stress for the selective killing of Myc-driven tumors. *Nature structural & molecular biology*, 18(12), p.1331.

Müller, C.A., Hawkins, M., Retkute, R., Malla, S., Wilson, R., Blythe, M.J., Nakato, R., Komata, M., Shirahige, K., de Moura, A.P. and Nieduszynski, C.A., 2014. The dynamics of genome replication using deep sequencing. *Nucleic Acids Research*, 42(1), pp.e3-e3.

Munkley, J., Copeland, N.A., Moignard, V., Knight, J.R., Greaves, E., Ramsbottom, S.A., Pownall, M.E., Southgate, J., Ainscough, J.F.X. and Coverley, D., 2011. Cyclin E is recruited to the nuclear matrix during differentiation, but is not recruited in cancer cells. *Nucleic acids research*, 39(7), pp.2671-2677.

Muñoz, S., Búa, S., Rodríguez-Acebes, S., Megías, D., Ortega, S., de Martino, A. and Méndez, J., 2017. In Vivo DNA Re-replication elicits lethal tissue dysplasias. *Cell reports*, 19(5), pp.928-938.

National Institute of Health¹, 2020, Phase II Trial of AZD6738 Alone and in Combination With Olaparib, National Institute of Health, view 20 May 2020, <https://clinicaltrials.gov/ct2/show/NCT03682289>>

National Institute of Health², 2020, Trial of M4344 and Niraparib in Patients With Poly (ADP-ribose) Polymerase (PARP) Resistant Recurrent Ovarian Cancer (PARP), National Institute of Health, view 20 May 2020, <<https://clinicaltrials.gov/ct2/show/NCT04149145>>

- National Institute of Health³, 2020, ATRi Transition Rollover Study, National Institute of Health, view 20 May 2020, <<https://clinicaltrials.gov/ct2/show/NCT03309150>>
- Nazareth, D., Jones, M.J. and Gabrielli, B., 2019. Everything in Moderation: Lessons Learned by Exploiting Moderate Replication Stress in Cancer. *Cancers*, 11(9), p.1320.
- Nazari, Z.E. and Gurevich, L., 2013. Molecular Combing of DNA: Methods and Applications. *Journal of Self-assembly and Molecular Electronics (same)*, 1(1), pp.125-148.
- NICE¹ 2020, Cytarabine, Nice, viewed 1 July 2020, <<https://bnf.nice.org.uk/drug/cytarabine.html>>
- NICE² 2020, Cisplatin, Nice, viewed 1 July 2020, <<https://bnf.nice.org.uk/drug/cisplatin.html>>
- NICE³ 2020, Doxorubicin Hydrochloride, Nice, viewed 1 July 2020, <<https://bnf.nice.org.uk/drug/doxorubicin-hydrochloride.html>>
- Nickerson, J.A., Krockmalnic, G., Wan, K.M. and Penman, S., 1997. The nuclear matrix revealed by eluting chromatin from a cross-linked nucleus. *Proceedings of the National Academy of Sciences*, 94(9), pp.4446-4450.
- Nie, L., Wei, Y., Zhang, F., Hsu, Y.H., Chan, L.C., Xia, W., Ke, B., Zhu, C., Deng, R., Tang, J. and Yao, J., 2019. CDK2-mediated site-specific phosphorylation of EZH2 drives and maintains triple-negative breast cancer. *Nature communications*, 10(1), pp.1-15.
- Nieminuszczy, J., Schwab, R.A. and Niedzwiedz, W., 2016. The DNA fibre technique—tracking helicases at work. *Methods*, 108, pp.92-98.
- Nishibe, R., Watanabe, W., Ueda, T., Yamasaki, N., Koller, R., Wolff, L., Honda, Z.I., Ohtsubo, M. and Honda, H., 2013. CIZ1, a p21Cip1/Waf1-interacting protein, functions as a tumor suppressor in vivo. *FEBS letters*, 587(10), pp.1529-1535.
- Nitiss, J.L., 2009. Targeting DNA topoisomerase II in cancer chemotherapy. *Nature Reviews Cancer*, 9(5), pp.338-350.
- Nombela, P., Lozano, R., Aytes, A., Mateo, J., Olmos, D. and Castro, E., 2019. BRCA2 and other DDR genes in prostate cancer. *Cancers*, 11(3), p.352.
- Noordermeer, S.M. and van Attikum, H., 2019. PARP inhibitor resistance: a tug-of-war in BRCA-mutated cells. *Trends in cell biology*, 29(10), pp.820-834.
- Oehlmann, M., Score, A.J. and Blow, J.J., 2004. The role of Cdc6 in ensuring complete genome licensing and S phase checkpoint activation. *The Journal of cell biology*, 165(2), pp.181-190.
- Ohkoshi, S., Yano, M. and Matsuda, Y., 2015. Oncogenic role of p21 in hepatocarcinogenesis suggests a new treatment strategy. *World journal of gastroenterology*, 21(42), p.12150.
- Olivier, M., Hollstein, M. and Hainaut, P., 2010. TP53 mutations in human cancers: origins, consequences, and clinical use. *Cold Spring Harbor perspectives in biology*, 2(1), p.a001008.

- O'Neil, N.J., Bailey, M.L. and Hieter, P., 2017. Synthetic lethality and cancer. *Nature Reviews Genetics*, 18(10), pp.613-623.
- Örd, M., Möll, K., Agerova, A., Kivi, R., Faustova, I., Venta, R., Valk, E. and Loog, M., 2019. Multisite phosphorylation code of CDK. *Nature structural & molecular biology*, 26(7), pp.649-658.
- Oren, M. and Rotter, V., 2010. Mutant p53 gain-of-function in cancer. *Cold Spring Harbor perspectives in biology*, 2(2), p.a001107.
- Papouli, E., Chen, S., Davies, A.A., Huttner, D., Krejci, L., Sung, P. and Ulrich, H.D., 2005. Crosstalk between SUMO and ubiquitin on PCNA is mediated by recruitment of the helicase Srs2p. *Molecular cell*, 19(1), pp.123-133.
- Park, S.Y., Im, J.S., Park, S.R., Kim, S.E., Wang, H.J. and Lee, J.K., 2012. Mimosine arrests the cell cycle prior to the onset of DNA replication by preventing the binding of human Ctf4/And-1 to chromatin via Hif-1 α activation in HeLa cells. *Cell Cycle*, 11(4), pp.761-766.
- Parra, I. and Windle, B., 1993. High resolution visual mapping of stretched DNA by fluorescent hybridization. *Nature genetics*, 5(1), pp.17-21.
- Pateras, I.S., Apostolopoulou, K., Niforou, K., Kotsinas, A. and Gorgoulis, V.G., 2009. p57KIP2: "Kip" ing the cell under control. *Molecular Cancer Research*, 7(12), pp.1902-1919.
- Patil, S., Majumdar, B., Awan, K.H., Sarode, G.S., Sarode, S.C., Gadbail, A.R. and Gondivkar, S., 2018. Cancer oriented biobanks: A comprehensive review. *Oncology reviews*, 12(1).
- Pauzaitė, T., Thacker, U., Tollitt, J. and Copeland, N.A., 2017. Emerging roles for CIZ1 in cell cycle regulation and as a driver of tumorigenesis. *Biomolecules*, 7(1), p.1.
- Pernas, S., Tolaney, S.M., Winer, E.P. and Goel, S., 2018. CDK4/6 inhibition in breast cancer: current practice and future directions. *Therapeutic advances in medical oncology*, 10, p.1758835918786451.
- Petermann, E., Maya-Mendoza, A., Zachos, G., Gillespie, D.A., Jackson, D.A. and Caldecott, K.W., 2006. Chk1 requirement for high global rates of replication fork progression during normal vertebrate S phase. *Molecular and cellular biology*, 26(8), pp.3319-3326.
- Petermann, E., Helleday, T. and Caldecott, K.W., 2008. Claspin promotes normal replication fork rates in human cells. *Molecular biology of the cell*, 19(6), pp.2373-2378.
- Petropoulos, M., Tsaniras, S.C., Taraviras, S. and Lygerou, Z., 2019. Replication licensing aberrations, replication stress, and genomic instability. *Trends in biochemical sciences*, 44(9), pp.752-764.
- Piovesan, A., Pelleri, M.C., Antonaros, F., Strippoli, P., Caracausi, M. and Vitale, L., 2019. On the length, weight and GC content of the human genome. *BMC research notes*, 12(1), p.106.
- Piunti, A., Rossi, A., Cerutti, A., Albert, M., Jammula, S., Scelfo, A., Cedrone, L., Fragola, G., Olsson, L., Koseki, H. and Testa, G., 2014. Polycomb proteins control proliferation and

transformation independently of cell cycle checkpoints by regulating DNA replication. *Nature communications*, 5(1), pp.1-14.

Planas-Silva, M.D. and Weinberg, R.A., 1997. Estrogen-dependent cyclin E-cdk2 activation through p21 redistribution. *Molecular and Cellular Biology*, 17(7), pp.4059-4069.

Platel, M., Goldar, A., Wiggins, J.M., Barbosa, P., Libeau, P., Priam, P., Narassimprakash, H., Grodzinski, X. and Marheineke, K., 2015. Tight Chk1 levels control replication cluster activation in *Xenopus*. *PloS one*, 10(6).

Pond, K.W., de Renty, C., Yagle, M.K. and Ellis, N.A., 2019. Rescue of collapsed replication forks is dependent on NSMCE2 to prevent mitotic DNA damage. *PLoS genetics*, 15(2), p.e1007942.

Prado, F. and Aguilera, A., 2005. Impairment of replication fork progression mediates RNA polIII transcription-associated recombination. *The EMBO journal*, 24(6), pp.1267-1276.

Prieur, A. and Peeper, D.S., 2008. Cellular senescence in vivo: a barrier to tumorigenesis. *Current opinion in cell biology*, 20(2), pp.150-155.

Primo, L.M. and Teixeira, L.K., 2020. DNA replication stress: oncogenes in the spotlight. *Genetics and Molecular Biology*, 43(1).

Qian, Y. and Chen, X., 2013. Senescence regulation by the p53 protein family. In *Cell Senescence* (pp. 37-61). Humana Press, Totowa, NJ.

Qie, S. and Diehl, J.A., 2016. Cyclin D1, cancer progression, and opportunities in cancer treatment. *Journal of Molecular Medicine*, 94(12), pp.1313-1326.

Qie, S. and Diehl, J.A., 2020, January. Cyclin D degradation by E3 ligases in cancer progression and treatment. In *Seminars in Cancer Biology*. Academic Press.

Quinet, A., Lemaçon, D. and Vindigni, A., 2017. Replication fork reversal: players and guardians. *Molecular cell*, 68(5), pp.830-833.

Quintás-Cardama, A. and Cortes, J., 2009. Molecular biology of bcr-abl1–positive chronic myeloid leukemia. *Blood*, 113(8), pp.1619-1630.

Rahman, F.A., Aziz, N. and Coverley, D., 2010. Differential detection of alternatively spliced variants of CIZ1 in normal and cancer cells using a custom exon-junction microarray. *BMC cancer*, 10(1), p.482.

Rao, P.N. and Johnson, R.T., 1970. Mammalian cell fusion: studies on the regulation of DNA synthesis and mitosis. *Nature*, 225(5228), pp.159-164.

Ren, B., Cam, H., Takahashi, Y., Volkert, T., Terragni, J., Young, R.A. and Dynlacht, B.D., 2002. E2F integrates cell cycle progression with DNA repair, replication, and G2/M checkpoints. *Genes & development*, 16(2), pp.245-256.

Resnitzky, D., Gossen, M., Bujard, H. and Reed, S.I., 1994. Acceleration of the G1/

S phase transition by expression of cyclins D1 and E with an inducible system. *Molecular and cellular biology*, 14(3), pp.1669-1679.

Rhind, N. and Gilbert, D.M., 2013. DNA replication timing. *Cold Spring Harbor perspectives in biology*, 5(8), p.a010132.

Ribeyre, C., Lebby, R., Patouillard, J., Larroque, M., Abou-Merhi, R., Larroque, C. and Constantinou, A., 2020. The isolation of proteins on nascent DNA (iPOND) reveals a role for RIF1 in the organization of replication factories. *bioRxiv*, p.669234.

Richmond, C.A., Shah, M.S., Carlone, D.L. and Breault, D.T., 2016. An enduring role for quiescent stem cells. *Developmental Dynamics*, 245(7), pp.718-726.

Ridings-Figueroa, R., Stewart, E.R., Nesterova, T.B., Coker, H., Pintacuda, G., Godwin, J., Wilson, R., Haslam, A., Lilley, F., Ruigrok, R. and Bageghni, S.A., 2017. The nuclear matrix protein CIZ1 facilitates localization of Xist RNA to the inactive X-chromosome territory. *Genes & development*, 31(9), pp.876-888.

Rivera-Mulia, J.C., Dimond, A., Vera, D., Trevilla-Garcia, C., Sasaki, T., Zimmerman, J., Dupont, C., Gribnau, J., Fraser, P. and Gilbert, D.M., 2018. Allele-specific control of replication timing and genome organization during development. *Genome research*, 28(6), pp.800-811.

Rivin, C.J. and Fangman, W.L., 1980. Replication fork rate and origin activation during the S phase of *Saccharomyces cerevisiae*. *The Journal of cell biology*, 85(1), pp.108-115.

Rivlin, N., Brosh, R., Oren, M. and Rotter, V., 2011. Mutations in the p53 tumor suppressor gene: important milestones at the various steps of tumorigenesis. *Genes & cancer*, 2(4), pp.466-474.

Rizzardi, L.F. and Cook, J.G., 2012. Flipping the switch from g1 to s phase with e3 ubiquitin ligases. *Genes & Cancer*, 3(11-12), pp.634-648.

Robinson, N.P. and Bell, S.D., 2005. Origins of DNA replication in the three domains of life. *The FEBS journal*, 272(15), pp.3757-3766.

Rodriguez, R. and Meuth, M., 2006. Chk1 and p21 cooperate to prevent apoptosis during DNA replication fork stress. *Molecular biology of the cell*, 17(1), pp.402-412.

Rodriguez-Acebes, S., Mourón, S. and Méndez, J., 2018. Uncoupling fork speed and origin activity to identify the primary cause of replicative stress phenotypes. *Journal of Biological Chemistry*, 293(33), pp.12855-12861.

Rossari, F., Minutolo, F. and Orciuolo, E., 2018. Past, present, and future of Bcr-Abl inhibitors: from chemical development to clinical efficacy. *Journal of hematology & oncology*, 11(1), p.84.

Roszbach, D. and Sclafani, R.A., 2016. Role of DDK in replication initiation. In *The Initiation of DNA Replication in Eukaryotes* (pp. 279-296). Springer, Cham.

Roy, R., Chun, J. and Powell, S.N., 2012. BRCA1 and BRCA2: different roles in a common pathway of genome protection. *Nature Reviews Cancer*, 12(1), pp.68-78.

- Rynearson, A.L. and Sussman, C.R., 2011. Nuclear structure, organization, and oncogenesis. *Journal of gastrointestinal cancer*, 42(2), pp.112-117.
- Sale, J.E., 2013. Translesion DNA synthesis and mutagenesis in eukaryotes. *Cold Spring Harbor perspectives in biology*, 5(3), p.a012708.
- Santocanale, C., Sharma, K. and Diffley, J.F., 1999. Activation of dormant origins of DNA replication in budding yeast. *Genes & development*, 13(18), pp.2360-2364.
- Scully, R. and Livingston, D.M., 2000. In search of the tumour-suppressor functions of BRCA1 and BRCA2. *Nature*, 408(6811), pp.429-432.
- Semmler, L., Reiter-Brennan, C. and Klein, A., 2019. BRCA1 and breast cancer: a review of the underlying mechanisms resulting in the tissue-specific tumorigenesis in mutation carriers. *Journal of breast cancer*, 22(1), pp.1-14.
- Semple, J.W., Da-Silva, L.F., Jervis, E.J., Ah-Kee, J., Al-Attar, H., Kummer, L., Heikkila, J.J., Pasero, P. and Duncker, B.P., 2006. An essential role for Orc6 in DNA replication through maintenance of pre-replicative complexes. *The EMBO journal*, 25(21), pp.5150-5158.
- Sen, T., Tong, P., Diao, L., Li, L., Fan, Y., Hoff, J., Heymach, J.V., Wang, J. and Byers, L.A., 2017. Targeting AXL and mTOR pathway overcomes primary and acquired resistance to WEE1 inhibition in small-cell lung cancer. *Clinical Cancer Research*, 23(20), pp.6239-6253.
- Shajani-Yi, Z., de Abreu, F.B., Peterson, J.D. and Tsongalis, G.J., 2018. Frequency of Somatic TP53 Mutations in Combination with Known Pathogenic Mutations in Colon Adenocarcinoma, Non-Small Cell Lung Carcinoma, and Gliomas as Identified by Next-Generation Sequencing. *Neoplasia*, 20(3), pp.256-262.
- Sheu, Y.J. and Stillman, B., 2006. Cdc7-Dbf4 phosphorylates MCM proteins via a docking site-mediated mechanism to promote S phase progression. *Molecular cell*, 24(1), pp.101-113.
- Sishc, B.J. and Davis, A.J., 2017. The role of the core non-homologous end joining factors in carcinogenesis and cancer. *Cancers*, 9(7), p.81.
- Sideridou, M., Zakopoulou, R., Evangelou, K., Lontos, M., Kotsinas, A., Rampakakis, E., Gagos, S., Kahata, K., Grabusic, K., Gkouskou, K. and Trougakos, I.P., 2011. Cdc6 expression represses E-cadherin transcription and activates adjacent replication origins. *Journal of Cell Biology*, 195(7), pp.1123-1140.
- Simon, A.C., Sannino, V., Costanzo, V. and Pellegrini, L., 2016. Structure of human Cdc45 and implications for CMG helicase function. *Nature communications*, 7, p.11638.
- Solimini, N.L., Luo, J. and Elledge, S.J., 2007. Non-oncogene addiction and the stress phenotype of cancer cells. *Cell*, 130(6), pp.986-988.
- Spencer, S.L., Cappell, S.D., Tsai, F.C., Overton, K.W., Wang, C.L. and Meyer, T., 2013. The proliferation-quiescence decision is controlled by a bifurcation in CDK2 activity at mitotic exit. *Cell*, 155(2), pp.369-383.

Speck, C. and Messer, W., 2001. Mechanism of origin unwinding: sequential binding of DnaA to double- and single-stranded DNA. *The EMBO journal*, 20(6), pp.1469-1476.

Srinivasan, S.V., Dominguez-Sola, D., Wang, L.C., Hyrien, O. and Gautier, J., 2013. Cdc45 is a critical effector of myc-dependent DNA replication stress. *Cell reports*, 3(5), pp.1629-1639.

Stepankiw, N., Kaidow, A., Boye, E. and Bates, D., 2009. The right half of the Escherichia coli replication origin is not essential for viability, but facilitates multi-forked replication. *Molecular microbiology*, 74(2), pp.467-479.

Stern, B. and Nurse, P., 1996. A quantitative model for the cdc2 control of S phase and mitosis in fission yeast. *Trends in Genetics*, 12(9), pp.345-350.

Strausfeld, U.P., Howell, M., Descombes, P., Chevalier, S., Rempel, R.E., Adamczewski, J., Maller, J.L., Hunt, T. and Blow, J.J., 1996. Both cyclin A and cyclin E have S-phase promoting (SPF) activity in Xenopus egg extracts. *Journal of cell science*, 109(6), pp.1555-1563.

Stern, B. and Nurse, P., 1996. A quantitative model for the cdc2 control of S phase and mitosis in fission yeast. *Trends in Genetics*, 12(9), pp.345-350.

Sunwoo, H., Colognori, D., Froberg, J.E., Jeon, Y. and Lee, J.T., 2017. Repeat E anchors Xist RNA to the inactive X chromosomal compartment through CDKN1A-interacting protein (CIZ1). *Proceedings of the National Academy of Sciences*, 114(40), pp.10654-10659.

Suryadinata, R., Sadowski, M. and Sarcevic, B., 2010. Control of cell cycle progression by phosphorylation of cyclin-dependent kinase (CDK) substrates. *Bioscience reports*, 30(4), pp.243-255.

Swaffer, M.P., Jones, A.W., Flynn, H.R., Snijders, A.P. and Nurse, P., 2016. CDK substrate phosphorylation and ordering the cell cycle. *Cell*, 167(7), pp.1750-1761.

Swarts, D.R., Stewart, E.R., Higgins, G.S. and Coverley, D., 2018. CIZ1-F, an alternatively spliced variant of the DNA replication protein CIZ1 with distinct expression and localisation, is overrepresented in early stage common solid tumours. *Cell Cycle*, 17(18), pp.2268-2283.

Tallet, A., Nault, J.C., Renier, A., Hysi, I., Galateau-Salle, F., Cazes, A., Copin, M.C., Hofman, P., Andujar, P., Le Pimpec-Barthes, F. and Zucman-Rossi, J., 2014. Overexpression and promoter mutation of the TERT gene in malignant pleural mesothelioma. *Oncogene*, 33(28), pp.3748-3752.

Taylor, M.R. and Yeeles, J.T., 2019. Dynamics of replication fork progression following helicase–polymerase uncoupling in eukaryotes. *Journal of molecular biology*, 431(10), pp.2040-2049.

Técher, H., Koundrioukoff, S., Nicolas, A. and Debatisse, M., 2017. The impact of replication stress on replication dynamics and DNA damage in vertebrate cells. *Nature Reviews Genetics*, 18(9), pp.535-550.

Thome, K.C., Dhar, S.K., Quintana, D.G., Delmolino, L., Shahsafaei, A. and Dutta, A., 2000. Subsets of human origin recognition complex (ORC) subunits are expressed in non-

proliferating cells and associate with non-ORC proteins. *Journal of Biological Chemistry*, 275(45), pp.35233-35241.

Thwaites, M.J., Cecchini, M.J., Passos, D.T., Zakirova, K. and Dick, F.A., 2019. Context dependent roles for RB-E2F transcriptional regulation in tumor suppression. *Plos one*, 14(1), p.e0203577.

Toledo, L.I., Altmeyer, M., Rask, M.B., Lukas, C., Larsen, D.H., Povlsen, L.K., Bekker-Jensen, S., Mailand, N., Bartek, J. and Lukas, J., 2013. ATR prohibits replication catastrophe by preventing global exhaustion of RPA. *Cell*, 155(5), pp.1088-1103.

Toren, P. and Zoubeidi, A., 2014. Targeting the PI3K/Akt pathway in prostate cancer: challenges and opportunities. *International journal of oncology*, 45(5), pp.1793-1801.

Tourrière, H., Saksouk, J., Lengronne, A. and Pasero, P., 2017. Single-molecule analysis of DNA replication dynamics in budding yeast and human cells by DNA combing. *Bio-protocol*, 7(11), p.e2305.

Trinkle-Mulcahy, L., 2019. Recent advances in proximity-based labeling methods for interactome mapping. *F1000Research*, 8.

Tuduri, S., Crabbé, L., Conti, C., Tourrière, H., Holtgreve-Grez, H., Jauch, A., Pantesco, V., De Vos, J., Thomas, A., Theillet, C. and Pommier, Y., 2009. Topoisomerase I suppresses genomic instability by preventing interference between replication and transcription. *Nature cell biology*, 11(11), pp.1315-1324.

Tudzarova, S., Mulholland, P., Dey, A., Stoeber, K., Okorokov, A.L. and Williams, G.H., 2016. p53 controls CDC7 levels to reinforce G1 cell cycle arrest upon genotoxic stress. *Cell Cycle*, 15(21), pp.2958-2972.

Turgeon, M.O., Perry, N.J. and Poulgiannis, G., 2018. DNA damage, repair, and cancer metabolism. *Frontiers in oncology*, 8, p.15.

Ubhi, T. and Brown, G.W., 2019. Exploiting DNA replication stress for cancer treatment. *Cancer research*, 79(8), pp.1730-1739.

Uhlmann, F., Bouchoux, C. and Lopez-Avilés, S., 2011. A quantitative model for cyclin-dependent kinase control of the cell cycle: revisited. *Philosophical Transactions of the Royal Society B: Biological Sciences*, 366(1584), pp.3572-3583.

van den Bosch, M., Bree, R.T. and Lowndes, N.F., 2003. The MRN complex: coordinating and mediating the response to broken chromosomes. *EMBO reports*, 4(9), pp.844-849.

Voitenleitner C, Rehfuess C, Hilmes M, O'Rear L, Liao PC, Gage DA, Ott R, Nasheuer HP, Fanning E. Cell cycle-dependent regulation of human DNA polymerase α -primase activity by phosphorylation. *Molecular and cellular biology*. 1999 Jan 1;19(1):646-56.

Wang, D.Q., Wang, K., Yan, D.W., Liu, J., Wang, B., Li, M.X., Wang, X.W., Liu, J., Peng, Z.H., Li, G.X. and Yu, Z.H., 2014. CIZ1 is a novel predictor of survival in human colon cancer. *Experimental Biology and Medicine*, 239(7), pp.862-870.

- Wang, D. and Gao, F., 2019. Comprehensive analysis of replication origins in *Saccharomyces cerevisiae* genomes. *Frontiers in microbiology*, 10, p.2122.
- Wang, S.C., Nakajima, Y., Yu, Y.L., Xia, W., Chen, C.T., Yang, C.C., McIntush, E.W., Li, L.Y., Hawke, D.H., Kobayashi, R. and Hung, M.C., 2006. Tyrosine phosphorylation controls PCNA function through protein stability. *Nature cell biology*, 8(12), pp.1359-1368.
- Wang, X., Fujimaki, K., Mitchell, G.C., Kwon, J.S., Della Croce, K., Langsdorf, C., Zhang, H.H. and Yao, G., 2017. Exit from quiescence displays a memory of cell growth and division. *Nature communications*, 8(1), pp.1-11.
- Wang, Y., Li, X., Zhang, J., Liu, Q., Gao, P., Li, D., Zhang, S. and Liu, J., 2019. CIZ1 Expression Is Upregulated in Hemangioma of the Tongue. *Pathology & Oncology Research*, 25(4), pp.1653-1658.
- Wasąg, P. and Lenartowski, R., 2016. Nuclear matrix-structure, function and pathogenesis. *Postepy higieny i medycyny doswiadczalnej (Online)*, 70, pp.1206-1219.
- Watanabe, K., Tateishi, S., Kawasuji, M., Tsurimoto, T., Inoue, H. and Yamaizumi, M., 2004. Rad18 guides pol η to replication stalling sites through physical interaction and PCNA monoubiquitination. *The EMBO journal*, 23(19), pp.3886-3896.
- Weinstein, J.N., Collisson, E.A., Mills, G.B., Shaw, K.R.M., Ozenberger, B.A., Ellrott, K., Shmulevich, I., Sander, C., Stuart, J.M. and Cancer Genome Atlas Research Network, 2013. The cancer genome atlas pan-cancer analysis project. *Nature genetics*, 45(10), p.1113.
- Wawrzyniak, P., Płucienniczak, G. and Bartosik, D., 2017. The different faces of rolling-circle replication and its multifunctional initiator proteins. *Frontiers in Microbiology*, 8, p.2353.
- Wilson, R.H. and Coverley, D., 2013. Relationship between DNA replication and the nuclear matrix. *Genes to Cells*, 18(1), pp.17-31.
- Wilson, R.H., Hesketh, E.L. and Coverley, D., 2016. The nuclear matrix: fractionation techniques and analysis. *Cold Spring Harbor Protocols*, 2016(1), pp.pdb-top074518.
- Wooster, R., Bignell, G., Lancaster, J., Swift, S., Seal, S., Mangion, J., Collins, N., Gregory, S., Gumbs, C., Micklem, G. and Barfoot, R., 1995. Identification of the breast cancer susceptibility gene BRCA2. *Nature*, 378(6559), pp.789-792.
- Wu, Z., Liu, J., Yang, H. and Xiang, H., 2014. DNA replication origins in archaea. *Frontiers in microbiology*, 5, p.179.
- Wu, J., Lei, L., Gu, D., Liu, H. and Wang, S., 2016. CIZ1 is upregulated in hepatocellular carcinoma and promotes the growth and migration of the cancer cells. *Tumor Biology*, 37(4), pp.4735-4742.
- Wu, D., Duan, C., Chen, L. and Chen, S., 2017. Efficacy and safety of different doses of cytarabine in consolidation therapy for adult acute myeloid leukemia patients: a network meta-analysis. *Scientific reports*, 7(1), pp.1-10.

- Xiao, J., Uitti, R.J., Zhao, Y., Vemula, S.R., Perlmutter, J.S., Wszolek, Z.K., Maraganore, D.M., Auburger, G., Leube, B., Lehnhoff, K. and LeDoux, M.S., 2012. Mutations in CIZ1 cause adult onset primary cervical dystonia. *Annals of neurology*, 71(4), pp.458-469.
- Yajima, H., Lee, K.J., Zhang, S., Kobayashi, J. and Chen, B.P., 2009. DNA double-strand break formation upon UV-induced replication stress activates ATM and DNA-PKcs kinases. *Journal of molecular biology*, 385(3), pp.800-810.
- Yan, Z., DeGregori, J., Shohet, R., Leone, G., Stillman, B., Nevins, J.R. and Williams, R.S., 1998. Cdc6 is regulated by E2F and is essential for DNA replication in mammalian cells. *Proceedings of the National Academy of Sciences*, 95(7), pp.3603-3608.
- Yao, G., 2014. Modelling mammalian cellular quiescence. *Interface focus*, 4(3), p.20130074.
- Ye, X., Nalepa, G., Welcker, M., Kessler, B.M., Spooner, E., Qin, J., Elledge, S.J., Clurman, B.E. and Harper, J.W., 2004. Recognition of phosphodegron motifs in human cyclin E by the SCFFbw7 ubiquitin ligase. *Journal of Biological Chemistry*, 279(48), pp.50110-50119.
- Yeeles, J.T., Deegan, T.D., Janska, A., Early, A. and Diffley, J.F., 2015. Regulated eukaryotic DNA replication origin firing with purified proteins. *Nature*, 519(7544), pp.431-435.
- Yeeles, J.T., Janska, A., Early, A. and Diffley, J.F., 2017. How the eukaryotic replisome achieves rapid and efficient DNA replication. *Molecular cell*, 65(1), pp.105-116.
- Yi, X., de Vries, H.I., Siudeja, K., Rana, A., Lemstra, W., Brunsting, J.F., Kok, R.M., Smulders, Y.M., Schaefer, M., Dijk, F. and Shang, Y., 2009. Stw1 modifies chromatin compaction and is required to maintain DNA integrity in the presence of perturbed DNA replication. *Molecular biology of the cell*, 20(3), pp.983-994.
- Yi, M., Dong, B., Qin, S., Chu, Q., Wu, K. and Luo, S., 2019. Advances and perspectives of PARP inhibitors. *Experimental Hematology & Oncology*, 8(1), p.29.
- Yin, Y., Shen, Q., Tao, R., Chang, W., Li, R., Xie, G., Liu, W., Zhang, P. and Tao, K., 2018. Wee1 inhibition can suppress tumor proliferation and sensitize p53 mutant colonic cancer cells to the anticancer effect of irinotecan. *Molecular medicine reports*, 17(2), pp.3344-3349.
- Young, C.P., Hillyer, C., Hokamp, K., Fitzpatrick, D.J., Konstantinov, N.K., Welty, J.S., Ness, S.A., Werner-Washburne, M., Fleming, A.B. and Osley, M.A., 2017. Distinct histone methylation and transcription profiles are established during the development of cellular quiescence in yeast. *BMC genomics*, 18(1), p.107.
- Yousefi, R. and Rowicka, M., 2019. Stochasticity of replication forks' speeds plays a key role in the dynamics of DNA replication. *PLoS computational biology*, 15(12), p.e1007519.
- Yu, Y., Cai, J.P., Tu, B., Wu, L., Zhao, Y., Liu, X., Li, L., McNutt, M.A., Feng, J., He, Q. and Yang, Y., 2009. Proliferating cell nuclear antigen is protected from degradation by forming a complex with MutT Homolog2. *Journal of Biological Chemistry*, 284(29), pp.19310-19320.
- Yuan, J. and Chen, J., 2010. MRE11-RAD50-NBS1 complex dictates DNA repair independent of H2AX. *Journal of Biological Chemistry*, 285(2), pp.1097-1104.

- Yuan, X., Srividhya, J., De Luca, T., Lee, J.H.E. and Pomerening, J.R., 2014. Uncovering the role of APC-Cdh1 in generating the dynamics of S-phase onset. *Molecular biology of the cell*, 25(4), pp.441-456.
- Yuan, Z., Georgescu, R., Bai, L., Zhang, D., Li, H. and O'Donnell, M.E., 2020. DNA unwinding mechanism of a eukaryotic replicative CMG helicase. *Nature communications*, 11(1), pp.1-10.
- Yurov, Y.B., 1980. Rate of DNA replication fork movement within a single mammalian cell. *Journal of molecular biology*, 136(3), pp.339-342.
- Zaboikin, M., Zaboikina, T., Freter, C. and Srinivasakumar, N., 2017. Non-homologous end joining and homology directed DNA repair frequency of double-stranded breaks introduced by genome editing reagents. *PloS one*, 12(1), p.e0169931.
- Zafar, M.K. and Eoff, R.L., 2017. Translesion DNA synthesis in cancer: molecular mechanisms and therapeutic opportunities. *Chemical research in toxicology*, 30(11), pp.1942-1955.
- Zarkowska, T.A., 1999. *Phosphorylation of the retinoblastoma protein, pRB, by CDK4-cyclin D1* (Doctoral dissertation, Institute of Cancer Research (University Of London)).
- Zeman, M.K. and Cimprich, K.A., 2014. Causes and consequences of replication stress. *Nature cell biology*, 16(1), pp.2-9.
- Zeng, X., Chen, S. and Huang, H., 2011. Phosphorylation of EZH2 by CDK1 and CDK2: a possible regulatory mechanism of transmission of the H3K27me3 epigenetic mark through cell divisions. *Cell cycle*, 10(4), pp.579-583.
- Zetterberg, A., Larsson, O. and Wiman, K.G., 1995. What is the restriction point?. *Current opinion in cell biology*, 7(6), pp.835-842.
- Zhan, T., Rindtorff, N. and Boutros, M., 2017. Wnt signaling in cancer. *Oncogene*, 36(11), pp.1461-1473.
- Zhang, D., Wang, Y., Dai, Y., Wang, J., Suo, T., Pan, H., Liu, H., Shen, S. and Liu, H., 2015. CIZ1 promoted the growth and migration of gallbladder cancer cells. *Tumor Biology*, 36(4), pp.2583-2591.
- Zhang, H. and Freudenreich, C.H., 2007. An AT-rich sequence in human common fragile site FRA16D causes fork stalling and chromosome breakage in *S. cerevisiae*. *Molecular cell*, 27(3), pp.367-379.
- Zhang, J., Si, J., Gan, L., Di, C., Xie, Y., Sun, C., Li, H., Guo, M. and Zhang, H., 2019. Research progress on therapeutic targeting of quiescent cancer cells. *Artificial cells, nanomedicine, and biotechnology*, 47(1), pp.2810-2819.
- Zhang, S., Zhou, Y., Trusa, S., Meng, X., Lee, E.Y. and Lee, M.Y., 2007. A Novel DNA Damage Response RAPID DEGRADATION OF THE p12 SUBUNIT OF DNA POLYMERASE δ . *Journal of Biological Chemistry*, 282(21), pp.15330-15340.
- Zhang, W., Nandakumar, N., Shi, Y., Manzano, M., Smith, A., Graham, G., Gupta, S., Vietsch, E.E., Laughlin, S.Z., Wadhwa, M. and Chetram, M., 2014. Downstream of mutant KRAS, the

transcription regulator YAP is essential for neoplastic progression to pancreatic ductal adenocarcinoma. *Science signaling*, 7(324), pp.ra42-ra42.

Zhang, X.H., Tee, L.Y., Wang, X.G., Huang, Q.S. and Yang, S.H., 2015. Off-target effects in CRISPR/Cas9-mediated genome engineering. *Molecular Therapy-Nucleic Acids*, 4, p.e264.

Zhao, Q.Y., Lei, P.J., Zhang, X., Zheng, J.Y., Wang, H.Y., Zhao, J., Li, Y.M., Ye, M., Li, L., Wei, G. and Wu, M., 2016. Global histone modification profiling reveals the epigenomic dynamics during malignant transformation in a four-stage breast cancer model. *Clinical epigenetics*, 8(1), pp.1-15.

Zhou, J.C., Janska, A., Goswami, P., Renault, L., Ali, F.A., Kotecha, A., Diffley, J.F. and Costa, A., 2017. CMG–Pol epsilon dynamics suggests a mechanism for the establishment of leading-strand synthesis in the eukaryotic replisome. *Proceedings of the National Academy of Sciences*, 114(16), pp.4141-4146.

Zhou, X., Liu, Q., Wada, Y., Liao, L. and Liu, J., 2018. CDKN1A-interacting zinc finger protein 1 is a novel biomarker for lung squamous cell carcinoma. *Oncology letters*, 15(1), pp.183-188.

Zhou, Y., Pozo, P.N., Oh, S., Stone, H.M. and Cook, J.G., 2020. Distinct and sequential re-replication barriers ensure precise genome duplication. *bioRxiv*, p.366666.

Zimmerman, K.M., Jones, R.M., Petermann, E. and Jeggo, P.A., 2013. Diminished origin-licensing capacity specifically sensitizes tumor cells to replication stress. *Molecular Cancer Research*, 11(4), pp.370-380.

Zlotorynski, E., Rahat, A., Skaug, J., Ben-Porat, N., Ozeri, E., Hershberg, R., Levi, A., Scherer, S.W., Margalit, H. and Kerem, B., 2003. Molecular basis for expression of common and rare fragile sites. *Molecular and cellular biology*, 23(20), pp.7143-7151.